U.PORTO

FEUP FACULDADE DE ENGENHARIA
UNIVERSIDADE DO PORTO

Application of phase change materials in thermally stressful situations

A thesis submitted in partial fulfilment of the requirements for
the degree of Doctor in Chemical and Biological Engineering of the Faculty of Engineering of the University of Porto,
by:

Jorge André Fonseca Malaquias

João Bernardo Lares Moreira de Campos – Supervisor

c e f t
TRANSPORT PHENOMENA RESEARCH CENTER

Department of Chemical Engineering,
Faculty of Engineering, University of Porto, Portugal

November 2021

This thesis was supported by national funds through FCT (Fundação para a Ciência e Tecnologia) under project UIDB/00532/2020 and grant PD/BD/ 135097/2017.

UNIÃO EUROPEIA

Fundo Social Europeu

Transport Phenomena Research Center
University of Porto – Faculty of Engineering
Rua Dr.Roberto Frias s/n, 4200-465 Porto
up201007676@up.pt

Acknowledgments

Antes de mais quero expressar os meus agradecimentos ao professor João Campos pelo seu suporte e supervisão desta tese. Um grande abraço aos meus amigos que me suportaram durante esta jornada e estiveram lá sempre para mim. Também quero agradecer aos meus colegas de trabalho pelo seu suporte e momentos hilariantes partilhados.

Queria agradecer á minha família em particular aos meus pais por me terem apoiado, e dado a oportunidade de seguir os meus sonhos e propósitos de vida. Amo-vos muito. Sem vocês nada disto seria possível.

Por último, queria dar um grande abraço ao meu sobrinho Gabriel ao qual eu dedico esta tese.

To Gabriel

Preface

This thesis was submitted for the fulfilment of the Doctor in Philosophy degree at the University of Porto – Faculty of Engineering (FEUP). The work outlined in this thesis was elaborated in the Transport Phenomena Research Center, (CEFT), at the Chemical Engineering Department of FEUP. Supervision was granted by Professor João Moreira de Campos from CEFT – FEUP. The major findings of this thesis are reported in four main chapters (chapters 3 - 6), each one corresponding to a research paper. These papers were written separately and thus may present language and nomenclature inconsistencies when compared to each other. Nonetheless, each of them contains enough information to be individually understood. They also follow a sequence of knowledge obtainance with a particular goal in mind, which resulted in the current thesis.

Table of contents

Application of phase change materials in thermally stressful situations

Abstract

As climate change becomes more evident in our everyday lives, heat stress illness is more likely to impact people around the globe in the various activities that they enroll on. Heat stress management solutions must become a top priority when humans are exposed to thermally stressful situations. Of such, probably one of the activities that is likely to suffer the most impact is firefighting. With rising temperature fluctuations and heat waves, fire occurrence is likely to become more frequent, exposing fire extinguishers to a greater risk of thermal damage. The potential application of phase change materials (PCM) to firefighting garments is studied in this thesis as a first step to the effective design of significantly improved protective garments for high temperature exposures.

In a first phase of this thesis, a numerical study is performed to analyze what properties a PCM must have in order to be an adequate candidate for its incorporation in a firefighting garment. Independent parametric studies are performed where the PCM properties and the fire exposure scenario are varied. Correlations are derived which enable the textile designer not only to check if a PCM choice is adequate from the thermal standpoint, but also to calculate the necessary PCM mass to be incorporated in the firefighting garment in order to achieve a desired protection level.

In a second phase, a numerical study is performed to augment the information on the correlations, considering the transient nature of the firefighting scenario in more detail. Besides considering the fire exposure phase, post – exposure and resting phases are included in much more detail in the calculations. Independent parametric studies are performed involving PCM choice as well as exposure scenario. The occurrence of PCM re-solidification after the exposure phase, exposes the firefighter to potential third – degree burn risk due to released latent heat towards the skin and thus is an aspect which must be taken into account.

In a third phase, heat and mass transport is studied in detail in a wet firefighting garment, identifying not only the influence of water presence on second – degree burn time for various exposure scenarios, but also environmental and garment conditions for which steam burn occurrence in firefighters is possible. Correlations are generated which indicate when the firefighter might suffer a burn and its nature. Critical knowledge regarding heat and mass transport in wet firefighting garments is gained.

Lastly in a fourth phase, the heat and mass transport phenomena are studied in a wet firefighting garment ensemble with an incorporated phase change material. A numerical study is performed utilizing a novel heat and mass transport model for PCM garments.

Independent parametric studies are performed involving PCM properties, water content and location, as well as exposure scenario. It is found that part of the steam that is generated inside the firefighting garment may condense at the phase change material and this has implications on optimal PCM choice and geometrical features.

Sumário

Os efeitos das alterações climáticas são cada vez mais visíveis no quotidiano das pessoas. O aumento da flutuação da temperatura bem como a frequência de vagas de calor faz com que, em certas profissões, a exposição a condições termicamente indesejáveis seja crescente. Por exemplo, no caso dos bombeiros, é expectável que os mesmos tenham que ser expostos com uma maior frequência a condições termicamente adversas devido ao aumento de incêndios. Daí serem cada vez mais necessárias soluções para mitigar o stress térmico no corpo humano, quando exposto a tais condições. A incorporação de materiais com mudança de fase (MMF) em vestuário de proteção, é vista com uma solução promissora e analisada em detalhe nesta tese para o caso específico dos bombeiros.

Numa primeira fase, são utilizadas ferramentas numéricas para estudar o transporte de calor num vestuário de bombeiros típico com uma camada de MMF incorporada no mesmo. São efetuados, estudos paramétricos independentes, considerando as propriedades termofísicas do MMF bem como o cenário de fogo a que o bombeiro é exposto. É utilizado o método das capacidades térmicas aparentes para simular a mudança de fase. No final, são geradas correlações que indicam o tempo de queimadura de segundo grau em função da temperatura de fusão, massa e energia latente do MMF, bem como em função do cenário de exposição. Tais correlações permitem a seleção adequada de um MMF.

Numa segunda fase, o momento pós – fogo é considerado com maior detalhe. Depois da exposição ao fogo, é assumido que o bombeiro está exposto a um meio ambiente suave em que há trocas de calor por convecção e radiação. Ferramentas numéricas são novamente utilizadas para executar um estudo paramétrico envolvendo parâmetros como a escolha do MMF e o cenário de exposição ao fogo. Demonstra-se que em certos casos ocorre re-solidificação do MMF depois da exposição ao fogo, o que promove um fluxo de calor latente para a pele, o que pode causar queimaduras de terceiro grau.

Numa terceira fase, é estudado o efeito da presença de água nas trocas de massa e calor num vestuário de bombeiros. São feitos estudos paramétricos independentes envolvendo a quantidade inicial bem como a localização da água, e a intensidade do fluxo de calor. No final, são gerados mapas indicando o tempo de queima de segundo grau em função da quantidade e localização da água no têxtil para vários fluxos de calor. A informação gerada permite também identificar a natureza das queimaduras sofridas pelo bombeiro, isto é, se o mesmo sofre queimaduras por escaldão, e em que condições.

Numa quarta e última fase, as trocas de massa e calor são estudadas num vestuário de bombeiros inicialmente molhado e com incorporação de MMFs. É sugerido um novo modelo

de transporte de calor e massa em vestuário contendo MMFs. São efetuados estudos paramétricos independentes envolvendo variáveis associadas ao MMF e à presença da água no têxtil. A presença inicial de água no têxtil faz com que vapor de água apareça durante a exposição. Este, em certas condições, pode condensar no MMF libertando calor e liquefazendo o MMF. Esta liquefação tem implicações nos mapas gerados para a escolha adequada de um MMF e nas propriedades geométricas para a sua incorporação num vestuário de bombeiros

Chapter 1

Introduction

1

Introduction

1.1 Phase change materials (PCMs)

1.1.1 Definition

Phase change materials may be defined as substances in which the latent heat associated with their phase change (usually solid-liquid) can be used to store or release heat at an almost, if not, constant temperature [1–4]. PCMs tend to change phase, depending on the temperature of their surroundings. If, for example, a PCM is initially in its solid-state, and the surrounding temperature suddenly increases to a temperature above its phase change temperature, the PCM will absorb part of the heat from the surroundings as latent heat and will melt (Figure 1.1). Consequently, the PCM enthalpy content increases (Figure 1.2). On the other hand, if the PCM is initially liquid and the surrounding temperature suddenly decreases below the phase change temperature, the PCM will solidify releasing heat towards the environment. This characteristic of storing and releasing energy at a specific temperature makes PCMs very attractive for thermal applications. In reality, however, PCMs tend to change phase not at a constant but rather over a narrow temperature region (i.e., mushy region), as most of them are not pure substances [1]. Nevertheless, the active principle is similar, but the phase change happens between a solidus and liquidus temperature, as shown in Figure 1.2b.

Figure 1.1 - Phase change material melting as it absorbs heat from the environment at the melting temperature.

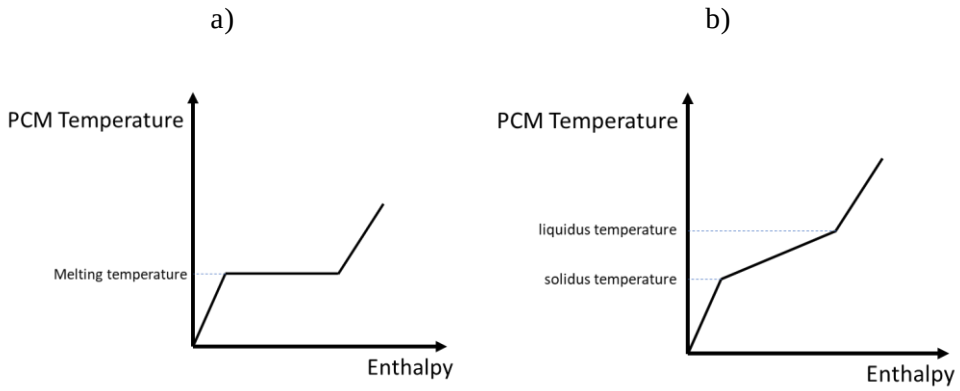

Figure 1.2 – Enthalpy evolution of PCM when heated from its initial solid phase to liquid phase: a) considering isothermal phase change (i.e., pure materials); b) considering non – isothermal phase change.

1.1.2 Types of PCMs

There are essentially two main categories into which most PCMs fall into: organics and inorganics.

Organic PCMs such as paraffins, and non – paraffins like fatty acids, have been widely studied and characterised in the literature. Organic PCMs present good chemical and thermal stabilities, but they tend to have low thermal conductivity, flammability issues, and low latent heat [1,3,5].

Inorganic PCMs, on the other hand, consist mainly of salt hydrates. These tend to have high latent heat and thermal conductivity, but they lack chemical and thermal stability and present phase segregation and corrosion phenomena.

Eutectic PCMs also exist, consisting of inorganic and/or organic components. Despite showing good phase changing behaviour, their latent heat tends to be very low and they are also costly [6,7].

1.2 Applications

As stated before, what makes PCMs attractive is their ability to store or release heat at an almost constant temperature. Several applications exist where this ability has been utilized either to promote energy savings in thermal storage systems or as an adequate tool for thermal management to prevent thermal hazards. The applications are discussed in terms of energy-saving applications and thermal management applications below [1].

1.2.1 Energy saving

When it comes to obtaining energy savings, the incorporation of PCMs has proven to be beneficial in various applications. PCM usage and research were firstly impulsed in the late 70s due to the energy crisis at the time. Afterward, the interest for research on the potential of such materials for energy savings disappeared but has re-emerged due to the current energy and climate crisis [4].

Solar heating systems with incorporated PCMs have received quite substantial attention in the literature. Solar water heating systems utilize PCMs to keep water warm even when no sunshine is available [3]. The latent energy stored in the PCM through its melting ensures that it will be available for later release. Other solar systems such as solar air heating systems, solar cookers, or solar greenhouses also utilize PCMs [3].

PCMs have found their way into a multitude of other applications also. They have been incorporated in wallboards, trombe walls, and shutters to reduce HVAC consumption in buildings [3,8]. Underfloor electric heating systems have also been combined with PCM layers to promote electricity savings [3,9]. Refrigerated transport trucks have been incorporated with PCMs to promote

refrigeration efficiency and thus reduce fuel costs [10]. Cooling of engines and vehicle exhaust heat recovery utilizing PCMs has been shown to reduce emissions towards the atmosphere and provide potential energy savings [11].

1.2.2 Thermal management

PCMs can also be used to provide adequate thermal management. These systems primarily aim to reduce the risk of some hazard occurring if some thermal limit is reached. A category of applications that meets such description is in the battery sector. PCMs have been shown to be an effective solution to keep batteries in the normal operating temperature ranges. A lack of control of such could promote thermal runaways and cause fires [12]. PCMs have also been shown to protect spacecraft equipment from thermal hazards, as short – term high heat flux exposures may render installed thermal control systems ineffective in doing so [13]. More recently, the application of PCMs in pavements has been gaining considerable attention in the literature [14]. Pavements with elevated temperatures contribute to the urban heat island effect, while low temperatures cause pavements to crack. Incorporating PCMs helps maintain pavement temperatures at an adequate level by storing and releasing latent heat. PCMs have also been applied in the textile sector to manage the microclimate temperature between the fabric and the skin and provide more comfort to the user when under thermally stressful conditions [15–18].

1.3 Heat stress

1.3.1 Definition

Heat stress is defined as the discomfort experienced by individuals when excess heat is present and can't be tolerated [19–21]. Heat stressful conditions may induce heat strain on individuals causing heat imbalance in the body. The heat balance equation is stated as follows:

$$S = M - Wk \pm K \pm R \pm C \pm C_{res} - E_{res} - E_{skin} \quad (1.1)$$

where S represents the body heat storage rate, M the metabolic energy expenditure, Wk the external work performed, and K, R, C represent the conductive, radiative, and convective heat exchanges between the environment and the skin, respectively. C_{res} and E_{res} represent the convective and evaporative respiratory heat losses, while E_{skin} represents the evaporative heat loss through the skin [22].

As is shown, heat strain can be induced by environmental and physiological factors. The body utilizes thermoregulatory mechanisms to maintain a neutral thermal condition (S = 0) as it will have a tendency to do so.

1.3.2 Thermoregulation

When thermal discomfort arises in an individual due to external or internal heat sources, the body tends to activate mechanisms to dissipate such heat. Consider an individual performing heavy-duty work. Under such conditions, the metabolic heat generated is substantial.

The hypothalamus, part of the brain, is responsible for the thermoregulation of the body. When thermosensitive neurons sense an increase in body temperature (either due to internal or external heat sources), the hypothalamus releases chemical compounds into the central nervous system to prompt reactions of the various organs to the heat strain that the body is experiencing. In the case of a temperature increase, there is vasodilation and an increase in the heart rate. These phenomena induce blood transport into the skin's surface, where heat exchanges now depend on the environmental conditions present [22–24]. Sweating also tends to occur, allowing for evaporative cooling to take place at the skin surface. Hence, as shown in equation 1.1, this heat gets rejected by convective, radiative, and evaporative means.

Note that if clothing is present, it could represent a barrier between the skin and the environment, retarding heat and evaporative transport rates and thus hindering body cooling. However, clothing becomes indispensable in various applications to prevent heat strain that external factors would otherwise induce.

1.3.3 High heat stress situations

One of the main reasons heat stress has become an essential topic in the literature is because of climate change phenomena and how such will impact the way humans interact with the environment [21,24]. Heatwaves are becoming more and more common, and their impact on human health is of concern. Thus heat stress is already an issue in our everyday lives [25].

In certain professions, humans tend to perform strenuous activities in undesirable environments characterised by high temperatures and humidity [26–28]. Such activities are present in the construction and agricultural sectors, for example, rendering workers to heat stress illness such as heat exhaustion, heat syncope, or even heat stroke. There are also professions where workers are exposed to extreme heat fluxes, such as in the metal and non – metal mineral industries [26]. Professions in the public sector such as firefighting also fall into this category where the heat strain experienced is unacceptable and life threatening.

Thus, it becomes clear that heat stress is present in our daily lives, but more so when humans undergo certain activities that require heavy-duty work under high heat and humidity exposures. Solutions to mitigate heat strain potential and contribute to body thermal neutrality under such conditions are thus necessary.

1.4 The firefighter problem

The firefighting occupation is among the most heat strenuous professions that humans can engage in [26,29]. Thus, in the ambit of this thesis, focus will

be given to the firefighter problem as representative of a typical high heat stressful situation that humans typically engage in.

Firefighters wear protective clothing assemblies, which usually consist of three main garment layer types: the outer shell, moisture barrier, and thermal inner. More than one layer of each type is possible, as shown in Figure 1.3, where two thermal inners are present in the firefighting protective clothing ensemble [30]. Each layer type has a specific function. The outer shell is essentially responsible for providing mechanical resistance to the firefighter. It is highly reflective to mitigate radiative heat transfer, and fire resistant as it could come into contact with fire sources. The moisture barrier is mainly responsible for configuring the firefighter with protection from liquid hazards such as blood pathogens and other toxic chemicals. This layer may or may not be impermeable to water vapour. The thermal inners main purpose is to provide the firefighter with thermal insulation.

The textile structure of each of the individual layer types is directly related to their specific function. Figure 1.3 shows a typical firefighting protective clothing ensemble and its textile structural characteristics. As can be seen, the inner layers tend to be non–woven fabrics providing the garments with still air entrapped between the fibres, increasing thermal insulation.

a.)

b.)

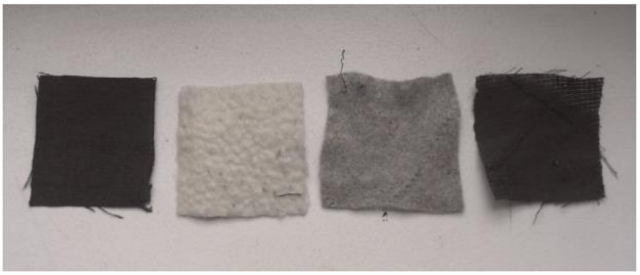

c.)

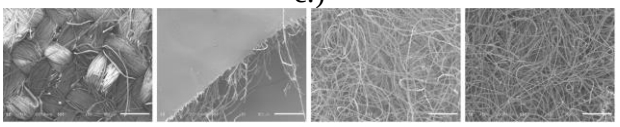

Figure 1.3 – Typical firefighting protective clothing ensemble consisting of an outer shell, moisture barrier, and two thermal inners, images taken from [30]; a) overall view of the garment ensemble; b) view of individual layers in the following order: outer shell, moisture barrier, thermal inner 1, thermal inner 2; c) SEM images of respective garment layers.

1.4.1 Firefighting scenarios

Firefighters tend to face high humid, radiative and convective heat flux exposures which renders them to heat stress illness and, in the worst cases, death [31]. The diversity of scenarios that firefighters face is immense, essentially due

to the nature of their profession. From rescue missions to combating fires, firefighters will naturally face various heat stress sources. Firefighters tend to sweat profusely during operations. Sweat rates as high as 3 liters/hour may be achieved under certain activities [32].

It is challenging to categorize firefighting scenarios essentially due to their high degree of variability. Nevertheless, some authors have published reports suggesting possible firefighting scenario characterization guidelines. Effectively, these firefighting scenarios are split into 3 or 4 thermal classes characterized by heat flux and air temperature faced by the firefighter, as shown in Figure 1.4 [33,34].

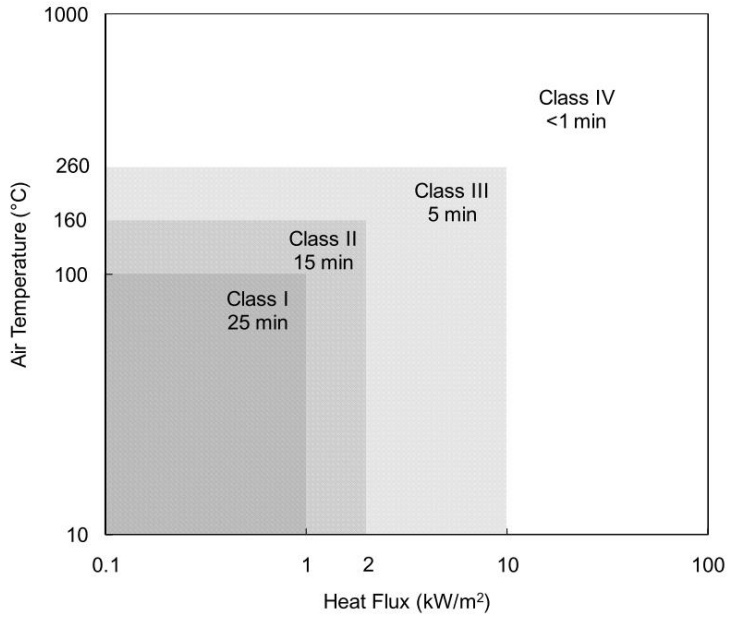

Figure 1.4 – Firefighting scenario types according to classification taken from [34].

Class I firefighting scenarios may be categorized as "routine", consisting of low temperature and low heat flux exposures in which firefighters may have a considerable tolerance time. Analogously for Class II, low heat fluxes and air temperatures dominate the characterization of such thermal class. From Class III onwards, firefighting scenarios may be categorized as hazardous or extreme.

Damage to electronic equipment and material deterioration is possible in this category [34]. The last Class IV includes flashover and backdraft type exposures where firefighters are exposed to critical environments and firefighting operations may not proceed. Firefighters are encouraged to escape such scenarios in seconds [31].

Due to the highly transient nature of firefighting scenarios and the limited amount of data used to generate the criteria shown above, it is challenging to categorize hazardous thermal environments. Further, the criteria above do not consider the humidity present in the air, which may be significant originating from hose spray during firefighting operations, for example [35].

Another aspect regarding firefighting scenarios that has gained limited attention in the literature is the post-fire exposure scenario [36–38]. When firefighters quit a firefighting scenario, they tend to be exposed to chilled environments. Nevertheless, if the firefighting garment is not doffed, the firefighter might unknowingly still be in danger due to the thermal energy accumulated in the garment [39]. Due to the high variability in post-fire exposure scenarios, it is also challenging to determine the thermal behaviour of firefighting protective clothing in these situations.

Thus, it is clear that firefighters may be exposed to extreme conditions. The clothing they wear must be able to manage this incoming heat, prevent it from reaching the skin, and thus avoid severe thermal hazards.

1.4.2 PCMs in firefighting garments

The idea of incorporating phase change materials in textile structures dates back to the 1980s when NASA decided to investigate the latent heat effect to keep astronauts protected from the heavy and highly transient thermal environment encountered in space [40]. The scientists at the time utilized a technique called microencapsulation, where the PCM was contained in microcapsules. The PCM microcapsules were then incorporated onto the textile substrate configuring it with latent heat. PCM microencapsulation is still used

today and has become a popular method to include PCMs in textiles. Microencapsulated PCMs have been incorporated in sportswear, bedding, and shoes [40].

However, one of the issues that arise with utilizing such a technique is the low PCM mass incorporated onto the textile. As a result, the thermal buffering effect observed seems to be limited [15,41]. Thus, other ways of incorporating PCMs in textile substrates still need to be found so that enough latent energy can be present to accommodate a substantial thermal buffering effect to the user.

Another way of assuring substantial thermal buffering effect to the user is by utilizing so-called PCM vests where the PCM is incorporated in a separate layer in the garment ensemble. PCM cooling vests have been the subject of much research in the literature.

PCM cooling vests consist of individual PCM packages distributed across a vest to cause an overall upper torso cooling effect (Figure 1.5). These vests have the potential to keep the user at a suitable temperature in cases where heat stress arises due to external weather conditions or due to high metabolic heat production.

Gao et al. [42] constructed a PCM cooling vest that consisted of 21 pockets to be inserted with PCM packs. A manikin with constant surface temperature of either 34 °C or 38 °C was used to test its potential cooling effect in a firefighter. The PCM vest was worn under a firefighting garment. Different PCM packets with different melting temperatures were tested to observe how PCM melting temperature affected the cooling rate. The authors found that a minimum difference of 6 °C must exist between the skin temperature and the PCM melting temperature for effective cooling. Gao et al. [43] then utilized a cooling vest on eight male subjects doing office work in a heated environment (i.e., 34 °C, 60 % RH) to analyse if such could keep the body cool in a potential heatwave environment (Figure 1.5a). The PCM utilized had a melting temperature of 21 °C, well below the skin and environment temperatures. The authors noticed a reduction in the torso skin temperature and a prolonged cooling effect.

a.) b.)

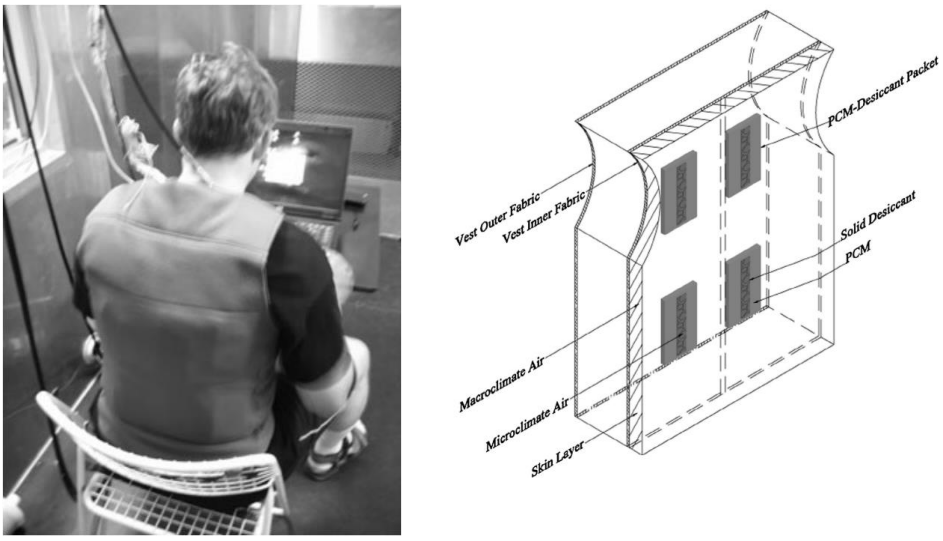

Figure 1.5 – a) User utilizing PCM cooling vest in a warm environment (34 °C, 60 % RH) [43]; b) PCM – desiccant cooling vest concept. [17]

Itani et al. [17] incorporated PCM – desiccant packets in a cooling vest to better manage the humidity in the microclimate between the garment and the skin (Figure 1.5b). The authors showed that the moisture in the microclimate is reduced due to the thermal interaction between PCM and the desiccant layer.

Some authors have already studied the effect of PCM incorporation on the thermal properties of the firefighting garment ensemble. Usually, in such studies, the PCM is inserted in the form of a microcapsule filling between two sewn layers, or as a separate layer containing PCM pockets [44,45]. Some authors also utilize coating technologies to incorporate a microcapsule PCM suspension directly onto the thermal inner surface [18,46]. The problem with such is that the breathability of the textile is highly affected, contributing to potential heat stress phenomena when the firefighter is under heavy metabolic activity. Nevertheless, the studies mentioned above demonstrate a positive, but limiting thermal effect caused by PCM incorporation.

Taking Barowy and Madrzykowski's study as an example [45], a sample of a typical firefighting protective clothing ensemble consisting of an outer shell,

moisture barrier, and thermal inner was modified with PCM PX -82 (Figure 1.6). The PCM filling was sewn in between the interior liner and batting layer, forming the modified thermal inner. The PCM firefighting assembly was then exposed to a full-scale room fire. Fabric temperatures as well as incoming heat fluxes were registered. The results show that despite clear evidence that the PCM reduces thermal damage to the firefighting garment (i.e., Figure 1.6c), it does not protect the firefighter from serious thermal hazards under such exposures. The reasons for such can vary from inadequate PCM selection to low PCM mass. Such matters need further study not only for diagnosis, but also to propose solutions so that adequate protection can be offered by the modified firefighting ensemble.

a.)

b.)

Figure 1.6 – Firefighting garment ensemble samples consisting of an outer shell, moisture barrier, and thermal inner seen from the backside [45]; a) before the fire exposure (garment ensemble on the left-hand side contains no PCM and the one on the right-hand side contains PCM); b) after exposure; garment ensemble on the left-hand side contains PCM, and the one in the right-hand side contains no PCM.

1.4.3 Challenges

Despite the promise the incorporation of phase change materials in firefighting garment assemblies shows, several questions in the literature remain unanswered. Namely, which PCM should be chosen so that a thermal buffering effect is provided and maximized? How much PCM mass should be incorporated to guarantee protection to the firefighter from thermal hazards? The need for selection criteria of phase change materials, especially in the firefighting application, is still lacking.

The firefighter scenario is a highly thermal transient scenario consisting of not only high-intensity exposure phases but also post-fire exposure and resting periods. The thermal behaviour of the PCM, and how this impacts the thermal damage delivered to the firefighter under such conditions is still unknown. Under certain circumstances, the inclusion of a PCM in a firefighting garment might be prejudicial. PCM selection criteria developed need to take such aspects into account.

Presence of water in a firefighting garment ensemble has been shown to influence fabric temperature considerably [47]. However, it is still unknown how PCM inclusion in wet firefighting garments affects heat and mass transport phenomena.

1.4.4 Motivation

Year upon year, various heat hazard injuries are reported by firefighters. In 2019 in the United States alone, 60,825 firefighter injuries occurred whilst on duty, of which 39 % occurred at the fire ground [48]. Also, in the same year, a total of 48 fatalities were registered [49]. Thus, with firefighting being a high-risk profession where injuries and deaths tend to happen, the challenge to develop solutions to mitigate heat hazards is of critical importance. One way of achieving such is to improve the protective performance of the clothing firefighters wear, considerably.

As already discussed, one possible way of achieving such is to introduce PCMs into the firefighting garment assembly. The PCM may absorb as latent heat part of the incoming heat flux from exposure, minimizing the garment temperatures over time, giving the firefighter a more significant time window to act in a fire scenario and protection from any other severe fires heat hazards. However, there are challenges regarding the incorporation of PCMs into firefighting garments.

In this thesis, such matters are addressed and discussed, further advancing the knowledge on the integration of PCMs in firefighting protective clothing and proving its effective potential in providing adequate protection towards the firefighter.

1.4.5 Outline

To investigate the issues addressed in Section 1.4.3, this thesis is divided into six chapters.

- The first chapter is introductory, where the different terms and challenges, motivation, and objectives are defined.
- The second chapter gives details on the materials and methods used throughout the thesis to meet the objectives.
- In the third chapter, PCM selection criteria are developed for the incorporation of PCMs in firefighting protective clothing ensembles. PCM optimal choice and mass are suggested depending on the fire exposure type encountered by the firefighter.
- In the fourth chapter, the PCM selection criteria are furthered by considering the influence of the post-fire exposure scenario.
- In the fifth chapter, the influence of water presence on the heat and mass transport in firefighting protective clothing ensembles is analysed and discussed without including the PCM. This study is justified as there is limiting knowledge in the literature regarding this aspect. It is useful to

investigate it before proceeding with the inclusion of the PCM under the presence of water.

- Hence, in the sixth chapter, the influence of water presence in the heat and mass transport in a PCM firefighting protective clothing ensemble is analysed, furthering the content of the PCM selection criterion to include such phenomena.
- Finally, in the seventh chapter, conclusions and future work are proposed.

References

[1] B. Zalba, Review on thermal energy storage with phase change: materials, heat transfer analysis and applications, Appl. Therm. Eng. 23 (2003) 251–283. https://doi.org/10.1016/S1359-4311(02)00192-8.

[2] Y. Dutil, D.R. Rousse, N. Ben Salah, S. Lassue, L. Zalewski, A review on phase-change materials: Mathematical modeling and simulations, Renew. Sustain. Energy Rev. 15 (2011) 112–130. https://doi.org/10.1016/j.rser.2010.06.011.

[3] A. Sharma, V. V. Tyagi, C.R. Chen, D. Buddhi, Review on thermal energy storage with phase change materials and applications, Renew. Sustain. Energy Rev. 13 (2009) 318–345. https://doi.org/10.1016/j.rser.2007.10.005.

[4] F. Agyenim, N. Hewitt, P. Eames, M. Smyth, A review of materials, heat transfer and phase change problem formulation for latent heat thermal energy storage systems (LHTESS), Renew. Sustain. Energy Rev. 14 (2010) 615–628. https://doi.org/10.1016/j.rser.2009.10.015.

[5] J. Liang, X. Zhang, J. Ji, Hygroscopic phase change composite material——A review, J. Energy Storage. 36 (2021) 102395. https://doi.org/10.1016/j.est.2021.102395.

[6] B.R. Anupam, U.C. Sahoo, P. Rath, Phase change materials for pavement applications: A review, Constr. Build. Mater. 247 (2020) 118553. https://doi.org/10.1016/j.conbuildmat.2020.118553.

[7] J. Liang, X. Zhang, J. Ji, Hygroscopic phase change composite material——A review, J. Energy Storage. 36 (2021) 102395. https://doi.org/10.1016/j.est.2021.102395.

[8] A.M. Borreguero, M. Luz Sánchez, J.L. Valverde, M. Carmona, J.F. Rodríguez, Thermal testing and numerical simulation of gypsum wallboards incorporated with different PCMs content, Appl. Energy. 88 (2011) 930–937. https://doi.org/10.1016/j.apenergy.2010.08.014.

[9] K. Lin, Y. Zhang, X. Xu, H. Di, R. Yang, P. Qin, Experimental study of

under-floor electric heating system with shape-stabilized PCM plates, Energy Build. 37 (2005) 215–220. https://doi.org/10.1016/j.enbuild.2004.06.017.

[10] M. Liu, W. Saman, F. Bruno, Development of a novel refrigeration system for refrigerated trucks incorporating phase change material, Appl. Energy. 92 (2012) 336–342. https://doi.org/10.1016/j.apenergy.2011.10.015.

[11] G.S. Wahile, P.D. Malwe, A. V. Kolhe, Waste heat recovery from exhaust gas of an engine by using a phase change material, Mater. Today Proc. 28 (2020) 2101–2107. https://doi.org/10.1016/j.matpr.2020.03.247.

[12] C. Liu, D. Xu, J. Weng, S. Zhou, W. Li, Y. Wan, S. Jiang, D. Zhou, J. Wang, Q. Huang, Phase change materials application in battery thermal management system: A review, Materials (Basel). 13 (2020) 1–37. https://doi.org/10.3390/ma13204622.

[13] W.F. Wu, N. Liu, W.L. Cheng, Y. Liu, Study on the effect of shape-stabilized phase change materials on spacecraft thermal control in extreme thermal environment, Energy Convers. Manag. 69 (2013) 174–180. https://doi.org/10.1016/j.enconman.2013.01.025.

[14] B.R. Anupam, U.C. Sahoo, P. Rath, Phase change materials for pavement applications: A review, Constr. Build. Mater. 247 (2020) 118553. https://doi.org/10.1016/j.conbuildmat.2020.118553.

[15] A. Izzo Renzi, C. Carfagna, P. Persico, Thermoregulated natural leather using phase change materials: An example of bioinspiration, Appl. Therm. Eng. 30 (2010) 1369–1376. https://doi.org/10.1016/j.applthermaleng.2010.02.026.

[16] B. Pause, Phase change materials and their application in coatings and laminates for textiles, Woodhead Publishing Limited, 2010. https://doi.org/http://dx.doi.org/10.1533/9781845697785.2.236.

[17] M. Itani, N. Ghaddar, K. Ghali, Innovative PCM-desiccant packet to provide dry microclimate and improve performance of cooling vest in hot environment, Energy Convers. Manag. 140 (2017) 218–227. https://doi.org/10.1016/j.enconman.2017.03.011.

[18] Y. Su, W. Zhu, M. Tian, Y. Wang, X. Zhang, J. Li, Intelligent bidirectional thermal regulation of phase change material incorporated in thermal protective clothing, Appl. Therm. Eng. 174 (2020) 115340. https://doi.org/10.1016/j.applthermaleng.2020.115340.

[19] A. Burgstall, A. Casanueva, S. Kotlarski, C. Schwierz, Heat warnings in Switzerland: Reassessing the choice of the current heat stress index, Int. J. Environ. Res. Public Health. 16 (2019). https://doi.org/10.3390/ijerph16152684.

[20] M.A. Borg, J. Xiang, O. Anikeeva, D. Pisaniello, A. Hansen, K. Zander, K. Dear, M.R. Sim, P. Bi, Occupational heat stress and economic burden: A review of global evidence, Environ. Res. 195 (2021) 110781. https://doi.org/10.1016/j.envres.2021.110781.

[21] T. Kjellstrom, D. Briggs, C. Freyberg, B. Lemke, M. Otto, O. Hyatt,

Heat, Human Performance, and Occupational Health: A Key Issue for the Assessment of Global Climate Change Impacts, Annu. Rev. Public Health. 37 (2016) 97–112. https://doi.org/10.1146/annurev-publhealth-032315-021740.

[22] M.N. Cramer, O. Jay, Biophysical aspects of human thermoregulation during heat stress, Auton. Neurosci. Basic Clin. 196 (2016) 3–13. https://doi.org/10.1016/j.autneu.2016.03.001.

[23] X. Yang, B. Li, Y. Li, Y. Wang, C. Zheng, A Research on Characteristics of Human Heat Stress in Dynamic Hot Environment, Procedia Eng. 205 (2017) 2749–2754. https://doi.org/10.1016/j.proeng.2017.09.870.

[24] J.R. Buzan, M. Huber, Moist Heat Stress on a Hotter Earth, Annu. Rev. Earth Planet. Sci. 48 (2020) 623–655. https://doi.org/10.1146/annurev-earth-053018-060100.

[25] T.E. Bernard, F.N. Dukes-Dobos, J.D. Ramsey, Evaluation and control of hot working environments: Part II-The scientific basis (knowledge base) for the guide, Elsevier Ergon. B. Ser. 1 (2000) 337–346. https://doi.org/10.1016/S1572-347X(00)80027-0.

[26] R. Bourbonnais, J. Zayed, M. Lévesque, M.A. Busque, P. Duguay, G. Truchon, Identification of workers exposed concomitantly to heat stress and chemicals, Ind. Health. 51 (2013) 25–33. https://doi.org/10.2486/indhealth.2012-0095.

[27] P. Boonruksa, T. Maturachon, P. Kongtip, S. Woskie, Heat stress, physiological response, and heat related symptoms among Thai sugarcane workers, Int. J. Environ. Res. Public Health. 17 (2020) 1–15. https://doi.org/10.3390/ijerph17176363.

[28] P. Acharya, B. Boggess, K. Zhang, Assessing heat stress and health among construction workers in a changing climate: A review, Int. J. Environ. Res. Public Health. 15 (2018). https://doi.org/10.3390/ijerph15020247.

[29] D. Barr, W. Gregson, T. Reilly, The thermal ergonomics of firefighting reviewed, Appl. Ergon. 41 (2010) 161–172. https://doi.org/10.1016/j.apergo.2009.07.001.

[30] A. Collin, A. Marchand, A. Kadi, Z. Acem, P. Boulet, J. Pageaux, S. Pinson, M. Lepelletier, Y. Van Waelfelghem, F. Magnolini, H. Charette, Study on visible-IR radiative properties of personal protective clothings for firefighting, Fire Saf. J. 71 (2015) 9–19. https://doi.org/10.1016/j.firesaf.2014.11.006.

[31] Y. Su, Y. Wang, J. Li, Evaluation method for thermal protection of firefighters' clothing in high-temperature and high-humidity condition: A review, Int. J. Cloth. Sci. Technol. 28 (2016) 429–448. https://doi.org/10.1108/IJCST-10-2015-0107.

[32] R.L. Barker, C. Guerth-Schacher, R. V. Grimes, H. Hamouda, Effects of Moisture on the Thermal Protective Performance of Firefighter Protective Clothing in Low-level Radiant Heat Exposures, Text. Res. J. 76 (2006) 27–31. https://doi.org/10.1177/0040517506053947.

[33] M.K. Donnelly, W.D. Davis, J. Lawson, M. Selepak, Thermal

Environment for Electronic Equipment Used by First Responders, Natl. Inst. Stand. Technol. Spec. Publ. 1474. (2006) 41.

[34] A. Mensch, G. Braga, N. Bryner, Fire Exposures of Fire Fighter Self-Contained Breathing Apparatus Facepiece Lenses, (2011) 36. https://www.nist.gov/publications/fire-exposures-fire-fighter-self-contained-breathing-apparatus-facepiece-lenses.

[35] J.R. Prasad, K., Twilley, W. H., & Lawson, Thermal Performance of Fire Fighters' Protective Clothing: Numerical Study of Transient Heat and Water Vapor Transfer., 2002. https://doi.org/https://doi.org/10.6028/NIST.IR.6881.

[36] Y. Su, J. He, J. Li, Modeling the transmitted and stored energy in multilayer protective clothing under low-level radiant exposure, Appl. Therm. Eng. 93 (2016) 1295–1303. https://doi.org/10.1016/j.applthermaleng.2015.10.089.

[37] H. Zhang, G. Song, Y. Gu, H. Ren, J. Cao, Effect of moisture content on thermal protective performance of fabric assemblies by a stored energy approach under flash exposure, Text. Res. J. 88 (2018) 1847–1861. https://doi.org/10.1177/0040517517712097.

[38] G. Song, W. Cao, F. Gholamreza, Analyzing stored thermal energy and thermal protective performance of clothing, Text. Res. J. 81 (2011) 1124–1138. https://doi.org/10.1177/0040517511398943.

[39] M. Tian, W. Song, L. Qu, S. Chen, S. Zhu, F. Ning, Thermal Response of Skin Underneath a Thermal Protective Garment During Post-fire Exposure, Int. J. Thermophys. 39 (2018) 1–17. https://doi.org/10.1007/s10765-018-2410-3.

[40] S. Mondal, Phase change materials for smart textiles - An overview, Appl. Therm. Eng. 28 (2008) 1536–1550. http://www.sciencedirect.com/science/article/B6V1Y-4PJ0538-3/1/57e5bbc8e42d18e28f62d9c18dc49c53.

[41] M.S. Tjønnås, H. Færevik, M. Sandsund, R.E. Reinertsen, The effect of melt-spun phase change material fibre garments on skin temperature in humans, in: Extrem. Physiol. Med., 2015. https://doi.org/10.1186/2046-7648-4-S1-A75.

[42] C. Gao, K. Kuklane, I. Holmér, Cooling vests with phase change material packs: the effects of temperature gradient, mass and covering area., Ergonomics. 53 (2010) 716–23. https://doi.org/10.1080/00140130903581649.

[43] C. Gao, K. Kuklane, F. Wang, I. Holmér, Personal cooling with phase change materials to improve thermal comfort from a heat wave perspective, Indoor Air. 22 (2012) 523–530. https://doi.org/10.1111/j.1600-0668.2012.00778.x.

[44] R. Rossi, W. Bolli, Phase change materials for improvement of heat protection, Adv. Eng. Mater. 7 (2005) 368–373. https://doi.org/10.1002/adem.200500064.

[45] A.M. Barowy, D.M. Madrzykowski, The Thermal Behavior of Structural Firefighting Protective Ensemble Samples Modified with Phase Change

Material and Exposed in Full - Scale Room Fires, Gaithersburg, MD, 2012.

[46] Y. Wang, Y. Ma, R. Chen, Y. Su, Thermal protective performance of firefighting protective clothing incorporated with phase change material in fire environments, Fire Mater. (2020) 1–11. https://doi.org/10.1002/fam.2928.

[47] Udayraj, P. Talukdar, A. Das, R. Alagirusamy, Heat and mass transfer through thermal protective clothing - A review, Int. J. Therm. Sci. 106 (2016) 32–56. https://doi.org/10.1016/j.ijthermalsci.2016.03.006.

[48] R. Campbell, B. Evarts, Firefighter Injuries in the United States in 2019, NFPA. (2020). https://www.nfpa.org/News-and-Research/Publications-and-media/NFPA-Journal/2020/November-December-2020/Features/FFI-Report.

[49] R. Fahy, J. Petrolli, J. Molis, NFPA: Firefighter Fatalities in the US-2019, NFPA Res. Rep. (2020). https://www.nfpa.org/News-and-Research/Publications-and-media/NFPA-Journal/2020/July-August-2020/Features/Firefighter-Fatalities.

2

Chapter 2

Modelling and numerical simulation of PCMs in textiles

2

Modelling and numerical simulation of PCMs in textiles

2.1. The Stefan problem

In 1889 Jozef Stefan proposed the first clear explanation of a model describing latent heat evolution in a material undergoing a solid-liquid phase change [1]. Stefan formulates the problem with various simplifying assumptions regarding the phase change. He assumes Fourier conductive heat transport to be the central heat transfer mechanism in the solid and liquid phases. Heat transport in the liquid phase is modeled according to equation 2.1.

$$\frac{\partial T_l}{\partial t} = \alpha_l \frac{\partial^2 T_l}{\partial x^2} \qquad 0 < x < X(t), \quad t > 0 \tag{2.1}$$

where T_l, α_l, t, and x represent liquid phase temperature, liquid phase thermal diffusivity, and time and space variables, respectively.

The equation above is solved solely in the liquid phase between 0 and $X(t)$, with $X(t)$ representing the position of the solid - liquid interface.

For the solid phase, the heat transport is modeled similarly:

$$\frac{\partial T_s}{\partial t} = \alpha_s \frac{\partial^2 T_s}{\partial x^2} \qquad X(t) < x, \quad t > 0 \tag{2.2}$$

where T_s, α_s, t, and x represent solid phase temperature, solid phase thermal diffusivity, and time and space variables, respectively. The above equation is solved solely in the solid phase, i.e., after position $X(t)$.

Regarding the conditions at the phase front, Stefan assumes a constant temperature condition, since the phase change is isothermal:

$$T(X(t), t) = T_m \qquad t > 0 \tag{2.3}$$

Stefan also assumes a shock condition at the phase front. Phase front movement occurs due to the difference in conductive heat fluxes between the phases. Such condition is mathematically formulated as follows:

$$k_s \frac{\partial T_s}{\partial x} - k_l \frac{\partial T_l}{\partial x} = \lambda \rho \frac{dX}{dt} \qquad x = X(t), \qquad t > 0 \qquad (2.4)$$

where k_s, k_l, λ, and ρ represent solid and liquid phase thermal conductivities, material latent heat, and density, respectively.

The model described above is the two - phase Stefan model since heat transport is assumed to occur in the solid and liquid phases [2]. If heat transport is solely considered in the liquid phase, the model is regarded as the one - phase Stefan model. Analytical solutions of this model exist for simplified geometries and boundary conditions. However, they are not physically representative, and thus are of limited use [2,3].

Proxy – analytical solutions are also available, but even though in some cases they represent a means to obtain rough estimates to the phase change problem, they tend to fail in several applications. Thus they are not reliable for general use [4].

Nevertheless, the two-phase Stefan model presents the first model that describes solid-liquid phase change, and it serves as the basis for more computationally adequate models, which are described below.

2.2. Modelling evolution of latent heat

The Stefan formulation of the solid - liquid phase change problem has no analytical solution for complex cases of interest. Numerical methods are thus an alternative to find solutions to the phase change problem in such situations. However, the nature of the Stefan model renders to numerical difficulties when the representative equations are discretized. One of the main reasons such happens is because the interface position *X(t)* is not known a priori and thus forms part of the solution. Also, discontinuities of the thermal properties between the solid and liquid phases might originate numerical difficulties [5].

Thus, the need for alternative formulations of the phase change problem become necessary.

2.2.1. Total enthalpy method

An alternative formulation of the phase change problem is the enthalpy formulation of the conservative energy equation. The main advantage of it, is that the interface position is implicitly taken into account, and thus it does not need to be tracked along the domain [5]. The total enthalpy method may be stated as follows [6]:

$$\frac{\partial H}{\partial t} = \frac{\partial}{\partial x}\left(k\frac{\partial T}{\partial x}\right) \qquad x > 0, \quad t > 0 \qquad (2.5)$$

where *H*, *k*, *t*, and *x* represent the total enthalpy, mixture thermal conductivity, and time and space variables, respectively.

If only two phases are present, the mixture enthalpy and thermal conductivities may be defined as follows [6]:

$$H = (1-f)\int_{T_{ref}}^{T} \rho_s C_s \, dT + f\int_{T_{ref}}^{T} \rho_l C_l \, dT + \rho_l f\lambda \;\; x > 0, \quad t > 0 \qquad (2.6)$$

$$k = (1-f)k_s + fk_l \qquad (2.7)$$

where *f*, *T*, ρ, *C*, and λ represent the liquid fraction, temperature, density, specific heat and latent heat, respectively. The indices *ref*, *s*, and *l* stand for reference, solid and liquid, respectively.

Compared to the Stefan model, the main advantages of this model are that only one equation needs to be solved throughout the solid - liquid domain, and the phase front position does not need to be known to solve the problem.

2.2.2. Source term method

There are several ways to formulate equation 2.5. Even though the physical interpretation of the model is still the same (based on the total energy equation), differences exist in the numerical schemes that result from the different formulations [7]. The source term method assumes that the total energy equation is expressed in the following way [5,6]:

$$C\frac{\partial T}{\partial t} = \frac{\partial}{\partial x}\left(k\frac{\partial T}{\partial x}\right) - \rho\lambda\frac{\partial f}{\partial t} \qquad x > 0, \quad t > 0 \qquad (2.8)$$

where C, T, k, ρ, f, x, and t represent the mixture specific heat, temperature, mixture thermal conductivity, mixture density, liquid fraction, space and time variables, respectively.

The mixture specific heat and mixture density are defined as follows:

$$C = (1-f)\rho_s C_s + f\rho_l C_l \qquad (2.9)$$

$$\rho = (1-f)\rho_s + f\rho_l \qquad (2.10)$$

where the subscripts *s* and *l* stand for solid phase and liquid phase, respectively. The liquid fraction may be assumed to be a function of temperature only.

In the source term method, it is assumed that sensible and latent heats are considered in separate terms instead of being accounted for in one lumped term (i.e., total enthalpy). Calculating the latent heat evolution in detached terms might bring advantages in numerical efficiency [8]. Source term methods are popular in the literature regarding the numerical simulation of phase change, especially when convective phenomena also need to be taken into account [9–11].

2.2.3. Apparent heat capacity method

The apparent heat capacity method is yet another way to express the conservative energy equation more straightforwardly. The apparent heat capacity (C_{app}) can be defined in the following way:

$$C_{app} = \frac{\mathrm{d}H}{\mathrm{d}T} \tag{2.11}$$

The apparent heat capacity includes both the sensible and latent heats (hence the name apparent). To relate the above expression to the total enthalpy equation 2.5, the following rates of change are utilized:

$$\frac{\partial H}{\partial T} = \frac{\mathrm{d}H}{\mathrm{d}T}\frac{\partial T}{\partial t} \tag{2.12}$$

Thus, the apparent heat capacity model is stated as follows:

$$\rho C_{app}\frac{\partial T}{\partial t} = \frac{\partial}{\partial x}\left(k\frac{\partial T}{\partial x}\right) \tag{2.13}$$

where C_{app}, T, k, x, and t represent the apparent heat capacity, temperature, mixture thermal conductivity, space, and time, respectively.

One of the different aspects between the apparent and total enthalpy methods lies on the transient derivative where in the former the temperature appears (i.e. equation 2.13, whilst in the latter the total enthalpy appears (i.e. equation 2.5). This subtle difference could have significant numerical implications [7].

One of the disadvantages of the apparent heat capacity method is that C_{app} is inevitably a discontinuous function for isothermal phase changes. Even when small mushy regions are assumed to counter such problem, the resulting solution to the phase change problem could contain significant numerical errors. In such cases, very small grid-sized meshes and low-time steps must be taken, making the method less efficient. If the time step is not small enough at a given node, the phase change might be totally ignored, underestimating the latent heat involved in the phase change process [12]. Researchers over time have proposed more efficient and accurate numerical schemes and features to solve this issue,

such as post-iterative numerical schemes to correct the temperature values when the latent heat is not correctly accounted for [11].

The apparent heat capacity method is one of the most utilized methods to solve phase change problems in the literature [6,11]. As Voller [6] pointed out, the choice of the method depends on the context of the problem and the researcher's preference. Thus, in this thesis, the apparent heat capacity method was utilized to solve PCM phase change problems due to its simplicity.

2.3. Heat and mass transport in textiles

A textile is, in its essence, a hygroscopic porous structure. Heat and mass transport in such structures has been subject to much research to understand the underlying heat and mass transport mechanisms. Several models have been proposed in the literature and improved over time. The first model which arose in the literature was by Henry [13] in 1939. In his model, Henry considered the coupled heat and mass transport diffusion through a cotton bale. However, his model had several assumptions, limiting its application when significant variations in water vapor concentration and temperature happen.

Nordon [14] dropped several assumptions made by Henry and considered a non – linear isotherm relation to obtain the relative humidity in the fiber , and also a conservative rate equation for water vapor mass transfer between the air and the fiber. Nordon highlighted the implications of the error caused by assuming instantaneous mass transfer between the fiber and gas phase, as was done in Henry's case. Nevertheless, years later, Gibson [15] suggested his own model. Based on Whitaker's theory which concerns heat and mass transport in porous media [16], Gibson extended such for hygroscopic media considering the fiber - water absorbing properties. Since then, various researchers have utilized Gibson's formulation to simulate heat and mass transport across multiple textile applications [17–20].

2.3.1. Considerations on the textile structure

The textile structure is essentially composed of individual fibers bundled together to form a hygroscopic porous structure. When the fibers are randomly bundled to form the textile, the resulting structure is considered non-woven. Such textiles tend to have high porosities (i.e., Figure 2.1b). The fibers may also be woven into specific forms (i.e., Figure 2.1a), such as yarns [21].

a) b)

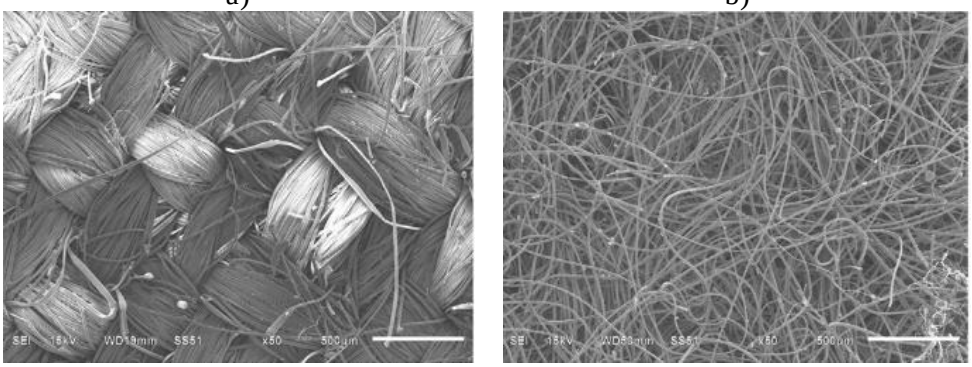

Figure 2.1 - SEM images, taken from [22], of: a) tightly woven outer shell fabric; b) non – woven inner layer.

When it comes to modeling the textile structure, several assumptions are made along this thesis. First and foremost, it is considered that the textile is a homogeneous structure consisting of different phases (i.e., fiber, air, water). Considerations regarding fiber orientation and other geometrical parameters are not done in detail. Instead, their influence on heat and mass transport throughout the textile is taken into account in lumped thermophysical properties of the textile, as will be shown in the model description section 2.3.2.

By surveying the literature it also becomes clear that one-dimensional numerical approaches are accurate enough to describe the structure of the textile for the purposes of studying heat and mass transport through it [19,23,24]. This option reduces computational cost and mesh requirements significantly. Thus in this thesis, one – dimensional approaches towards modeling the heat and mass transport in textiles are considered.

2.3.2. Model without PCM

The model utilized in this thesis to model the heat and mass transport in textiles is analogous to Gibson's model [15]. Such is considered due to its success in modeling similar systems of the sort [19,23,24]. Most assumptions and model equation derivations are shown in this section.

The heat transport equation through a hygroscopic porous medium is derived by formulating an infinitesimal balance to the average volume δV shown in Figure 2.2.

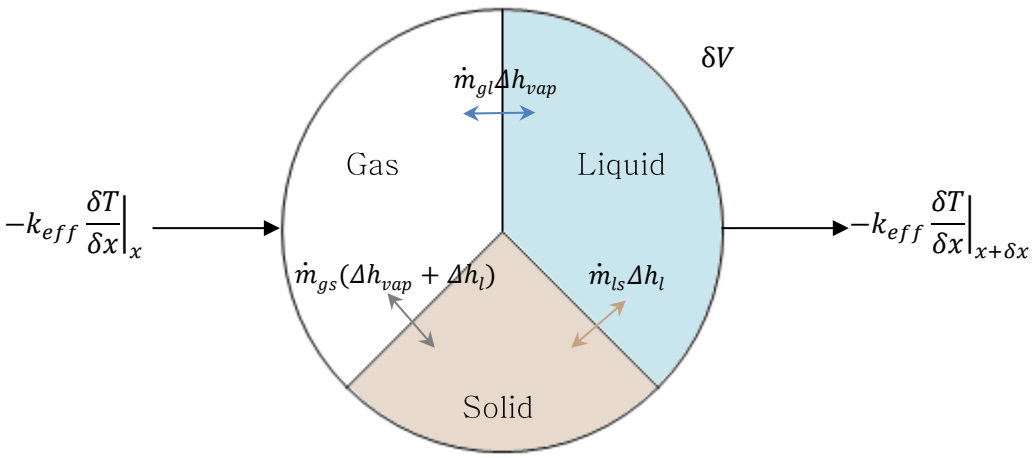

Figure 2.2 – Constituent element of the heat transfer equation in hygroscopic porous media.

One-dimensional Fourier type conductive heat transport is assumed to be the essential heat transfer mechanism through the textile, neglecting any convective and radiative heat transfer phenomena. Local thermal equilibrium is assumed, and thus the temperature of the different phases is equivalent [23]. Hence, the energy balance of the constituent element may be stated as follows:

$$-k_{eff}\frac{\delta T}{\delta x}\Big)_{x+\delta x}\delta t-\left[-k_{eff}\frac{\delta T}{\delta x}\Big)_{x}\delta t\right] = \rho C_{eff}\delta T\delta x+\dot{m}_{gl}\Delta h_{vap}\delta t\delta x + \dot{m}_{gs}\left(\Delta h_{vap}+\Delta h_{l}\right)\delta t\delta x+\dot{m}_{ls}\Delta h_{l}\delta t\delta x \tag{2.14}$$

where T, h_{vap}, h_l, x and t represent the temperature, water vaporization latent heat, liquid water - fiber association heat, and space and time variables, respectively. The variables $\dot{m}_{gs}$, $\dot{m}_{gl}$, and $\dot{m}_{ls}$ are gas - solid, gas - liquid, and liquid - solid water species transfer rates, respectively. Lastly, ρ_{eff}, c_{eff}, k_{eff} represent the effective density, specific heat, and thermal conductivities respectively defined by the following equations:

$$\rho_{eff} = \varepsilon_{bw}\rho_w + \varepsilon_\gamma\rho_\gamma + \varepsilon_{ds}\rho_{ds} + \varepsilon_l\rho_w \tag{2.15}$$

$$C_{eff} = \frac{\varepsilon_{bw}\rho_w c_{p,w} + \varepsilon_\gamma(\rho_a C_a + \rho_v C_v) + \varepsilon_{ds}\rho_{ds}C_{ds} + \varepsilon_l\rho_w C_w}{\rho_{eff}} \tag{2.16}$$

$$k_{eff} = k_\gamma\left\{\frac{\varepsilon_\gamma k_\gamma + [1+\varepsilon_{bw}+\varepsilon_{ds}+\varepsilon_l]k_\sigma}{\varepsilon_\gamma k_\sigma + [1+\varepsilon_{bw}+\varepsilon_{ds}+\varepsilon_l]k_\gamma}\right\} \tag{2.17}$$

where ε_{bw}, ε_γ, ε_{ds}, and ε_l represent the bound water volume fraction, gas-phase fraction, textile fiber fraction, and the liquid fraction, respectively. The subscripts bw, w, ds, v, a, γ, σ , stand for bound water, water, fiber material, water vapor, air, gas phase, and solid phase, respectively. The variables k_σ and k_γ represent the thermal conductivity of the solid and gas phases defined by the following equations:

$$k_\sigma = \frac{k_w\rho_w\varepsilon_{bw} + k_{ds}\rho_{ds}\varepsilon_{ds} + k_w\rho_w\varepsilon_l}{\rho_w\varepsilon_{bw} + \rho_{ds}\varepsilon_{ds} + \rho_w\varepsilon_l} \tag{2.18}$$

$$k_\gamma = \frac{k_v\rho_v + k_a\rho_a}{\rho_v + \rho_a} \tag{2.19}$$

Notice that the thermophysical properties of the textile are in function of each of the different components of the average volume (gas, liquid, solid). The effective density is calculated using the volume fraction weighted approach

(ρ_{eff}). This approach is also done for the effective specific heat (C_{eff}). For the effective thermal conductivity, an approach based on Maxwell's theorem [25] was utilized by Gibson and Charmchi [24] and also by Chitrphiromsri [23]. The same approach is utilized in this thesis (equation 2.17).

Re-arranging equation 2.14 and taking the limits concerning space and time, the heat transfer equation is obtained (equation 2.21):

$$\lim_{\delta t,\delta x\to 0}\frac{-k_{eff}\frac{\delta T}{\delta x}\Big)_{x+\delta x}-\left[-k_{eff}\frac{\delta T}{\delta x}\Big)_{x}\right]}{\delta x} = \lim_{\delta t,\delta x\to 0}\left\{\rho C_{eff}\frac{\delta T}{\delta t}+\dot{m}_{gl}\Delta h_{vap} + \dot{m}_{gs}\left(\Delta h_{vap}+\Delta h_{l}\right)+\dot{m}_{ls}\Delta h_{l}\right\} \tag{2.20}$$

$$\rho_{eff}C_{eff}\frac{\partial T}{\partial t}+\frac{\partial}{\partial x}\left(-k_{eff}\frac{\partial T}{\partial x}\right)-\dot{m}_{gs}\left(\Delta h_{vap}+\Delta h_{l}\right)-\dot{m}_{gl}\Delta h_{vap} - \dot{m}_{ls}\Delta h_{l}=0 \tag{2.21}$$

The first term on the left-hand side of the equation accounts for the sensible heat accumulation. The second term accounts for conductive heat flux debits, while the remaining three terms for the latent energy associated with water adsorption, condensation, and liquid water - fiber association, respectively.

Regarding the conservation of mass in the constituent element, several assumptions are made. Quasi-stationary approaches are utilized to describe the mass transfer rates between each of the phases (i.e., equations 2.32, 2.35, 2.39). Hence, three continuity equations regarding each phase must be solved for each volume fraction.

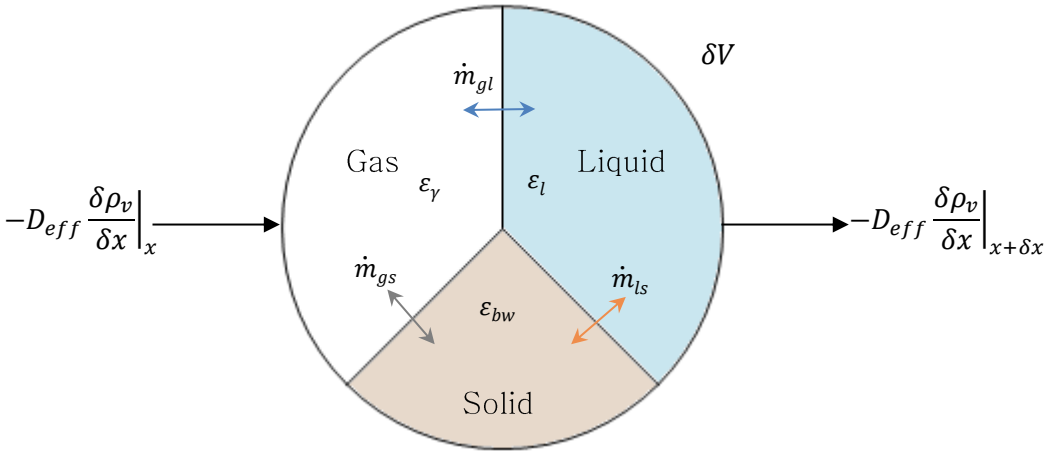

Figure 2.3 - Constituent element of the mass conservation equation in hygroscopic porous media.

Water vapor diffusion in the gas phase is assumed be the principal water species transport mechanism in the textile domain. Convective transport in the gaseous, liquid (i.e., wicking phenomena), and solid phases (i.e., fiber swelling) is neglected. The infinitesimal water vapor mass balance is then formulated as follows:

$$-D_{eff}\frac{\delta\rho_v}{\delta x}\Big)_{x+\delta x}\delta t-\left[-D_{eff}\frac{\delta\rho_v}{\delta x}\Big)_{x}\delta t\right] = \delta(\varepsilon_\gamma\rho_v)\delta x+\dot{m}_{gl}\delta t\delta x+\dot{m}_{gs}\delta t\delta x \tag{2.22}$$

where D_{eff} and ρ_v represent the effective diffusivity calculated by equation 2.25 and the water vapor concentration, respectively. The other variables have the same meanings as described in the section above.

Re-arranging and taking the limits concerning space and time of equation 2.22, the gas phase continuity equation is obtained (equation 2.24):

$$\lim_{\delta t,\delta x\to 0}\frac{-D_{eff}\frac{\delta\rho_v}{\delta x}\Big)_{x+\delta x}-\left[-D_{eff}\frac{\delta\rho_v}{\delta x}\Big)_{x}\right]}{\delta x} = \lim_{\delta t,\delta x\to 0}\left\{\frac{\delta(\varepsilon_\gamma\rho_v)}{\delta t}+\dot{m}_{gl}+\dot{m}_{gs}\right\} \tag{2.23}$$

$$\frac{\partial(\varepsilon_\gamma\cdot\rho_v)}{\partial t}+\frac{\partial}{\partial x}\left(-D_{eff}\frac{\partial\rho_v}{\partial x}\right)+\dot{m}_{gl}+\dot{m}_{gs}=0 \tag{2.24}$$

$$D_{eff}=\frac{\varepsilon_\gamma\cdot D_a}{\tau} \tag{2.25}$$

where ε_γ, D_a and τ represent the gas phase volume fraction, water vapor diffusivity in air, and fabric tortuosity, respectively.

The first term on the left-hand side of equation 2.24 accounts for the accumulation of water vapor in the pores. The second term accounts for the water vapor diffusive flux debits, and the third and fourth terms for water adsorption and condensation rates, respectively.

As stated before, water vapor may condense or adsorb in the fibers altering the volume fractions of the liquid and solid phases, respectively. Thus, continuity equations regarding these phases must also be formulated. Regarding the continuity equation of the liquid phase, no water advection is assumed to occur (i.e., wicking). Thus, the change in liquid water content is due to condensation and adsorption by the fibers. Hence, the infinitesimal liquid water mass balance is as follows:

$$\rho_w\delta\varepsilon_l=\dot{m}_{sl}\delta t+\dot{m}_{gl}\delta t \tag{2.26}$$

Re-arranging and taking the limits concerning space and time variables, the continuity equation for the liquid phase is formulated as follows:

$$\lim_{\delta t,\delta x\to 0}\rho_w\frac{\delta\varepsilon_l}{\delta t}=\lim_{\delta t,\delta x\to 0}\left\{\dot{m}_{sl}+\dot{m}_{gl}\right\} \tag{2.27}$$

$$\rho_w\frac{\partial\varepsilon_l}{\partial t}=\dot{m}_{sl}+\dot{m}_{gl} \tag{2.28}$$

Regarding the solid phase continuity equation, it is assumed that there is no bulk movement of the solid phase (i.e., no swelling of the fibers). Thus, solid phase volume fraction only changes due to a change in bound - water volume fraction (ε_{bw}). The infinitesimal bound-water mass balance is thus stated as follows:

$$\rho_w \delta\varepsilon_{bw} = \dot{m}_{gs}\delta t + \dot{m}_{ls}\delta t \tag{2.29}$$

Re-arranging and taking the limits with respect to space and time, the overall solid-phase continuity equation is obtained:

$$\lim_{\delta t,\delta x\to 0} \rho_w \frac{\delta\varepsilon_{bw}}{\delta t} = \lim_{\delta t,\delta x\to 0}\{\dot{m}_{gs} + \dot{m}_{ls}\} \tag{2.30}$$

$$\rho_w \frac{\partial\varepsilon_{bw}}{\partial t} = \dot{m}_{gs} + \dot{m}_{ls} \tag{2.31}$$

Assuming steady-state diffusion of water in the fiber, the water vapor adsorption rate may be stated as follows [23,26]:

$$\dot{m}_{gs} = \frac{8D_f\rho_{ds}}{d_f^2}\left(Regain_{eq} - Regain_f\right) \tag{2.32}$$

where D_f, ρ_{ds}, d_f, $Regain_{eq,}$ and $Regain_f$ represent the fiber diffusion, fiber density, fiber diameter, equilibrium, and fabric regain, respectively. The fabric regain is defined as follows:

$$Regain_f = \frac{\varepsilon_{bw}\rho_w}{\varepsilon_{ds}\rho_{ds}} \tag{2.33}$$

The equilibrium fabric regain is calculated as follows:

$$\begin{aligned} Regain_{eq} = \frac{\varepsilon_{bw}|_{eq}\cdot\rho_w}{\varepsilon_{ds}\rho_{ds}} \\ = 0.578\cdot Regain_{f(\emptyset=65\,\%)}\cdot\emptyset \\ \cdot\left[(0.321+\emptyset)^{-1} + (1.262-\emptyset)^{-1}\right] \end{aligned} \tag{2.34}$$

where Ø and $Regain_{f(Ø=65\%)}$ represent the relative humidity and the fabric regain at 65 % relative humidity, respectively.

Regarding the water condensation/evaporation rate inside the fabric pore, it is assumed that condensation happens instantaneously when the air becomes saturated. This behavior may occur in practice due to the presence of nuclei (such as dust particles) in the air inside the pores. Thus evaporation and condensation phenomena are described by the following expression [27].

$$\dot{m}_{gl} = \begin{cases} c \cdot \left(\rho_v - \rho_{v,sat}\right) & \rho_v \geq \rho_{v,sat} \\ h_m a_s \frac{\varepsilon_l}{\varepsilon_l^{cr}} \left(\rho_v - \rho_{v,sat}\right) & \rho_v < \rho_{v,sat} \end{cases} \tag{2.35}$$

where c, $\rho_{v,}$ and $\rho_{v,sat}$ represent the condensation law correction coefficient, the water vapor concentration, and the saturated water vapor concentration, respectively. The variable h_m is the mass transfer coefficient between the liquid water and pore gas, while a_s and ε_l^{cr} represent the specific area of the fiber and the critical liquid water fraction, respectively, calculated by the following expressions:

$$a_s = \frac{4\varepsilon_{ds}}{d_f} \tag{2.36}$$

$$\varepsilon_l^{cr} = s_{im} \cdot \varepsilon_{g,init} \tag{2.37}$$

where s_{im} represents the immobile saturation limit from which liquid water movement occurs in the textile.

It is assumed that liquid water volume fraction (ε_l) present in the textile can not exceed ε_l^{cr}. If it does, the excess water is assumed to drip off the textile. The liquid water absorption rate by the fiber is described by the following expression [23,26]:

$$\dot{m}_{ls} = h_m a_s \gamma_{ls} \frac{\varepsilon_l}{\varepsilon_l^{cr}} \left(\frac{Regain_{eq}}{Regain_f} - 1\right) \tag{2.38}$$

where γ_{ls} represents the absorption proportionality constant of water by the fiber.

The volume fraction balance follows directly from the application of the average volume theorem. It is stated as follows [15]:

$$\varepsilon_{ds} + \varepsilon_{bw} + \varepsilon_{\gamma} + \varepsilon_{l} = 1 \tag{2.39}$$

The gas in the pores is assumed to be ideal, and thus the following thermodynamic relationships are valid:

$$p_{v} = \frac{\rho_{v} RT}{M_{H_2O}} \tag{2.40}$$

$$\rho_{\gamma} = \rho_{v} + \rho_{a} \tag{2.41}$$

$$p_{a} = p_{\gamma} - p_{v} \tag{2.42}$$

where p, ρ, R, T, M_{H_2O}, represent pressure, density, universal gas constant, temperature, and molecular water mass, respectively. The subscripts v,a, and γ stand for vapor, air, and gas phases, respectively.

2.3.3. Model with PCM

In this thesis, heat and mass transport through fire protective clothing ensembles containing PCMs is studied. However, in an initial phase, no water presence is considered in the fire protective clothing containing PCMs and thus no mass transport model is needed. In such cases, the model is vastly simplified. The textile layers are considered impermeable, and the PCM is considered as a separate layer (i.e., PCM slab). In the cases where wet fire protective ensembles are used, the textile is considered to be a hygroscopic porous structure, and a modified version of Gibson's Model is utilized to include the PCM phase in the textile [15].

2.3.3.1. Considering textile as impermeable structure

When the different textile layers are considered impermeable, no mass transport is assumed through them. Fourier heat transport and temperature-dependent thermophysical properties are in turn assumed. The PCM layer is considered as a separate impermeable layer (essentially a PCM slab). Such configuration happens in practice with PCM pockets in cooling vests, for example. The apparent heat capacity model is utilized to simulate phase change in the PCM. The model is formulated by considering the following constituent elements:

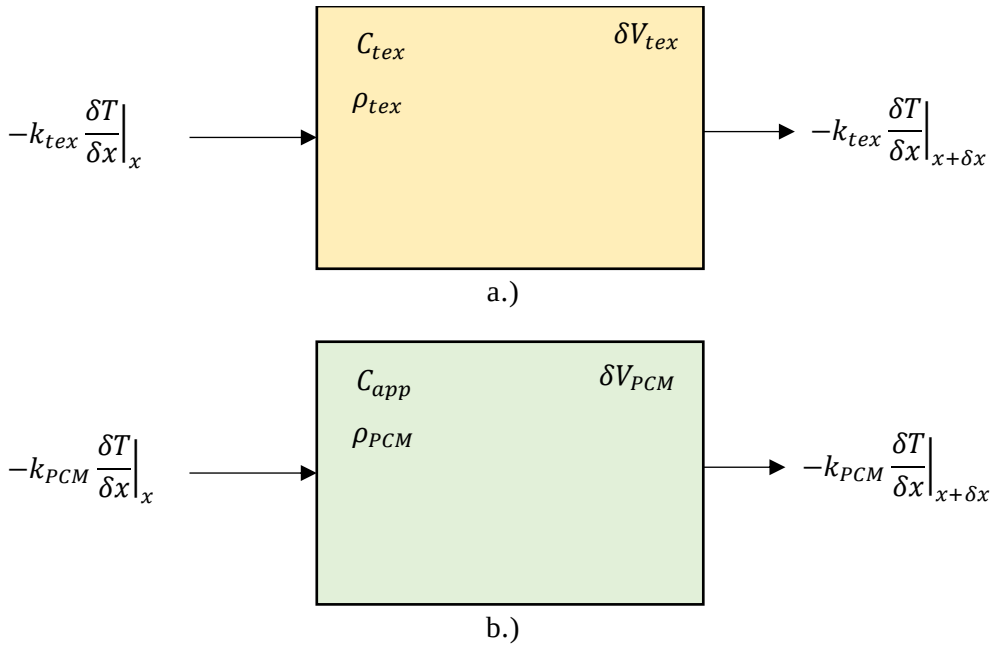

Figure 2.4 Constituent elements of: a) textile; b) PCM for heat transport model formulation.

The infinitesimal balance of the textile element is expressed as follows:

$$-k_{tex}\frac{\delta T}{\delta x}\Big|_{x+\delta x}\delta t-\left(-k_{tex}\frac{\delta T}{\delta x}\Big|_{x}\right)\delta t \;=\; C_{tex}\rho_{tex}\delta T\delta x \tag{2.43}$$

Re – arranging and taking the limits with respect to space and time, the energy balance for an impermeable textile layer is obtained (equation 2.46);

$$\lim_{\delta t,\delta x\to 0}\frac{-k_{tex}\frac{\delta T}{\delta x}\Big|_{x+\delta x}-\left(-k_{tex}\frac{\delta T}{\delta x}\Big|_{x}\right)}{\delta x} = \lim_{\delta t,\delta x\to 0} C_{tex}\rho_{tex}\frac{\delta T}{\delta t} \tag{2.44}$$

$$\frac{\partial}{\partial x}\left(-k_{tex}\frac{\partial T}{\partial x}\right) = C_{tex}\rho_{tex}\frac{\partial T}{\partial t} \tag{2.45}$$

where the subscript *tex* stands for textile, while the others variables shown have their usual meanings.

For the PCM layer, convective heat transfer phenomena in the liquid phase are neglected. Thus, the infinitesimal balance of the PCM element is stated as follows:

$$-k_{PCM}\frac{\delta T}{\delta x}\Big|_{x+\delta x}\delta t-\left(-k_{PCM}\frac{\delta T}{\delta x}\Big|_{x}\right)\delta t \;=\; C_{app}\rho_{PCM}\delta T\delta x \tag{2.46}$$

Taking the limits with respect to space and time, the energy balance of the PCM layer is obtained:

$$\lim_{\delta t,\delta x\to 0}\frac{-k_{PCM}\frac{\delta T}{\delta x}\Big|_{x+\delta x}-\left(-k_{PCM}\frac{\delta T}{\delta x}\Big|_{x}\right)}{\delta x} = \lim_{\delta t,\delta x\to 0} C_{app}\rho_{PCM}\frac{\delta T}{\delta t} \tag{2.47}$$

$$\frac{\partial}{\partial x}\left(-k_{PCM}\frac{\partial T}{\partial x}\right) = C_{app}\rho_{PCM}\frac{\partial T}{\partial t} \tag{2.48}$$

where C_{app} stands for the apparent heat capacity.

This model is applied in chapters 3 and 4 to study the influence of the PCM layer on the thermal performance of the firefighting garment assembly with only heat transport present.

2.3.3.2. *Considering textile as a permeable structure*

The following model description considers the textile as a permeable structure with incorporated PCM. In this case, the PCM is considered as a new phase in the average volume, as shown in the following figure:

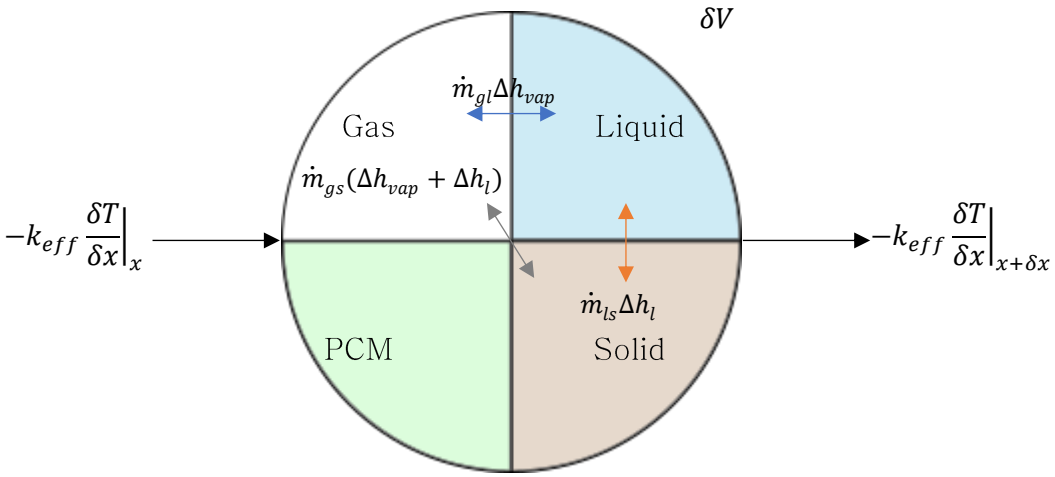

Figure 2.5 - Consituent element of the PCM textile heat transport equation.

As shown in Figure 2.5, the latent heat terms are identical to those in Gibson's model [15]. No water migration is assumed towards the PCM, and thus no latent heats associated with such are considered. Also, the water phase change rates (i.e., equations 2.32, 2.35, 2.38) are assumed unaffected by the presence of the PCM phase. The infinitesimal balance to the constituent element shown in Figure 2.5 is as follows:

$$-k_{eff}\frac{\delta T}{\delta x}\Big)_{x+\delta x}\delta t - \left[-k_{eff}\frac{\delta T}{\delta x}\Big)_{x}\delta t\right] = \rho_{eff}C_{eff}\delta T\delta x + \dot{m}_{gl}\Delta h_{vap}\delta t\delta x + \dot{m}_{gs}\left(\Delta h_{vap} + \Delta h_l\right)\delta t\delta x + \dot{m}_{ls}\Delta h_l\delta t\delta x \quad (2.49)$$

where C_{eff}, k_{eff}, and ρ_{eff} represent the effective specific heat, effective thermal conductivity, and effective density calculated as follows:

$$\rho_{eff} = \varepsilon_{bw}\rho_w + \varepsilon_\gamma\rho_\gamma + \varepsilon_{ds}\rho_{ds} + \varepsilon_l\rho_w + \varepsilon_{PCM}\rho_{PCM} \quad (2.50)$$

$$C_{eff} = \frac{\varepsilon_{bw}\rho_w C_w + \varepsilon_\gamma(\rho_a C_a + \rho_v C_v) + \varepsilon_{ds}\rho_{ds}C_{ds} + \varepsilon_l \rho_w C_w + \varepsilon_{PCM}\rho_{PCM}C_{app}}{\rho_{eff}} \quad (2.51)$$

$$k_{eff} = k_\gamma \left\{ \frac{\varepsilon_\gamma k_\gamma + [1 + \varepsilon_{bw} + \varepsilon_{ds} + \varepsilon_l + \varepsilon_{PCM}]k_\sigma}{\varepsilon_\gamma k_\sigma + [1 + \varepsilon_{bw} + \varepsilon_{ds} + \varepsilon_l + \varepsilon_{PCM}]k_\gamma} \right\} \quad (2.52)$$

The variables k_σ and k_γ represent the solid and gas phase thermal conductivities, respectively. The solid phase now includes the PCM, and thus its thermal conductivity is obtained as follows:

$$k_\sigma = \frac{k_w\rho_w\varepsilon_{bw} + k_{ds}\rho_{ds}\varepsilon_{ds} + k_w\rho_w\varepsilon_l + k_{PCM}\rho_{PCM}\varepsilon_{PCM}}{\rho_w\varepsilon_{bw} + \rho_{ds}\varepsilon_{ds} + \rho_w\varepsilon_l + \rho_{PCM}\varepsilon_{PCM}} \quad (2.53)$$

$$k_\gamma = \frac{k_v\rho_v + k_a\rho_a}{\rho_v + \rho_a} \quad (2.54)$$

The energy balance is obtained by re-arranging and taking the limits of equation 2.49 with respect to space and time (equation 2.55).

$$\lim_{\delta t, \delta x \to 0} \frac{-k_{eff}\frac{\delta T}{\delta x}\Big)_{x+\delta x} - \left[-k_{eff}\frac{\delta T}{\delta x}\Big)_x\right]}{\delta x} = \lim_{\delta t, \delta x \to 0} \left\{ \rho C_{eff}\frac{\delta T}{\delta t} + \dot{m}_{gl}\Delta h_{vap} + \dot{m}_{gs}\left(\Delta h_{vap} + \Delta h_l\right) + \dot{m}_{ls}\Delta h_l \right\} \quad (2.55)$$

$$\rho_{eff}C_{eff}\frac{\partial T}{\partial t} + \frac{\partial}{\partial x}\left(-k_{eff}\frac{\partial T}{\partial x}\right) - \dot{m}_{gs}\left(\Delta h_{vap} + \Delta h_l\right) - \dot{m}_{gl}\Delta h_{vap} - \dot{m}_{ls}\Delta h_l = 0 \quad (2.56)$$

The energy balance of the PCM textile model is analogous to the energy balance of the model without PCM. Thus, the model assumes thermal equilibrium between all phases.

The gas, solid, and liquid phase continuity equations are equivalent to those derived for the textile model without PCM inclusion (i.e., equations 2.22 -2.38).

However, as the PCM phase is now present, the total volume conservation equation now becomes:

$$\varepsilon_{ds} + \varepsilon_{bw} + \varepsilon_{\gamma} + \varepsilon_{l} + \varepsilon_{PCM} = 1 \tag{2.57}$$

The remaining thermodynamic relationships for this model are also equivalent to the textile model without PCM (equations 2.40 -2.42).

The models used throughout the textile – PCM structure are described above. However, a thermal performance criterion is necessary to measure the textile thermal performance under a given heat exposure scenario. In this thesis, a skin burn criterion is utilized as a significant indicator of the thermal performance of the textile.

2.3.4. Skin–burn criteria

During a fire exposure, firefighters may obtain burns on their skin which can vary in size and depth. Based on these aspects, burns can be arranged into essentially three categories: first, second and third-degree burns [28]. First-degree burns are superficial burns at the epidermis of the skin. Typically, these burns do not represent a significant hazard, and healing is possible within a time frame of a few days [28,29]. Second–degree burns, on the other hand, are categorized by damage not only in the epidermis but also in the dermis layer of the skin. Redness and blisters tend to appear on the skin, but healing is possible within a few weeks. Third-degree burns involve the destruction of the epidermis and dermis layers of the skin. In these types of burns, natural healing of the skin is not possible. Damage to internal organs is included in this burn type.

To mathematically account for burns in a given heat exposure is challenging. Stoll [30] noticed that a burn caused to the skin by heat exposure not only depends on its intensity, but also on the exposure time. Stoll developed a criterion to quantify the time to second - degree burn based on the exposure heat flux [30]. Even though this criterion is practical and easy to use, several aspects make it limiting. First, it can only be used for a limited set of heat flux exposures. Extrapolation is necessary if it is to be used for another range of heat

fluxes. Also, heat exposures towards the skin under a garment tend to be variant and not constant over time. Stoll's criterion is for constant heat flux exposures directly towards the skin. To overcome this, researchers multiply the heat flux exposure by the respective tolerance time given by the Stoll criterion to obtain accumulated energy for the second-degree burn [30]. However, this is still a simplification of the phenomena.

On the other hand, mathematical models are based on a physical interpretation of the skin damage phenomena. It is assumed that cell degradation due to heat exposure follows first - order kinetics. Henriques' applied these assumptions to formulate the Henriques' burn criterion stated as follows [31]:

$$\Omega = \int_0^t P \cdot exp\left(\frac{-E_a}{RT}\right) dt \tag{2.58}$$

where Ω, P, E_a, R, and t represent the damage integral function, pre-exponential factor, activation energy, universal gas constant, and time, respectively. The variable T represents the skin temperature at the epidermis/dermis or dermis/subcutaneous boundaries, depending on the degree burn type. If second - degree burn time is the objective, the temperature utilized is at the epidermis/dermis boundary and happens when $\Omega = 1$. The second-degree burn time is then obtained by solving the equation for the upper limit of the integral.

For a third-degree burn calculation, the temperature at the dermis/subcutaneous boundary is considered, and similarly, the third-degree burn time is evaluated for when $\Omega = 1$.

In the Henrique's burn criterion, P and E_a are dependent on the heat flux history at the skin surface. As in Stoll's criterion, such parameters were derived for rectangular heat flux pulses directed towards the skin. For this reason, the burn time obtained with Henriques' criterion may have a significant error associated with it.

Despite these issues, the Henriques burn criterion has been vastly utilized in the literature to analyze skin burns and thus will also be used in this thesis as the best criterion for thermal performance determination of the PCM firefighting garment. The values utilized for P and E_a are taken from Stoll & Weave [32].

Notation

Latin	Definition	Units
A	Area	[m^2]
a_s	Textile fiber specific surface area	[1/m]
C	Specific heat	[J/(kg·K)]
c	Condensation law correction factor	[1/s]
D	Water vapor Diffusivity	[m^2/s]
d	Diameter	[m]
E_a	Activation energy	[J/mol]
f	PCM liquid fraction	[-]
H	Enthalpy	[J/kg]
k	Thermal conductivity	[W/(m·K)]
$\dot{m}_{gs}$	Gas to solid phase mass transfer rate	[kg/(m^3·s)]
$\dot{m}_{gl}$	Gas to liquid phase mass transfer rate	[kg/(m^3·s)]
$\dot{m}_{ls}$	Liquid to solid phase mass transfer rate	[kg/(m^3·s)]
P	Pre – exponential factor	[1/s]
R	Universal gas constant	[J/(mol·K)]
$Regain_f$	Fabric regain	[kg_{H2O}/kg_{fiber}]
T	Temperature	[K]
t	Time	[s]
V	volume	[m^3]
x	Space coordinate	[m]

Greek	Definition	Units
γ_{ls}	Proportionality constant associated to liquid water absorption by fiber	[kg/m^3]
Δh_{vap}	heat of water vaporization	[J/kg]
Δh_l	heat of water association into textile fiber	[J/kg]
ε	Volume fraction	[-]
λ	Latent heat	[kJ/kg]
ρ	Density	[kg/m^3]
τ	Tortuosity	[-]
$\emptyset$	Relative humidity	[-]
Ω	Skin damage function	[-]

Subscripts	Definition
a	Air
app	Apparent
bw	Bound water

cr	Critical
ds	Fiber
eff	Effective
eq	Equilibrium
gs	Gas - solid
gl	Gas -liquid
init	Initial
l	Liquid
ls	Liquid -solid
m	Melting
o	Floating variable
PCM	Phase change material
sat	Saturated
v	Water vapor
w	Water
γ	Gas phase
σ	Solid phase

References

[1] B. Sarler, Stefan ' s work on solid-liquid phase changes, 7997 (1995) 83–92.

[2] H. Hu, S. a Argyropoulos, Mathematical modelling of solidification and melting: a review, Model. Simul. Mater. Sci. Eng. 4 (1999) 371–396.

[3] Solomon, An easily computable solution to a two-phase Stefan problem, Sol. Energy. 23 (1979) 525–528.

[4] V. Alexiades, A.D. Solomon, Mathematical Modeling of Melting and Freezing Processes, Taylor & Francis, 1993.

[5] Y. Dutil, D.R. Rousse, N. Ben Salah, S. Lassue, L. Zalewski, A review on phase-change materials: Mathematical modeling and simulations, Renew. Sustain. Energy Rev. 15 (2011) 112–130.

[6] V.R. Voller, C.R. Swaminathan, B.G. Thomas, Fixed grid techniques for phase change problems: A review, Int. J. Numer. Methods Eng. 30 (1990) 875–898.

[7] D. Poirier, M. Salcudean, On Numerical Methods Used in Mathematical Modeling of Phase Change in Liquid Metals, J. Heat Transfer. 110 (1988) 562.

[8] V.R. Voller, Implicit Finite-difference Solutions of the Enthalpy Formulation of Stefan Problems, IMA J. Numer. Anal. (1985) 201–214.

[9] A.D. Brent, V.R. Voller, K.J. Reid, Enthalpy-porosity technique for modeling convection-diffusion phase change: Application to the melting of a pure metal, Numer. Heat Transf. 13 (1988) 297–318.

[10] V.R. Voller, M. Cross, N.C. Markatos, An enthalpy method for convection/diffusion phase change, Int. J. Numer. Methods Eng. 24 (1987) 271–284.

[11] C.R. Swaminathan, V.R. Voller, On the enthalpy method, Int. J. Numer. Methods Heat Fluid Flow. 3 (1993) 233–244.

[12] J.S. Hsiao, An efficient algorithm for finite-difference analyses of heat transfer with melting and solidification, Numer. Heat Transf. 8 (1985) 653–666.

[13] T.R. Society, Diffusion in absorbing media, Proc. R. Soc. London. Ser. A. Math. Phys. Sci. 171 (1939) 215–241.

[14] P. Nordon, H.G. David, Coupled diffusion of moisture and heat in hygroscopic textile materials, Int. J. Heat Mass Transf. 10 (1967) 853–866.

[15] P. Gibson, Governing Equations for Multiphase Heat and Mass Transfer in Hygroscopic Porous Media With Applications to Clothing Materials, Natick, Massachusetts, 1994.

[16] S. Whitaker, Simultaneous Heat, Mass, and Momentum Transfer in Porous Media: A Theory of Drying, Adv. Heat Transf. 13 (1977) 119–203.

[17] P. Chitrphiromsri, A. V. Kuznetsov, Modeling heat and moisture transport in firefighter protective clothing during flash fire exposure,

Heat Mass Transf. Und Stoffuebertragung. 41 (2005) 206–215.
[18] G. Song, P. Chitrphiromsri, D. Ding, Numerical Simulations of Heat and Moisture Transport in Thermal Protective Clothing Under Flash Fire Conditions, Int. J. Occup. Saf. Ergon. 14 (2015) 89–106.
[19] Y. Su, J. Li, X. Zhang, A Coupled Model for Heat and Moisture Transport Simulation in Porous Materials Exposed to Thermal Radiation, Transp. Porous Media. 131 (2020) 381–397.
[20] S.F. Neves, J.B.L.M. Campos, T.S. Mayor, Effects of clothing and fibres properties on the heat and mass transport, for different body heat/sweat releases, Appl. Therm. Eng. 117 (2017) 109–121.
[21] N. Pan, P. Gibson, Thermal and Moisture Transport in Fibrous Materials, Woodhead Publishing Limited, Cambridge, 2006.
[22] A. Collin, A. Marchand, A. Kadi, Z. Acem, P. Boulet, J. Pageaux, S. Pinson, M. Lepelletier, Y. Van Waelfelghem, F. Magnolini, H. Charette, Study on visible-IR radiative properties of personal protective clothings for firefighting, Fire Saf. J. 71 (2015) 9–19.
[23] P. Chitrphiromsri, Modeling of Thermal Performance of Firefighter Protective Clothing during the Intense Heat Exposure, NCSW, 2004.
[24] P. Gibson, M. Charmchi, The use of volume-averaging techniques to predict temperature transients due to water vapor sorption in hygroscopic porous polymer materials, J. Appl. Polym. Sci. 64 (1997) 493–505.
[25] R.C. Progelhof, J.L. Throne, R.R. Ruetsch, Methods for predicting the thermal conductivity of composite systems: A review, Polym. Eng. Sci. 16 (1976) 615–625.
[26] C. V. le, N.G. ly, R. Postle, Heat and Moisture Transfer in Textile Assemblies: Part I: Steaming of Wool, Cotton, Nylon, and Polyester Fabric Beds, Text. Res. J. 65 (1995) 203–212.
[27] C. V. Le, N.G. Ly, R. Postle, Heat and mass transfer in the condensing flow of steam through an absorbing fibrous medium, Int. J. Heat Mass Transf. 38 (1995) 81–89.
[28] M. Gasperin, D. Juricić, The uncertainty in burn prediction as a result of variable skin parameters: an experimental evaluation of burn-protective outfits., Burns. 35 (2009) 970–82.
[29] Johnson, R. M., & Richard, R. (2003). Partial-Thickness Burns: Identification and Management. Advances in Skin & Wound Care, 16(4), 178–187.
[30] L.N. Zhai, J. Li, Prediction methods of skin burn for performance evaluation of thermal protective clothing, Burns. 41 (2015) 1385–1396.
[31] F.C. Henriques, Studies of thermal injury V. The predictability and the significance of thermally induced rate processes leading to irreversible epidermal injury, Arch. Pathol. 43 (1947) 489–502.
[32] J.A. Weaver, A.M. Stoll, Mathematical model of skin exposed to thermal radiation., Aerosp. Med. (1969).

3

Chapter 3

Guidelines for the specification of a PCM layer in fire protective clothing ensembles

3

Guidelines for the specification of a PCM layer in firefighting protective clothing ensembles

The first objective of this thesis was to establish basic guidelines regarding the PCM incorporation in a dry FPC. This is useful since it provides the designer with information regarding the PCM choice and its geometrical parameters when it comes to its incorporation in FPC. The text written in this chapter resulted in the following publication:

Fonseca, A., Mayor, T. S., & Campos, J. B. L. M. (2018). Guidelines for the specification of a PCM layer in firefighting protective clothing ensembles. *Applied Thermal Engineering*, 133(March 2017), 81–96.

Abstract

Phase change materials are increasingly seen not only as a solution to reduce the mismatch between demand and supply of energy, but also as an adequate tool for heat management. Firefighters usually encounter high heat flux exposures, which can cause severe burns. The addition of a PCM layer into a typical firefighting garment en- semble can be used to mitigate this effect, increasing the time to second-degree burns. A numerical approach was used to investigate the effect of PCM latent heat, mass, melting temperature, and position within the garment ensemble, to assess the implications in terms of thermal performance and time to second-degree burns, under high-, medium- and low-intensity heat exposures. Guidelines for the specification of PCM characteristics are provided with respect to the heat exposure scenario considered, to enable informed decisions regarding the choice and features of the PCM, in function of the intended application and required time-windows without burns. The data discussed in this work provide insight on how a PCM layer influences the thermal burden on a firefighter, which enables the

estimation of optimal PCM masses, and thus the minimization of the load to be carried by the firefighter, and the costs associated with the integration of high loads of PCM in a garment.

3.1 Introduction

Phase Change Materials (PCMs) are substances that can be used to absorb/release energy in the form of latent heat usually through a solid/liquid phase change. PCMs have been subject to much research for the last 30 years due to the big concern of pollution and shortage of fossil fuels [1]. The vast number of PCMs available are essentially ca- tegorized into two major groups: organics and inorganics [2]. PCMs have been applied in solar panels, construction wallboards, textiles, power plants, as a means to reduce the gap between energy demand and supply and therefore to eliminate excessive energy waste [3]. Energy in the form of latent heat as opposed to sensible heat allows for a greater heat storage using a much lower mass, and it also allows its efficient usage, as such energy is stored at almost constant temperature [3].

Firefighters are usually exposed to high levels of thermal strain which negatively affect their microclimate near the skin [4]. This may lead to severe burns, or even death. It is therefore of crucial importance to assess if the inclusion of a PCM layer in a firefighting protective clothing (FFPC) ensemble, augments its thermal performance by storing, as latent heat, part of the energy coming from the external source. The idea of incorporating PCMs into firefighting protective clothing is not new. Zhu et al. [5] studied the incorporation of a PCM coated layer into a FFPC ensemble and tested it also for various exposure conditions. The authors used PCMs with different melting temperatures, and almost equal remaining thermophysical properties, and also they varied the configuration. They concluded that a melting temperature of about 52 °C and a configuration closer to the skin is beneficial to thermal performance. Hu et al. [6] numerically studied, using a one-dimensional heat transfer model, the inclusion of a PCM layer in an FFPC ensemble including the various skin layers. The authors varied the mass of the PCM layer and its

position, and exposed the FFPC-skin ensemble to a variable ambient temperature. They concluded that a higher mass and a position towards the skin decrease the temperatures developed along the FFPC over time. Phelps et al. [7] studied the effect of PCM position on the FFPC ensemble under low and medium intensity heat exposure scenarios. They concluded that a PCM position further away from the skin enhanced its effect on the thermal performance of the FFPC suit. Huang et al. [8] numerically studied the influence of melting temperature on the thermal performance of a FFPC-skin system assuming the same boundary conditions as in [6]. The authors considered additionally the effect of sweat on thermal performance. They concluded that PCM melting temperature had an effect on the thermal performance and that a PCM melting temperature of 132 °C allows it to have the most effect in thermal performance.

Despite the above mentioned interesting contributions, there are inconsistencies as to what the optimal choice of PCM parameters should be for a given heat exposure scenario. By consequence, it is challenging to draw quantitative conclusions from the existing works, as the para- meters of interest (PCM latent heat, mass, melting temperature and position) were mostly studied for different boundary conditions and with different PCMs. In light of this, extensions to the current knowledge of the effects of PCM latent heat, mass, melting temperature, and position on a FFPC garment ensemble are proposed in this work. A one- dimensional numerical study is carried out where the influence of the four mentioned variables is studied in a systematic way, considering a series of parametric variations in each of the variables to allow for quantitative conclusions. Three heat exposure scenarios are considered to simulate low-, medium- and high-intensity heat exposures usually encountered by firefighters. The PCM effect is studied for these heat exposures and guidelines are then drawn to assist in the specification of a PCM layer for a firefighting protective clothing ensemble. This data is important to enable the prediction, for instance, of the PCM mass, latent heat and melting temperature ranges, needed to ensure a pre-defined tolerance time, where a firefighter can operate under a given heat exposure scenario, without the risk of second-degree burns.

3.2 Materials and methods

3.2.1 Problem description

A typical firefighting protective clothing (FFPC)-skin system was used (Figure 3.1), consisting of a series of garment and skin layers, in order to analyse the effect of PCMs in enhancing the garment thermal protection ([9,10]). The outer shell and thermal inner layers were considered to be a Kevlar®/PBI fire resistant fabric and an Aralite ® fabric, respectively ([11,12]). To address the worst possible situation, no air gaps (i.e. microclimates) were considered between the different garment layers, and perfect contact was assumed between the garment inner layer and the skin (e.g. as in [6,10,13]). The external surface of the garment (boundary 1 in Figure 3.1) was subject to a sudden heat flux for a certain amount of time. Three fluxes were chosen to reflect different scenarios that firefighters can encounter: 84, 12 and 5 kW/m^2 [10]. For each of the different fluxes, variables associated with the PCM layer were varied independently. PCM latent heat, mass, melting temperature, and position were varied and the data analysed to study their effects on the temperature profiles across the FFPC-skin system. These variables are reported to have an influence in the thermal performance of the PCM.

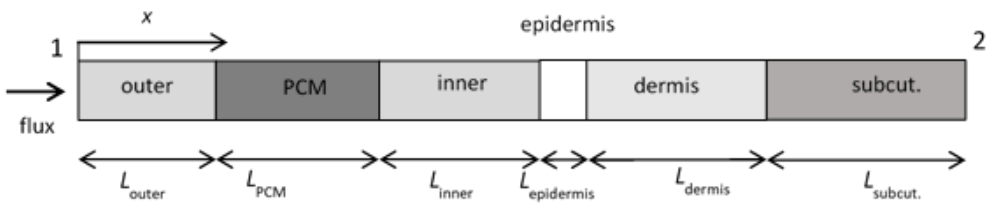

Figure 3.1- Geometry and boundaries of garment-skin system.

3.2.2 Geometries and boundary conditions

The firefighting garment is essentially composed of an outer layer, a thermal inner, and a PCM layer (Figure 3.1). The general dimensions of the various layers in the FFPC-skin system are shown in Table 3.1.

Firefighters encounter various types of exposure scenarios, from mild exposures in which the firefighter doesn't need special clothing, to flash fire scenarios where the firefighter must have special protective clothing [14].

McCarthy and co-workers [15] used exposures of 2.5, 10, and 20 kW/m^2 for 15 min, 5 min, and 30 s, respectively, as boundary conditions for the external garment layer. Other researchers [9] used exposures of 83.2 kW/m^2 and 1.2 kW/m^2 for periods of 5 min and 3 s respectively, to simulate low and high intensity firefighting. In this work, three heat exposure scenarios were considered (Table 3.2). They include a low - and medium-intensity exposures (5 and 12 kW/m^2 for 5 min, cases C and B in Table 3.2) describing, pre-flashover conditions, and a high intensity exposure (84 kW/m^2 for 8 s, Case A in Table 3.2) representing flash fire conditions [10]. These scenarios represent an incoming energy into the FFPC suit of 672, 3600, and 1500 kJ/m^2 respectively (Table 3.2).

Table 3.1- General geometry dimensions (following [6,8–10,12,11]).

Domain dimensions [mm]
L_{Outer} = 0.6
L_{PCM} = 0.6 - 6
L_{Inner} = 3.59
$L_{Epidermis}$ = 0.08
L_{Dermis} = 2.0
L_{Subcut} = 10

Table 3.2 - Boundary conditions (named according to Figure 3.1) and energy associated to heat exposures.

Exposure	Boundary 1	Boundary 2	Energy [kJ/m^2]
A (high – intensity)	84 kW/m^2 for 8 s	37 °C	672
B (medium – intensity)	12 kW/m^2 for 5 min	37 °C	3600
C (Low – intensity)	5 kW/m^2 for 5 min	37 °C	1500

To fully observe the effect of the heat exposure on the garment skin system, the simulation times were higher than the exposure times. For Case A, the simulation time was 1 min whilst for Cases B and C they were 15 min. After the end of the heat exposure, null heat flux in the garment external surface was assumed, in order to address the worst possible scenario from the thermal point of view (i.e. the most demanding situation for the garment and firefighter), and thus generate safer pessimistic estimates of the relevant data (e.g. PCM loads, duration of burn-free periods).

3.2.3 Mathematical model

The apparent heat capacity method was used to simulate the phase change (Eq. (3.1)) in the PCM layer. The apparent heat capacity method derives from a weak formulation of the phase change problem, namely the enthalpy formulation. Essentially, the position of the interface is implicitly taken into account by an apparent heat capacity, which not only considers the sensible, but also the latent heat associated with the phase change [16]. This makes it possible to avoid problems associated with interface tracking methods [17].

$$\rho C_{app} \frac{\partial T}{\partial t} = \nabla \cdot (k \nabla T) \tag{3.1}$$

where ρ, C_{app}, T, t and k, represent, respectively, density in kg/m^3, apparent specific heat in J/(kg·K), temperature in K, time in s, and thermal conductivity

in W/(m·K). The index app stands for apparent. Eq. (3.1) is applied in the PCM domain, considering a one-dimensional approach.

The apparent specific heat curve was assumed to have the following form ([6,8–10]):

$$C_{app} = \frac{dH}{dT} = \frac{d}{dT}\left[0.5 \times \lambda \times erf\left(\frac{T - T_m}{T_0}\right) + C_{PCM}(T - T_m)\right] = \lambda \times \frac{exp\left(-\frac{T - T_m}{T_0}\right)^2}{T_0\sqrt{\pi}} + C_{PCM} \quad (3.2)$$

where H, T_m, λ, and C_{PCM} are, respectively, the total enthalpy in J/kg, the melting temperature in K, the latent heat in J/kg and the specific heat in J/kg/K, and T_0 is the floating variable used to fit the experimental curve. Further information about the application of (Eq. (3.2)) is shown in Section 3.5.1.

For the dermis and subcutaneous regions, the one-dimensional heat transfer was simulated according to Eq. (3.3), where the second term on the right-hand side represents the heat removal by blood circulation. In the remaining domains, the heat transfer is modelled using the Fourier equation (Eq. (3.4)).

$$\rho C_p \frac{\partial T}{\partial t} = \nabla \cdot (k \nabla T) - G \rho_b C_b (T - T_c) \quad (3.3)$$

$$\rho C_p \frac{\partial T}{\partial t} = \nabla \cdot (k \nabla T) \quad (3.4)$$

where the indexed b and c stand for blood and core, respectively.

The following boundary conditions are considered:

$$-k \frac{\partial T}{\partial x}\Big|_{x=0} = q \quad for\ 0 < t \leq t_{exp} \quad (3.5)$$

$$-k \frac{\partial T}{\partial x}\Big|_{x=0} = 0 \quad for\ t > t_{exp} \quad (3.6)$$

where t_{exp} is the heat flux exposure time, depending on the case scenario being considered (Table 3.2). The core body temperature was assumed constant at 37

°C ([6,8–10]), and the initial clothing layers were assumed to be at 34 °C. The initial temperature of the different skin layers was assumed to vary linearly between 37 °C (core) and 34 °C (skin-clothing interface) [10,13].

3.2.4 General assumptions

The phase change was modelled (Section 3.2.3) using the apparent heat capacity method. One-dimensional heat conduction was assumed to be the major heat transfer mechanism, neglecting radiant exchange between the garment layers and convection. Heat removal through blood circulation was considered in the dermis and subcutaneous layers ([6,9,10]). Air gaps between the garment layers and the skin were neglected to simulate the worst possible case in terms of thermal performance [13], and generate safer pessimistic data on time to burn and PCM requirements. Moisture transport across the clothing layers (as in [18–21]) was not considered as the effect of PCM is larger than that of moisture transfer ([9]). Regarding the garment ensemble materials, the following assumptions were made:

- Temperature dependant thermophysical properties were assumed for the various fabric layers (except density). Regarding the PCM, the thermophysical properties were solely phase dependant [12,11,22].
- The latent heat associated with the PCM was obtained via the differential scanning calorimetry curve given in [23]. The resulting thermogram in turn was approximated by a function through a minimizing square technique. This function was then used and adapted for all simulation cases (i.e. changing the fitting curve as needed to represent the hypothetical PCM being considered in each parametric analysis; details in Annex 6.1). Both melting and re-solidification processes (i.e. charge and discharge processes) were assumed to be described by the experimental curve mentioned above.
- Blood perfusion rates were assumed constant in dermis and subcutaneous layers [6,8,10].

- A skin burn model was used to estimate the time for a second-degree burn to occur. This was done following the initial work of Henriques [24], which tries to quantify the thermal damage to the skin based on the burn integral obtained from the evolution of temperature over time. A second-degree burn at the epidermis/dermis interface was acknowledged when the Henriques' burn integral (with parameters based in [25]), implied Ω values equal to unity. The time needed for that to happen was considered to represent the time needed for the occurrence of a second-degree burn (t_{2nd}).

3.2.5 Properties of the different layers

Properties of the different garment layers are shown in Table 3.3. The firefighting garment ensemble may also contain a moisture barrier [6], but that was not considered in this work, following related works in the literature ([9,10]). This simplification is reasonable as the addition of an extra thermal resistance should not affect the qualitative conclusions on the variables influencing the thermal performance.

Table 3.3 - Thermophysical properties of the various garment and skin layers ([12,11]); ρ, C, k and G stand for, respectively, density, specific heat, thermal conductivity and blood perfusion rate. K_{air} and k_{fibre} stand for the air and clothing fibre thermal conductivity, respectively.

Property	ρ [kg/m^3]	C [J/kg/K]	k [W/m/K]	G [s^{-1}]
Outer	323	1300+1.6·(T [K]-300)	0.8·k_{air}+ 0.2·k_{fibre}	
PCM (sol./liq.)	862	2100/3000	0.37/0.19	
Inner	74.2	10.4·T [ºC]+1225	0.0003·T [ºC]+0.0304	
Epidermis	1200	3600	0.24	
Dermis	1200	3300	0.45	1.25 x 10^{-3}
Subcutaneous	1000	2500	0.18	1.25 x 10^{-3}

3.2.6 Calculation and discretization settings

Simulations were performed on a FEM platform in a computer with 2 processors Intel® Xeon® CPU E5-2620 v2 @ 2.10 GHz. Grid independency tests regarding time and space were performed. It was concluded that a maximum time step of 0.1 s for the high- and 1 s for the medium- and low-heat exposure scenarios were adequate. Also, a spatial mesh of 800 elements (of which 200 in the PCM) was considered. A backward finite difference time step update scheme was used with relative and absolute tolerances both set to 10−3 with respect to temperature. The time step chosen was controlled by the mentioned tolerances and hence it varied throughout the simulations. For example, in a typical flash fire simulation (Case A), the time step could vary between 0.001 and 0.04 s (see more details in Section 3.2.8).

3.2.7 Code verification and study configurations

The present modelling and simulation approach was used to replicate several works in the literature, involving melting of PCM layers during exposure to heat. Comparisons were done against:

(i) Experimental data of temperature of a PCM layer placed between a layer of clothing and a warm cylinder (mimicking a human torso protected by clothing; [26]);

(ii) Numerical predictions of temperature histories along a firefighting garment-skin system containing a PCM layer [9];

(iii) Analytical solutions for the temperature profiles over time, for 1D heat transfer along a semi-infinite PCM slab exposed to a constant temperature in one boundary [27].

As shown in Figure 3.2a-c, excellent agreement was obtained between the predictions with the present model, and the data from the mentioned works, which indicates that the present model can be used for studying the effect of a PCM layer in the heat transport across a firefighter garment.

The addition of a PCM layer to the FFPC-skin system introduces thermal storage in the form of latent heat. In general, the PCM considered in this work (capric acid) has a melting temperature of 50.6 °C and a latent heat of 199.8 kJ/kg. Also, a PCM layer with a mass of 0.2 kg was assumed unless said otherwise.

The position of the PCM layer, latent heat, mass, and melting temperature were all subject to independent studies so as to observe their effects on the thermal performance of the FFPC. The specific parameters considered in each of the independent studies (i.e. Sections 3.3.1-3.3.4, respectively) are shown in Table 3.4. The range of thicknesses considered for the PCM layer (0.6–6 mm) addresses different possibilities in terms of PCM application, e.g. from thin PCM-rich layers to thicker PCM packs. For the calculation of the thickness of the PCM layer, it was assumed that the PCM layer covered the entire surface of the body region (i.e. the upper anterior body part, specifically 0.35 m^2 obtained based on a height of 0.73 m and a waist circumference with 0.97 m [8]).

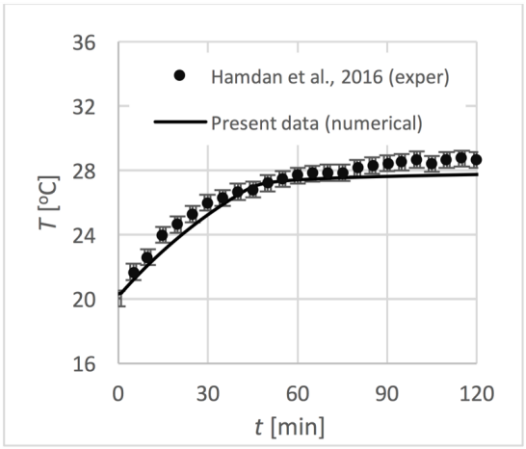

a.)

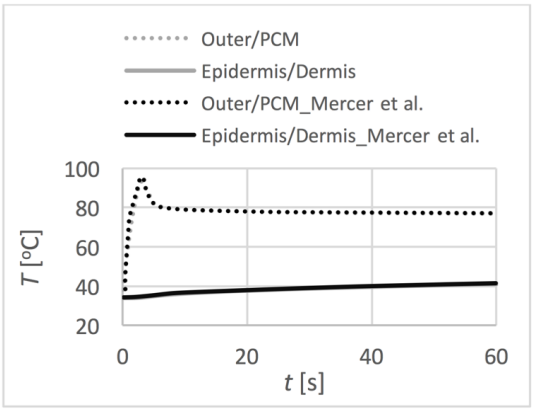

b.)

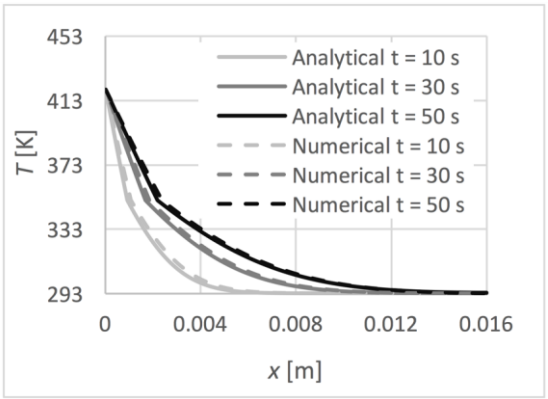

c.)

Figure 3.2 - Comparison between predictions of temperature obtained with the present model and simulation approach against previous experimental, numerical and analytical data from the literature. (a) Temperature over time for a PCM layer placed

between a layer of clothing and a warm cylinder [26]; (b) temperature over time along a firefighting garment-skin system incorporating a PCM layer [9]; and (c) temperature profiles over time, along a PCM slab exposed to a constant temperature in one boundary.

Table 3.4 - Specific parameters considered in each of the independent studies (Sections 3.3.1-3.3.4); *d* is the distance of the PCM layer relative to typical position between the outer shell and the thermal inner. T_m, λ, m, L_{PCM}, E_λ and ΔT_m are the PCM melting temperature, latent heat, mass, thickness, total latent energy and width of the mushy region (i.e. temperature interval where phase change occurs), respectively

Variable	**relevant section**	***d*** **[mm]**	T_m **[ºC]**	λ **[kJ/kg]**	***m*** **[kg]**	L_{PCM} **[mm]**	E_λ **(=*m*·λ) [kJ]**	ΔT_m **[K]**
Latent heat (λ)	3.1	0	50.6	100-300	0.2	1	20-60	20
PCM mass (*m*)	3.2	0	50.6	199.8	0.2-2	0.6-6	40-400	20
Melting temperature (T_m)	3.3	0	50-200	199.8	0.2	1	40	20
		0	50-200	199.8	0.2-2	0.6-6	40-400	20
PCM position (*d*)	3.4	0-0.95	50.6	199.8	0.2	1	40	20

3.2.8 Grid independence tests

Grid indepence tests in time and space were done in order to assure accurate solutions and, at the same time, computational efficiency (Table 3.5).

Table 3.5 - Meshes used in convergence tests.

Mesh	Elements in PCM	Elements in each of the other domains
1	50	5
2	200	100
3	500	200

As it can be seen in Figure 3.3, spatial mesh independence is obtained with Mesh 2 and time step independence with a maximum time step of 0.1 s. The following grid independence tests were run for the high – intensity heat exposure scenario. For lower heat intensity scenarios, the maximum time step could be increased to 1 s without loss of accuracy.

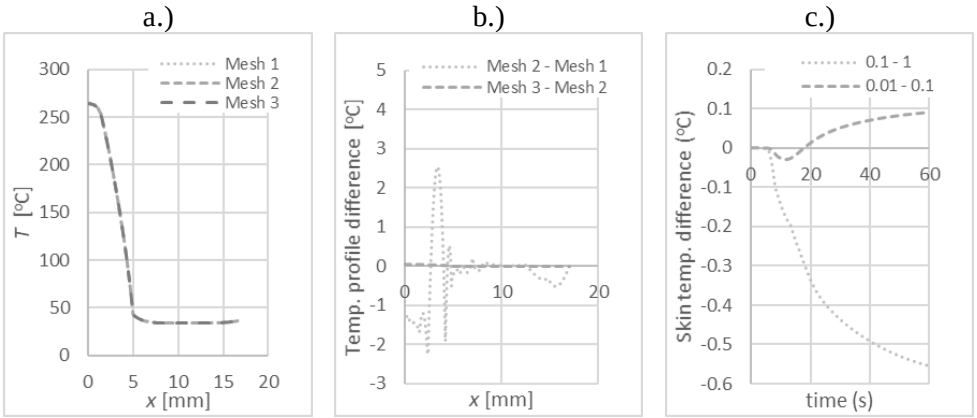

Figure 3.3 - Grid tests performed for high-intensity exposure (84 kW/m^2 for 8 s): (a) temperature profiles obtained with the indicated meshes at t = 20 s; (b) difference between temperature profiles obtained with the indicated meshes; (c) difference between skin temperature histories obtained with the indicated maximum time steps.

3.3 Results and discussion

In general, in a firefighting garment ensemble, there is an exposure to an external heat flux which originates a rise in temperature in the firefighting suit and consequently in the PCM layer. If the heat flux is big enough to melt the PCM, part of the energy entering the garment is stored as latent heat (in the PCM) in a narrow temperature range around the melting temperature (T_m) namely, between the liquidus and solidus temperatures (ΔT_m). If no PCM was present, this energy would instead be stored as sensible heat at higher temperatures in the garment ensemble.

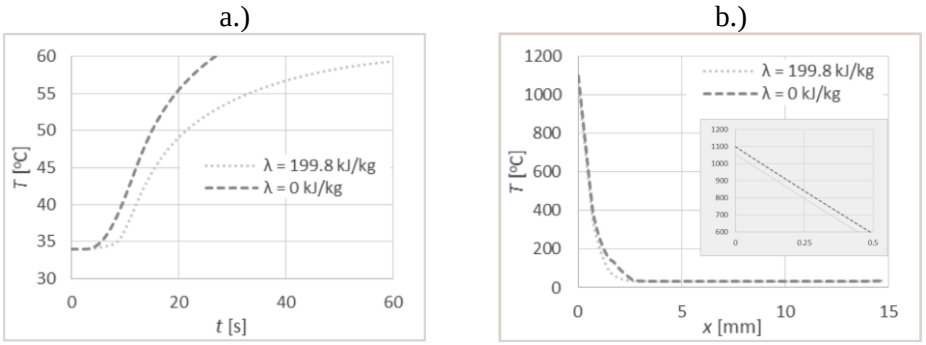

Figure 3.4 - Temperature histories and profiles obtained for the heat exposure scenario of 84 kW/m^2 during 8 s, considering a PCM layer with and without latent heat (i.e. λ = 199.8 kJ/kg and λ = 0 kJ/kg, respectively) with constant thermophysical properties for all garment layers. a) Temperature history obtained at epidermis/dermis boundary and; b) Temperature profiles across the FFPC - skin ensemble for t = 8 s; x is the coordinate along the thickness of the garment, starting from the external clothing surface (see Figure 3.1).

Figure 3.4 shows the effect of the addition of latent heat to the firefighting garment system. As can be seen, this addition delays and dampens the temperature rise at the epidermis/dermis boundary (λ = 199.8 kJ/kg, Figure 3.4a, t > 8 s). This is a natural consequence of the development of lower temperatures throughout the FFPC system (Figure 3.4b).

3.3.1 Influence of latent heat

Latent heat is the energy associated with a phase change, which in PCMs is usually from solid to liquid or vice versa (storage/release of latent heat, respectively). The presence of latent heat makes it that a portion of the incoming energy is stored at a lower temperature, which in turn is expected to originate lower temperatures throughout the garment-skin system, enhancing therefore the time the firefighter can be exposed to such heat fluxes before he/she gets a second-degree skin burn. So, a high latent heat is usually recommended when choosing a PCM ([2,3]), so that a relevant portion of the incoming energy can be stored in the PCM layer. To the knowledge of the authors, there exists no study on the influence of PCM latent heat on the thermal performance of a firefighting garment ensemble in the literature.

Figure 3.5 shows the temperature histories for different PCM latent heats obtained for the three exposure scenarios outlined in Table 3.2. As can be seen, an increase in PCM latent heat causes a decrease in the temperature obtained at the epidermis/dermis layer over time. Initially, for all heat fluxes, the temperature increases at a small rate (e.g. λ = 300 kJ/kg, $0 < t < 40$ s, Figure 3.5b), but after some time, the temperature suddenly rises at a much higher rate. This is registered for all exposure scenarios and latent heats considered. This change in the temperature increase marks the moment when the full capacity of the PCM effect is reached, i.e. when the PCM is completely melted and thus, no more storage of latent energy is possible and its effect is no longer felt at the skin. Moreover, for the most intense and short exposure scenario (84 kW/m^2 for 8 s, Figure 3.5a), the temperature at the skin starts to level out, for times above 20 s, for all latent heats considered. After the exposure, i.e. for $t > 8$ s, the temperature in the garments is still high. The heat accumulated in the garments will tend to flow towards the skin, increasing its temperature. As the heat is transferred to/ through the skin, the energy accumulated in the garment decreases and the temperature gradients across the garment become less steep.

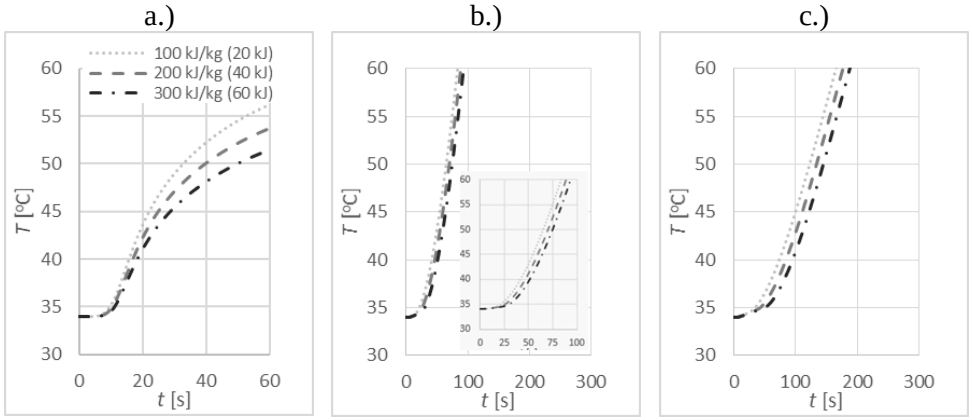

Figure 3.5 - Temperatures obtained at epidermis/ dermis boundary for the indicated latent heats and energies, for the outside exposures of: (a) 84 kW/m^2 for 8 s; (b) 12 kW/m^2 for 5 min; (c) 5 kW/m^2 for 5 min.

Figure 3.6 shows the heat flux that reaches the skin for all cases and latent heats considered. The heat flux reaching the skin increases, in full agreement with the increase in temperature registered in Figure 3.5, over time. At early times, the heat flux reaching the skin seems to stabilize (e.g. 20 < t < 80 s, λ = 300 kJ/kg, Figure 3.6c), when there are low rates of temperature rise (Figure 3.5c). It is the PCM effect being felt by the skin, when part of the incoming energy is stored as latent heat, at a lower temperature in the FFPC ensemble. The higher the latent heat, the more evident this effect, and the lower the temperatures and heat fluxes registered at the skin over time (Figure 3.5 and Figure 3.6). For the short high-intensity exposure (Case A, Table 3.2), after some time, one observes a decrease in the flux reaching the skin (t > 20 s, Figure 3.6a), which is in line with the lower temperature rise registered for later times (t > 20 s, Figure 3.5a). That this happens for the more intense but shorter exposure is not a coincidence, because it directly depends on the importance of the available latent energy (up to 60 kJ) relatively to the total incoming energy. Indeed, a PCM layer with a latent heat of 300 kJ/kg can absorb, as latent energy, 25% of the total energy entering the garment during the 8 s of the high-intensity exposure (672 kJ/m^2=84 kW/m^2 × 8 s, Table 3.2). This is about 5-fold and 2-fold more than for the medium- and low-intensity exposures, respectively, where only 4.6% and 11.2% of the incoming energy (i.e. 3600 kJ/m^2 and 1500 kJ/m^2) can be retained by the PCM layer. This is why the effect of the PCM

layer is more pronounced in the temperature and heat flux curves corresponding to the short high-intensity exposure.

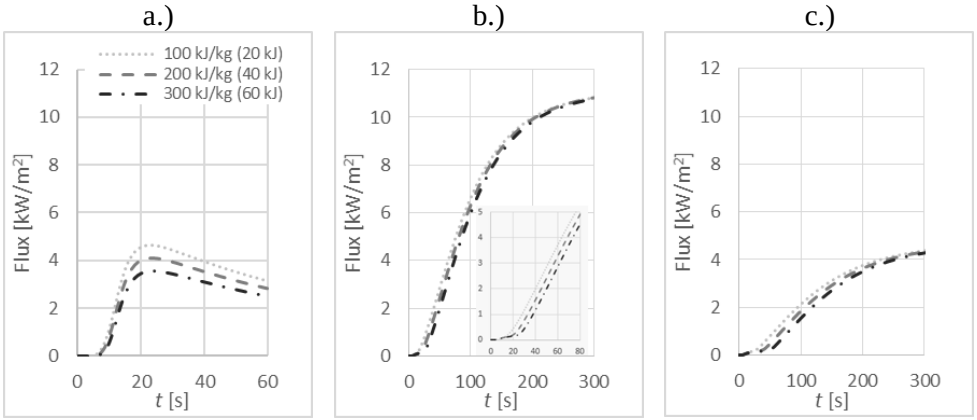

Figure 3.6 - Heat fluxes obtained at epidermis/dermis boundary for the indicated latent heats and energies, for the outside exposures of: (a) 84 kW/m^2 for 8 s; (b) 12 kW/m^2 for 5 min; (c) 5 kW/m^2 for 5 min.

Figure 3.7 shows the liquid fraction of PCM over time for the different heat exposure scenarios (details on the liquid fraction calculation are in appendix). As expected from previous discussion, the phase change begins at a very early stage in the process (e.g. Figure 3.7a, $0 < t < 6$ s). This is consistent with the stabilization of the heat fluxes reaching the skin and the low rates of temperature rise discussed above. Once the phase change is complete (i.e. when liquid fraction reaches 1), the energy coming from the external source starts being stored in the PCM layer as sensible rather than latent heat. This, in turn, causes a rise in the rates of temperature increase (Figure 3.5) and heat fluxes at the skin (Figure 3.6).

The phase change takes longer for decreasing external heat fluxes and increasing latent heats, as the latent energy is used up at a slower rate (Figure 3.7). An interesting aspect is to quantify the time it takes to reach a skin burn for a given exposure scenario and PCM latent heat, as that informs about the time a firefighter can work safely. The Henriques burn model [24] was used to estimate the time needed for the occurrence of a second-degree burn at the epidermis/dermis interface (t_{2nd}). We calculated also a dimensionless time to second-degree burn (τ_{2nd}), defined as the percentage increase obtained in the

time to second-degree burn, relative to the lowest time obtained when studying the effect of increasing values of a given parameter (in this case latent heat; see appendix for more details on the calculation). Figure 3.8 shows the time it takes to reach a second-degree skin burn under the different exposure scenarios, considering the chosen PCM latent heats/energies.

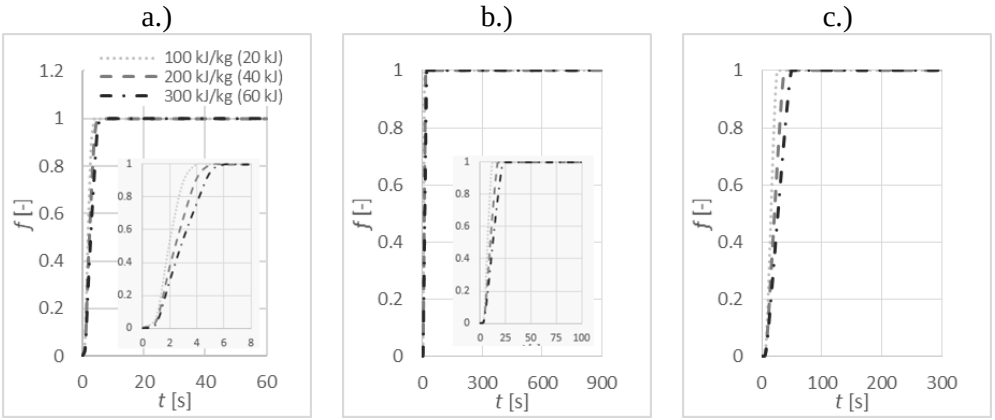

Figure 3.7- PCM liquid fractions for the indicated latent heats and energies, for the outside exposures of: (a) 84 kW/m^2 for 8 s; (b) 12 kW/m^2 for 5 min; (c) 5 kW/m^2 for 5 min.

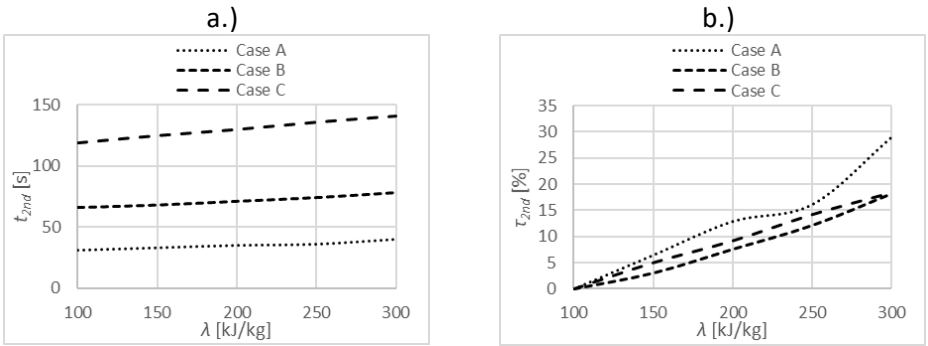

Figure 3.8 - Time to second-degree burn for high-, medium- and low-intensity exposures (Cases A, B and C, respectively, Table 3.2): (a) absolute times to second-degree burns; (b) dimensionless times to second-degree burns in percentage relative to the lowest time obtained for the series of parameters being considered.

As shown and expected, the time to reach a second-degree burn increases with an increasing latent heat, as more of the incoming heat is stored in the PCM. Naturally, higher time to second-degree burn is obtained for decreasing incoming heat fluxes. The trends of the curves obtained are approximately linear

for all exposure scenarios meaning t_{2nd} is approximately proportional to the latent heat. This is clearly shown by the dimensionless time to 2nd-degree burns (τ_{2nd}; Figure 3.8b).

A higher latent heat implies that, as long as the PCM melts, more heat is stored in the latent form, and hence a higher time to second- degree burn is achieved (which implies improved thermal performance of the garment).

3.3.2 Influence of PCM mass

An increase in PCM mass means that more PCM is available to melt. Hence, more energy can be stored in the latent form, as when increasing latent heat (Section 3.3.1). However, since the thickness of the PCM now increases with an increasing mass, the thermal resistance and the sensible heat (that can be accumulated) also increase, thus changing the transport rates.

The influence of PCM mass on the temperature profiles obtained throughout the garment-skin system has been studied to a limited extent by Hu and co-workers [6]. They considered a limited number of PCM mass configurations which render difficult to elaborate on how exactly the PCM mass influences thermal performance.

In the present study, different PCM masses were considered up to 2 kg [28], corresponding to latent energies up to 400 kJ. The thickness of the PCM layer was calculated assuming that only the upper anterior body part of the suit had an integrated PCM layer, and that the latter covered all its surface area (i.e. 0.35 m^2). This implied considering PCM layers with up to 6.5 mm of thickness and hence a thermal resistance of 4×10^{-2} m^2K/W (for the PCM mass of 2 kg). Temperature profiles along the garment-skin system for various times and temperature histories at the epidermis/dermis layer were then obtained.

Figure 3.9 shows the temperature histories obtained at the epidermis/dermis boundary for the different exposure scenarios. As shown, an increase in PCM mass originates a decrease in temperature throughout time. More energy is stored at a lower temperature (i.e. melting temperature T_m) in the form of latent

heat. This is associated with a lower heat flux reaching the epidermis/dermis boundary (Figure 3.10). As discussed in Section 3.3.1, at initial time the rise of the temperature at the epidermis/dermis boundary is delayed due to the phase change but once this is over, the temperature rises at a much higher rate (e.g. Figure 3.9c and Figure 3.11, m = 1000 g, t > 200 s).

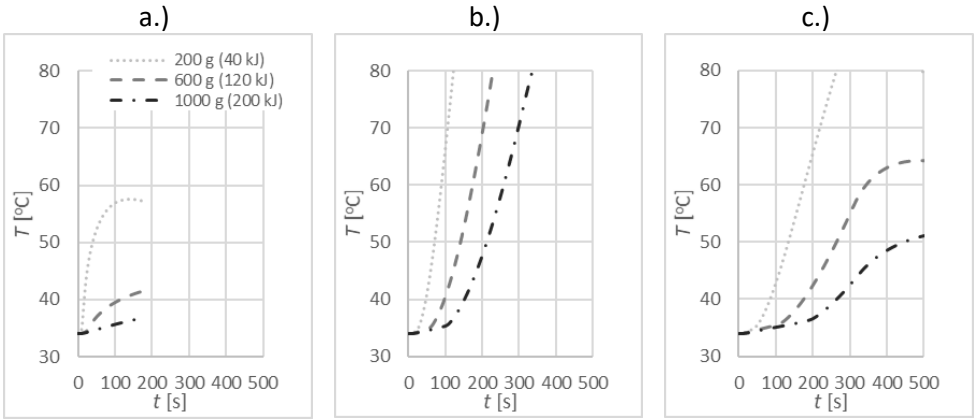

Figure 3.9 - Temperature obtained at epidermis/ dermis boundary for the indicated PCM masses and latent energies, for the outside exposures of: (a) 84 kW/m^2 for 8 s; (b) 12 kW/m^2 for 5 min; (c) 5 kW/m^2 for 5 min.

However, for the high-intensity exposure (Case A, Table 3.2), the change in temperatures with respect to PCM mass is a lot greater than for the other two less intense exposures (Cases B and C, Table 3.2; Figure 3.9). This has to do with a very high amount of energy entering the garment in a very short amount of time, for the high-intensity exposure (Case A, Table 3.2). This means the PCM melts very fast for the smaller PCM mass (m = 200 g/E_λ = 40 kJ), but on the other hand, it does not undergo full melting during the exposure time (t = 8 s), for higher PCM masses (600 g or 1000 g/120 kJ or 200 kJ, Figure 3.9a). For the medium- and low- intensity exposures (Cases B and C, Table 3.2), the exposure times (5 min) are greater which in turn allows for the full melting of the PCM, for the masses/latent energies considered (i.e. Figure 3.11b and c).

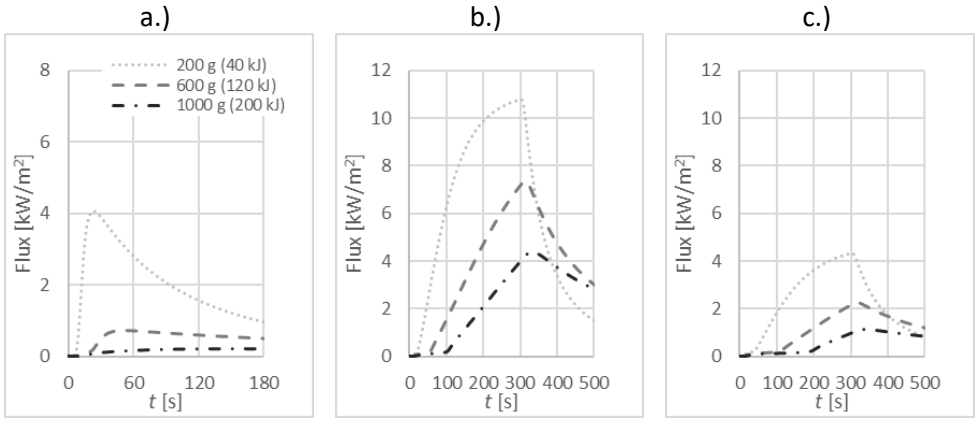

Figure 3.10 - Heat fluxes obtained at epidermis/ dermis boundary for the indicated PCM masses, for the outside exposures of: (a) 84 kW/m^2 for 8 s; (b) 12 kW/m^2 for 5 min; (c) 5 kW/m^2 for 5 min.

Figure 3.11 shows the liquid fractions obtained over time for the different exposure scenarios. The PCM liquid fraction increases over time as the PCM stores part of the incoming energy, in the latent form. Notice that, for the high-intensity exposure (Case A, Table 3.2), the lower PCM mass (i.e. m = 200 g / E_λ = 40 kJ) is clearly not enough to deal with the incoming energy, as the corresponding phase change finishes when only 63% of the exposure has been completed (i.e. at t = 5 s, for an exposure time of 8 s). On the contrary, the higher masses shown in the chart (600 g or 1000 g/120 kJ or 200 kJ, Figure 3.9a) are more adequate to hold the incoming heat front as only about 60% and 35% of the corresponding PCM melts during the 8 s exposure (Figure 3.11a). Furthermore, for the higher mass shown in the chart (1000 g/200 kJ, Figure 3.11a), not only there is no full phase change during the entire simulation time, but there is actually re-solidifying after the initial liquefying process, as the PCM liquid fraction starts to decrease after a certain point (t > 100 s, m=1000 g, Figure 3.11a).

The fact that, with both 600 and 1000 g of PCM there is still solid PCM after the exposure, implies that part of the energy entering the garment during the exposure may be absorbed by the PCM layer after the exposure, thus influencing the time to second-degree burns. To study this effect, Figure 3.12a and b show

the absolute and dimensionless times until occurrence of second-degree burns, respectively, for PCM masses of 200-2000 kg (i.e. latent energies of 40-400 kJ).

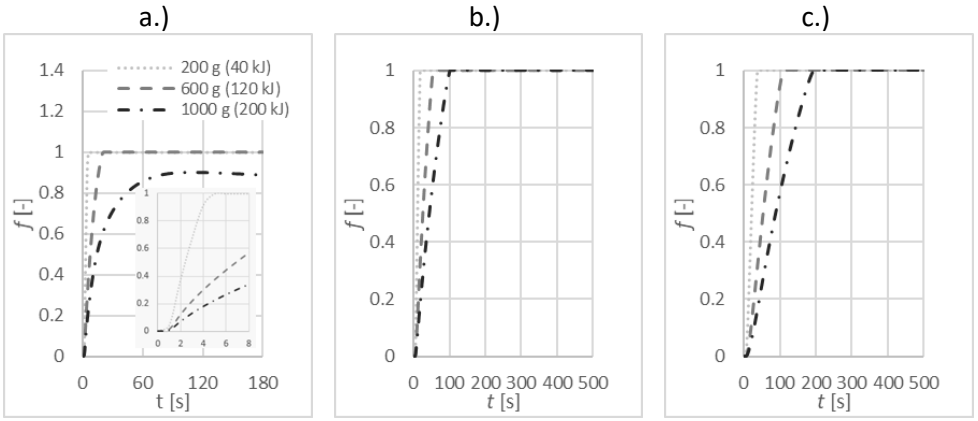

Figure 3.11 - PCM liquid fractions for the indicated PCM masses, for the outside exposures of: (a) 84 kW/m^2 for 8 s; (b) 12 kW/m^2 for 5 min; (c) 5 kW/m^2 for 5 min.

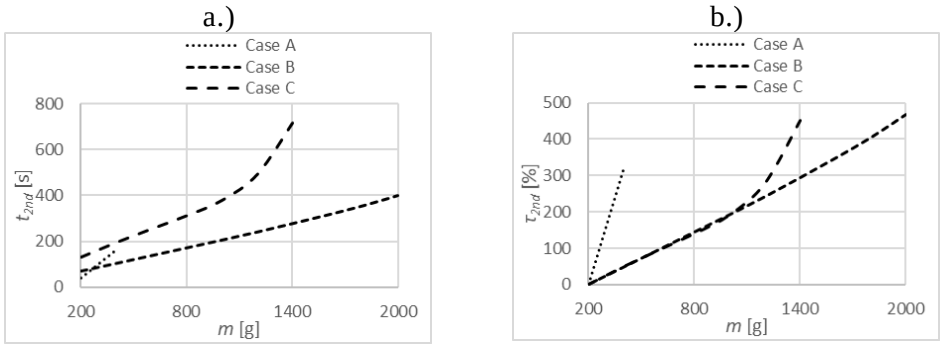

Figure 3.12 - Time to second-degree burn for high-, medium- and low-intensity exposures (Cases A, B and C, respectively, Table 3.2): (a) absolute times to second-degree burns; (b) dimensionless times to second-degree burns in percentage relative to the lowest time obtained for the series of para- meters being considered

As expected, there is an increase in time to second-degree burns, with an increase in PCM mass (or latent energy). This increase is approximately linear, for most of the masses and exposures considered. However, an exception is worth mentioning (Figure 3.12b). The time for a second-degree burn to occur under the low-intensity exposure (Case C, Table 3.2) initially varies in an approximately linear way (m < 1000 g/ E_λ < 200 kJ, "Case C", Figure 3.12b), but has an approximately exponential growth for PCM masses above 1000 g (m > 1000 g/E_λ > 200 kJ, "Case C", Figure 3.12b). This change happens when the

available latent energy (200 kJ) accounts for a fairly relevant portion of the total incoming energy (37%).

The mentioned exponential increases in the time to burn curves indicate the presence of solid PCM after the heat exposure, which partially absorbs the energy already inside the garment (but still in the outer layer), thus delaying and dampening the temperature rise at the skin. Considering the high – exposure intensity "Case A" notice that, for m > 200 g, solid PCM is readily present after the exposure. Hence, the greater linear increase in τ_{2nd} compared to the other cases (Figure 3.12).

Finally, an increase in PCM mass means more heat from the external source can be stored, not only as latent but also as sensible heat, which implies an increase in the thermal performance of the garment, as both contribute to increase the time-window without burns. Nevertheless, after the relationship between the time to burns and the mass becomes exponential, there is no advantage in adding more PCM to the garment, as it will not change phase, serving only as a thermal resistance. Therefore, to increase further the time window without burns, it is preferable to add more thermal insulation, avoiding unnecessary costs and excessive loading of the firefighter.

3.3.3 Influence of melting temperature

The melting temperature of a PCM is the temperature at which it changes phase, if pure. A higher melting temperature of a PCM in a given position, and for a given mass and thermophysical properties, implies that, during an exposure to heat, the PCM will only change phase at a higher temperature. The melting temperature of the PCM has been reported to have an influence on clothing applications involving PCMs ([8,29–31]). However, conclusions differ as to what the best choice of the melting temperature is. This is also naturally dependent on the boundary conditions considered. To the best of our knowledge, for the exposure scenarios considered in this study, no detailed study on the influence of melting temperature on the thermal performance of a FFPC has been undertaken.

One has to keep in mind that raising the melting temperature of the PCM makes it change phase at a later time during a charge process (i.e. exposure to heat), or not change phase at all if, during the exposure, T_m is not reached at the PCM layer due to the low intensity of heat reaching the PCM. If that is the case, then more energy is accumulated as sensible heat, higher temperatures are obtained, and a higher heat flux is observed at the skin. This also implies that certain values of T_m might allow for only a partial melting of the PCM during a heat exposure. For instance, with very high PCM melting temperatures, less PCM melts and therefore less latent heat is used to absorb the energy from the external source. Thus, as a general principle, one aims to identify the ranges of melting temperature that imply full melting of the PCM, or as much phase change as possible, with the lowest possible amount of PCM. This allows to draw the maximum benefit from the PCM storage capacity, while minimizing the load to be carried by the firefighter (by eliminating the PCM portions that do not change phase).

Simulations were run for melting temperatures of the PCM between 50 and 200 °C, for a constant latent energy of 40 kJ. For each melting temperature, the temperature and heat flux history at the epidermis/ dermis layer were obtained, together with profiles of PCM liquid fraction over time. This was done for the three exposure scenarios outlined in Table 3.2.

Figure 3.13 shows the temperature histories obtained at the epidermis/dermis boundary for the three exposure scenarios. For all, an increase in the melting temperature of the PCM originates a rise in the temperature curves. Initially, the temperature curves rise due to the external heat flux (e.g. Figure 3.13b, T_m = 100 °C, $0 < t < 20$ s). After some time, the temperature increases at a low rate, corresponding to the period over which the phase change effect is felt at the skin (e.g. Figure 3.13b, T_m = 100 °C, $20 < t < 50$ s). When this happens, it depends on the melting temperature considered (e.g. Figure 3.13c, T_m = 50 °C, $0 < t < 50$ s and T_m = 100 °C, $50 < t < 70$ s), with higher melting temperature implying later occurrence of the phase change. This is fully in line with the heat fluxes at the skin, which level out as the PCM undergoes phase change (e.g. Figure 3.14c, T_m = 50 °C, $0 < t < 50$ s and T_m = 100 °C, $40 < t < 70$ s).

A PCM with a higher melting temperature implies that the PCM layer will be at a higher temperature when changing phase. This in turn means that the rest of the garment system is also warmer. Hence, a higher heat flux is allowed to reach the skin whilst phase change occurs, when considering increasing melting temperatures (e.g. Figure 3.14c, T_m = 50 °C, 0 < t < 50 s and T_m = 100 °C, 40 < t < 70 s). Note that for the high-intensity exposure (Case A, Table 3.2), the heat fluxes registered for all melting temperatures start to decrease from a certain point in time (e.g. Figure 3.14a, T_m = 150 °C, t > 20 s).

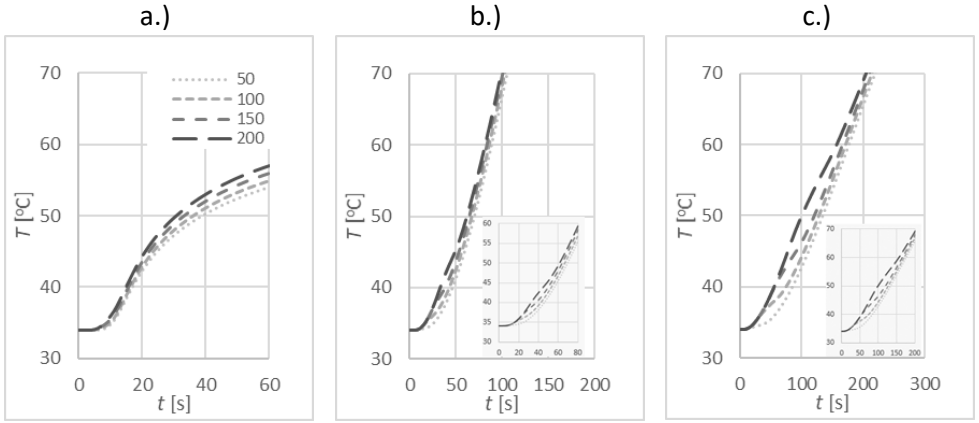

Figure 3.13 - Temperatures obtained at epidermis/ dermis boundary for the indicated melting temperatures (in °C), for the outside exposures of: (a) 84 kW/m^2 for 8 s; (b) 12 kW/m^2 for 5 min; (c) 5 kW/m^2 for 5 min.

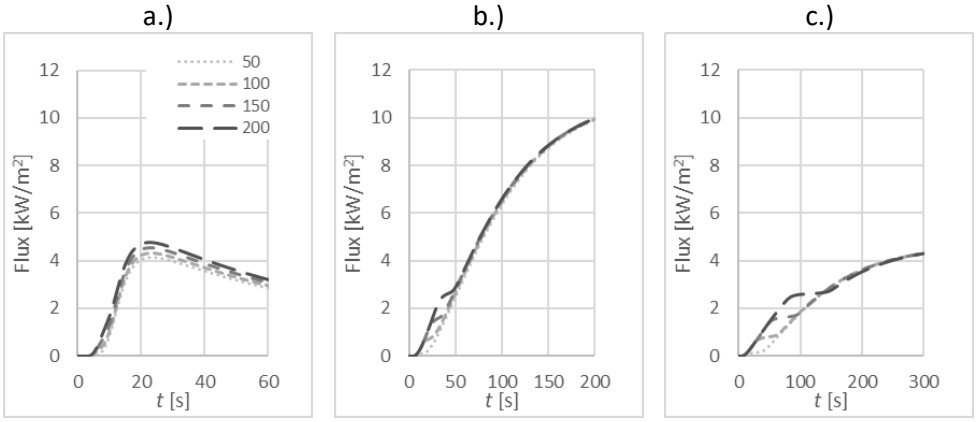

Figure 3.14 - Heat fluxes obtained at epidermis/dermis boundary for the indicated temperatures (in °C), for the outside exposures of: (a) 84 kW/m^2 for 8 s; (b) 12 kW/m^2 for 5 min; (c) 5 kW/m^2 for 5 min.

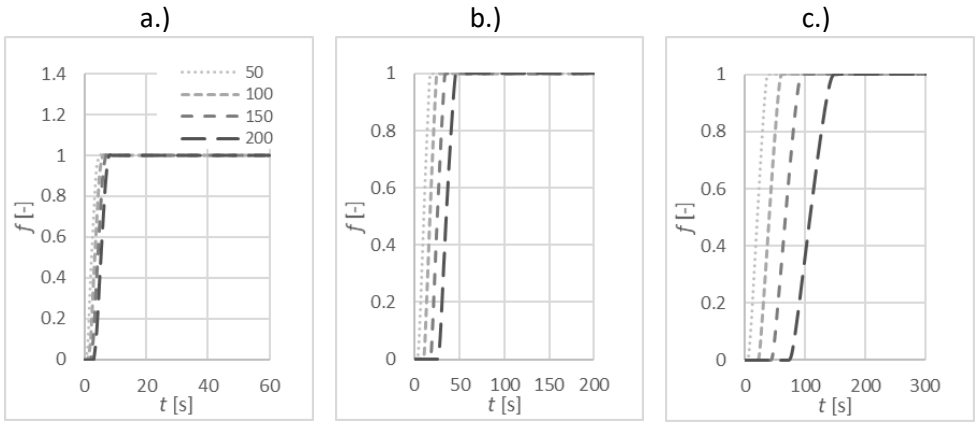

Figure 3.15 - PCM liquid fractions for the indicated melting temperatures (in °C), for the outside exposures of: (a) 84 kW/m^2 for 8 s; (b) 12 kW/m^2 for 5 min; (c) 5 kW/m^2 for 5 min.

Figure 3.16 shows the absolute and relative times to second-degree burns for the three heat exposure scenarios. For all cases considered, an increase in the melting temperature (T_m) originates a decrease in the time to second-degree burns (t_{2nd}). To understand the effect of Tm in more detail consider, for instance, the curve for the low-intensity exposure ("Case C" in Figure 3.16a), where we observe a clear change below and above a melting temperature of 150 °C. Below 150 °C, there is a relatively small but gradual decrease in t_{2nd} with increasing T_m, which is due to the different thermal properties of the solid and liquid PCM. When T_m increases, the PCM liquefies at a later stage, thus the PCM is in its solid state for a longer time, before a burn is reached. Hence, as T_m increases, the thermal properties of the solid PCM have an increasing footprint in the time to burn obtained. Because the solid PCM has a much higher thermal conductivity and much lower specific heat compared to the liquid PCM (two effects that increase the rate of heat transport), this results in the observed gradual reduction in the time to burn, for increasing T_m.

On the contrary, for increasing melting temperatures above 150 °C, there is a much steeper decrease in the time to burn (Figure 3.16, T_m > 150 °C), which is related to a reduction in the portion of PCM melted by the time a burn occurs

(i.e. there is partial melting of the PCM, thus increasing amounts of heat reaching the skin and burns occurring increasingly sooner; more details on this reasoning can be found in Appendix 3.5.4).

Similar trends are observed for the high- and medium-intensity scenarios, but the effect of the melting temperature on the time to burn is less pronounced because partial melting is not observed in either of the scenarios, for all T_m considered (Figure 3.15). In other words, for the high- and medium-intensity scenarios, full melting of the PCM is observed before the second-degree burn, throughout the whole range of T_m considered, whereas for the low-intensity scenario, full melting is only promoted in the range 50 °C < T_m < 150 °C.

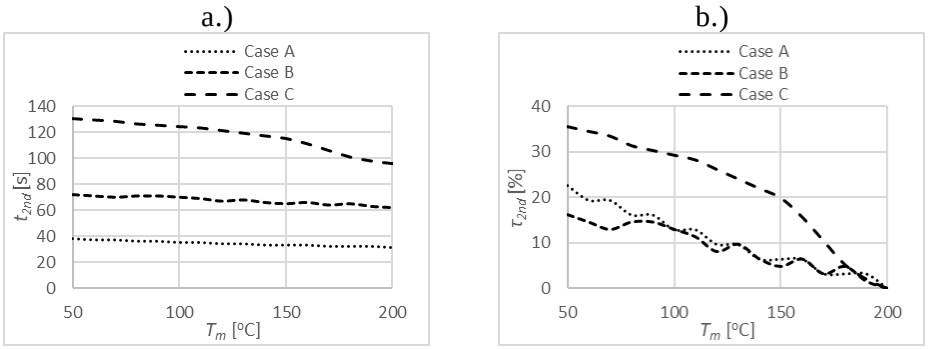

Figure 3.16 - Time to second-degree burn for high-, medium- and low-intensity exposures (Cases A, B and C, respectively, Table 2): (a) absolute times to second-degree burns; (b) dimensionless times to second-degree burns in percentage relative to the lowest time obtained for the series of parameters being considered.

Whenever full melting is not promoted, a practical solution would be to replace the non-melted PCM by an insulating layer. In this way, the time to burn intended can be obtained with lower loads on the firefighter and lower cost of the PCM layer.

Nevertheless, it is important to note that the results shown above refer to the case where all the other parameters are held constant and their values are equal to those reported in this work. However, the conclusions mentioned above might differ if certain parameters change. For instance, it is possible that the PCM mass (m) and latent heat (λ) may have an influence on the range of T_m values found to be ideal, for a given heat exposure. This is because, as the available latent energy ($m \cdot \lambda$) increases, more solid PCM may persist after a given

exposure, for a given T_m. Hence, it is logical that higher latent energies (i.e. higher PCM masses/latent heats) will imply lower or narrower ranges of T_m to allow for full melting of the PCM. Furthermore, a change in PCM mass (m) will also affect the sensible heat accumulated in the PCM.

To study this in more detail, Figure 3.17 shows the time to second-degree burns (t_{2nd}) for the various heat exposure scenarios, for different T_m (50-200 °C) and PCM masses (200-2000 kg). As expected (Sections 3.3.1-3.3.2), increasing PCM mass (or latent energy), increases the time- window without burns, because of the increasing storage capacity of the PCM. Furthermore, there is a clear change in the t_{2nd} curves above certain masses/latent energies, as regions where full melting occurs become shorter, namely for the higher PCM masses (e.g. Figure 3.17c, m = 1400 g / E_λ = 280 kJ). As discussed earlier, this means that the PCM no longer fully melts before the burn (see Appendix 3.5.4), indicating that the phase change starts too late to enable the full usage of the PCM storage capacity.

As predicted, increasing PCM mass/latent energy implies a narrowing of the melting temperature range that originates full melting of the PCM. This is indicated by the decreasing length of the less steep portion of the t_{2nd} curve versus T_m (e.g. Figure 3.17, from 50-200 °C to 50-110 °C, for PCM layers from 200 g / 40 kJ to 2000 g / 400 kJ, respectively). The extent of this effect is, however, different in the different exposure scenarios, as it depends on the importance of the available latent energies, relative to the corresponding total incoming energies, i.e. on the capacity of the PCM loads to absorb relevant portions of the incoming heat.

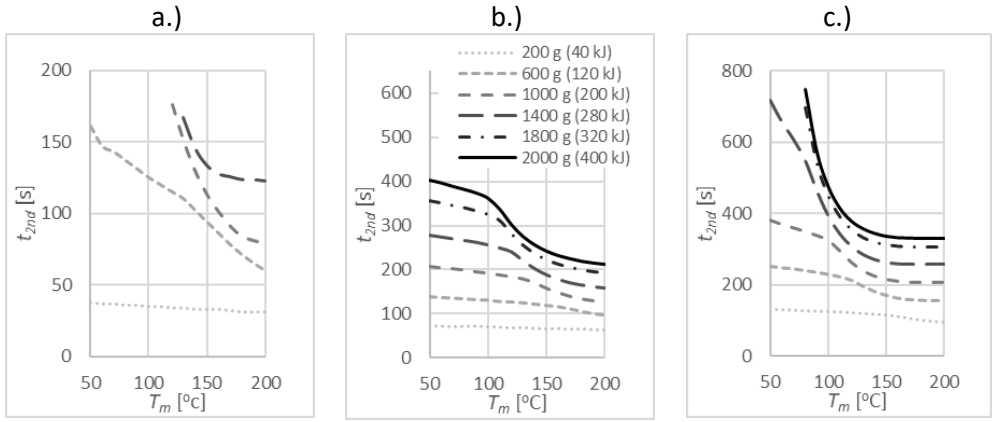

Figure 3.17 - Times for epidermis/dermis boundary to reach second-degree burns for the indicated masses and melting temperatures for outside exposures of: (a) 84 kW/m^2 for 8 s; (b) 12 kW/m^2 for 5 min; (c) 5 kW/m^2 for 5 min.

An increase in PCM mass essentially leads to more PCM available for melting during the exposure as well as a greater thermal resistance. This means that the PCM will take longer to melt and hence it is more likely for a burn to occur before the full melting of the PCM. In such cases, solid PCM will be present after the exposure which will serve only as a thermal resistance. The replacement of this solid PCM by a thermal insulator could be beneficial in terms of cost and exertion of the firefighter, because of the reduction in the total amount of PCM present in the garment.

3.3.4 Influence of position

When a PCM melts, the absorbed energy implies lower temperature in the firefighting garment system, as discussed earlier. Another way to interpret this is to consider that the PCM has a variable thermal inertia throughout the phase change, which is always higher than that of any other layer in the garment. A higher thermal inertia means that, over time in a charge process (i.e. heat exposure), it takes longer for the PCM temperature to rise.

The position of the PCM layer should be chosen so that it favours its full phase change before the skin burn is achieved to take full advantage of its latent heat (i.e. high thermal inertia during the phase change). However, few studies

in the literature address the effect of position of the PCM layer [5,6] and in these, different positions are reported as providing better performance. Therefore, to clarify this, we changed the position of the PCM in a gradual way to investigate the implications in terms of temperature histories and transport rates along the garment.

A spatial co-ordinate d was defined, ranging from 0 to 3.59 mm, to represent different positions of the PCM layer: when d = 0 mm, the PCM layer is located between the outer shell and the thermal inner (i.e. the most outer position) and when d = 3.59 mm, is located between the thermal inner and the epidermis (i.e. the most inner position). Figure 3.18 shows the temperature histories obtained at the epidermis/dermis boundary for the three heat exposures considered. As shown, for all the exposures, an inner position of the PCM layer (i.e. higher d) originates higher temperatures at the epidermis/dermis boundary. The temperature at initial times rises slowly due to the phase change (Figure 3.18a, $0 < t < 10$ s; 3.18b, $0 < t < 40$ s; and 3.19c, $0 < t < 70$ s). This is consistent with the initial lower heat flux histories obtained at the epidermis/dermis boundary (Figure 3.19), and the initial lower liquid fraction histories (Figure 3.20). Naturally, with a decreasing exposure heat flux, the phase change takes longer (e.g. $10 < t < 50$ s, d = 3.59 mm, Figure 3.20b, and between $40 < t < 110$ s in Figure 3.20c), and the heat flux reaching the epidermis/dermis boundary decreases (Figure 3.19). Notice also that with an increase in d, for the same heat exposure, the phase change starts later and takes longer as a smaller heat flux reaches the PCM over time due to its more inner position (e.g. Figure 3.20c).

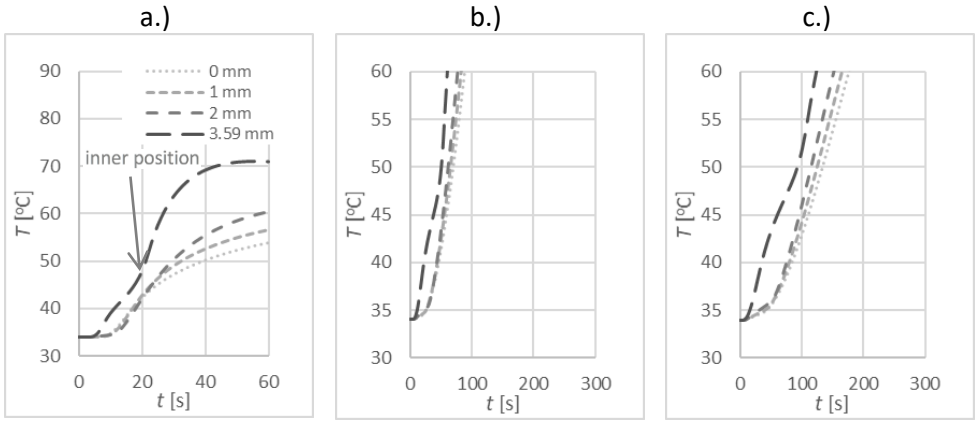

Figure 3.18 - Temperatures obtained at epidermis/ dermis boundary for the indicated positions, for the outside exposures of: (a) 84 kW/m^2 for 8 s; (b) 12 kW/m^2 for 5 min; (c) 5 kW/m^2 for 5 min.

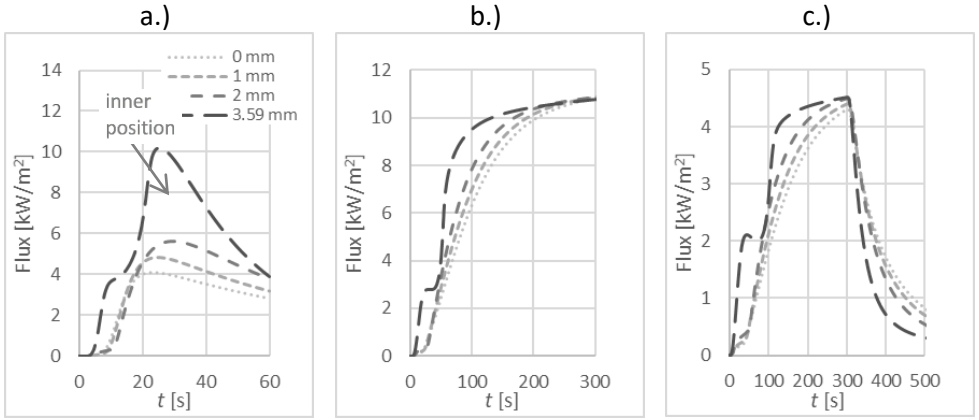

Figure 3.19 - Heat fluxes obtained at epidermis/dermis boundary for the indicated positions, for the outside exposures of: (a) 84 kW/m^2 for 8 s; (b) 12 kW/m^2 for 5 min; (c) 5 kW/m^2 for 5 min.

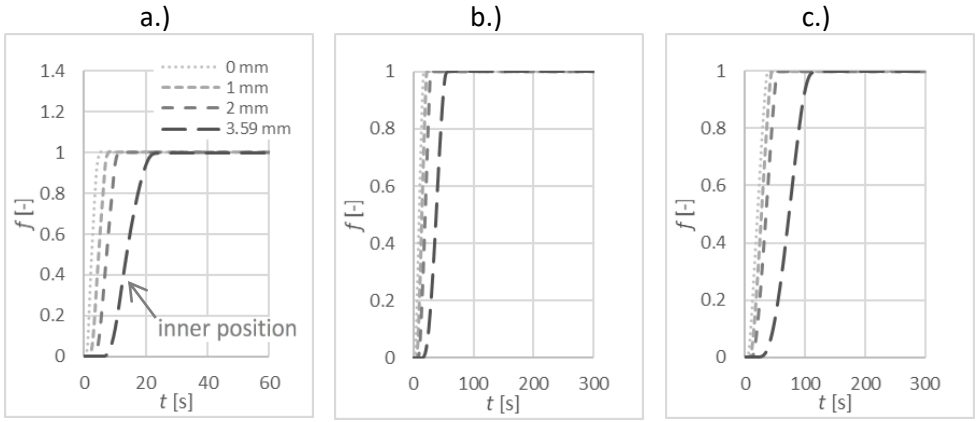

Figure 3.20 - PCM liquid fractions for the indicated positions, for the outside exposures of: (a) 84 kW/m^2 for 8 s; (b) 12 kW/m^2 for 5 min; (c) 5 kW/m^2 for 5 min.

Figure 3.21 shows the absolute and relative time to second-degree burns under various PCM layer positions. For all heat exposure scenarios considered, an inward position (i.e. higher *d*) originates lower times to second-degree burns, because of the higher temperatures at the skin (Figure 3.18), as a result of the higher heat fluxes (Figure 3.19). This is fully in line with a lower portion of PCM changing phase (Figure 3.20) before the burn is reached, as the PCM layer moves closer to the skin, thus away from the external heat source.

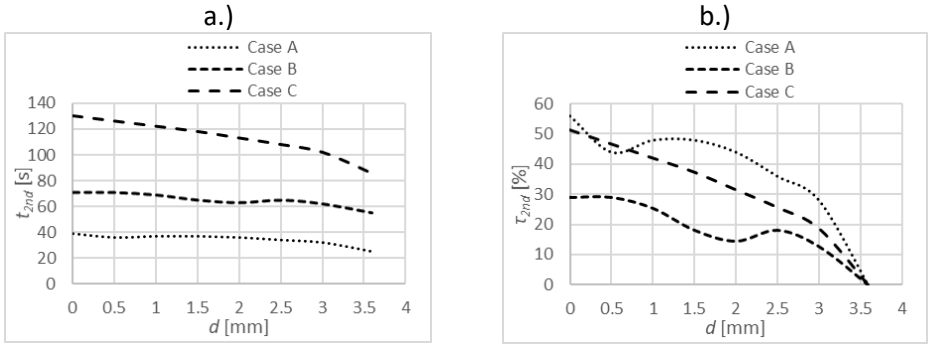

Figure 3.21 - Time to second-degree burn for high-, medium- and low-intensity exposures (Cases A, B and C, respectively, Table 3.2): (a) absolute times to second-degree burns; (b) dimensionless times to second-degree burns in percentage relative to the lowest time obtained for the series of parameters being considered.

The results discussed above show that, in the case of a charge scenario (heat exposure) the PCM layer should be positioned closest to the external source. If

so, lower temperatures in the garment are obtained over time, resulting in longer time to burns. This was observed for all heat exposure scenarios considered.

3.3.5 Use of generated data

The data generated in this work can be used in different ways to assist in the design of a firefighting garment ensemble with an incorporated PCM layer. They help to choose the adequate PCM for a given application or to assess if a given PCM can successfully deal with a given thermal load. Furthermore, it enables the estimation of its ideal position and mass (see Section 3.3.4 and Section 3.3.3/Figure 3.17, respectively). From a choice of PCMs, the generated data help in determining which ones originate the lowest mass needed to reach a certain tolerance time (i.e. time-window without burns), under a given heat exposure scenario. The data can also be used to obtain, for a given PCM, a rough estimate of the proportion that melts under a given heat exposure scenario, for a given exposure time. This enables to decide between adding a significant mass of PCM or seek alternative solutions (like adding more insulation) to reach a required exposure time (see Section 3.3.3).

3.3.6 Limitations and suggestion of future work

This section discusses limitations of the present work and need for future research.

Effect of clothing air gaps - In this work, no air gaps (or microclimates) were considered between the different garment layers, in order to address the worst possible case in terms of thermal load on the firefighter. Although this represents body regions where, either because of gravity or compression, it is reasonable to assume a perfect contact between the different garment layers, there are other body regions where it may be more reasonable to consider the existence of air gaps between the different garment layers. In that case, the predictions in this work (e.g. skin temperature and heat fluxes) are slight

overestimations because the air layers trapped within the garment would serve as additional thermal resistances ([9–11,32]). Furthermore, if the geometries and thermal conditions in the air gaps would allow for natural convection to occur, then the local transport rates may be very different from a purely conductive heat transfer ([32–36]). Moreover, radiant exchange across the air gaps would have to be considered in the calculations, as it could have a relevant footprint in the overall heat transfer and affect even the (naturally occurring) convective transport via changes in the temperature fields across the air gaps ([35,37,38]). Thus, it would be important to study the effect of different air gaps, on the transport rates across firefighting protective garments, for different heat exposure scenarios.

Effect of underwear and moisture transport - Perfect contact (i.e. without underwear layer) between the garment and the skin was assumed in this work, to address the most thermally-demanding situation. The existence of an underwear layer between the garment and the skin, would imply slightly lower temperatures and heat flux at the skin, and therefore, slightly longer periods without burns, because of the added thermal resistance of the underwear. Although the latter is small compared to the total thermal resistance the garment ensemble, its effect would vary with the underwear thermal properties and moisture content, as these may affect the evolution of temperature over time ([20,21,39]). In this regard, and although the PCM effect is reported to be larger than that of the moisture transfer ([9]), it would be interesting to incorporate in the present model, the effect of mass transfer across all the garment/underwear layers (including the energy exchange due to water/sweat phase change), to investigate its implications in terms of heat fluxes at the skin, temperature distributions across the garment layers and its overall thermal performance.

Effect of pumping - The present work regards static conditions, where it is reasonable to assume negligible motion of the garment layers relative to the skin. However, if air gaps were to be considered between the garment layers or between these and the skin, then it could be relevant to assess also the importance of the “pumping” effect, i.e. the motion of the garment layers relative to the body (e.g. because of the motion of the firefighter), as this may change the transport processes within and around the garment ([11,40,41]).

Need for experimental tests - Although the results obtained in this work have been validated against previous results in the literature (i.e. [9,26,27]), and the modelling approach used is reported to produce good predictions of the thermal effect of PCM layers, it would be important to conduct flame manikin tests with a small number of prototypes of firefighting garments incorporating PCM layers built following the guidelines derived in this work. Such experimental tests would be important to test and fine-tune the obtained predictions, and thus contribute to a body of knowledge on the best way to use the PCM latent storage capacity, to improve the thermal performance of firefighting protective clothing.

Need for analyses including PCM resolidification – Most results obtained in this work address thermal scenarios implying melting of the PCM layer (i.e. charge process), with only very few exceptions implying also resolidification (i.e. discharge process) in the end of the analyses. Although many of the situations encountered by firefighters can lead to melting of a PCM layer integrated in the garment, there are others where resolidification may also be present and even have relevance footprint in the overall temperature histories across the garment. This may happen, for instance, during intermittent heat exposures, or when the transport rates to/from the garment external surface suddenly decrease (e.g. because of a change in ambient temperature and level of convection/ventilation around the firefighter). In these cases, the process of resolidification of the PCM layer may lead to relevant changes in the transport rates across and within the garment, and affect the relations discussed in this work. For this reason, it would be important to investigate the effect of the mentioned changes in the thermal environments surrounding the firefighters, on the performance of a fire- fighting garment incorporating a PCM layer.

3.4 Conclusions

A numerical study was conducted to investigate the role of PCM mass, latent heat, melting temperature and position, over the thermal performance of a firefighting protective clothing ensemble (FFPC) incorporating a PCM layer. Parametric analyses were done for high-, medium- and low-intensity thermal

exposures, i.e. 84 kW/m^2 for 8 s, 12 kW/m^2 for 5 min and 5 kW/m^2 for 5 min, respectively. The obtained data show that PCMs can contribute to an enhancement in the thermal performance of a FFPC by absorbing part of the incoming energy, in the form of latent heat. As a result of the parametric study, the following conclusions can be drawn:

- Full melting of the PCM before the occurrence of a skin burn is needed to fully use its storage capacity, i.e. to draw full benefit from the available latent energy, to absorb part of the incoming heat. For this to happen, due attention must be given to the choice of melting temperature, as this directly influences the temperature range around which the phase change takes place, as well as how soon it starts after the onset of the exposure to heat. The melting temperature of the PCM should be high enough so its melting does not commence before the exposure onset (e.g. due to heat coming from the body), but also low enough to promote its full melting.
- For a latent energy of 40 kJ and the low-intensity exposure considered in this work, full melting occurs before second-degree burns for PCM with melting temperatures of 50–150 °C. For the high- and medium-intensity exposure, full melting is observed before the second-degree burn, for the whole range of melting temperatures considered (50–200 °C).
- The ranges of melting temperature that promote full melting of the PCM vary with the latent energy available in the garment, with higher latent energies implying lower or narrower ranges of melting temperature. During an exposure to heat, increasing latent energies require the PCM to start melting sooner (thus at lower temperatures) to reach full melting before a skin burn occurs.
- The PCM mass (m) and latent heat (λ) directly influence the latent energy ($E_\lambda = m \cdot \lambda$) available in the garment to absorb part of the heat coming from the external source. These parameters should be high enough for E_λ to represent relevant portions of the total incoming energy, because, in general, the higher these portions, the longer it takes for a skin burn to occur (e.g. the time for second-degree burns

to occur vary in an approximately liner way with both PCM mass and latent heat). However, care should be taken to avoid overestimation of the latent energies to integrate in the garment, to minimize the load to be carried by the firefighter (by incorporating only the PCM mass that can fully melt, for the intended thermal exposure).

- The optimum position of the PCM layer was found to be closest to the external heat source, thus furthest from the skin. This hinders the development of higher temperatures in the garment-skin system, favours a higher use of the PCM storage capacity and takes advantage of its high thermal inertia in a more efficient way.

Acknowledgments

The authors gratefully acknowledge the financial support from FEDER through the Operational Programme for Competitiveness Factors – COMPETE, ON.2 – O Novo Norte – North Portugal Regional Operational Programme and National Funds through FCT – Foundation for Science and Technology - under projects PEst-OE/EME/UI0532 and NORTE-07-0124-FEDER-000025-RL2-Environment & Health.

3.5 Appendix

3.5.1 Differential scanning calorimetry (DSC) curve utilized

The type of equation fitted to the DSC experimental curve is shown below (equation 3.7). The variable T_0 was used as the floating variable to fit the experimental curve via a minimizing square technique (Figure 3.22). The following fitting equation was obtained:

$$C_{app} = \lambda \times \frac{\exp\left(-\frac{T - T_m}{T_0}\right)^2}{T_0\sqrt{\pi}} + C_{PCM}$$
$$= \left(199.8 \times 10^3 \frac{\text{J}}{\text{kg}}\right) \times \frac{\exp\left(-\frac{T - (50.6 + 273)\text{K}}{5.2\ \text{K}}\right)^2}{(5.2\ \text{K})\sqrt{\pi}} + 3000 \frac{\text{J}}{\text{kg} \cdot \text{K}} \quad (3.7)$$

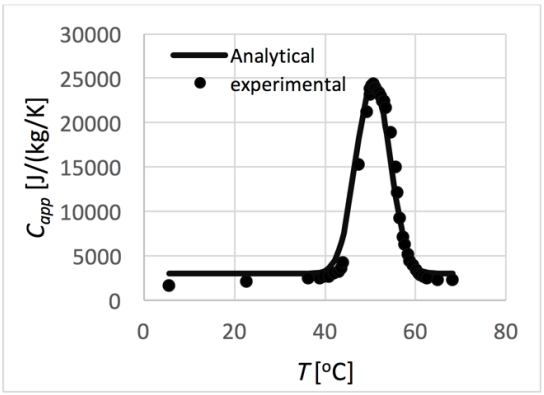

Figure 3.22 - Comparison between experimental DSC curve obtained from [23], and fitted equation (equation 3.7)

In the parametric analyses discussed in Sections 3.3.1-3.3.3, the above-mentioned fitting curve was adapted as needed to represent the hypothetical PCM considered in each case. For instance, in Sections 3.3.1-3.3.2, the maximum value of the fitting curve for C_{app} was increased as needed (to generate the corresponding total latent energies) and, in Section 3.3.3, the fitting curve was shifted to higher melting temperatures. The fitting was done assuming that the specific heat of the PCM is 3000 J/(kg·K) in both phases.

3.5.2 Liquid fraction calculation

The latent energy used along a given phase change process was calculated by integrating, between the boundaries x_1 and x_2 of the PCM domain, the latent portion of the PCM apparent C_p:

$$E_\lambda = \rho_{PCM} A \int_{x=x_1}^{x=x_2} C_{app}^{lat}\, \mathrm{d}x + \frac{1}{2}\rho_{PCM} L_{PCM} \lambda A \tag{3.8}$$

where E_λ is the total latent energy used at a given time, and ρ_{PCM}, A, and λ, represent the PCM density, the surface area occupied by PCM in m^2, and the latent heat in J/kg.

The second term in the right side of the above equation is a vertical shift so that the error function varies between 0 and 1, instead of −1/2 and 1/ 2, so that when the latent heat is zero, E_λ is also zero.

3.5.3 Time to burns calculation

It is of use to estimate the time it takes for the epidermis/dermis layer to suffer second-degree burns (t_{2nd}) in relative terms. The relative time it takes for the epidermis/dermis layer to suffer a burn is defined relative to the shortest t_{2nd} obtained, in a systematic analysis of the effect of a given parameter:

$$\tau_{2nd} = \frac{t_{2nd} - t_{2nd,min}}{t_{2nd,min}} \times 100 \tag{3.9}$$

where t_{2nd} is the time it takes for the epidermis/dermis layer to suffer a second-degree burn, $t_{2nd,\mathrm{min}}$ is the minimum t_{2nd} obtained and τ_{2nd} represents the relative time for the second-degree burn, compared to the lowest time obtained. For instance, a value of τ_{2nd} = 20% for a given value of say PCM mass, means the time it takes for the epidermis/dermis to suffer a second-degree burn is 20% bigger than the lowest value of t_{2nd} obtained for the masses being compared.

3.5.4 Relation between proportion of liquefied PCM, and curves of time to second-degree burn

When a change in T_m significantly alters the time until a burn occurs, that means there is a significant change in the amount of heat allowed to reach the skin, because of a change in the amount of energy stored in the PCM in the latent form. This means the PCM is only partially melted, and that the proportion of liquid PCM is changing with the change in T_m. This is why one can assume there is partial melting of a PCM if the curves of t_{2nd} versus T_m (e.g. Figure 3.17) vary significantly with the choice of T_m.

On the other hand, if a change in Tm does not change significantly the time to burn, then the heat reaching the skin must be approximately the same for the different T_m. This implies that the energy stored as latent heat must be null or constant, for the different T_m. In other words, that none or all the PCM melts before the burn takes place. Because in our study the lower values of T_m were chosen to ensure at least partial melting of the PCM, one can assume that complete melting of the PCM must take place before the occurrence of the skin burn, for the predictions of time to burn to be approximately independent of the chosen T_m, for the lower values of T_m. This is why the presence or absence of a approximate plateau in the left portion of the curves of t_{2nd} versus T_m (e.g. Figure 3.17) can be used to identify the full or partial melting of the PCM layer, respectively.

References

[1] F. Agyenim, N. Hewitt, P. Eames, M. Smyth, A review of materials, heat transfer and phase change problem formulation for latent heat thermal energy storage systems (LHTESS), Renew. Sustain. Energy Rev. 14 (2010) 615–628, http://dx.doi.org/10. 1016/j.rser.2009.10.015.

[2] B. Zalba, Review on thermal energy storage with phase change: materials, heat transfer analysis and applications, Appl. Therm. Eng. 23 (2003) 251–283, http://dx. doi.org/10.1016/S1359-4311(02)00192-8.

[3] A. Sharma, V.V. Tyagi, C.R. Chen, D. Buddhi, Review on thermal energy storage with phase change materials and applications, Renew. Sustain. Energy Rev. 13 (2009) 318–345, http://dx.doi.org/10.1016/j.rser.2007.10.005.

[4] D. Barr, W. Gregson, T. Reilly, The thermal ergonomics of firefighting reviewed, Appl. Ergon. 41 (2010) 161–172, http://dx.doi.org/10.1016/j.apergo.2009.07.001.

[5] F.L. Zhu, Q.Q. Feng, R.T. Liu, B.G. Yu, Y. Zhou, Enhancing the thermal protective performance of firefighters' protective fabrics by incorporating phase change ma- terials, Fibres Text. East. Eur. 23 (2015) 68–73.

[6] Y. Hu, D. Huang, Z. Qi, S. He, H. Yang, H. Zhang, Modeling thermal insulation of firefighting protective clothing embedded with phase change material, Heat Mass Transf. 49 (2012) 567–573, http://dx.doi.org/10.1007/s00231-012-1103-x.

[7] H. Phelps, H. Sidhu, L. Sidhu, Modelling heat transport in protective fire fighting clothing containing phase change materials, in: Chemeca, Perth, Western Australia, 2014.

[8] D. Huang, Y. Li, L. Tong, H. Yang, H. Zhang, Modeling heat transfer in phase change material bedded firefighting protective clothing under fire exposure, in: L. Shengcai, W. Weiye, A. Ying (Eds.), Proc. 2010 Int. Symp. Saf. Sci. Technol., 2010, pp. 921–926.

[9] G.N. Mercer, H.S. Sidhu, Mathematical modelling of the effect of fire exposure on a new type of protective clothing, Anziam J. 49 (2008) 289–305.

[10] H. Phelps, H. Sidhu, A mathematical model for heat transfer in fire fighting suits containing phase change materials, Fire Saf. J. 74 (2015) 43–47, http://dx.doi.org/ 10.1016/j.firesaf.2015.04.007.

[11] A. Ghazy, Air gap in protective clothing during flash fire exposure, University of Saskatchewan, 2011.

[12] J.R. Lawson, W.D. Walton, N.P. Bryner, F.K. Amon, Estimates of thermal properties for fire fighters' protective clothing materials, 2005.

[13] G.N. Mercer, H.S. Sidhu, A theoretical investigation into phase change clothing benefits for firefighters under extreme conditions, Chem. Prod. Process Model. 4 (2009), http://dx.doi.org/10.2202/1934-2659.1349.

[14] Udayraj, P. Talukdar, A. Das, R. Alagirusamy, Heat and mass transfer through thermal protective clothing - A review, Int. J. Therm. Sci. 106 (2016) 32–56, http:// dx.doi.org/10.1016/j.ijthermalsci.2016.03.006.

[15] L.K. McCarthy, M. Marzo, The application of phase change material in fire fighter protective clothing, Fire Technol. 48 (2012) 841–864, http://dx.doi.org/10.1007/ s10694-011-0248-3.

[16] V.R. Voller, C.R. Swaminathan, B.G. Thomas, Fixed grid techniques for phase change problems: A review, Int. J. Numer. Methods Eng. 30 (1990) 875–898, http://dx.doi.org/10.1002/nme.1620300419.

[17] Y. Dutil, D.R. Rousse, N. Ben Salah, S. Lassue, L. Zalewski, A review on phase change materials: Mathematical modeling and simulations, Renew. Sustain. Energy Rev. 15 (2011) 112–130, http://dx.doi.org/10.1016/j.rser.2010.06.011.

[18] J. Fan, Heat and moisture transfer with sorption and phase change through clothing assemblies: Part I: experimental investigation, Text. Res. J. 75 (2005) 99–105, http://dx.doi.org/10.1177/004051750507500202.

[19] S.F. Neves, J.B.L.M. Campos, T.S. Mayor, Numerical simulation study on the heat and mass transfer through multi-layer textile assemblies, in: Comsol Conf. Eur., Milan, 2012.

[20] S.F. Neves, J.B.L.M. Campos, T.S. Mayor, On the determination of parameters re- quired for numerical studies of heat and mass transfer through textiles – Methodologies and experimental procedures, Int. J. Heat Mass Transf. 81 (2015) 272–282, http://dx.doi.org/10.1016/j.ijheatmasstransfer.2014.09.038.

[21] S.F. Neves, J.B.L.M. Campos, T.S. Mayor, Effects of clothing and fibres properties on the heat and mass transport, for different body heat/sweat releases, Appl. Therm. Eng. 117 (2017) 109–121, http://dx.doi.org/10.1016/j.applthermaleng.2017.01. 074.

[22] R. Vettori, Estimates of Thermal Conductivity for Unconditioned and Conditioned Materials Used in Fire Fighters â€TM Protective Clothing Estimates of Thermal Conductivity for Unconditioned and Conditioned Materials Used in Fire Fighters â €TM Protective Clothing, n.d.

[23] A.A.F. Al-Hamadani, S.K. Shukla, Water distillation using solar energy system with lauric acid as storage medium, Int. J. Energy Eng. 1 (2012) 1–8, http://dx.doi.org/ 10.5923/j.ijee.20110101.01.

[24] F.C. Henriques, Studies of thermal injury V. The predictability and the significance of thermally induced rate processes leading to irreversible epidermal injury, Arch. Pathol. 43 (1947) 489–502.

[25] L.N. Zhai, J. Li, Prediction methods of skin burn for performance evaluation of thermal protective clothing, Burns. 41 (2015) 1385–1396, http://dx.doi.org/10. 1016/j.burns.2015.02.019.

[26] H. Hamdan, N. Ghaddar, D. Ouahrani, K. Ghali, M. Itani, PCM cooling vest for improving thermal comfort in hot environment, Int. J. Therm. Sci. 102 (2016) 154–167, http://dx.doi.org/10.1016/j.ijthermalsci.2015.12.001.

[27] Solomon, An easily computable solution to a two-phase Stefan problem, Sol. Energy. 23 (1979) 525–528. doi:10.1016/0038-092X(79)90077-X.

[28] J.R. House, H.C. Lunt, R. Taylor, G. Milligan, J.a. Lyons, C.M. House, The impact of a phase-change cooling vest on heat strain and the effect of different cooling pack melting temperatures, Eur. J. Appl. Physiol. 113 (2013) 1223–1231, http://dx.doi. org/10.1007/s00421-012-2534-2.

[29] C. Chou, Y. Tochihara, T. Kim, Physiological and subjective responses to cooling devices on firefighting protective clothing, Eur. J. Appl. Physiol. (2008) 369–374, http://dx.doi.org/10.1007/s00421-007-0665-7.

[30] C. Gao, K. Kuklane, I. Holmér, Cooling vests with phase change material packs: the effects of temperature gradient, mass and covering area, Ergonomics 53 (2010) 716–723, http://dx.doi.org/10.1080/00140130903581649.

[31] C. Gao, K. Kuklane, I. Holmér, Cooling vests with phase change materials: The ef- fects of melting temperature on heat strain alleviation in an extremely hot en- vironment, Eur. J. Appl. Physiol. 111 (2011) 1207–1216, http://dx.doi.org/10. 1007/s00421-010-1748-4.

[32] T.S. Mayor, S. Couto, A. Psikuta, R.M. Rossi, Advanced modelling of the transport phenomena across horizontal clothing microclimates with natural convection, Int. J. Biometeorol. 59 (2015) 1875–1889, http://dx.doi.org/10.1007/s00484-015- 0994-x.

[33] M.P. Sobera, Flow, Heat and Mass Transfer through Protective Textiles, Tecnische Universiteit Czçestochowa geboren te Ilza, Polen, 2006.

[34] T.S. Mayor, S. Couto, A. Psikuta, R.M. Rossi, A numerical analysis on the transport phenomena across horizontal clothing microclimates, in: 6th Eur. Conf. Prot. Cloth., Bruges, Belgium, 2014, pp. 34.

[35] T.S. Mayor, D. Oliveira, R.M. Rossi, S. Annaheim, Numerical simulation of the transport phenomena in tilted clothing microclimates, in: XVI Int. Conf. Environ. Ergon., Portsmouth, UK, 2015.

[36] M.S. Santos, D. Oliveira, J.B.L.M. Campos, T.S. Mayor, Numerical analysis of the flow and heat transfer in cylindrical clothing microclimates - influence of the mi- croclimate thickness ratio, Int. J. Heat Mass Transf. 117 (2018) 71–79.

[37] V. Vivek, A.K. Sharma, C. Balaji, Interaction effects between laminar natural con- vection and surface radiation in tilted square and shallow enclosures, Int. J. Therm. Sci. 60 (2012) 70–84, http://dx.doi.org/10.1016/j.ijthermalsci.2012.04.021.

[38] T.S. Mayor, S. Couto, A. Psikuta, R.M. Rossi, Transport phenomena in clothing wavy microclimates – a numerical study, in: Sci. Conf. Smart Funct. Text. Well-Being, Therm. Comf. Clothing, Des. Therm. Manikins Model. (Ambience14 10i3m), Tampere, Finland, 2014.

[39] R.L. Barker, G. Song, H. Hamouda, D.B. Thompson, A.V. Kuznetsov, A.S. Deaton, P. Chitrphiromsri, Modeling of thermal protection outfits for fire exposures F01-NS50, North Caroline State, 2004.

[40] F. Wang, L.Y. Lin, M. Ribeiro, S. Ferraro, T.S. Mayor, V. Molinaro, C. Gao, K. Kuklane, I. Holmér, Localized evaporative resistance: correction

for body and air movement, in: Stylianos Kounalakis · Maria Koskolou (Eds) (Ed.), XIV Int. Conf. Environ. Ergon., Nafplio, Greece, 2011, pp. 101–102.

[41] F. Wang, S. Ferraro, L.Y. Lin, T.S. Mayor, V. Molinaro, M. Ribeiro, C. Gao, K. Kuklane, I. Holmér, Localised boundary air layer and clothing evaporative re- sistances for individual body segments, Ergonomics 55 (2012) 799–812, http://dx. doi.org/10.1080/00140139.2012.668948.

4

Chapter 4

Thermal performance of a PCM firefighting suit considering transient periods of fire exposure, post – fire exposure and resting phases

4

Thermal performance of a PCM firefighting suit considering transient periods of fire exposure, post – fire exposure and resting phases

In this chapter, the concept of thermal performance regarding the PCM FPC is extended to include the influence of the post – fire exposure and resting phases. It is shown that second – degree burns can happen after the fire exposure, due to the re-solidification of the PCM. This can have implications regarding the PCM choice. The information shown in this chapter resulted in the following publication:

Fonseca, A., Neves, S. F., & Campos, J. B. L. M. (2020). Thermal performance of a PCM firefighting suit considering transient periods of fire exposure, post – fire exposure and resting phases. *Applied Thermal Engineering*, 182(July 2020), 115769.

Abstract

Firefighting scenarios may be characterized by various transient periods (i.e. phases), which consist of diverse environmental conditions. Firefighters usually encounter fire exposure, post fire exposure and resting phases. Development of new and improved protective clothing must be able to provide protection throughout all these phases, as burnouts may still occur after fire exposure due to accumulation of heat in the garment. The incorporation of phase change materials (PCMs) in firefighting garments has been shown to minimize the potential of heat hazards only during fire exposure. Thus to get more knowledge on their thermal performance, in the present study, the effect of PCM incorporation in post fire and resting phases were also numerically studied. The numerical code was validated for all phases. Five potential PCM candidates were considered. Exposure phases were characterized by high- medium and low-

heat flux intensities (84, 12 and 5 $kW \cdot m^{-2}$) with variable exposure times whilst post –exposure and resting phases where characterized by different wind speeds (i.e. ambient convective coefficients). Optimal PCM masses, times to second and third – degree burns as well as PCM suit cooling times were calculated to reflect thermal protective performance in each respective phase. The data generated allows for PCM short-listing from a set of potential PCM candidates along with its geometrical parameters, considering a wide range of characteristics of the various phases that consist a typical firefighting scenario.

4.1 Introduction

Firefighters face thermal stressful situations that may cause severe burns or even death. To avoid such situations, the suit has an important role to fulfill [1]. Hence, improvements in firefighting garments are justified. A possibility of improvement relies on the increase of the garment thermal performance by the inclusion of phase change materials (PCM) [2–6]. In the literature, some works show guidelines to estimate PCM properties, mass and its position in the firefighters suit [5–9]. However, despite the extensive research on the application of PCMs for the fire exposure phase, the fire scenarios considered are limited to specific fire heat fluxes and exposure times. Additionally, the analyses were done neglecting the effect of the accumulated energy in the suit, on the firefighter's skin. Another aspect which still needs to be investigated is how the suit thermally behaves during a resting phase, where the firefighter doffs the garment and leaves it to cool down. Without the consideration of these additional aspects, misleading conclusions about the choice of adequate PCMs is inevitable. Hence in the present work, a detailed investigation of the heat transport in a firefighting suit with PCM considering these additional phases (i.e. exposure, post-fire and resting phases) is justified.

In order to obtain optimal performances, the inclusion of PCMs in firefighting garments requires knowledge about the PCM choice and its mass. The mass to be incorporated depends on many factors. In the present study, a PCM mass choice criteria for firefighting garments is suggested, considering a

wide range of possible exposure scenarios that the firefighter can face. PCM mass choice is also a problem in other PCM applications such as in the automobile sector and clothing industry [10–12]. Several authors report the masses used, however, justification of their choice is, usually, not reported. Others perform parametric studies to observe the influence of the mass on the PCM cooling effect, but the analysis is usually done for only one PCM and does not take into account an optimal performance criteria. Oró et al. [13] incorporated 4 kg of a PCM (RT-27) into the inner roof of a car to control its inner temperature during hot summer days. The authors reported a cooling effect that lasted for about 80 min and recognized the necessity of a mathematical model in order to predict optimal PCM masses in function of the process variables such as external ambient conditions and parking time. Hamdan et al. [14] suggested and validated an integrated PCM- fabric bio-heat model which was used to study the effects of melting temperature and mass of the incorporated PCM. Chou et al. [15] studied the effect of using different PCMs with different melting temperatures (i.e. Ice, PCM(5) and PCM(20)) on the cooling of a firefighter during a treadmill exercise. The subjects faced a warm environment during the treadmill (30 °C, 50% RH) and the masses used for Ice, PCM(5) and PCM (20) were 1.05, 1.69 and 1.34 kg, respectively. The PCMs provided cooling effect throughout the exercise, however it is unclear whether the PCM masses used were the optimum.

Typically, skin burns are classified according to injury depth. They are organized in four categories [39]: Superficial (S), Superficial Partial-thickness (SP), Deep Partial – thickness (DP), and Full – Thickness (FT). S burns are usually referred to as first degree burns, whilst SP and DP refer to second degree burns. Third degree burns correspond to FT type burns. Occurrence of 2^{nd} and 3^{rd} degree burns is likely during firefighting exposures. In 2^{nd} degree burns, the firefighter suffers damage both in the epidermis and dermis regions, and natural healing is still possible [16]. Whilst for 3^{rd} degree burns, there is destruction of blood vessels, hindering the possibility of natural healing [16]. As adequate PCMs promote the storage of incoming heat at lower temperatures during fire exposure phase, it is to expect that this stored heat will have a great influence on the post-fire exposure phase, where third degree burnouts are likely to happen

[6]. Hence, it is rather of interest not only to analyze how the inclusion of adequate PCMs relates to the time to second degree burnout (exposure phase), but also to see how much longer the firefighter has until a third degree burnout occurs (post-exposure phase).

Information about the post fire stage regarding the design of PCM fire protective clothing (PCM FPC) is scarce in the literature. Properties associated to the ambient encountered by firefighters in the post exposure phase may change the thermal behavior of the firefighting garment. Torvi et al. [17] proposed and validated a heat transfer model for a firefighting garment, and conducted a parametric study involving different ambient convective heat fluxes, supposing a high – intensity heat exposure. They concluded that the ambient convective heat flux had a marginal effect on the temperatures obtained after the fire exposure. Song et al. [18] considered different garment configurations and experimentally analyzed how stored thermal energy influences the occurrence of burns, for different heat exposure scenarios. They concluded that thicker fabrics promote stored energy burns (i.e. burns after fire exposure). The authors mention that, in some cases, the release of stored energy towards the skin can make up to 50% of the total skin damage required for a burnout. The same authors in a similar study [19] proposed correlations relating the fabric thickness with the time to burnout. The authors considered low radiant heat exposures. Su et al. [20] proposed and validated a heat transfer model for a three layer firefighting garment assembly. The authors analyzed the effect of stored energy on thermal performance. According to this study, ambient temperature marginally influences thermal performance.

In the recovery phase, the firefighter usually doffs the firefighting garment and rests. During this time, the firefighting garment cools down, releasing the remaining accumulated energy from the fire exposure. The existence of PCMs in the firefighting garment prolongs the cooling time, as it needs to re-solidify [3]. The choice of a PCM with adequate properties to minimize the garment cooling time is also important so the firefighter can don the PCM garment again.

In resume, in the present study, both PCM optimal choice and mass were calculated taking not only into account the exposure phase, but also the post –

exposure and recovery phases as well. A list of five potential PCM candidates was considered. PCM minimum masses were calculated for high – medium – and low- intensity heat flux exposures, for various exposure durations. The difference between second and third degree burn times was afterwards calculated for the post-exposure period in function of the previous exposure intensity and duration. This difference in burnout times was labeled alarm time, i.e. the time that the firefighter has until suffering irreversible burns. Second and third degree burnouts have had special attention devoted in previous works also regarding thermal performance in PCM FPC [20–23]. Different post – exposure scenarios characterized by different ambient convective coefficients were considered. Lastly, it was assumed that the firefighter doffs the PCM firefighting suit at the end of the exposure phase and the cooling time was obtained for the different PCMs.

4.2 Materials and methods

4.2.1 Problem description

In order to analyze the effect of PCMs in enhancing the garment thermal protection [5,24], a typical firefighting protective clothing (FFPC)-skin system was used (Figure 4.1). The simulation domain consists in a series of layers of garment (i.e. outer shell, PCM and thermal inner layer; at blue in Figure 4.1) and of skin (i.e. epidermis, dermis and subcutaneous; at orange in Figure 4.1). Air gaps between the garment layers and the skin were not considered in order to address the worst possible case in terms of thermal load on the firefighter, and generate safer pessimistic data on time to burn and PCM requirements. The performance of the PCM FFPC clothing is studied for a dynamic scenario which consists of a fire exposure, post-fire exposure and a resting phase. In the fire exposure period, the external surface of the garment (boundary 1 in Figure 4.1a) is initially subject to a sudden heat flux for a given exposure time (i.e. mimicking the exposure to flame) that ensures almost a reversible burn (i.e. a second-degree burn). Afterwards, the garment is no longer in direct exposure to

the flame and the heat exchange between the garment and the environment can occur by convection and radiation (Figure 4.1b and c). During this time, we were interested in studying how long the firefighter can handle without getting a third degree burn or how long the firefighter should wait until the garment is completely cooled down. This may happen in two ways: i) the firefighter is wearing the PCM FPC and the simulation domain is the system FFPC-skin (post - fire phase, Figure 4.1b) or ii) the PCM FPC is taken out and the simulation domain consists only in the garment with both the boundaries exposed to the environment conditions (resting phase, Figure 4.1c). Three heat fluxes were chosen to reflect the different fire scenarios that firefighters can encounter: 84, 12 and 5 $kW \cdot m^{-2}$ [5]. For the post-fire exposure and resting phase, the garment performance was assessed for windy and no wind conditions (e.g. inside a fire truck).

The PCMs considered in the present work are shown in Table 4.1[25]. These PCMs were chosen essentially based on their melting temperatures. Rubitherm PX 82, however, has been previously incorporated in firefighting garments [3]. The melting temperature has to be low enough not only because the PCM should melt for the different exposure scenarios [6], but also because the skin burn should, if at all, happen after the PCM is fully melted (i.e. maximum PCM efficiency). The PCM mass also influences the PCM efficiency, as a higher PCM mass takes a longer time to melt. The data outlined in [6 - Figure 17], gives rough estimates of melting temperatures and PCM mass ranges which could potentially provide maximum PCM efficiency and protection to the firefighter, for each of the exposure scenarios. It was based on these data that the PCMs listed in Table 4.1 were chosen. In the simulation, a variation in the PCM mass was considered by changing the PCM thickness while ensuring constant density.

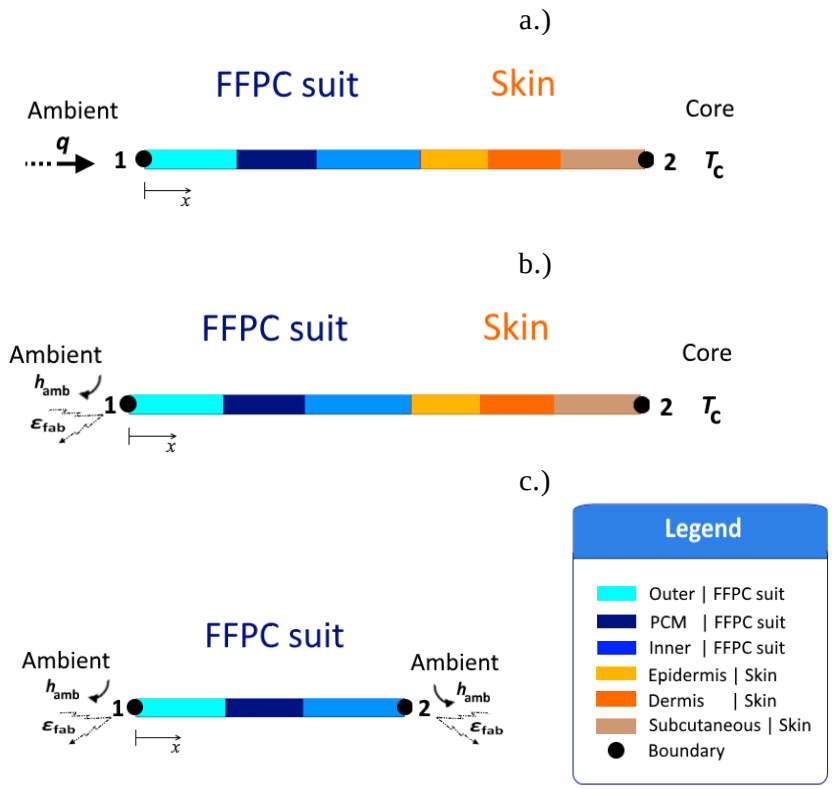

Figure 4.1 - Geometry and boundaries of (FFPC)- skin system: a.) for heat exposure; b.) for post - fire period when PCM FFPC is not removed; c.) for resting period when garment is removed.

Table 4.1 - PCMs and their thermophysical properties used in the present study (retrieved from [25]); T_m, ΔH_m, Cp_s, Cp_l, k_s, k_l, and ρ_s stand for melting temperature, latent heat of fusion, solid specific heat, liquid specific heat, solid thermal conducitvity, liquid thermal conductivity and density of the solid phase, respectively.

Phase change material	T_m (°C)	ΔH_m (kJ/kg)	Cp_s (kJ/kg/K)	Cp_l (kJ/kg/K)	k_s (W/m/K)	k_l (W/m/K)	ρ_s (kg/m^3)
Stearic acid	54	157	1.76	2.27	0.29	0.17	940
Sodium acetate trihydrate	58	266	1.68	2.37	0.43	0.34	1450
Barium hydroxide octahydrate	78	280	1.34	2.44	1.26	0.66	2180
Rubitherm PX82	82	105	1.6	1.6	0.1	0.1	690
Magnesium nitrate hexahydrate	89	140	2.5	3.1	0.65	0.5	1640

4.2.2 Boundary conditions

Firefighters encounter several types of heat exposure scenarios, from mild exposures in which the firefighter doesn't need special clothing, to flash fire scenarios where the firefighter must have special protective clothing [26]. McCarthy and co-workers [27] used exposures of 2.5, 10, and 20 $kW \cdot m^{-2}$ for 15 min, 5 min, and 30 s, respectively, as boundary conditions for the external garment layer. Other researchers [24] assumed exposure scenarios of 83.2 $kW \cdot m^{-2}$ and 1.2 $kW \cdot m^{-2}$ for periods of 3 s and 5 min respectively, to simulate high and low intensity firefighting. In the present study the firefighter was exposed to three heat exposure intensities as described in [6]. They include low and medium-intensity exposures (5 and 12 $kW \cdot m^{-2}$) corresponding to pre-flashover conditions, and a high intensity exposure (84 $kW \cdot m^{-2}$) representing flash fire conditions [5]. However, the novelty of the present study is that the exposure times were not fixed, in order to obtain more generic results regarding the exposure scenario the firefighters are subjected to.

Also the model developed in [6] was extended in the present study in order to include the post fire and resting phases. After the heat exposure scenario, the firefighter is likely to be exposed to a windy environment as well as to a reduced ambient temperature. Torvi et al. [17] characterized the post fire environmental scenario as having a constant ambient temperature (27 °C), and convective heat coefficients in the range of 2–10 $W \cdot m^{-2} \cdot K^{-1}$. Ghazy et al. [28] considered an equivalent temperature, but used a correlation for natural convection to estimate the ambient convective heat flux. Su et al. [20] considered ambient temperatures in the range of 0–50 °C and a correlation to estimate the ambient convective heat flux. Li et al. [29] used different wind speeds to characterize the thermal protection, implying different convective heat fluxes. Butler et al. [30] provides a list of typical ambient temperatures and wind speeds found in firefighting scenarios, as they are data taken from live fires. From the works above, it was possible to define an ambient temperature and the ranges in which the convective fluxes should be taken. The ambient temperature was assumed constant and equal to 25 °C. The convective heat coefficients considered were varied from 0 $W \cdot m^{-2}\ K^{-1}$ to 90 $W \cdot m^{-2}\ K^{-1}$. That is, it varied from when no

convection was present (e.g. inside fire truck), to cases where strong winds were up to 25 m·s^{-1} (e.g. exposed to forest fires or to blower fans). Thus, the following boundary conditions were considered:

$$-k\frac{\partial T}{\partial x}\Big|_{x=0} = q \quad for\ 0 < t \leq t_{exp} \tag{4.1}$$

$$-k\frac{\partial T}{\partial x}\Big|_{x=0} = -h_{\text{amb}}(T_{\text{fab}} - T_{\text{amb}}) - \varepsilon_{\text{fab}}\sigma(T_{\text{fab}}^4 - T_{\text{amb}}^4) \quad \text{for } t > t_{\text{exp}} \tag{4.2}$$

where q (W·m^{-2}) is the exposure intensity, t_{exp} (s) is the heat flux exposure time and h_{amb}, (W·m^{-2} ·K^{-1})T_{fab}(K), T_{amb}(K) and ε_{fab} represent the ambient convective heat flux, the fabric surface temperature, the ambient temperature, and the fabric emissivity respectively (i.e. ε_{fab} = 0.9 [31]).

4.2.3 Mathematical model and assumptions

The firefighting garment is essentially composed of an outer garment layer, a PCM layer and a thermal inner layer (Figure 4.1). The general dimensions of the various layers in the FFPC-skin system are shown in Table 4.2. The outer shell and thermal inner layers of the garment were considered to be a Kevlar®/PBI fire resistant fabric and an Aralite ® fabric, respectively [15,16]. The firefighting garment ensemble may also contain a moisture barrier [9], but, following related works in the literature [5,14], it was not considered in the present study as the thermal effect of PCM is larger than that of the moisture barrier [24].

Conductive heat transport in the outer and inner domains was modeled using the Fourier equation [6]. Their thermophysical properties were assumed temperature dependent (Table 4.2).

Table 4.2 - Thermophysical properties of the outer and inner layer of the garment and skin layers [32,33]; ρ, Cp, k, and L stand for, respectively, density, specific heat, thermal conductivity, and layer thickness. k_{air} and k_{fibre} stand for the air and clothing fiber thermal conductivity, respectively.

Property	ρ [kg/m^3]	C [J/kg/K]	k [W/m/K]	L [mm]
Outer	323	1300 + 1.6·(T [K]-300)	0.8·k_{air} + 0.2·k_{fibre}	0.6
Inner	74.2	10.4·T [°C] + 1225	0.0003·T [°C]+0.0304	3.59
Epidermis	1200	3600	0.24	0.08
Dermis	1200	3300	0.45	2
Subcutaneous	1000	2500	0.18	10

The apparent heat capacity method was used to simulate the phase change (Equation 4.3) in the PCM layer. The apparent heat capacity method is derived from a weak formulation of the phase change problem, namely the enthalpy formulation. Essentially, the position of the interface is implicitly taken into account by an apparent heat capacity (C_{app}), which not only considers the sensible, but also the latent heat associated with the phase change [34]. This makes it possible to avoid problems associated with interface tracking methods [35]. The following conservative one-dimensional energy equation is then applied in the PCM domain:

$$\rho C_{app} \frac{\partial T}{\partial t} = \frac{\partial}{\partial x} \cdot \left(k \frac{\partial T}{\partial x} \right) \tag{4.3}$$

where ρ (kg·m^{-3}), T (K), t (s) and k (W·m^{-1}·K^{-1}), represent, respectively, density, temperature, time and thermal conductivity. The index app stands for apparent. The PCM thermophysical properties in Equation 4.3 were considered solely phase dependent (Table 4.1).

The apparent specific heat curve was assumed to have the following form [5,9,24,36]:

$$\begin{aligned} C_{app} = \frac{dH}{dT} = \frac{d}{dT}\left[0.5 \times \lambda \times erf\left(\frac{T - T_m}{T_0}\right) + C_{PCM}(T - T_m)\right] \\ = \lambda \times \frac{exp\left(-\frac{T - T_m}{T_0}\right)^2}{T_0\sqrt{\pi}} + C_{PCM} \end{aligned} \tag{4.4}$$

where H ($J \cdot kg^{-1}$), T_m (K), λ ($J \cdot kg^{-1}$), and C_{PCM} ($J \cdot kg^{-1} \cdot K^{-1}$) are, respectively, the total enthalpy, the melting temperature, the latent heat, the specific heat and T_0 (K) is a variable associated to the mushy region. Identical mushy regions were assumed for all PCMs. Both melting and re-solidification processes (i.e. charge and discharge processes) were assumed to be described by the same apparent heat capacity relationship with temperature.

For the skin layers, the one-dimensional heat transfer was simulated according to equation 4.5, where the second term on the right-hand side represents the heat removed through blood circulation (only applied for dermis and subcutaneous layers [5,9,24]):

$$\rho C \frac{\partial T}{\partial t} = \frac{\partial}{\partial x} \cdot \left(k \frac{\partial T}{\partial x} \right) - G \rho_b C_b (T - T_c) \tag{4.5}$$

where the indexes b and c stand for blood and core, respectively. Blood perfusion rates (G) were assumed constant in dermis and subcutaneous layers (i.e. 1.25×10^{-3} s^{-1} [5,9,36]) and the blood density (ρ_b) was set at 1060 $kg \cdot m^{-3}$ for all skin layers.

A skin burn model was used to estimate the time for a second and third degree burns to occur. This was done following the initial work of Henriques [37], which tries to quantify the thermal damage to the skin through the so-called burn integral, obtained from the evolution of skin temperature over time. A second-degree burn at the epidermis/dermis interface was acknowledged when the Henriques' burn integral implied Ω values equal to unity (with the parameters from [38]). An identical procedure was done for the third degree burns, but at the dermis/ subcutaneous interface. The difference between both was considered the alarm time. It should be noted that different people may have different epidermis widths. However, this does not alter the skin temperature histories obtained as the width of the epidermis is very small compared to the width of the other layers.

At the initial time, the clothing layers were assumed to be at 34 °C, whilst throughout the simulation, the core body temperature was assumed constant at 37 °C. The body core temperature may vary somewhat over time; however, this

is unlikely to have a significant influence in the thermal performance of the FPC PCM due to its small change. The initial temperature of the different skin layers was assumed to vary linearly between 34 °C (epidermis – garment inner layer interface) and 37 °C (core; [5,24]).

The equations above (equations 4.1-4.5) were modeled in a FEM platform. A weak formulation of the problem was utilized to avoid numerical issues regarding property discontinuities along the different domains representing the different textile and skin layers.

4.2.4 Grid independence tests

Grid independence tests with regards in time and space were performed in order to obtain accurate results with good computational efficiency. Such tests were done considering a FPC PCM with 0.5 kg of barium hydroxide octahydrate that was exposed to a high – intensity scenario (84 $kW \cdot m^{-2}$), for an exposure time of 40 s. After the exposure, the firefighting garment was exposed to the environment simulating a post fire exposure phase. The meshes shown in Table 4.1 were considered for the grid independence tests (Figure 4.2a).

In the numerical procedure, an adaptive time step was calculated considering the backward differential method (function of maximum time step threshold) and a relative and absolute tolerance of 10^{-5}. For the time independence tests, different maximum time-step thresholds and tolerances were tested (Figure 4.2b and c).

As it can be seen from Figure 4.2, the difference in skin temperatures obtained between mesh 2 and mesh 3 is less than 0.05 °C (Figure 4.2a). Hence, mesh 2 was chosen as an adequate spatial mesh. Also, marginal difference in skin temperatures is attained when the time step tolerance is less than 10^{-5} (Figure 4.2b). A change in the maximum time step did not result in significant differences in the skin temperatures obtained (Figure 4.2c). Nevertheless, and due to the low computational cost, a maximum time step of 0.1 s was employed

for the high intensity exposure. For the medium and low- intensity, a maximum time step of 1 s was employed.

Table 4.3 – Meshes used in grid independence tests

Mesh number	No. of elements
Mesh 1	160 (100 in PCM layer)
Mesh 2	800 (500 in PCM layer)800 (500 in PCM layer)
Mesh 3	1600 (1000 in PCM layer)

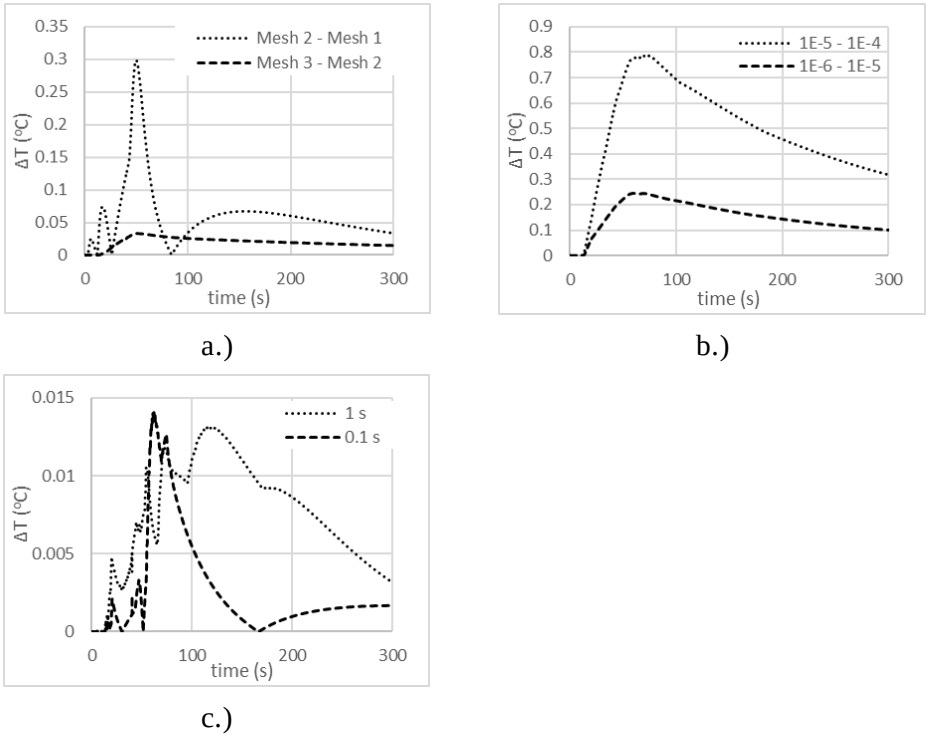

Figure 4.2 - Grid and time sensitivity tests for high intensity heat exposure (84 kW · m^{-2}): a.) Difference in temperature histories obtained at the skin (ΔT) for the meshes in Table 4.3 b.) Difference in temperature histories for the indicated time step tolerances c.) and for the maximum time step threshold.

4.2.5 Model validation

In our previous work [6], the model predictions of temperature histories were validated against experimental and numerical results found in the literature [14,24], obtained during the fire exposure phase. In the present study, the accuracy of the model to predict the cooling phase was evaluated by comparison of temperature predictions obtained from Ghazy ([31]; Figure 4.3). Ghazy [31] performed a numerical study on a typical firefighting garment assembly considering exposure and post-exposure phases. Temperature histories along the FFPC suit and skin layers over time were obtained (Figure 4.3).

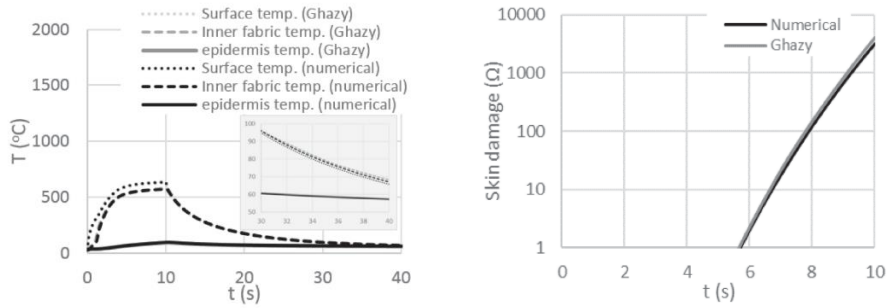

a.) b.)

Figure 4.3 - Temperature history comparison between numerical results and those obtained from Ghazy [31] for different position in the firefighting garment - skin system.

As shown in Figure 4.3a, differences in the temperature profiles obtained are negligible. The skin damage calculated at the epidermis/dermis surface is almost the same as that obtained by Ghazy [31] indicating that the current model is able to predict second degree burns accurately (Figure 4.3b).

4.3 Results and discussion

The mass that is incorporated in an FFPC needs to be minimized, as weight is a critical factor for the firefighter. Firstly, for the exposure phase, optimal/minimal (just to prevent a 2nd degree burn) PCM masses m_{PCM} (kg) for the different exposure heat flux intensities and durations (i.e. t_{exp}) were obtained

for each PCM (Section 4.3.1). For the post- exposure phase, the alarm time t_{alarm} (s) was calculated for the intended exposure heat flux intensities and durations (t_{exp}), taking into account also the effect of the ambient conditions (i.e. variable h_{amb}). Lastly, it was assumed that the firefighter doffs the PCM FPC during the resting phase (i.e. right after the exposure) and the PCM FPC cooling time $t_{cooling}$ (s) for the intended exposure times (t_{exp}) was obtained for the different PCMs (Section 4.3.3).

The masses shown below refer to an area coverage of 0.35 m^2, which corresponds approximately to the front upper body area of the firefighter [6].

4.3.1 PCM mass calculation during fire exposure

The optimal/minimum PCM mass (m_{PCM}) essentially depends on the PCM properties, as well as on the intended exposure intensity and duration (t_{exp}).

Figure 4.4 shows the minimum PCM masses needed for the firefighter to survive the fire exposure without burns (i.e. without 2nd degree burn), for the three exposure heat flux intensities.

For the FFPC suit without the PCM layer (not included in the figures), maximum exposure times (i.e. without 2nd degree burn) of 12 s, 34 s, and 55 s were obtained for the high – medium- and low- intensity heat exposures. If these values are compared with those of Figure 4.4, it can be concluded that there is a very significant increase of time to reach a 2nd degree burn when a PCM is used, particularly for the medium and low – intensity exposures

According to Figure 4.4, the required PCM mass (m_{PCM}) increases linearly with the intended exposure time (t_{exp}) for almost all exposure intensities. For example, for the low – intensity exposure (Figure 4.4c), sodium acetate trihydrate increases linearly from a mass requirement of ~0.2 to ~1.9 kg in order to increase exposure sustenance from 141 to 563 s, respectively. This tendency is in accordance with findings from previous works [6].

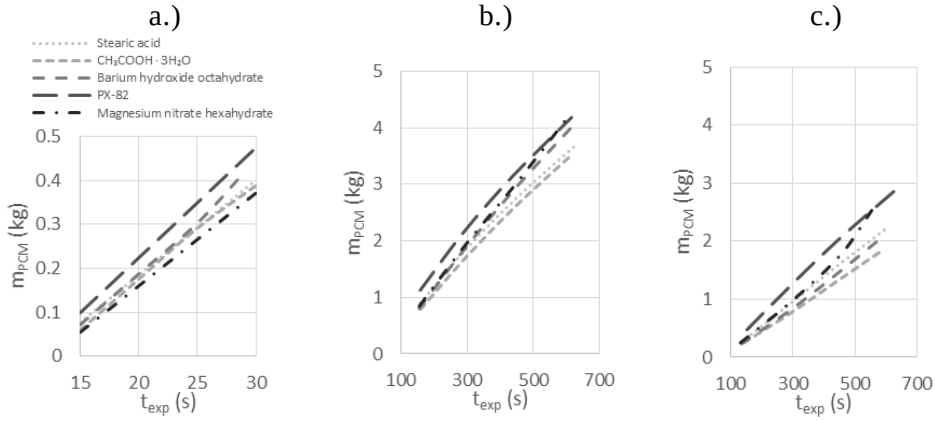

Figure 4.4 - Minimal PCM masses (m_{PCM}) obtained for different exposure times (t_{exp}) and indicated PCMs for a.) high - b.) medium- and c.) low - intensity heat exposures.

The best PCM choice is naturally the one that requires the lowest minimum mass (m_{PCM}), however, this choice depends on the intended exposure time (t_{exp}). For example, for the medium – intensity heat exposure scenario (Figure 4.4b), whilst magnesium nitrate hexahydrate might be the PCM with the lowest mass requirement for short exposure times (i.e. $t_{exp} < 150$ s), the contrary is true for longer exposure times (i.e. $t_{exp} > 150$ s). Furthermore, an oversight in the PCM choice can lead to a significantly increase in the firefighter load, particularly for higher exposure times (e.g. a maximum deviation of ~0.6 kg is obtained for 600 s; Figure 4.4b).

For the high- intensity heat exposure scenario (Figure 4.4a), the PCM with the lowest mass requirement is magnesium nitrate hexahydrate, for all t_{exp} considered. Even though, magnesium nitrate hexahydrate is the PCM with the lowest latent heat and the highest melting temperature, it has a significantly higher specific heat than the others (Table 4.1). In a high- intensity heat exposure, a significant amount of energy is stored in the PCM as sensible heat in the liquid phase. PX-82 is the PCM with the highest mass requirement because it has the lowest specific heat (1.6 $kJ \cdot kg^{-1} \cdot K^{-1}$). So, it can be concluded that the latent heat present does not influence the exposure times greatly for high – intensity short duration exposures. This puts into question whether or not the inclusion of a PCM is justified for high intensity short duration exposures such as these.

For the medium – intensity heat exposure scenario (Figure 4.4b), as less heat is accumulated in the sensible and more in the latent form, the PCM latent heat and melting temperature become more important on the minimal mass obtained. For a given mass, PCMs with higher latent heats and lower melting temperatures have the capacity to store greater amounts of energy at lower temperatures. So, the mass requirements for a given t_{exp} will be lower for such materials. sodium acetate trihydrate originates the lowest mass requirement. For t_{exp} = 600 s, the mass requirement for the PCM with the highest melting temperature and lowest latent heat (i.e. magnesium nitrate hexahydrate) is 4.1 kg whilst for sodium acetate trihydrate is 3.5 kg. Barium hydroxide octahydrate has a slightly higher latent heat, but a much higher melting temperature, hence the mass requirement, especially for higher t_{exp}, is greater (Figure 4.4b). For the low – intensity exposure, similar trends are registered (Figure 4.4c). Contrary to the medium intensity exposure, Barium hydroxide octahydrate originates a lower mass requirement than stearic acid. That is, the difference in melting temperatures between the two PCMs does not influence the mass requirements as much as the difference in latent heat, in this exposure intensity.

Hence, for the high- medium- and low-intensity heat exposures, magnesium nitrate hexahydrate and sodium acetate trihydrate are the PCMs with the lowest mass requirements respectively. To note that for the high – intensity exposure, the inclusion of a PCM might not be justified as most of the incoming heat is accumulated in the sensible form.

4.3.2 Alarm time during post-fire exposure

One of the benefits of incorporating a PCM in a firefighting suit is the accumulation of incoming heat energy at lower temperatures. This allows for extending the exposure time before a second-degree burn occurs as shown in Section 4.3.1. Despite this, the accumulated energy in the PCM is eventually released towards the environment and the firefighters' skin during the post-fire exposure. This exposes the firefighter to a third degree burnout risk which must be addressed.

Using the minimal masses calculated above (i.e. m_{PCM}), the alarm time (t_{alarm}), defined as the difference between times to second and third degree burnout, has been obtained as an indicator for the adequacy of a PCM choice for the post – fire exposure phase. Figure 4.5 shows that a PCM choice based on this criterion is heavily dependent on the exposure time considered (t_{exp}) as well as on the ambient conditions and exposure scenarios.

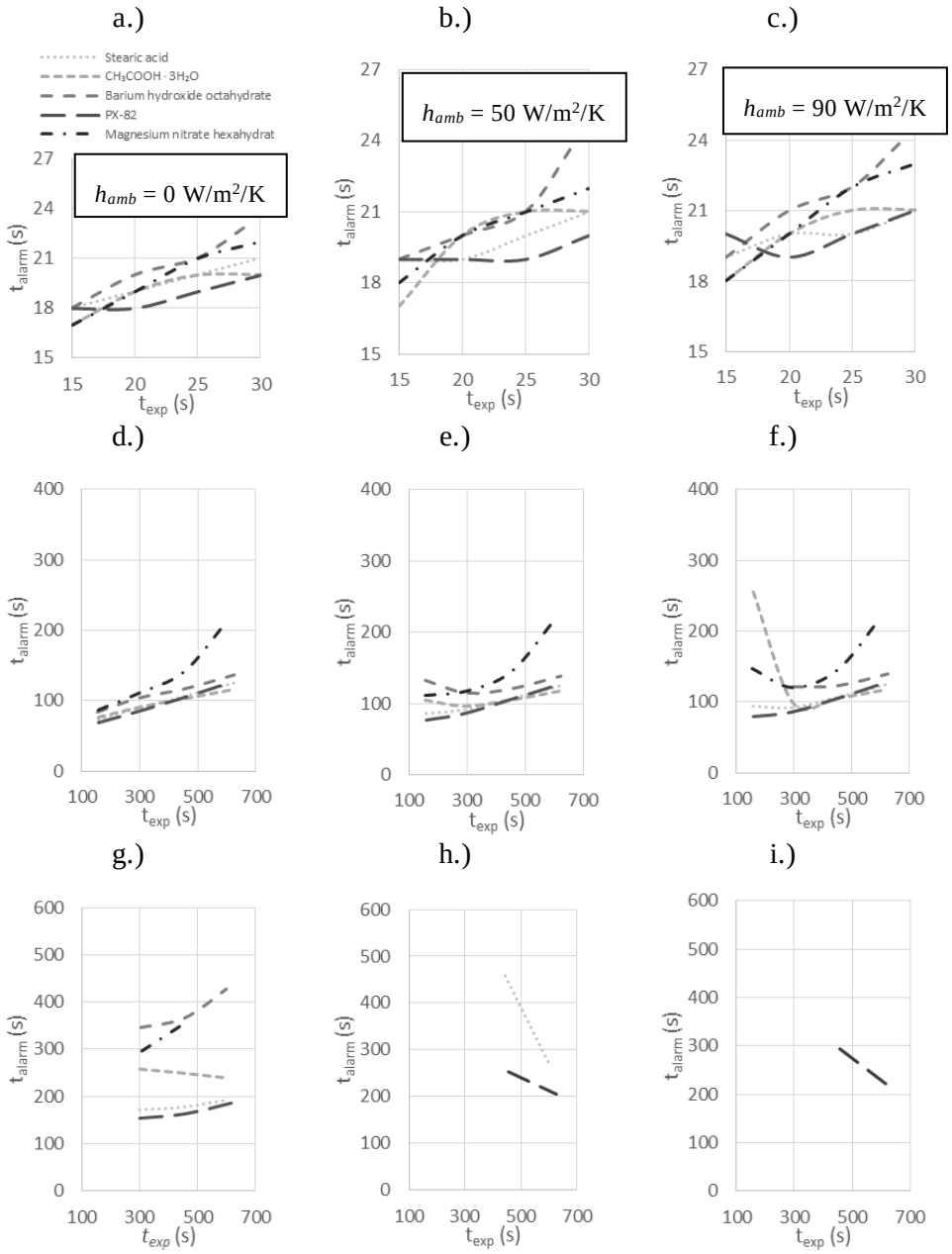

Figure 4.5 - Alarm times (t_{alarm}) obtained for different exposure times (t_{exp}) and indicated PCMs for the a-c.) high – d-f.) medium – g-i.) low intensity heat exposure, for the indicated h_{amb}.

Firstly, let us compare the alarm times of Figure 4.5 obtained for the high-intensity heat exposure (a-c) with a reference FFPC that does not contain a PCM layer. With the reference FFPC the obtained alarm times are 19 s, 20, and 21 s

for h_{amb} = 0, 50 and 90 $W \cdot m^{-2} \cdot K^{-1}$, respectively. These values are not far off when compared to the ones with PCM inclusion (i.e. Figure 4.5a-c). But, for the medium and low – intensity exposures however, it turns out that if a PCM layer is not included, the alarm time does not exist (i.e. no third degree burn is reached); the accumulated heat is smaller and it is mostly removed to the environment. However, it should be highlighted that the inclusion of a PCM allows for greater exposure times (it is possible to double the exposure time without any second degree burn occurring; Figure 4.4). With this in mind, again, consider the post fire scenarios after a high – intensity exposure (Figure 4.5a-c). For h_{amb} = 0 $W \cdot m^{-2} \cdot K^{-1}$, the alarm times obtained for all exposure durations are in the range of 18–24 s for all PCMs. The way t_{alarm} varies with t_{exp} is different for each PCM. For example, for PX-82, t_{alarm} stays constant for 15 s < t_{exp} < 20 s and then rises almost linearly to a t_{alarm} of 20 s (Figure 4.5a). On the other hand, if barium hydroxide octahydrate is the incorporated PCM, t_{alarm} increases to a maximum of 20 s and then stabilizes. These variations can be explained essentially by the nature of the Henriques burn criteria [37]. The Henriques burn criteria depends on the temperature histories obtained at the skin for a given incorporated PCM with enough mass to sustain a given t_{exp}. For different t_{exp}, different temperature histories are obtained. If these are very different from each other, this will enhance the influence of the exponential nature of the Henriques integral on the time to burn obtained and hence on the alarm time. This is also true for other h_{amb}. Little variation on the t_{alarm} exists when h_{amb} is increased to 50 $W \cdot m^{-2} \cdot K^{-1}$ and 90 $W \cdot m^{-2} \cdot K^{-1}$. However, there are slight variations in the nature of the tendencies of t_{alarm} with t_{exp}, for each respective PCM.

For the medium – intensity exposure, the tendencies registered are different (Figure 4.5d-f). Consider the case for h_{amb} = 0 $W \cdot m^{-2} \cdot K^{-1}$ (Figure 4.5d). For all PCMs, there is a general increase of t_{alarm} with t_{exp}. This is due to the increase of the thermal resistance provided by the incorporated PCM. For magnesium nitrate hexahydrate however, an exponential rise occurs for t_{exp} > 450 s. This is because solid PCM might be present in the PCM after the exposure [6]. This also occurs for the remaining h_{amb}. For h_{amb} = 50 $W \cdot m^{-2} \cdot K^{-1}$, apart from there being a general difference in the t_{alarm} obtained for all PCMs and t_{exp}, differ-

ences in the tendencies exist for low t_{exp}. For example, for Barium hydroxide octahydrate, t_{alarm} decreases with t_{exp} for 150 s < t_{exp} < 350 s. It reaches a minimum for a t_{exp} of 350 s. Notice however that such minimum is still greater than the t_{alarm} obtained for h_{amb} = 0 $W \cdot m^{-2} \cdot K^{-1}$, for the same t_{exp}. If a lower t_{exp} is considered, less heat is stored in the PCM FPC and hence it cools down faster due to heat rejection towards the ambient originating less heat flowing towards the skin and causing skin damage over time. When t_{exp} is big enough so that the rejected heat towards the environment does not affect the heat flowing to the skin, a minimum t_{alarm} is reached. Similar phenomena are observed for h_{amb} = 90 $W \cdot m^{-2} \cdot K^{-1}$. The absence of t_{alarm} values for a given t_{exp} simply means that a third degree burn for that PCM and t_{exp} is not reached. This happens because the rejected heat towards the environment is considerable (e.g. Barium hydroxide octahydrate, t_{exp} < 300 s,, Figure 4.5f).

Figure 4.5g-i show the t_{alarm} obtained for the different t_{exp} and PCMs for the low – intensity exposure. As can be seen, for h_{amb} = 0 $W \cdot m^{-2} \cdot K^{-1}$, no t_{alarm} is obtained for t_{exp} < 300 s, for any of the PCMs. The incoming energy from the exposure is much lower due to the lower intensity when compared to the medium- exposure intensity. For h_{amb} = 50 $W \cdot m^{-2} \cdot K^{-1}$ and 90 $W \cdot m^{-2} \cdot K^{-1}$, the occurrence of a third degree burn for any PCM and t_{alarm} becomes almost non – existent except for a few cases. Hence, the cases of greatest benefit of adding a PCM are those where no alarm times are registered for the medium and low – intensity heat exposures (e.g. Figure 4.5g; 100 < t_{exp} < 300 s; for all PCMs). Otherwise the inclusion of a PCM layer on one hand will allow for greater exposure times (Figure 4.4), but on the other hand, it will also promote the occurrence of third degree burns causing the firefighter to have a limited time to remove the firefighting garment (i.e. t_{alarm}). However as shown above, this limited time is considerable, especially for medium- and low- intensity heat exposures.

4.3.3 Cooling time during resting phase

Another important aspect that influences PCM choice is the time the FPC PCM takes to cool down, so that the firefighter can don it again. Different PCMs will result in different cooling times. PCMs with higher melting temperatures and lower latent heats will cool faster. In this section, it is assumed that the firefighter takes off the PCM FPC when the exposure ends (i.e. at t_{exp}).This implies that the inner garment surface is no longer exposed to the skin, but to the environment. With this in mind, cooling times were calculated for the various PCMs for the different scenarios (Figure 4.6).

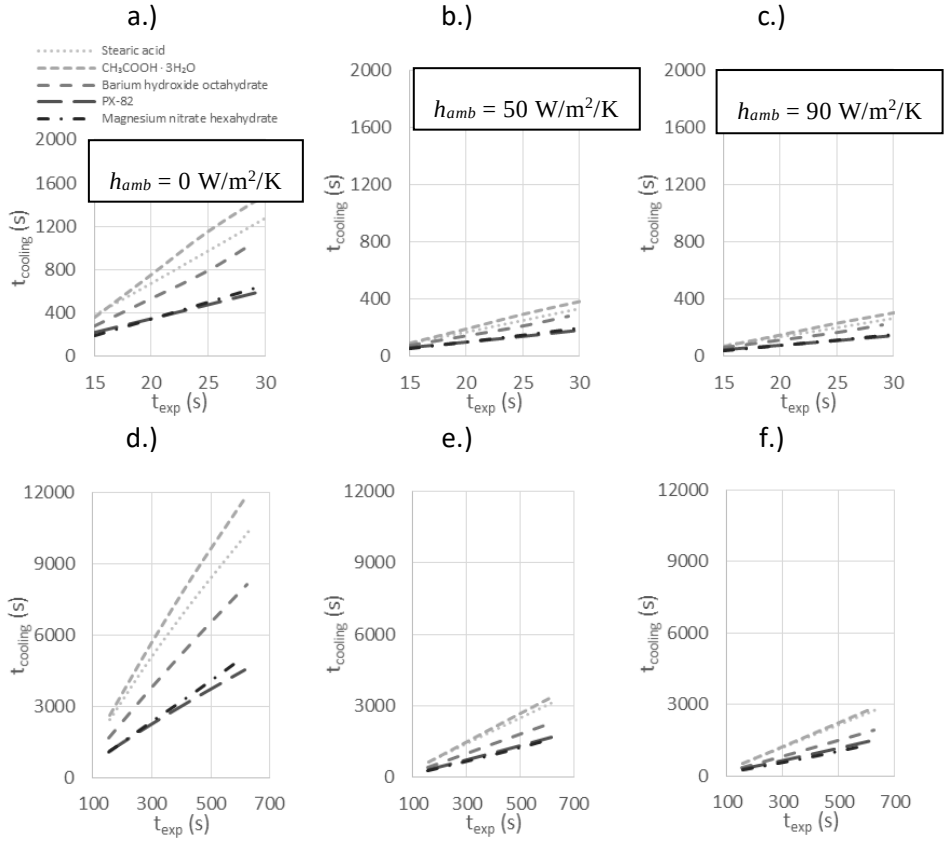

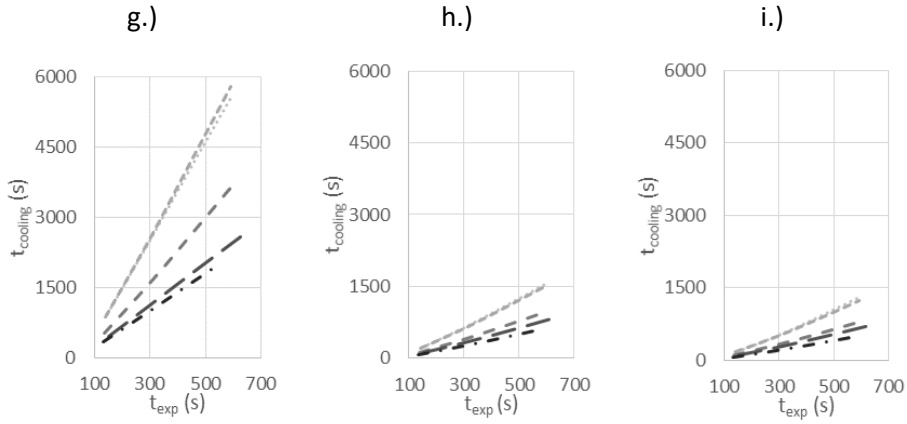

Figure 4.6 - Cooling times ($t_{cooling}$) obtained for different exposure times (t_{exp}) and indicated PCMs for the a-c.) high – d-f.) medium – g-i.) low intensity heat exposure, for the indicated h_{amb}.

For the exposure time (t_{exp}) and wind conditions (i.e. h_{amb}) ranges considered in the present study (Figure 4.6), an FFPC without PCM would take between 32–175 s, 22–145 s, and 17–122 s to cool down, for the high – medium and low – intensity heat exposures respectively. Notice that, by rough inspection these values are significantly smaller than the ones obtained when a PCM layer is considered (Figure 4.6).

PCM FPC tend to take long times to cool down especially when no wind is present (h_{amb} = 0 $W \cdot m^{-2} \cdot K^{-1}$). Even if the firefighter takes out the protective clothing in a chilled environment, the firefighter will have to wait a considerable time in order for it to cool down. For example, for the medium – intensity heat exposure scenario and no wind conditions (Figure 4.6d), for t_{exp} = 300 s, cooling times ($t_{cooling}$) vary between 2192 and 5606 s for all PCMs. The reason for such substantial cooling times is due to the presence of latent heat in the PCM. However, when the protective clothing is left in a windy environment, cooling times can drop significantly. For example, at moderate wind conditions (h_{amb} = 50 $W \cdot m^{-2} \cdot K^{-1}$), the cooling times referred above drop to 675–1464 s (Figure 4.6e). Windy conditions may be due to natural or forced convection. For example, blower fans may be available in the fire trucks nearby for cooling down purposes. However, from a certain h_{amb} upwards, the cooling times only decrease marginally. As an example, consider the case when very windy

conditions are present (i.e. h_{amb} = 90 $W \cdot m^{-2} \cdot K^{-1}$); the cooling times referred above only further drop to 554 s-1204 s (Figure 4.5f)). When h_{amb} becomes significant, the cooling time obtained is essentially determined by the thermal resistance to heat transfer of the PCM FPC. Hence, there is no point in increasing the wind speed.

Thus, it becomes clear that submitting the protective clothing to high speed cooling winds may drastically decrease the cooling time, up to a certain point. Another thing to point out is the significant difference in the cooling times obtained, for the different PCMs. To note from the example above, that this difference is almost 4 – fold when h_{amb} = 0 $W \cdot m^{-2} \cdot K^{-1}$ and drops to about 2-fold when h_{amb} = 90 $W \cdot m^{-2} \cdot K^{-1}$. This shows that PCM choice has less influence in the cooling time for higher h_{amb} (higher wind speeds), and this is understandable because the heat is rapidly dissipated towards the environment, rendering the transient heat transfer phenomena in the PCM negligible. But, even so, for increasing h_{amb}, the cooling times of the different PCMs tend to diverge for higher t_{exp}; for example, for the medium – intensity heat exposure when h_{amb} = 0 $W \cdot m^{-2} \cdot K^{-1}$ and t_{exp} = 150 s, PCM cooling times range from 1087 -2643 s whilst for t_{exp} = 600 s, they range from 4574 - 11828 s. This tendency is simply explained by the increase in PCM mass present in the FFPC, allowing for a greater heat storage in it, and hence a bigger influence of its properties on the cooling time.

Speaking about the PCM properties, for all exposure scenarios and ambient environments considered, the incorporation of magnesium nitrate hexahydrate tends to result in the lowest cooling time with a few exceptions (Figure 4.6). In fact, the PCMs are ordered in the figure by decreasing cooling times, for all exposure scenarios and exposure times. For example, for the low – intensity heat exposure scenario, when no air movement is considered (Figure 4.6g), sodium acetate trihydrate, stearic acid, barium hydroxide octahydrate and PX-82, result in cooling times, in the t_{exp} range of about 150–600 s, between 935–5638 s, 875–5794 s, 521–3702 s, 463–2572 s respectively, whilst magnesium nitrate hexahydrate results in a cooling time between 329 and 2023 s. This order is inversely related with the melting temperatures of the respective PCMs. That is, magnesium nitrate hexahydrate having the highest melting temperature (T_m) of

89 °C, results in the lowest $t_{cooling}$, followed by PX -82 with a T_m of 82 °C and barium hydroxide octahydrate, stearic acid, and sodium acetate trihydrate each having a T_m of 78 °C, 58 °C and 54 °C respectively. Hence, the melting temperature strongly affects the $t_{cooling}$. This was expected, since higher melting temperatures allow for a greater temperature gradient between the PCM and environment. The melting temperature becomes specially significant when the latent energy in the PCM FPC is substantial and also for high values of PCM masses (and consequently high t_{exp}). This further explains the huge discrepancy of obtained cooling times for high t_{exp}, for the different PCMs.

Thus, for most exposure intensities and durations, magnesium nitrate hexahydrate would be the PCM which results in the lowest cooling time, and hence would satisfy the best criterion. Other PCMs can be chosen depending on the time the firefighter has to recover during the resting period.

4.4 Conclusions

Numerical simulations were conducted to study the effect of PCM choice and optimal mass on the thermal behavior of a PCM firefighting suit, considering a dynamic scenario of fire exposure, post-fire exposure and resting phase. The following specific conclusions were obtained:

- For a high – intensity (84 $kW \cdot m^{-2}$) and short duration exposure, the inclusion of a PCM might not be justified as most heat is accumulated in the sensible form. The addition of a material with a high specific heat could provide enough protection without the need for it to change phase.
- For a medium ($12kW \cdot m^{-2}$) and low-intensity (5 $kW \cdot m^{-2}$) long duration exposures, sodium acetate trihydrate is the PCM with lowest mass requirements due to its high latent heat and low melting temperature. For exposures in the range of ~150–600 s, sodium acetate trihydrate masses of ~1 kg–3.5 kg and ~0.5–2 kg should be sufficient to provide full protection during the exposure, for medium- and low– intensity exposures respectively. If a different PCM is

considered, the required mass should in principle not be very far off the ranges of PCM masses analysed in the present study, as long as full melting is verified during the exposure and before a second – degree burn is reached. Hence, they can for example be used as initial mass estimates for a potential PCM that has not been considered in tthe present study.

- Regarding the post – fire exposure, for low exposure times, sodium acetate trihydrate tends to originate the highest alarm times. Whilst for high exposure times, magnesium nitrate hexahydrate tends to originate the highest.
- For medium and low-intensity exposures, wind strength (i.e. h_{amb}) has a major influence in the alarm time obtained, especially for PCMs with low melting temperature and high latent heat such as sodium acetate trihydrate and barium hydroxide octahydrate.
- The cooling of a PCM FPC is strongly correlated to the melting temperature of the PCM in consideration. A PCM such as magnesium nitrate hexahydrate originates low cooling times whilst sodium acetate trihydrate is exactly the opposite. Big differences between the cooling times are obtained for low h_{amb}. For high h_{amb}, such differences become negligible.

The data shown above can help a PCM FPC designer in the initial stages of research and development. Tangible guidelines and estimates of key parameters are provided associated to the PCM choice, and the PCM FPC performance.

Acknowledgments

This work was supported by national funds through FCT –Fundação para a Ciência e a Tecnologia, I.P., within the scope of the project UIDB/00532/2020 as well as by PCIF/SSO/0106/2018 - Project for “Development of an innovative

firefighter's coat", funded by national funds through FCT/MCTES (PIDDAC). Fonseca acknowledges the financial support provided by FCT through the PhD Grant PD/BD/ 135097/2017.

References

[1] A.M. Raimundo, A.R. Figueiredo, Personal protective clothing and safety of fire- fighters near a high intensity fire front, Fire Saf. J. 44 (2009) 514–521, https://doi. org/10.1016/j.firesaf.2008.10.007.

[2] A. Shaid, L. Wang, R. Padhye, The thermal protection and comfort properties of aerogel and PCM-coated fabric for firefighter garment, J. Ind. Text. 45 (2016) 611–625, https://doi.org/10.1177/1528083715610296.

[3] F.L. Zhu, Q.Q. Feng, R.T. Liu, B.G. Yu, Y. Zhou, Enhancing the thermal protective performance of firefighters' protective fabrics by incorporating phase change ma- terials, Fibres Text. East. Eur. 23 (2015) 68–73.

[4] M. Fu, W. Weng, H. Yuan, Effects of multiple air gaps on the thermal performance of firefighter protective clothing under low-level heat exposure, Text. Res. J. 84 (2014) 968–978, https://doi.org/10.1177/0040517513512403.

[5] H. Phelps, H. Sidhu, A mathematical model for heat transfer in fire fighting suits containing phase change materials, Fire Saf. J. 74 (2015) 43–47, https://doi.org/ 10.1016/j.firesaf.2015.04.007.

[6] A. Fonseca, T.S. Mayor, J.B.L.M. Campos, Guidelines for the specification of a PCM layer in firefighting protective clothing ensembles, Appl. Therm. Eng. 133 (2018) 81–96, https://doi.org/10.1016/j.applthermaleng.2018.01.028.

[7] H.L. Phelps, S.D. Watt, H.S. Sidhu, L.A. Sidhu, Using phase change materials and air gaps in designing fire fighting suits: a mathematical investigation, Fire Technol. (2018), https://doi.org/10.1007/s10694-018-0794-z.

[8] G.N. Mercer, H.S. Sidhu, A theoretical investigation into phase change clothing benefits for firefighters under extreme conditions, Chem. Prod. Process Model. 4 (2009), https://doi.org/10.2202/1934-2659.1349.

[9] Y. Hu, D. Huang, Z. Qi, S. He, H. Yang, H. Zhang, Modeling thermal insulation of firefighting protective clothing embedded with phase change material, Heat Mass Transf. 49 (2012) 567–573, https://doi.org/10.1007/s00231-012-1103-x.

[10] S. Mondal, Phase change materials for smart textiles - An overview, Appl. Therm. Eng. 28 (2008) 1536–1550.

http://www.sciencedirect.com/science/article/B6V1Y- 4PJ0538-3/1/57e5bbc8e42d18e28f62d9c18dc49c53.

[11] K. Pielichowska, K. Pielichowski, Phase change materials for thermal energy sto- rage, Prog. Mater. Sci. 65 (2014) 67–123, https://doi.org/10.1016/j.pmatsci.2014. 03.005.

[12] V. Tesař, J. Kordík, Energy storage in macro-capsules for thermal comfort garments, J. Energy Storage. 25 (2019) 100842, , https://doi.org/10.1016/j.est.2019.100842.

[13] E. Oró, E. de Jong, L.F. Cabeza, Experimental analysis of a car incorporating phase change material, J. Energy Storage 7 (2016) 131–135, https://doi.org/10.1016/j. est.2016.05.003.

[14] H. Hamdan, N. Ghaddar, D. Ouahrani, K. Ghali, M. Itani, PCM cooling vest for improving thermal comfort in hot environment, Int. J. Therm. Sci. 102 (2016) 154–167, https://doi.org/10.1016/j.ijthermalsci.2015.12.001.

[15] C. Chou, Y. Tochihara, T. Kim, Physiological and subjective responses to cooling devices on firefighting protective clothing, Eur. J. Appl. Physiol. 104 (2008) 369–374, https://doi.org/10.1007/s00421-007-0665-7.

[16] M. Gasperin, D. Juricić, The uncertainty in burn prediction as a result of variable skin parameters: an experimental evaluation of burn-protective outfits, Burns. 35 (2009) 970–982, https://doi.org/10.1016/j.burns.2008.12.018.

[17] D.A. Torvi, T.G. Threlfall, Heat transfer model of flame resistant fabrics during cooling after exposure to fire, Fire Technol. 42 (2006) 27–48, https://doi.org/10. 1007/s10694-005-3733-8.

[18] G. Song, W. Cao, F. Gholamreza, Analyzing stored thermal energy and thermal protective performance of clothing, Text. Res. J. 81 (2011) 1124–1138, https://doi. org/10.1177/0040517511398943.

[19] S. Guowen Song, R. Paskaluk, E.M. Sati, J.D. Crown, M.A. Dale, Thermal protective performance of protective clothing used for low radiant heat protection, Text. Res. J. 81 (2011) 311–323, https://doi.org/10.1177/0040517510380108.

[20] Y. Su, J. He, J. Li, Modeling the transmitted and stored energy in multilayer pro- tective clothing under low-level radiant exposure, Appl. Therm. Eng. 93 (2016) 1295–1303, https://doi.org/10.1016/j.applthermaleng.2015.10.089.

[21] M. Gašperin, Đ. Juriˇ, B. Musizza, I. Mekjaviˇ, A model-based approach to the evaluation of flame-protective garments, 47 (2008) 198–210. doi:10.1016/j.isatra. 2007.12.003.

[22] H. Phelps, H. Sidhu, L. Sidhu, Modelling heat transport in protective fire fighting clothing containing phase change materials, Chemeca, Perth, Western Australia, 2014.

[23] Y. Su, J. Li, G. Song, The effect of moisture content within multilayer protective clothing on protection from radiation and steam, Int. J. Occup.

Saf. Ergon. 24 (2018) 190–199, https://doi.org/10.1080/10803548.2017.1321890.

[24] G.N. Mercer, H.S. Sidhu, Mathematical modelling of the effect of fire exposure on a new type of protective clothing, Anziam J. 49 (2008) 289–305.

[25] J. Pereira da Cunha, P. Eames, Thermal energy storage for low and medium tem- perature applications using phase change materials - a review, Appl. Energy 177 (2016) 227–238, https://doi.org/10.1016/j.apenergy.2016.05.097.

[26] P. Udayraj, A. Talukdar, R. Das, Alagirusamy, Heat and mass transfer through thermal protective clothing - a review, Int. J. Therm. Sci. 106 (2016) 32–56, https://doi.org/10.1016/j.ijthermalsci.2016.03.006.

[27] L.K. McCarthy, M. Marzo, The application of phase change material in fire fighter protective clothing, Fire Technol. 48 (2012) 841–864, https://doi.org/10.1007/ s10694-011-0248-3.

[28] A. Ghazy, D.J. Bergstrom, Numerical simulation of heat transfer in firefighters' protective clothing with multiple air gaps during flash fire exposure, Numer. Heat Transf. Part A Appl. 61 (2012) 569–593, https://doi.org/10.1080/10407782.2012. 666932.

[29] J. Li, M. Tian, Personal thermal protection simulation under diverse wind speeds based on life-size manikin exposed to flash fire, Appl. Therm. Eng. 103 (2016) 1381–1389, https://doi.org/10.1016/j.applthermaleng.2016.04.155.

[30] B.W. Butler, Wildland firefighter safety zones: a review of past science and summary of future needs, Int. J. Wildl. Fire. 23 (2014) 295–308, https://doi.org/10.1071/ WF13021.

[31] A. Ghazy, Numerical study of the air gap between fire-protective clothing and the skin, J. Ind. Text. 44 (2014) 257–274, https://doi.org/10.1177/ 1528083713483784.

[32] A. Ghazy, Air gap in protective clothing during flash fire exposure, University of Saskatchewan (2011).

[33] J.R. Lawson, W.D. Walton, N.P. Bryner, F.K. Amon, Estimates of thermal properties for fire fighters' protective clothing materials, 2005.

[34] V.R. Voller, C.R. Swaminathan, B.G. Thomas, Fixed grid techniques for phase change problems: a review, Int. J. Numer. Methods Eng. 30 (1990) 875–898, https://doi.org/10.1002/nme.1620300419.

[35] Y. Dutil, D.R. Rousse, N. Ben Salah, S. Lassue, L. Zalewski, A review on phase- change materials: mathematical modeling and simulations, Renew. Sustain. Energy Rev. 15 (2011) 112–130, https://doi.org/10.1016/j.rser.2010.06.011.

[36] D. Huang, Y. Li, L. Tong, H. Yang, H. Zhang, Modeling Heat Transfer in Phase Change Material Bedded Firefighting Protective Clothing under Fire Exposure, in: L. Shengcai, W. Weiye, A. Ying (Eds.), Proc. 2010 Int. Symp. Saf. Sci. Technol., 2010: pp. 921–926.

[37] F.C. Henriques, Studies of thermal injury V. The predictability and the significance of thermally induced rate processes leading to irreversible epidermal injury, Arch. Pathol. 43 (1947) 489–502.

[38] L.N. Zhai, J. Li, Prediction methods of skin burn for performance evaluation of thermal protective clothing, Burns 41 (2015) 1385–1396, https://doi.org/10.1016/ j.burns.2015.02.019.

[39] Lara Devgan, Satyanarayan Bhat, S. Aylward, Robert Spence, Modalities for the Assessment of Burn Wound Depth, J. Burns Wounds 5 (2006) 7–15.

5

Chapter 5

The impact of water on firefighter protective clothing thermal performance and steam burn occurrence in firefighters

5

The impact of water on firefighter protective clothing thermal performance and steam burn occurrence in firefighters

Presence of water in FPCs tends to be quite common and can influence the temperatures in the FPC quite substantially. As information regarding this topic lacks in the literature and is critical to the design of PCM FPCs, such was of interest to investigate. The text in this chapter resulted in the following publication:

Fonseca Malaquias, A., Neves, S. F., & Campos, J. B. L. M. (2022). The impact of water on firefighter protective clothing thermal performance and steam burn occurrence in firefighters. Fire Safety Journal, 127(November 2021). https://doi.org/10.1016/j.firesaf.2021.103506

Abstract

Exposure to oscillating heat fluxes while having variable water contents in the thermal protective clothing (T.P.C) is possible in a real firefighting scenario. The occurrence of steam burns becomes inevitable in certain conditions which are still unidentified in the literature. In light of such, in this study, the effect of water distribution on thermal protective clothing (T.P.C) performance is studied for various environmental conditions (i.e., fixed and transient values of heat flux). A numerical approach is used to simulate heat and mass transport in the T.P.C.. Parametric studies are performed, where the exposure heat flux (0–80 kW/m^2) and initial quantities of water in the T.P.C. are varied and correlated with second–degree burn times. The presence of water in the outer shell increases second-degree burn times, while water in the inner layer has the opposite effect for high heat fluxes. For the tested heat fluxes, burns obtained are majorly of a scald nature. The results generated allow for identifying environmental and protective clothing conditions where steam burns may

become a potential hazard. This study can directly impact the proceedings for firefighters to take in certain environmental conditions and aid in the design of more effective firefighting protective suits.

5.1 Introduction

Firefighters face high heat flux and humid scenarios, exposing them to potential heat stress illness and skin burns [1–3]. During fire combat, firefighters may suffer burns caused by direct heat from the flame and high-temperature vapor reaching the skin and condensing [4,5].

High humid environments in firefighting make the task of designing adequate firefighting clothing challenging. The presence of water in firefighting garments is frequent, either due to firefighters sweating during strenuous exercise or due to external sources [3,6,7]. Water presence in a firefighting garment assembly significantly alters its thermal performance. However, the current evaluation norms do not consider transient moisture effects when measuring firefighting clothing performance [8].

In the meantime, various researchers have, mostly experimentally, studied the influence of moisture in firefighting clothing performance.

Su et al. [5] studied the effects of different initial moisture contents in firefighting clothing thermal performance. Two thermal inners with different weights were initially incorporated with various amounts of water (0–100 % wt. of turnout system), simulating the presence of sweat in the firefighting jacket. Afterward, the layers were exposed to radiative heat flux of 8.5 kW/m^2. The authors increased the initial water content and a convex trend was noticed for second-degree burn time (i. e., a minimum occurs at 50 % wt. of turnout system). A similar conclusion was reached, for third-degree burn time, with the minimum verified at 15 % wt.

He et al. [9] used a modified thermal protective performance (T.P.P.) test apparatus to study the exposure of pre-moistened firefighting jackets (0–70 % wt. of turnout system) to a radiative heat flux of 21 kW/m^2. The authors also studied the influence of air gap size and location. Second-degree burn time decreased with an increase in moisture content for most air gap configurations. A minimum trend with water content was also observed, at 20 % wt. of moisture content for most cases. Barker et al. [10] also experimentally studied the effect of different moisture contents initially present (0–100 % wt. of turnout system) in the thermal inner, on the second-degree burn time, for a heat flux of 6.3 kW/m^2. However, contrary to the previously mentioned studies, more complicated moisture effects were observed; a maximum burn time for 50 % wt. moisture incorporation, superior to that of the dry textile (i.e., 0 % wt.).

Lawson et al. [7] utilized four different two-layered firefighting jackets to study the influence of moisture. The outer shell and thermal inners were either assumed to be dry, conditioned at specific atmospheric conditions, or in their saturated state. The fabric system was exposed to low–radiant flux (10 kW/m^2) or high-radiant flux (83 kW/m^2). The authors showed that water in the outer layer was beneficial for high heat fluxes but prejudicial in the inner layer. For low heat fluxes, however, water in the thermal inner was advantageous towards thermal performance. They also highlighted the dependence of the results on the textile materials used in the experiments.

Keiser & Rossi [11] incorporated moisture in the thermal barrier (278%–696 % wt. of thermal barrier) or underwear (70%–176 % wt. of underwear), and exposed a 5–layered firefighting jacket to a radiative flux of 5 kW/m^2 for 10 min. The authors concluded that the presence of moisture decreases the temperatures in the garment. The same group performed a study using X-ray radiography [4] and validated the temperature sensor-based approach to measure, indirectly, the humidity concentrations in the previous study. They confirmed that the moisture initially present in outer layers might re-condense near the skin, originating steam burns.

Onofrei et al. [12] also studied the effect of moisture presence on thermal performance for low–heat fluxes. They incorporated the moisture in the thermal inner (120%–200 % wt. of thermal inner) of a 3 or 4 layer firefighting jacket exposed to a low radiant heat flux of 1.1 kW/m^2. They found that the presence of moisture decreases temperatures in the protective clothing over the exposure time. Zhang et al. [6] studied the effect of the moisture in the outer shell and in the thermal inner of a 3-layered firefighting garment when exposed to a heat flux of 15.4 kW/m^2. The authors noticed an increase in second-degree burn time with outer shell moisture but a diminishment when moisture was also present in the thermal inner.

From the studies above, precise conclusions about the influence of moisture on thermal performance under diverse heat exposures are hard to obtain. This difficulty is due to several issues, including different material properties, experimental conditions, and set-ups. Also, contradictory results between some works exist, and the reasons why are not well understood.

In parallel, several authors have developed numerical models to understand better heat and mass transfer mechanisms in firefighting garments. Chitrphiromsri [13] incorporated a heat and moisture transfer model to study heat transfer in a flash fire scenario (84 kW/m^2 for 4 s) with the presence of liquid water in a typical 3– layered firefighting jacket. The authors assumed an initial moisture content present in all 3 –layers corresponding to 10% of the saturation point of each respective layer.

Prasad et al. [3] proposed a heat and moisture transfer model for a firefighting jacket and validated it for an exposure of 2.5 kW/m^2 for 750 s, assuming an initially wet thermal inner. The authors showed a thermal performance enhancement with moisture incorporation in the thermal inner compared to dry textiles. Su et al. [14] numerically studied the heat and moisture transport in a 3 –layer firefighting jacket exposed to a low heat flux (8.5 kW/m^2 for 300 s followed by a 200 s cooling period). The authors concluded that while moisture

decreases the heat flux towards the skin, it increases thermal hazard due to higher stored energy in the garment. Huang et al. [15] numerically studied the relative humidity (0–90% R.H) effect on the thermal performance of a 3 – layer protective firefighting jacket exposure to a flux of 5 kW/m^2. They found a positive trend between relative humidity and second–degree burn time. Łapka et al. [16] outlined a heat and moisture transport model for a three-layer firefighting protective clothing fabric. The model accounted for fabric movement and its influence on heat and water vapor transport in the garment.

In resume, in the literature, most studies in the area are experimental. It is hard to achieve coherent conclusions in these studies as different experimental set-ups and garments, measuring techniques, and protocols are utilized. No systematic study has been conducted considering a wide range of heat flux scenarios, nor real exposure scenarios. Hence any comparison, and trends, between the studies are not conclusive. Also, current numerical models in the literature lack details regarding the condensation phenomena in the textile when mass fluxes are significant. No results have been shown or discussed for cases when the different garment layers contain different saturation levels of free water. This aspect is essential to consider, as it can happen in real firefighting scenarios.

Hence, in light of such, an extensive and systematic numerical study was carried out. Firstly, the apart effects of the initial moisture content in the outer shell and thermal inner were studied for a wide variety of heat fluxes. Then, both layers were assumed to have different initial water quantities simultaneously. The effect of such water distribution in the thermal performance was analyzed for various heat flux exposures. Lastly, to apply the concepts, a live-fire training exercise consisting of a highly transient heat flux exposure was considered, and the respective effects on temperature and water profiles were discussed.

5.2 Materials and methods

5.2.1 Problem description

A typical 3-layered firefighting protective clothing (F.F.P.C) was assumed (Figure 5.1). Also, a 3 –layered skin model was used to simulate the firefighter's presence in contact with the F.F.P.C.

Initially, a firefighter wearing the F.F.P.C. is exposed to an external thermal hazard (boundary 1, Figure 5.1). Consequently, the temperature in the layers of the garment starts rising. Liquid water initially present in the garment due to sweat or ambient exposure starts evaporating and diffusing, reducing the temperature rate increase. Some of this vapor may be rejected towards the ambient (i.e., evaporative cooling) or diffuse and re-condense near the skin, liberating condensation heat. After some exposure time, the firefighter may suffer skin burns due to the direct heat from the thermal hazard or moisture re-condensation near the skin or a combination of both.

Core body temperature was assumed constant at 37 °C (boundary 2, Figure 5.1) throughout the exposure. Firefighters may have a higher core temperature when entering a fire scenario (e.g., 38 °C); however, such is unlikely to influence second-degree burn times due to the thermal resistance between the core and the epidermis (2*). Fabrics' properties are shown with their respective sources in Table 5.1. Some of the properties missing had to be estimated to perform numerical simulations.

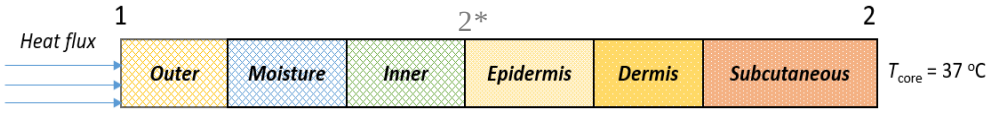

Figure 5.1- F.F.P.C. skin system used in the numerical simulations with the indication of the boundary numbers.

The moisture distribution effect on the thermal protective performance was studied, assuming a uniform initial moisture distribution in each fabric layer. Similar water distribution was taken by Chitrphiromsri [13]. The initial temperature at the skin layers was assumed to have a linear profile between the core temperature (37 °C) and skin temperature (34 °C). The garment's initial temperature and relative humidity were assumed to be 34 °C and 65 %, respectively.

Table 5.1 – Properties of the various layers consisting of the firefighting protective clothing.

Property	Outer shell	Moisture Barrier	Thermal inner	Source
Thickness (w) mm	0.39	0.45	2.24	[6]
Density (ρ_{ds}) kg/m^3	1460	1460	1440	[6]
Specific heat (c_{ds}) J/(kg·K)	1086	1086	1421	[17]
Thermal conductivity (k_{ds}) W/(m·K)	0.25	0.25	0.21	[17,18]
Fiber volume fraction (ε_{ds})	0.36	0.16	0.09	Estimated [6,19]
Tortuosity (τ)	2.32	2.87	1.32	Estimated [12]
Fiber diameter (d_f) µm	15	15	15	[6,20]
Regain at 65 % RH	0.0485	0.0485	0.0397	[14]
Diffusivity of water in fiber (D_f) m^2/s	6×10^{-14}	6×10^{-14}	6×10^{-14}	[13]
Proportionality constant for liquid water sorption in fibres (γ_{ls}) kg/m^3	5×10^{-4}	5×10^{-4}	5×10^{-4}	[13]

5.2.2 Mathematical model and assumptions

5.2.2.1 Textile model

A model similar to the one suggested by Chitrphiromsri [13], based on Gibson's model [21], was assumed to perform the one-dimensional numerical analysis. The most important assumption is that homogeneous phases can well describe the heterogeneous porous hygroscopic structure of the textile layer with different materials (i.e., gas, solid, liquid) [21]. Heat and moisture transport occur throughout and between the phases where moisture may transfer (e.g., water from gas to liquid phase). Using Gibson's model, problems associated with geometric domain definition are eliminated, promoting computer efficiency.

The model in the textile layers comprises one global energy balance and three species transport balances (i.e., water transport in the gas, fiber, and liquid phase). Fourier type heat transfer is assumed to simulate the heat transport in the firefighting garment. Hence for a hygroscopic medium, where water sorption and condensation may take place, and assuming heat conduction to be the effective heat transfer mechanism, the global energy balance is written as follows:

$$\rho_{eff} C_{eff} \frac{\partial T}{\partial t} + \frac{\partial}{\partial x}\left(-k_{eff} \frac{\partial T}{\partial x}\right) - \dot{m}_{gs}\left(\Delta h_{vap} + \Delta h_l\right) - \dot{m}_{gl} \Delta h_{vap} - \dot{m}_{ls} \Delta h_l = 0 \quad (5.1)$$

$$\rho_{eff} = \varepsilon_{bw} \rho_w + \varepsilon_\gamma \rho_\gamma + \varepsilon_{ds} \rho_{ds} + \varepsilon_l \rho_w \quad (5.2)$$

$$C_{p,eff} = \frac{\varepsilon_{bw} \rho_w c_{p,w} + \varepsilon_\gamma \left(\rho_a c_{p,a} + \rho_v c_{p,v}\right) + \varepsilon_{ds} \rho_{ds} c_{p,ds} + \varepsilon_l \rho_w c_{p,w}}{\rho_{eff}} \quad (5.3)$$

$$k_{eff} = k_\gamma \left\{ \frac{\varepsilon_\gamma k_\gamma + [1 + \varepsilon_{bw} + \varepsilon_{ds} + \varepsilon_l] k_\sigma}{\varepsilon_\gamma k_\sigma + [1 + \varepsilon_{bw} + \varepsilon_{ds} + \varepsilon_l] k_\gamma} \right\} \quad (5.4)$$

where, ρ_{eff}, C_{eff}, k_{eff}, $\dot{m}_{gs}$, $\dot{m}_{gl}$, $\dot{m}_{ls}$, Δh_{vap} and Δh_l represent the effective density (kg/m^3), effective specific heat (J/(kg K)), effective thermal conductivity (W/(m K)), gas sorption/desorption rate (kg/(m^3·s)), vaporization/condensation rate (kg/(m^3 s)), liquid sorption/desorption rate (kg/(m^3·s)), water vaporization heat (J/kg), and liquid sorption/desorption heat (J/kg), respectively. ε represents the phase volume fraction, and the subscripts *bw, w, γ, ds,* and *l* stand for bounded water, water, gas, fiber, and liquid, respectively.

The first term on the left-hand side of equation 5.1 accounts for the heat accumulation in the garment. The second term accounts for the conductive heat fluxes, while the third, fourth and fifth terms account for the latent heat associated with water sorption/desorption, vaporization/condensation and liquid sorption/desorption into the fibers, respectively. k_σ and k_γ represent the solid and gas phases thermal conductivity respectively, and they are calculated as follows:

$$k_\sigma = \frac{k_w \rho_w \varepsilon_{bw} + k_{ds} \rho_{ds} \varepsilon_{ds} + k_w \rho_w \varepsilon_l}{\rho_w \varepsilon_{bw} + \rho_{ds} \varepsilon_{ds} + \rho_w \varepsilon_l} \tag{5.5}$$

$$k_\gamma = \frac{k_v \rho_v + k_a \rho_a}{\rho_v + \rho_a} \tag{5.6}$$

where subscripts *v, a*, refer to the water vapor and air, respectively.

Water vapor transport in the gas phase is calculated as follows:

$$\frac{\partial(\varepsilon_\gamma \cdot \rho_v)}{\partial t} + \frac{\partial}{\partial x}\left(-D_{eff} \frac{\partial \rho_v}{\partial x}\right) + \dot{m}_{gs} + \dot{m}_{gl} = 0 \tag{5.7}$$

$$D_{eff} = \frac{\varepsilon_\gamma \cdot D_a}{\tau} \tag{5.8}$$

$$D_a = 2.23 \cdot 10^{-5} \left(\frac{T}{273.15}\right)^{1.75} \tag{5.9}$$

where ρ_v, D_{eff}, D_a, and τ stand for water vapor density (kg/m^3), effective diffusivity throughout the textile layer (m^2/s), water vapor diffusivity in the air (m^2/s), and fabric tortuosity, respectively.

The first term of equation 5.7 refers to vapor accumulation in the gas phase, the second term accounts for diffusive water vapor transport, and the third and fourth terms account for sorption/desorption and condensation/evaporation of water, respectively.

The liquid water and bounded water transport balances are as follows:

$$\rho_w \frac{\partial \varepsilon_l}{\partial t} = \dot{m}_{sl} + \dot{m}_{vl} \tag{5.10}$$

$$\rho_w \frac{\partial \varepsilon_{bw}}{\partial t} = \dot{m}_{gs} + \dot{m}_{ls} \tag{5.11}$$

As can be seen, there is no convective or diffusive transport of liquid and bounded water. Only terms associated with water phase changes are considered. They are calculated as follows:

$$\dot{m}_{gs} = \frac{8 D_f \rho_{ds}}{d_f^2} \left(Regain_{eq} - Regain_f \right) \tag{5.12}$$

where D_f, d_f, and *Regain* represent water diffusivity in the clothing fiber (m^2/s), fiber diameter (m), and fabric regain, respectively.

$$\dot{m}_{gl} = \begin{cases} c \cdot \left(\rho_v - \rho_{v,sat} \right) \\ h_m a_s \frac{\varepsilon_l}{\varepsilon_l^{cr}} \left(\rho_v - \rho_{v,sat} \right) \end{cases} \tag{5.13}$$

where c represents a correction factor (i.e., 10^5 s^{-1}) which accounts for the instantaneous condensation when the pores become saturated with water vapor. The variable ε_l^{cr} represents the critical liquid water fraction for which water movement starts occurring in the pores (defined as $\varepsilon_l^{cr} = s \cdot \varepsilon_g^{init}$ where s stands for the saturation level in which liquid water movement starts occurring in the textile). In this work, the saturation levels were defined as 0.77, 0.1, 0.27 for the outer, moisture, and thermal inner, respectively. The variables h_m and a_s represent the mass transfer coefficient between the fiber and the surrounding air (m/s), and the specific surface area (m^{-1}) is defined as:

$$a_s = \frac{4\varepsilon_{ds}}{d_f} \tag{5.14}$$

$$\dot{m}_{ls} = h_m a_s \gamma_{ls} \frac{\varepsilon_l}{\varepsilon_l^{cr}} \left(\frac{Regain_{eq}}{Regain_f} - 1 \right) \tag{5.15}$$

where γ_{ls} is the sorption proportionality constant of liquid water in the fiber; the subscripts *eq* and *f* stand for equilibrium and fabric, respectively.

The fabric regain is calculated as follows:

$$Regain_f = \frac{\varepsilon_{bw}\rho_w}{\varepsilon_{ds}\rho_{ds}} \tag{5.16}$$

and the equilibrium regain by:

$$\begin{aligned} Regain_{eq} = \frac{\varepsilon_{bw}|_{eq} \cdot \rho_w}{\varepsilon_{ds}\rho_{ds}} \\ = 0.578 \cdot Regain_{f(\emptyset=65\,\%)} \cdot \emptyset \\ \cdot [(0.321 + \emptyset)^{-1} + (1.262 - \emptyset)^{-1}] \end{aligned} \tag{5.17}$$

where Ø is the relative humidity.

Lastly, the volume fractions of each phase must satisfy the following constraint:

$$\varepsilon_{ds} + \varepsilon_{bw} + \varepsilon_\gamma + \varepsilon_l = 1 \tag{5.18}$$

Other thermodynamic relations regarding the model are below:

$$p_v = \frac{\rho_v R T}{M_{H_2O}} \tag{5.19}$$

$$\rho_\gamma = \rho_v + \rho_a \tag{5.20}$$

$$p_a = p_\gamma - p_v \tag{5.21}$$

where p_v, p_v, R and M_{H_2O} stand for the total pressure (Pa), partial vapor pressure (Pa), universal gas constant (J/(mol·K)) and water molecular mass (kg/mol), respectively.

5.2.2.2 Skin model

The Pennes' bio-heat model was assumed to describe the heat exchanges in the firefighter's skin layers. The following equations describe heat transport in the epidermis, dermis and subcutaneous:

$$\rho_{ep} C_{ep} \frac{\partial T}{\partial t} = \frac{\partial}{\partial x}\left(k_{ep} \frac{\partial T}{\partial x}\right) \tag{5.22}$$

$$\rho_{derm} C_{derm} \frac{\partial T}{\partial t} = \frac{\partial}{\partial x}\left(k_{derm} \frac{\partial T}{\partial x}\right) - G\rho_b c_b (T - T_c) \tag{5.23}$$

$$\rho_{subcut} C_{subcut} \frac{\partial T}{\partial t} = \frac{\partial}{\partial x}\left(k_{subcut} \frac{\partial T}{\partial x}\right) - G\rho_b c_b (T - T_c) \tag{5.24}$$

where G, ρ_b, c_b and T_c represent the volumetric blood flow, blood density (kg/m^3), specific heat (J/(kg·K)) and core body temperature (K), respectively. The subscripts *ep*, *derm*, and *subcut* stand for epidermis, dermis and subcutaneous, respectively. The properties of the skin layers are in Table 5.2.

Like other studies in the field, Henriques' burn criterion was utilized to calculate second-degree burn time [22].

Table 5.2 - Properties of skin layers taken from [13].

Property	epidermis	dermis	Subcutaneous
Thermal conductivity (k) W/(m·K)	0.255	0.523	0.167
Specific heat (c_p) J/(kg·K)	3600	3400	3060
Density (ρ) kg/m^3	1200	1200	1000
Thickness (w) mm	0.08	2	10
Blood perfusion rate (G) s^{-1}	1.25×10^{-3}	1.25×10^{-3}	1.25×10^{-3}

5.2.3 Boundary and initial conditions

Donnelly et al. [23] divided the firefighting scenario into four thermal classes that a firefighter can face. These classes are categorized based on the heat flux and air temperature. In this work, an effort to consider heat flux exposures covering all types was made. Total heat fluxes in the range from 5-80 kW/m^2 were selected to simulate pre-flashover and flash fire conditions (Neumann condition imposed at boundary 1, Figure 5.1). A constant core body temperature of 37 °C (Dirichlet condition imposed at boundary 2, Figure 5.1) and ambient temperature of 34 °C with 65 % R.H. were considered throughout the simulation. A Newmann boundary condition in the outer shell for mass transfer between the garment and the environment was assumed (equation 5.25; imposed at boundary 1, Figure 5.1), while a mass insulation condition at the boundary facing the skin (2*, Figure 5.1) was set:

$$k_c(\rho_v - \rho_{amb}) = -D_{eff,outer} \left.\frac{\partial \rho_v}{\partial x}\right|_{x=0} \tag{5.25}$$

where k_c represents the mass transfer coefficient (0.021 m/s) [13].

The initial conditions assumed are shown in Table 5.3.

Table 5.3 - Initial conditions assumed for the firefighting protective clothing

Property	Outer shell	Moisture Barrier	Thermal Inner
$\varepsilon_{l,init}$	Distribution (0 to 0.27) (i.e. wetness level 0 to 1)	0	Distribution (0 to 0.25) (i.e. wetness level 0 to 1)
$\varepsilon_{b,init}$	0.025	0.007	0.008
T_{init}	34 °C	34 °C	34 °C
$\emptyset_{init}$	0.65	0.65	0.65

The initial temperature at the skin is assumed to be a linear gradient between 34 °C at the epidermis surface and 37 °C at the subcutaneous core. Note that the distributions mentioned for the initial water fractions correspond to wetness levels between 0 and 1 for the outer shell and thermal inner.

5.2.4 Grid independence tests

To ensure solution accuracy and promote computational efficiency, grid convergence tests concerning time and space were performed. Figure 5.2a shows the difference in skin temperature histories obtained with the different indicated meshes in Table 5.4. As can be seen, spatial mesh independence is obtained with Mesh 2. The same can be said regarding vapor densities, vaporization/condensation and sorption rates near the skin (Figure 5.2c, e and g). A backward differentiation formula solver was used to choose the best time step, utilizing a relative tolerance as a criterion. The best relative tolerance obtained was 10^{-4} and a residual-based termination criterion was used (Figure 5.2b, d, f and g).

Table 5.4 - Meshes used to test spatial mesh independence

Mesh no.	Elements in textile	Elements in skin
Mesh 1	50	5
Mesh 2	500	50
Mesh 3	1000	100

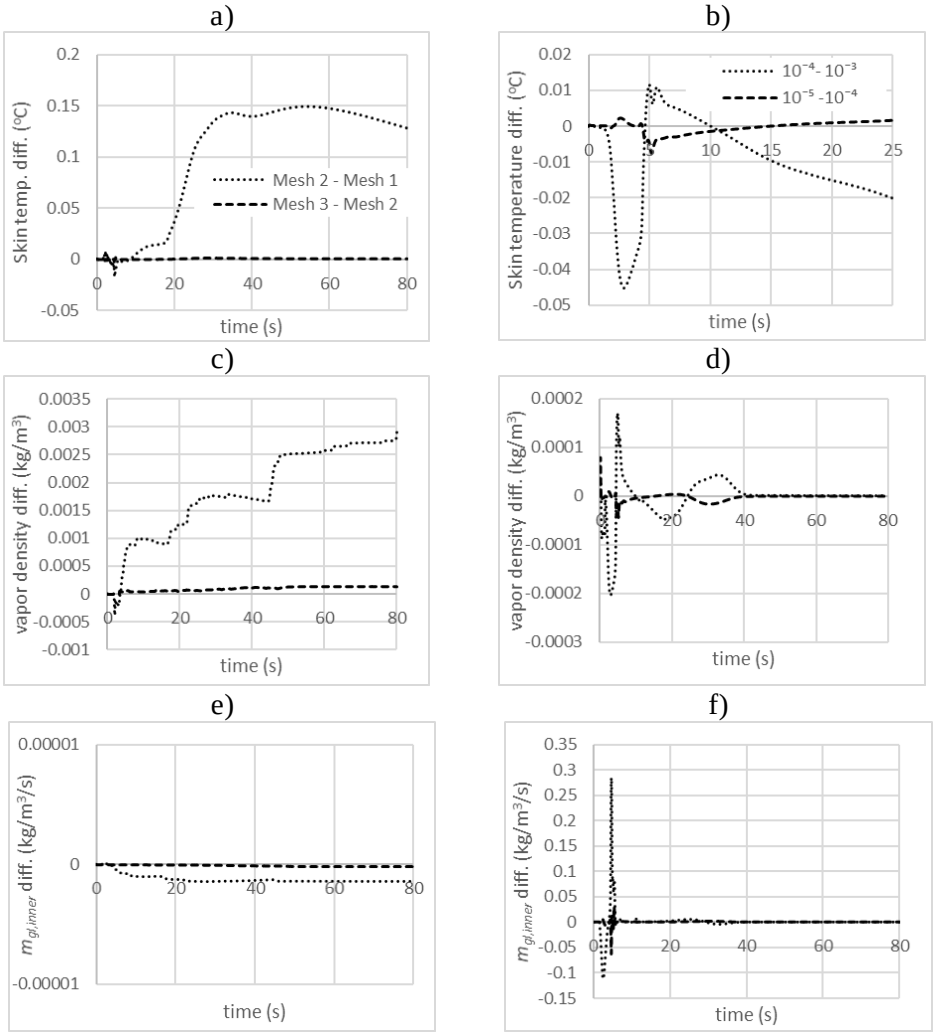

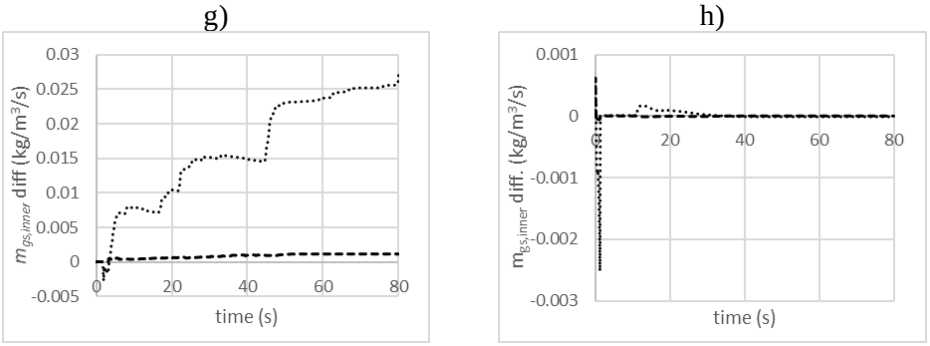

Figure 5.2 - Differences in the: a) skin temperature; c) water vapor densities; e) vaporization/condensation rate and; g)sorption rate histories near the skin, obtained with the indicated meshes. Differences in the: b) skin temperature d); water vapor densities; f) vaporization/condensation rate and; h) sorption rate histories near the skin, obtained with the indicated relative tolerances.

5.2.5 Model validation

The textile model was validated with the experimental results outlined in Ref. [6]. The firefighting jacket used in the experiments consists of an outer shell (93 % meta-aramid/5 % para-aramid/2 % antistatic), moisture barrier (P.T.F.E./nonwoven meta-aramid), and thermal inner (100 % para-aramid).

Before a heat exposure, the outer shell or/and thermal inner were initially pre-wetted. Then, a total heat flux of 15.4 kW/m^2 was irradiated on the outer shell through a quartz tube heat source. A skin simulant sensor was used to register the heat flux reaching the backside of the fabric. Such a sensor imitates the thermal properties of the skin. Thus its registered heat flux is then used as an input to calculate second–degree burn times using equations 5.22 – 5.24 and utilizing the properties outlined in Table 5.2 [6,24].

Figure 5.3 shows the obtained experimental and numerical skin temperatures and heat fluxes at the skin simulant sensor in the case where the outer shell fabric was initially saturated with water. Saturation corresponds to a wetness level of unity according to the wetting protocol utilized in Ref. [6].

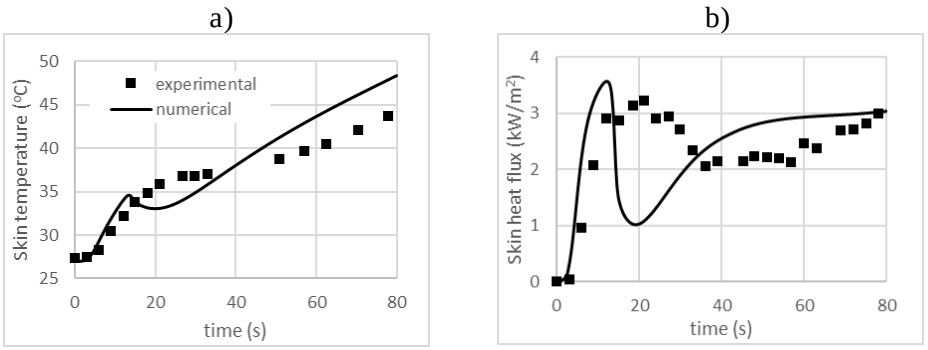

Figure 5.3 - Comparison between experimental [6] and numerical results for radiant exposure of 15.4 kW/m^2 for an outer shell initially saturated with water; a) skin temperature and b) skin heat flux over time.

As can be seen, good agreement between numerical and experimental data is obtained. Initially, the firefighting garment is exposed to a heat hazard, which causes the moisture present in the outer shell to evaporate, forming steam. This steam is rejected towards the environment or diffuses throughout the textile layers, eventually reaching the skin. As the skin is at a much lower temperature than the heated steam, the vapor is sorbed in the fiber of the textile, close to the skin (i.e., thermal inner), and it also condenses, liberating latent heat and thus raising the skin temperature (i.e., Figure 5.3a and b, $5 < t < 15$ s). Once the moisture in the outer shell has fully evaporated, there is no more steam diffusing towards and condensing near the skin. The water present near the skin starts to evaporate as the temperatures in the textile are high due to the condensation which happened previously near the skin (i.e., evaporative cooling). This creates a sudden temperature fall (Figure 5.3a, $15 < t < 20$ s). In this phase, deviations from the experimental data in skin temperatures and skin heat fluxes are observed. Several reasons could be behind this deviation. The condensate could have dripped off the garment or wicked into the suit's outer layers, which are not considered in the numerical model. For $t > 20$ s, the skin temperature steadily rises due to the temperature increase in the fire protective clothing. At the same time, the evaporation of the condensate restrained in the thermal inner layer also takes place.

5.3 Results

5.3.1 Water presence in the outer shell

Figure 5.4a shows the second–degree burn times for the various exposure intensities and outer shell wetness levels considered. An increase in second-degree burn time with outer shell wetness level can be observed for all heat exposures considered. For example, for a heat exposure of 5 kW/m^2, a rise in the outer shell wetness level from 0 to 1 causes an increase in second-degree burn time from 71.7 s to 116.5 s. Such represents an increase of 62 % relative to the dry case (Figure 5.4b). However, the increase in second-degree burn time tends to be minor for higher heat fluxes. For example, considering exposure of 80 kW/m^2, the second-degree burn time rises from 17.8 s to 19.3 s when the outer shell wetness level increases from 0 to 1. According to Figure 5.4b, such represents a relative increase of 8 % compared to the dry case.

This minor increase in the protective effect for high heat fluxes is primarily due to the heat liberated by vapor condensation near the skin. Figure 5.5a shows the second-degree burn time when such heat is neglected in the simulations. As shown and expected, second-degree burn times are significantly greater, demonstrating how latent heat impacts thermal performance. For example, for a heat exposure of 5 kW/m^2, considering an initially saturated outer shell, the time to second-degree burn increases from 116.5 s to 136 s (Figure 5.4a and Figure 5.5a). Figure 5.5b illustrates the relative increase in second–degree burn time to show this effect clearly. As can be seen, there is a more significant increase in thermal performance with an increase in wetness level when compared to the original case (i.e., Figure 5.4b) for all heat exposures. For example, considering exposure of 80 kW/m^2, a relative increase in second-degree burn time of 37 % is achieved when steam condensation and sorption in the garment are not considered (Figure 5.5b). Instead, only an 8 % increase for a fully saturated outer shell is observed (Figure 5.4b).

In resume, for high-intensity exposures, both the steam condensation and sorption are responsible for at least a 29 % decrease in T.P.C. thermal performance. Such steam condensation tends to happen in the layers closest to the skin. Figure 5.4c shows the fraction of liquid water contained in the inner layer at the time of the second-degree burn (i.e., $f_{inner,\ 2nd}$). As can be seen, there is a decrease in the fraction of remaining liquid water with an increase in initial wetness level for all heat exposures considered. This behavior happens because a higher amount of water is initially present, (i.e. higher outer shell wetness level). And, as the amount of water condensing near the skin before a second-degree burn is more or less the same, its percentage representation decreases. Also, note that for heat fluxes above 20 kW/m^2, the remaining liquid water fraction tends to be independent of the heat flux exposure considered. This behavior happens because steam sorption and condensation in the thermal inner become major determinants to skin temperature rise and damage. Hence, when the presence of water in the outer shell is significant, the T.P.C could be designed in such a way as to mitigate the diffusion and condensation of water in the inner layers of the garment. In this way, significant gains in thermal performance can be achieved.

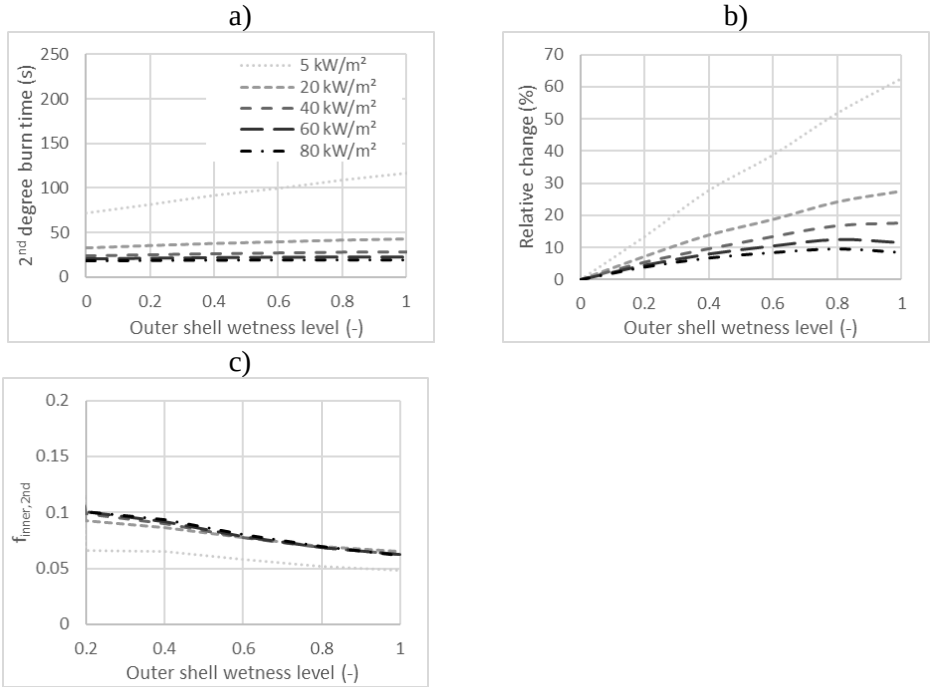

Figure 5.4 - a) second-degree burn times obtained for the indicated outer shell wetness levels and heat flux exposure intensities; b) relative change in second-degree burn time when compared to the dry case for corresponding wetness levels and heat fluxes; c) Remaining free water fraction ($f_{inner,2nd}$) in the thermal inner at the time when a second-degree burn occurs.

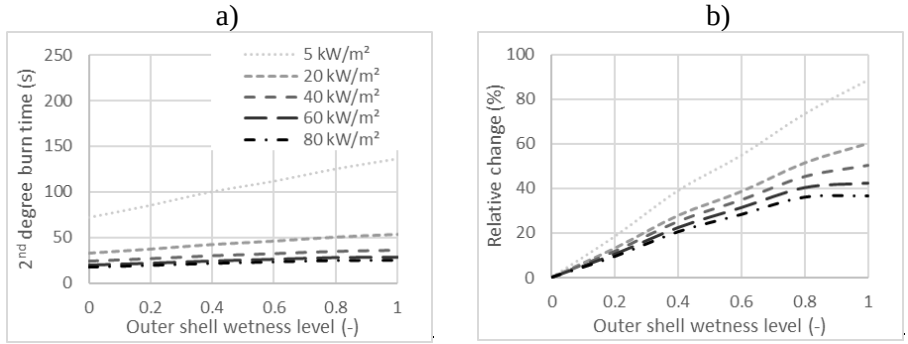

Figure 5.5 - Results obtained when condensation and sorption heat in the textile fiber are neglected: a) second-degree burn times for indicated heat fluxes and wetness levels in the outer shell; b) relative changes in second-degree burn times when compared to the dry case for the indicated outer shell wetness levels and heat exposures.

When a firefighter faces a low heat flux exposure, water in the outer shell increases second-degree burn time. However, the increase in thermal performance is marginal for higher heat fluxes due to more significant steam condensation near the skin. Hence, T.P.C. thermal performance can be considered independent of the water content in the outer shell for high heat fluxes. Steam burns may become common in such conditions. If this steam is prevented from reaching the skin by, for example, using less porous textiles [25], a significant rise in thermal performance can be achieved.

5.3.2 Water presence in the thermal inner

Figure 5.6a shows the second-degree burn times obtained for the indicated heat flux scenarios when the inner layer has different initial water content. For low heat flux exposures (i.e., 5 kW/m^2), second-degree burn time increases non - linearly with initial wetness level increase. This behavior is clearly observed when relative changes in second-degree burn times are considered (Figure 5.6b). There is a sharp linear increase in second-degree burn time for low heat fluxes (i.e., < 5 kW/m^2) for low initial water content. The linear increase is due to the onset of the latent heat associated with water desorption and vaporization. Then, the second-degree burn time decreases between wetness levels of 0.2 and 0.4, reaching a minimum, and steadily rises again (Figure 5.6b). This increase is justified because, when a large amount of water is present in the thermal inner, some of it will not evaporate, remaining in the clothing even after the firefighter obtains a second-degree burn (e.g., for a wetness level of 1, the inner layer contains around 60 % of the initial water content; Figure 5.6c). At the same time, water evaporation happens further away from the skin, and less vapor diffuses and condenses at the skin. This phenomenon occurs because the pores become more saturated as the initial presence of water increases.

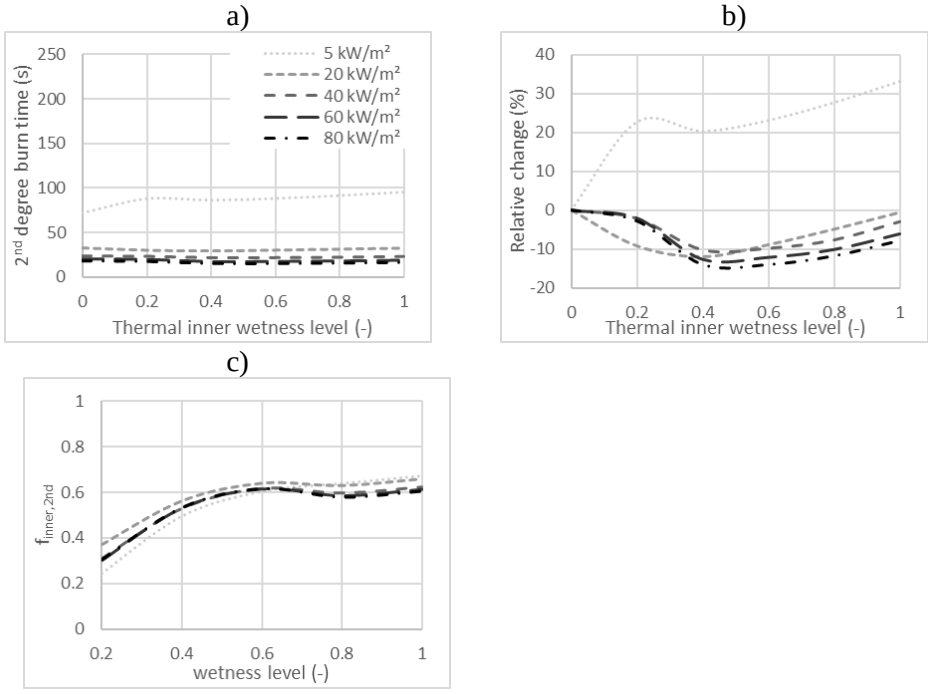

Figure 5.6 - a) second-degree burn times obtained for the indicated thermal inner wetness levels and heat flux exposure intensities; b) relative change in second degree burn time when compared to the dry case for corresponding wetness levels and heat fluxes; c) Remaining free water fraction ($f_{inner,2nd}$) in the thermal inner at the time when a second-degree burn occurs.

Second-degree burn time presents similar relationships for more significant heat fluxes, reaching a minimum at about 0.4 wetness level for heat exposures in the range of 20 to 80 kW/m^2 (Figure 5.6b).

However, above a certain wetness level, the second-degree burn time decreases relative to the dry case (e.g., Figure 5.6b, 20 kW/m^2, wetness level > 0.2). The quantity of steam that reaches the skin and condenses is significant enough to cause more heat transfer towards it. For greater wetness levels (above 0.5), similar to low heat fluxes, water is still present in the thermal inner after a second-degree burn time (Figure 5.6c). Phenomena associated with water vaporization and moisture condensation are behind the observed second-degree burn time tendencies.

To emphasize and show more clearly the steam phenomena discussed above, the relative and second-degree burn times without condensation phenomena

should again be analyzed (Figure 5.7). The impact of moisture condensation on thermal performance is quite significant. For example, for an exposure of 20 kW/m^2 and initially saturated thermal inner, moisture sorption and condensation are responsible for a 225 % decrease in the thermal performance.

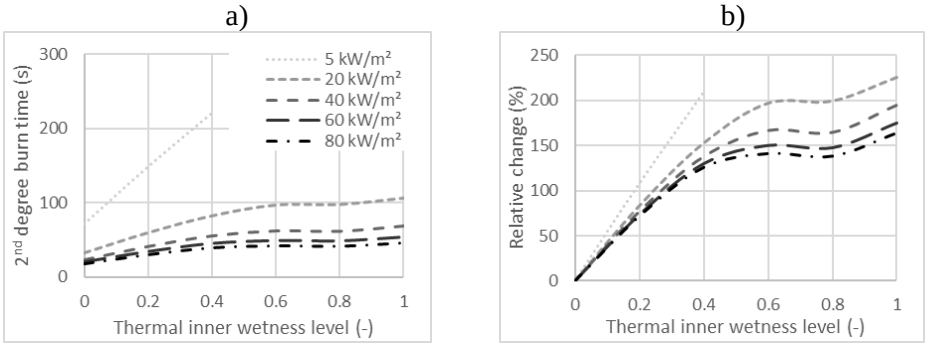

Figure 5.7 - Results obtained when condensation and sorption heat in the textile fiber are neglected: a) second-degree burn times for indicated heat fluxes and wetness levels; b) relative changes in second-degree burn times compared to the dry case for the indicated outer shell wetness levels and heat exposures.

Lastly, the liquid fraction present after the exposure in the thermal inner is quite significant, tending to a plateau of 0.6 with increasing wetness levels (Figure 5.6c). This behavior happens because steam sorption and condensation in the thermal inner become determinants for skin temperature rise and damage.

In conclusion, water presence in the thermal inner during firefighting can be prejudicial towards the firefighter for high heat fluxes. Solutions to mitigate such hazards and enhance thermal performance would have to ensure that the generated steam would be expelled to the environment rather than allowed to reach the firefighters' skin. An alternative would be, for example, to introduce a thermal inner with higher evaporative resistance but also a lower fiber fraction to not allow for moisture accumulation, decreasing steam burn risk.

5.3.3 Water presence in the outer shell and thermal inner

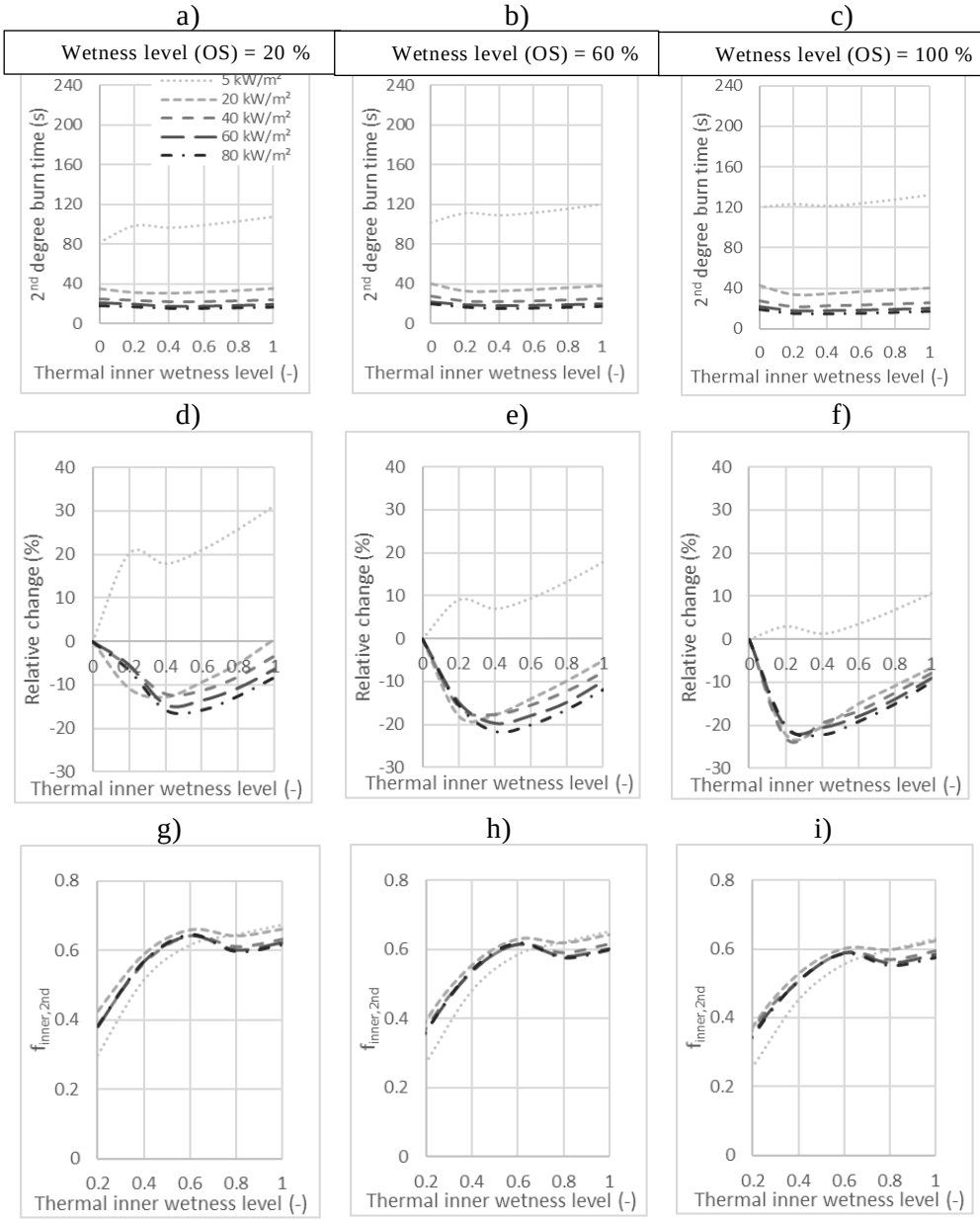

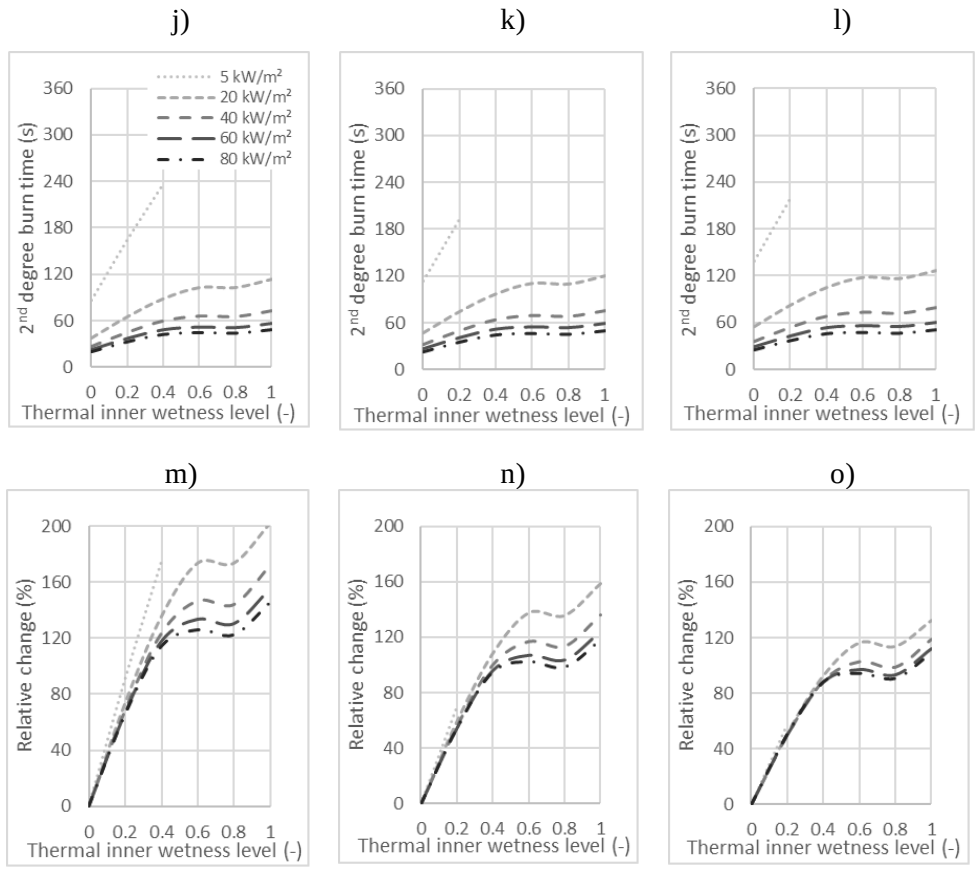

Figure 5.8 - a-c) Second-degree burn times obtained for the indicated outer shell (0.2, 0.6, and 1 wetness levels for a-c respectively) and thermal inner wetness levels, for different heat flux exposure intensities; d-f) relative change in second-degree burn time when compared to the dry case for corresponding wetness levels and heat fluxes; g-I) remaining free water fraction ($f_{inner,2nd}$) in the thermal inner when a second-degree burn occurs; j-l) second-degree burn times when no heat of condensation and sorption are considered in the textile; m-o) relative change in second-degree burn times when no heat of condensation and sorption are considered.

During a firefighter scenario, there may be situations where both the thermal inner and outer shell may be wet due to internal (e.g., sweating) and external (e.g., hose spraying) water sources. Hence in such cases, it is also of interest to study the thermal behavior of the T.P.C. Figure 5.8a-c shows the second-degree burn times for the indicated thermal inner wetness levels and wetness levels of 0.2, 0.6, and 1 in the outer shell, respectively. As can be seen for a heat flux exposure of 5 kW/m^2, the second-degree burn time rises with increased thermal

inner and outer shell wetness levels. However, for heat flux exposures above 20 kW/m^2, the second-degree burn time tends to present a minimum trend for all outer shell wetness levels considered (Figure 5.8a-c). For example, for a wetness level of 0.2 in the outer shell and heat exposure of 20 kW/m^2, second-degree burn time shows a decreasing trend for thermal inner wetness levels between 0.2 - 0.4 (Figure 5.8a), reaching a minimum at 0.4 of about 30.9 s. It then rises for wetness levels above 0.4, reaching 35.6 s when saturated.

Relative second-degree burn times emphasize the variations that occur with thermal inner wetness levels (Figure 5.8d-f). For example, for a heat flux exposure of 5 kW/m^2, the relative rises in second-degree burn time barely pass the 30 % mark, independently of the outer shell initial wetness level. For higher heat fluxes, above 20 kW/m^2, the minimum trend with thermal inner wetness level is verified. For example, for an outer shell wetness level of 0.2, the minimum tends to happen around a thermal inner wetness level of 0.5, between -10 % and -20 % depending on the heat flux exposure considered (Figure 5.8d).

Steam condensation/sorption is mainly responsible for the second-degree burn tendencies with wetness levels obtained. Figure 5.8g-i show the remaining water liquid fraction at the thermal inner when the exposure ends for the various wetness levels. As can be seen, the remaining liquid fractions have similar values and tendencies to those obtained when only the thermal inner is initially wet (Section 5.3.3). This behavior was e expected as most of the water present in the outer shell evaporated and diffused towards the environment instead of the skin (Section 5.3.2). Figure 5.8j-l show the second-degree burn times when condensation/sorption phenomena are not taken into account. Compared to the original case (i.e., Figure 5.8a-c), we can observe that condensation heat near the skin plays a crucial role in decreasing thermal performance. For example, suppose the firefighter faces an exposure of 20 kW/m^2 when the wetness level at the outer shell is 0.6 and 0.2 at the thermal inner. In that case, the presence of steam condensation reaching the skin will account for a 41.7 s decrease in the second-degree burn time (Figure 5.8b and k). This effect represents a difference of 78 % in thermal performance.

In conclusion, when the water is present both in the outer shell and thermal inner, there tends to be an increase in thermal performance for low heat fluxes, while for high heat fluxes, a diminishing in thermal performance happens. However and once more, if correctly managed, the water present in the garment can positively impact thermal performance if it is not allowed to reach and condense near the skin:

5.3.4 Real heat flux scenario

The data and phenomena discussed in previous sections with constant heat fluxes can be applied to analyze the impact of moisture presence on thermal performance for firefighting exercises. Firefighters usually face non – constant heat exposures from the environment, and hence a real case heat flux from a live-fire training exercise will be considered in this section. The live training exercise was performed in a structure where firefighters wore heat flux sensors to monitor their heat exposure throughout the activity [26]. Below, the registered heat flux for the firefighting exercise is shown (Figure 5.9a).

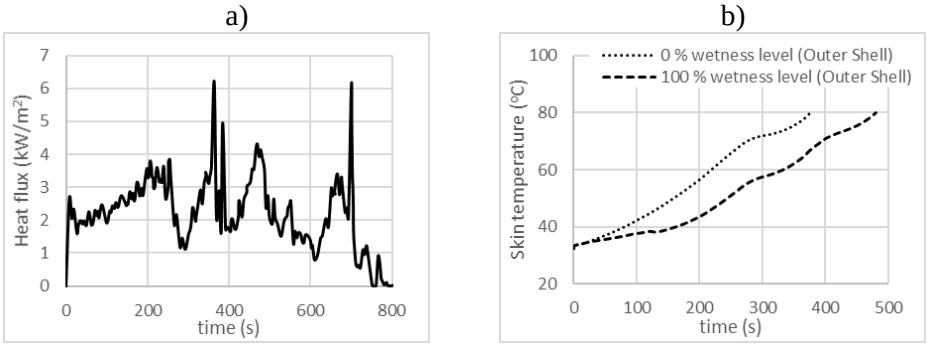

Figure 5.9 - a) heat flux data retrieved from a live-fire training exercise [26]; b) skin temperature obtained by simulation when the heat flux is considered a boundary condition for the indicated wetness levels.

Figure 5.9b shows the skin temperature profiles obtained when the textile is dry and when the outer shell is saturated. As can be seen, the temperature increase rate tends to vary over time, essentially due to the varying intensity of the external heat flux.

Figure 5.10a shows the second-degree burn time obtained for various inner and outer layer wetness levels. As is shown, an increase in second-degree burn time happens with an increase in thermal inner wetness level. This effect was expectable because the radiated heat flux is low–intensity (Figure 5.10a). Also, the increase in outer shell wetness level causes an increase in second-degree burn time. Relative increases in second-degree burn time are also more significant when the outer shell is dry (about 50 % increase when the inner layer

is fully saturated; Figure 5.10b). Figure 5.10c shows the fractions of free water obtained after the exposure. And as can be seen, the tendencies are similar to those obtained when constant heat fluxes were simulated in the previous sections for low heat fluxes.

Hence, the data and phenomena discussed in previous sections with constant heat fluxes can explain the tendencies observed in thermal behavior and guide possible thermal performance improvement solutions.

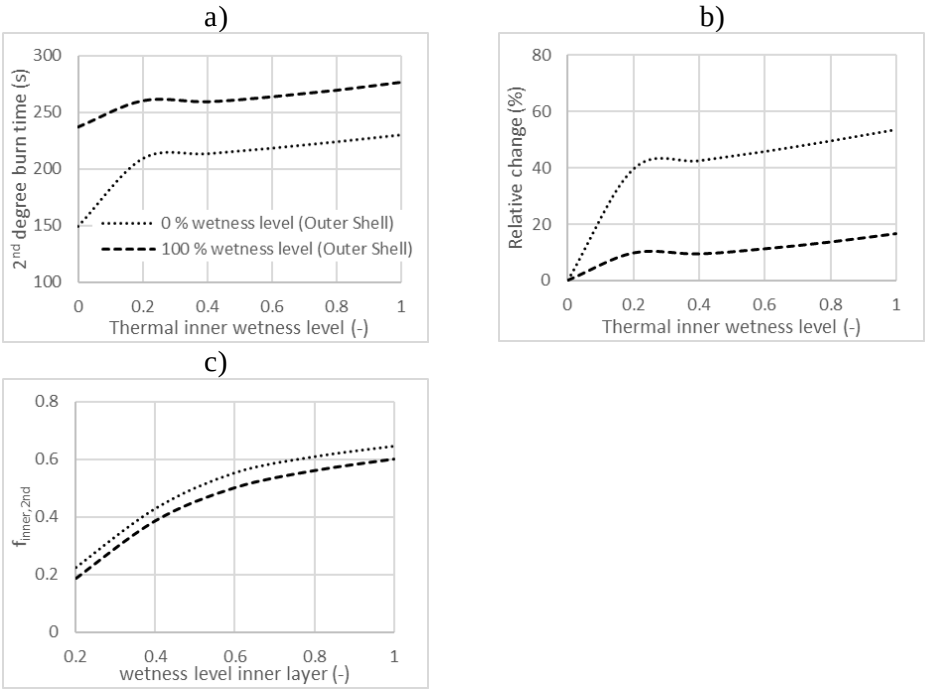

Figure 5.10 - a) second degree burn times obtained for the indicated outer shell and thermal inner wetness levels; b) relative change in second-degree burn time when compared to the dry case for corresponding wetness levels; c) remaining free water fraction ($f_{inner,2nd}$) in the thermal inner at the time when a second-degree burn occurs.

5.4 Conclusions

In this study, a one-dimensional numerical analysis of heat and moisture transport in a 3 –layered firefighting garment was performed. The thermal performance according to a second-degree burn criterion was analyzed. Different initial moisture quantities present in the inner layer and outer shell and different heat flux exposures were considered to generate maps and identify conditions for which moisture presence was impactful, specifying the reasons. The following specific conclusions were obtained:

- The presence of moisture in the outer shell increases second–degree burn time. However, this increase tends to be marginal for high heat fluxes (above 20 kW/m^2). Hence, moisture in the outer shell does not influence thermal performance for high heat fluxes.
- The presence of moisture in the inner layer generally decreases second-degree burn time and shows the worse performance at a wetness level of 50 % for heat flux exposures above 20 kW/m^2. For low-intensity exposure, however, the presence of moisture increases second-degree burn time.
- The simultaneous presence of water in the outer shell and thermal inner causes an increase in second-degree burn time, but only for low heat exposures (i.e., 5 kW/m^2). For higher heat exposures, it decreases and shows a minimum trend with the thermal inner wetness level.
- Decreases in thermal performance, especially for high heat fluxes, are essentially due to moisture condensation near the skin, as the liberated heat will provoke scald burns.

Lastly, it is essential to note that if we prevent the water vapor from reaching the skin, water in the textile, in all cases, provides significant gains in second-degree burn time. Nevertheless, in practical terms, such is challenging to achieve as the firefighter sweats and water vapour must be allowed to be

released from the skin to the environment; otherwise, the firefighter might overheat.

However, a good textile selection contributes to noteworthy gains in thermal performance. One of the options that is currently gaining attention in the literature is to use janus wetting and wicking properties to allow for better moisture management [27]. The authors would also like to point out that in a future study, textile compression phenomena could be incorporated in the model, as in such, situations burn injuries could occur due to the movement of hot water in the textile assembly and not necessarily due to steam condensation near the skin [28].

5.5 Appendix

5.5.1 Influence of an air gap

Figure 5.11 shows the second–degree burn times obtained when there is no air gap and when a 6.4 mm air gap is considered. The model described in section 5.2.2 was slightly modified to include the air gap domain (between fabric and skin) and conductive and radiative heat transport (assuming both skin and fabric to be grey bodies with an emissivity of 0.9) through it. Water vapor transport was considered to occur through the air gap where condensation could occur according to an equation similar to equation 5.13. Instantaneous condensation could happen in the air gap due to the presence of a nuclei in the air (e.g., dust particles).

The addition of an air gap between the fabric and the skin will cause a positive shift in the second-degree burn – times obtained for the various wetness levels. Such shifts roughly represent increases of about a factor of 2 when an air gap of 6.4 mm is present. In this work, the authors intended to simulate the worst possible case scenario where vapor mass transfer and heat transfer towards the skin would be the greatest. And such happens when no air gaps are considered.

The addition of an air gap does not change the quality of the results generated (Figure 5.11). Except for the resistance role of the air gap, no new physical phenomena are observed when an air gap is considered.

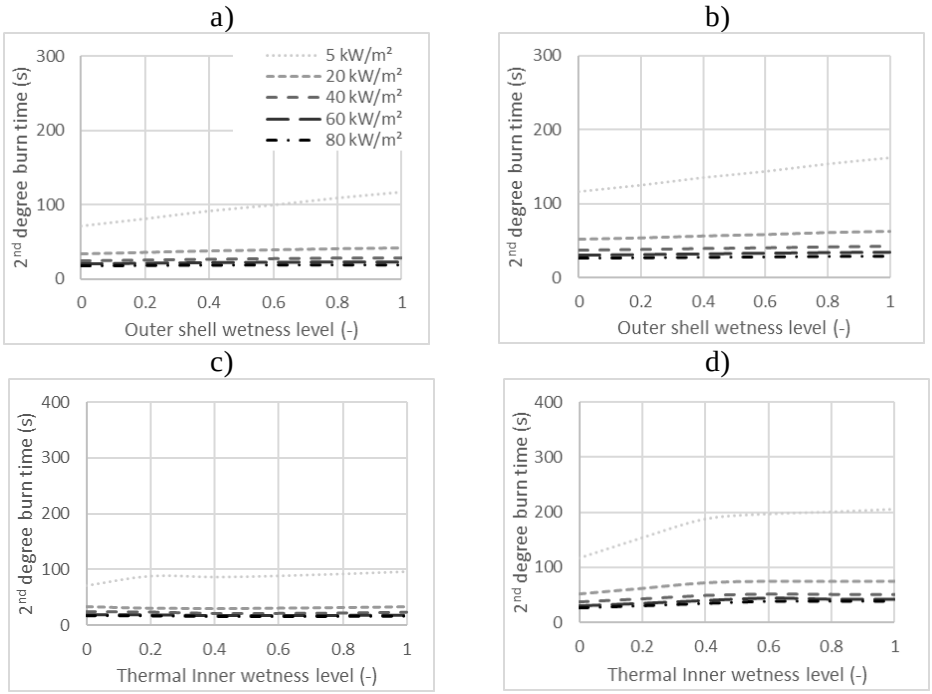

Figure 5.11 - Second degree - burn times obtained for indicated wetness levels considering: a,c.) no air gap b,d.) 6.4 mm air gap between skin and fabric.

Acknowledgments

National funds supported the present study through F.C.T. –Fundação para a Ciência e a Tecnologia, I.P., within the scope of the project UIDB/00532/2020 as well as by PCIF/SSO/0106/2018 - Project for "Development of an innovative firefighter's jacket", funded by national funds through FCT/MCTES (PIDDAC). Malaquias acknowledges the financial support provided by F.C.T. through the PhD Grant PD/BD/ 135097/2017.

References

[1] A. Morel, G. Bedek, F. Salaün, D. Dupont, A review of heat transfer phenomena and the impact of moisture on firefighters' clothing and protection, Ergonomics 57 (2014) 1078–1089, https://doi.org/10.1080/00140139.2014.907447.

[2] A.M. Raimundo, A.R. Figueiredo, Personal protective clothing and safety of firefighters near a high intensity fire front, Fire Saf. J. 44 (2009) 514–521, https:// doi.org/10.1016/j.firesaf.2008.10.007.

[3] J.R. Prasad, K. Twilley, W.H. Lawson, Thermal Performance of Fire Fighters' Protective Clothing: Numerical Study of Transient Heat and Water Vapor Transfer, Natl. Inst. Stand. Technol. Gaithersburg, 2002, pp. 1–32. MD 20899-8660.

[4] C. Keiser, P. Wyss, R.M. Rossi, Analysis of steam formation and migration in firefighters' protective clothing using x-ray radiography, Int. J. Occup. Saf. Ergon. 16 (2010) 217–229, https://doi.org/10.1080/10803548.2010.11076839.

[5] Y. Su, J. Li, G. Song, The effect of moisture content within multilayer protective clothing on protection from radiation and steam, Int. J. Occup. Saf. Ergon. 24 (2018) 190–199, https://doi.org/10.1080/10803548.2017.1321890.

[6] H. Zhang, G. Song, H. Ren, J. Cao, The effects of moisture on the thermal protective performance of firefighter protective clothing under medium intensity radiant exposure, Textil. Res. J. 88 (2018) 847–862, https://doi.org/10.1177/ 0040517517690620.

[7] L.K. Lawson, E.M. Crown, M.Y. Ackerman, J.D. Dale, Moisture effects in heat transfer through clothing systems for wildland firefighters, Int. J. Occup. Saf. Ergon. 10 (2004) 227–238, https://doi.org/10.1080/10803548.2004.11076610.

[8] M. Guan, A. Psikuta, M. Camenzind, J. Li, S. Mandal, R. Michel Rossi, S. Annaheim, Effect of perspired moisture and material properties on evaporative cooling and thermal protection of the clothed human body exposed to radiant heat, Textil. Res. J. 89 (2019) 3663–3676, https://doi.org/10.1177/0040517518817067.

[9] H. He, Z.C. Yu, G. Song, The effect of moisture and air gap on the thermal protective performance of fabric assemblies used by wildland firefighters, J. Text. Inst. 107 (2016) 1030–1036, https://doi.org/10.1080/00405000.2015.1083258.

[10] R.L. Barker, C. Guerth-Schacher, R.V. Grimes, H. Hamouda, Effects of moisture on the thermal protective performance of firefighter protective clothing in low-level radiant heat exposures, Textil. Res. J. 76 (2006) 27–31, https://doi.org/10.1177/ 0040517506053947.

[11] C. Keiser, R.M. Rossi, Temperature analysis for the prediction of steam formation and transfer in multilayer thermal protective clothing at low

level thermal radiation, Textil. Res. J. 78 (2008) 1025–1035, https://doi.org/10.1177/ 0040517508090484.
[12] E. Onofrei, T.C. Codau, S. Petrusic, G. Bedek, D. Dupont, D. Soulat, Analysis of moisture evaporation from underwear designed for fire-fighters, Autex Res. J. 15 (2015) 35–47, https://doi.org/10.2478/aut-2014-0015.
[13] P. Chitrphiromsri, Modeling of Thermal Performance of Firefighter Protective Clothing during the Intense Heat Exposure, NCSW, 2004.
[14] Y. Su, J. Li, X. Zhang, A coupled model for heat and moisture transport simulation in porous materials exposed to thermal radiation, Transport Porous Media 131 (2020) 381–397, https://doi.org/10.1007/s11242-019-01347-2.
[15] D. Huang, S. He, Influence of initial moisture content on heat and moisture transfer in firefighters' protective clothing, Sci. World J. 2017 (2017), https://doi.org/ 10.1155/2017/9365814.
[16] P. Łapka, P. Furma´nski, Modeling and analysis of the influence of the protective garment movement on the skin temperature and burn degree, Fire Saf. J. 111 (2020), https://doi.org/10.1016/j.firesaf.2019.102916.
[17] DuPont, Technical Guide for NOMEX Brand Fiber, 2001.
[18] J.W.S. Hearle, M.W. E, Physical Properties of Textile Fibres, fourth ed., Woodhead Publishing Limited, 2008.
[19] S.F. Neves, J.B.L.M. Campos, T.S. Mayor, On the determination of parameters required for numerical studies of heat and mass transfer through textiles - methodologies and experimental procedures, Int. J. Heat Mass Tran. 81 (2015) 272–282, https://doi.org/10.1016/j.ijheatmasstransfer.2014.09.038.
[20] D.A. Torvi, Heat Transfer in Thin Fibrous Materials under High Heat Flux Conditions, 1997.
[21] P. Gibson, Governing Equations for Multiphase Heat and Mass Transfer in Hygroscopic Porous Media with Applications to Clothing Materials, 1994.
[22] F.C. Henriques, Studies of thermal injury V. The predictability and the significance of thermally induced rate processes leading to irreversible epidermal injury, Arch. Pathol. 43 (1947) 489–502.
[23] M.K. Donnelly, W.D. Davis, J. Lawson, M. Selepak, Thermal environment for electronic equipment used by first responders, Natl. Inst. Stand. Technol. Spec. Publ. 1474 (2006) 41.
[24] H. Zhang, G. Song, Y. Gu, H. Ren, J. Cao, Effect of moisture content on thermal protective performance of fabric assemblies by a stored energy approach under flash exposure, Textil. Res. J. 88 (2018) 1847–1861, https://doi.org/10.1177/ 0040517517712097.
[25] Y. Su, R. Li, G. Song, J. Li, C. Xiang, Modeling steam heat transfer in thermal protective clothing under hot steam exposure, Int. J. Heat Mass Tran. 120 (2018) 818–829, https://doi.org/10.1016/j.ijheatmasstransfer.2017.12.074.

[26] J.M. Willi, G.P. Horn, D. Madrzykowski, Characterizing a firefighter's immediate thermal environment in live-fire training scenarios, Fire Technol. 52 (2016) 1667–1696, https://doi.org/10.1007/s10694-015-0555-1.

[27] X. Guan, X. Wang, Y. Huang, L. Zhao, X. Sun, H. Owens, J.R. Lu, X. Liu, Smart textiles with janus wetting and wicking properties fabricated by graphene oxide coatings, Adv. Mater. Interfaces 8 (2021), https://doi.org/10.1002/ admi.202001427.

[28] S. Mandal, G. Song, F. Gholamreza, A novel protocol to characterize the thermal protective performance of fabrics in hot-water exposure, J. Ind. Textil. 46 (2016) 279–291, https://doi.org/10.1177/1528083715580522.

6

Chapter 6

Incorporation of phase change materials in fire protective clothing considering the presence of water

6

Incorporation of phase change materials in fire protective clothing considering the presence of water

With the knowledge gained in the previous chapter regarding wet FPCs, the influence of the incorporation of a PCM can now be analyzed more clearly. The text written in this chapter resulted in the following publication:

Fonseca Malaquias, A., Neves, S. F., & J.B.L.M., C. (2022). Incorporation of phase change materials in fire protective clothing considering the presence of water. *International Journal of Thermal Sciences*. – Submitted and under revision.

Abstract

When firefighters face a heat exposure, free water may be present in the fire protective clothing (F.P.C.). Recently, the incorporation of Phase Change Materials (PCMs) into FPC has shown great promise to increase thermal performance when in the dry state. However, the presence of water in firefighting garments is expected and how this alters the thermal behavior of a PCM FPC still remains to be discussed in the literature. Hence, in this study, the effect of free water presence in the outer shell and/or thermal inner of a PCM FPC consisting of 3 layers is investigated. A new mathematical model is proposed where the PCM is assumed to be incorporated in the thermal inner. A numerical parametric analysis is performed where PCM incorporated mass, water distribution, and heat flux intensity are independently varied. Skin temperature, skin heat flux, and PCM liquid fraction profiles are obtained along with second-degree burn times to measure thermal performance. It is found that steam condensation at the skin greatly reduces time to second –degree burn window, dispromoting full PCM melting before such occurs. This study tends

to shine a light on the importance of considering moisture management in PCM FPCs so as to promote maximum PCM efficiency.

6.1 Introduction

The presence of moisture in textiles tends to have a major influence on their thermal performance. Water sources may be external or internal, such as that coming from the users' sweat. Firefighter garments are not an exception. During activities, firefighters may sweat profusely and be exposed to external water sources such as high – humidity environments and hose spraying. Hence, the development of improved firefighter garments demands the most increased understanding of the interdependency of the thermal performance of fire protective clothing with the contained water.

In the literature, there are several studies regarding the heat and moisture transport in a typical fire protective clothing (FPC). Barker et al. [1] experimentally studied the effect of free water presence in thermal inners when the FPC is subject to a low-heat flux exposure. They utilized a quartz tube heat source along with a calorimeter to measure the incoming heat flux from the turnout gear. Su et al. [2] used an improved benchtop tester to determine firefighters' second–degree burnouts when exposed to a radiative flux and hot steam. They used a black–ceramic heat source to produce a low–heat flux exposure and a water-cooled Schmidt-Boetler thermopile type sensor to register the incoming heat flux from the turnout suit. Keiser et al. [3] analyzed moisture distribution in FPC using a sweating torso equipment that mimicked the firefighters' continuous sweating. FPC layers were weighed before and after each trial to account for the presence of water in each of the garment layers. The same sweating torso equipment was utilized in a later study where a radiative heat exposure was also considered, and the interaction between continuous perspiration and radiative heat exposure on the FPC was analyzed [4]. Keiser et al. [5] measured the temperature of the layers of an FPC sample initially wet and exposed to an infrared lamp heat source in a PEEK tube. The temperature profiles obtained indicated moisture transport in the FPC, which, in a subsequent

study, was confirmed utilizing X-ray radiography to analyze the position and quantity of water in the FPC [6]. Mandal et al. [7] suggested a new protocol to characterize the thermal protective performance of fabrics in hot water exposure where heat and mass transfer through the FPC is emphasized.

Several numerical studies also exist in the literature regarding heat and mass transport in FPCs. Chitrphiromsri et al. [8] adapted Gibson's model [9] to numerically study heat and mass transport in an FPC with initial free water presence under high-intensity heat exposure. Huang et al.[10] also proposed a heat and mass transfer model for FPCs considering air gaps between the textile layers. Su et al. [11] developed and validated a heat and mass transfer model for FPCs subject to hot steam exposure. The authors report on the importance of mass transfer under such conditions as the hot steam diffuses rapidly through the turnout and condenses near the sensor. Su et al. [12] then suggested and validated a heat and mass transfer model for FPCs under low dry heat exposures where the initial presence of moisture in the FPC was considered.

Efforts to improve the thermal performance of fire protective clothing are vast, and researchers are constantly trying to find new ways to enhance firefighter microclimate management and resistance to flame [13–16]. One of the solutions that is being looked upon with promise is the incorporation of phase change materials in firefighting garments. A phase change material (PCM) is a substance in which the latent heat associated with its phase change (solid-liquid) can be used to improve thermal management. In the case of incorporation into fire protective clothing, the PCM would have the role of absorbing part of the incoming heat flux from the flame as latent energy, originating lower temperature in the fire protective clothing and thus at the firefighters' skin. A few studies exist in the literature reporting on the potential benefits of PCM incorporation in fire protective clothing [17–22].

In the literature, it is not common to find PCMs in textile applications where the effect of heat and moisture is simultaneously studied. Fengzhi et al. [23] proposed a heat and mass transport mathematical model for textiles with incorporated micro-PCMs (mPCMs). The model was validated for an ambient step temperature variation. Itan et al. [24] studied the incorporation of PCM –

desiccant packets onto a cooling vest that was subject to a hot humid environment. A mathematical model was proposed and validated. A decrease in the humidity content at the microclimate and an increase in the amount of liquefied PCM were observed. Wan et al. [25] proposed a heat and moisture transfer model for hybrid personal cooling garments incorporating PCMs and ventilation fans. The model was validated with experimental data, and good agreement was found. Zhao et al. [26] reported on the disadvantages of wearing PCM cooling vests in hot dry conditions, as the presence of PCM packets dramatically reduces the permeability of the fabric, hindering evaporative cooling from the user.

In practice, several techniques exist to incorporate PCMs into a textile [27]. The PCM can be already encapsulated in a micro or nanocapsule and then incorporated into the textile. Renzi et al. [28] incorporated mPCMs into a leather textile utilizing a wet soaking and a dry coating method. The authors found a limiting thermal effect on the jacket and reported that such depends on the percentage of incorporated PCM. Fiber latent heat of 20.4 J/g was reported for a 40 % wt mPCM incorporation. Bendkowska et al. [29] applied mPCMs through a coating method to non-woven textiles and noticed a thermoregulating effect. The authors note that the extension of such effect depends on the amount of incorporated PCM, its distribution, and position in the textile. Yoo et al. [30] incorporated 100 % cotton textiles with mPCMs using the knife over roll technique and studied the thermal response of a multilayer garment system consisting of such layers. Different configurations considering the presence of mPCMs were tested. The authors noticed a thermal buffering effect that depended on the number of layers that incorporated mPCMs and their position. Rossi et al. [31] incorporated mPCMs into a foam which was then coated onto the thermal inner of a firefighting garment assembly. The PCM foam layer weighed about 180 g/m^2. The authors found a thermal buffering effect when the mPCM garment was exposed to a heat source. Su et al. [19] coated different contents of mPCMs, with different melting temperatures, onto a thermal protective clothing garment and studied the performance of the assembly under hot contact exposure. The authors noticed a beneficial thermal effect that depended on the incorporated PCM quantity, melting temperature, and latent

heat. In the literature, several authors report their PCM textile fibers to have latent heats in the range 1 – 44 J/g [27].

Currently, according to the authors' knowledge, there is no numerical study in the literature analyzing heat and moisture transport in a PCM FPC (i.e., phase change material incorporated in fire protective clothing). In previous works, we studied correlations regarding the choice of a PCM to be incorporated in a dry firefighting garment [17,22], thus neglecting the effect of moisture on the performance of the PCM FPC. Hence, the presence of free water and moisture transport in a PCM FPC suit was considered in this study, and their effects in the PCM selection criteria were discussed. Moreover, in this study, the layer with PCM was considered permeable, rather than impermeable, to water and to water vapor (in our previous works [17,22], the layer was a PCM slab). Firstly, the effect of incorporating different PCM quantities in the thermal inner on thermal performance was studied, initially considering a saturated wet outer shell. Then, the effect of PCM melting temperature on second-degree burn time was analyzed for dry and wet PCM FPC samples with different initial water contents; for high – medium- and low – intensity exposures.

6.2 Materials and methods

6.2.1 Problem description

Consider a typical 3 – layered firefighting garment, composing of an outer shell, moisture barrier, and thermal inner, as shown in Figure 6.1. In this work, to increase the thermal performance of the firefighting garment, a phase change material (PCM) was added to the thermal inner, creating a phase change material fire protective clothing (PCM FPC) garment. The properties of each of the fabric layers utilized (without the incorporation of PCM) are shown in Table 6.1, while the PCM properties are shown in Table 6.2.

The PCM FPC was assumed to be in direct contact with the firefighters' skin composed of three layers: the epidermis, dermis and subcutaneous regions

(Figure 6.1). The outer shell, thermal inner, or both layers were assumed to be initially wet.

The PCM FPC was then exposed to a given heat flux. In such scenario, garment and skin temperatures rise, and the water initially present in the garment evaporates. Some of the vapor diffuses towards the skin, and the rest towards the environment. The vapor which diffuses towards the skin may re-condense, increasing the skin temperature. We aim to understand how adding a thermal inner layer with incorporated PCMs alters the suit's moisture and heat transfer rates. Furthermore, it is also expected that the PCM latent energy present in the thermal inner is not only used to absorb thermal energy from the incoming heat flux, but also for water vapor condensation heat absorption. The melting of the PCM originates lower temperatures in the garment.

As the temperature of the PCM FPC rises, the PCM melts, and the water vaporizes and re-condenses near the skin, promoting, eventually, a skin burn. A mathematical model considering the interdependency between moisture and heat transfer phenomena was developed to study the correlation between PCM properties and second – degree burn time window.

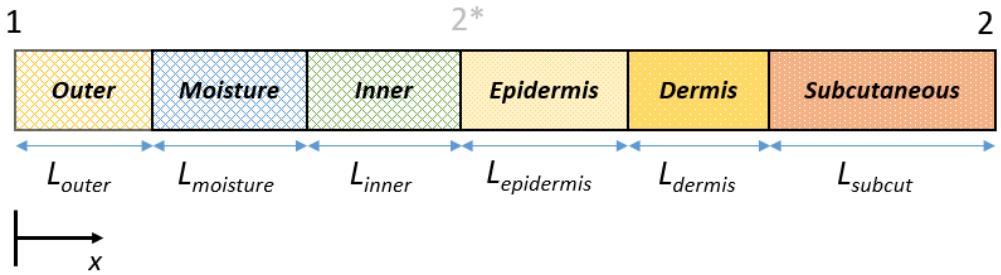

Figure 6.1- PCM FPC - skin system used in numerical simulations.

Table 6.1 – Properties of the various layers consisting of the firefighting protective clothing.

Property	Outer shell	Moisture Barrier	Thermal inner	Source
Thickness (w) mm	0.39	0.45	2.24	[32]
Density (ρ_{ds}) kg/m^3	1460	1460	1440	[33]
Specific heat (c_{ds}) J/(kg K)	1086	1086	1421	[34]
Thermal conductivity (k_{ds}) W/(m K)	0.25	0.25	0.21	[33][34]
Fiber volume fraction (ε_{ds})	0.36	0.16	0.09	Estimated [32,35]
Tortuosity (τ)	2.32	2.87	1.32	Estimated [36]
Fiber diameter (d_f) µm	15	15	15	[37,38]
Regain at 65 % RH	0.0485	0.0485	0.0397	[39]
Diffusivity of water in fiber (D_f) m^2/s	6×10^{-14}	6×10^{-14}	6×10^{-14}	[8]
Proportionality constant for liquid water sorption in fibres (γ_{ls}) kg/m^3	5×10^{-4}	5×10^{-4}	5×10^{-4}	[8]

6.2.2 Incorporation of PCM in the thermal inner

In practice, several techniques exist to incorporate a PCM into a textile [27]. Beyond direct incorporation, the PCM can be encapsulated in micro or nanocapsules and then incorporated into the textile. However, whether the thermal buffering effect offered by such textiles is sufficient or not, is debatable. This doubt exists because current micro or nanocapsule incorporation techniques simply do not allow enough PCM mass to be incorporated into the textile to notice a substantial thermal buffering effect [40].

Thus, to link our work to current methods of incorporation of PCM, a maximum practical value of textile latent heat (i.e., 40 J/g) was set considering experimental data found in the literature [27]. Also, in this study, higher fiber latent heats are considered, representing a new incorporation method where more PCM is retained in the textile fiber, as such could be possible in the future. It is assumed that the PCM distribution along the thermal inner textile is perfectly homogeneous and does not influence the hygroscopic properties of the textile. The properties of the incorporated PCM are shown in Table 6.2. The textile latent heats considered in the simulations are shown in Table 6.3.

Table 6.2 - Properties of Rubitherm® RT42 [41].

Property	Value
Latent heat (λ)	220 kJ/kg
Specific heat (C_{PCM})	2 kJ/(kg·K)
Solid density (ρ_{PCM})	800 kg/m^3
Thermal conductivity (k_{PCM})	0.2 W/(m·K)
Melting temperature (T_m)	42.5 ºC
Floating variable (T_0)	1 ºC

Table 6.3 - Fiber latent heats and respective PCM volume fraction s

Property	Value
PCM volume fraction (ε_{PCM})	0.04 – 0.60
Fiber latent heat ($\lambda_{fiber,eff}$)	40 – 170 J g^{-1}

6.2.2.1 Textile model

The model utilized in this work is in the sequence of a previous one, developed by our group, now including the PCM effect. The textile is considered a structure where the fiber, air pore and PCM are assumed to be homogeneous. Thus, the constitutive element of the model contemplates the presence of all phases. In this way, the model is simplified and problems with geometrical boundaries regarding the different phases are eliminated [9].

More details about the model can be found in a previous work by the same group [42]. In this section, emphasis will be majorly put on the altered parts.

With the inclusion of a PCM phase, the energy balance in the thermal inner is stated as follows:

$$\rho_{eff} C_{eff} \frac{\partial T}{\partial t} + \frac{\partial}{\partial x}\left(-k_{eff} \frac{\partial T}{\partial x}\right) - \dot{m}_{gs}\left(\Delta h_{vap} + \Delta h_l\right) - \dot{m}_{gl} \Delta h_{vap} - \dot{m}_{ls} \Delta h_l = 0 \tag{6.1}$$

$$\rho_{eff} = \varepsilon_{bw}\rho_w + \varepsilon_\gamma \rho_\gamma + \varepsilon_{ds}\rho_{ds} + \varepsilon_{PCM}\rho_{PCM} + \varepsilon_l \rho_w \tag{6.2}$$

$$C_{eff} = \frac{\varepsilon_{bw}\rho_w C_{p,w} + \varepsilon_\gamma\left(\rho_a C_{p,a} + \rho_v C_{p,v}\right) + \varepsilon_{ds}\rho_{ds} C_{p,ds} + \varepsilon_l \rho_w C_{p,w} + \varepsilon_{PCM}\rho_{PCM} C_{app}}{\rho_{eff}} \tag{6.3}$$

$$k_{eff} = k_\gamma \left\{\frac{\varepsilon_\gamma k_\gamma + [1 + \varepsilon_{bw} + \varepsilon_{ds} + \varepsilon_{PCM} + \varepsilon_l]k_\sigma}{\varepsilon_\gamma k_\sigma + [1 + \varepsilon_{bw} + \varepsilon_{ds} + \varepsilon_{PCM} + \varepsilon_l]k_\gamma}\right\} \tag{6.4}$$

where, ρ_{eff}, C_{eff}, k_{eff}, $\dot{m}_{gs}$, $\dot{m}_{gl}$, $\dot{m}_{ls}$, Δh_{vap} and Δh_l represent the effective density, effective specific heat, effective thermal conductivity, gas sorption/desorption rate, vaporization/condensation rate, liquid sorption/desorption rate, water vaporization heat, and liquid sorption/desorption heat, respectively. ε represents the phase volume fraction, and the subscripts bw, w, γ, ds, and l stand for bounded water, water, gas, fiber, and liquid, respectively. The apparent PCM specific heat (C_{app}) is defined as follows:

$$\begin{aligned} C_{\text{app}} = \frac{\mathrm{d}H}{\mathrm{d}T} &= \frac{\mathrm{d}}{\mathrm{d}T}\left[0.5 \times \lambda \times \operatorname{erf}\left(\frac{T - T_m}{T_0}\right) + C_{\text{PCM}}(T - T_m)\right] \\ &= \lambda \times \frac{\exp\left(-\frac{T - T_m}{T_0}\right)^2}{T_0\sqrt{\pi}} + C_{\text{PCM}} \end{aligned} \tag{6.5}$$

where T, T_m, λ, T_0, C_{PCM} stand for the temperature, melting temperature, latent heat, floating variable associated to mushy region, and PCM specific heat, respectively.

The first term on the left-hand side of equation 6.1 accounts for the heat accumulation in the garment. The second term accounts for the conductive heat fluxes, while the third, fourth and fifth terms account for the latent heat

associated with water sorption/desorption, vaporization/condensation and liquid sorption/desorption into the fibers, respectively. k_σ and k_γ represent the solid and gas phases thermal conductivity respectively, and they are calculated as follows:

$$k_\sigma = \frac{k_w \rho_w \varepsilon_{bw} + k_{ds} \rho_{ds} \varepsilon_{ds} + k_{PCM} \rho_{PCM} \varepsilon_{PCM} + k_w \rho_w \varepsilon_l}{\rho_w \varepsilon_{bw} + \rho_{ds} \varepsilon_{ds} + \rho_{PCM} \varepsilon_{PCM} + \rho_w \varepsilon_l} \tag{6.6}$$

$$k_\gamma = \frac{k_v \rho_v + k_a \rho_a}{\rho_v + \rho_a} \tag{6.7}$$

where subscripts *v* and *a*, refer to the water vapor and air, respectively.

The moisture mass balance in the gas phase is stated as follows:

$$\frac{\partial(\varepsilon_\gamma \cdot \rho_v)}{\partial t} + \frac{\partial}{\partial x}\left(-D_{eff} \frac{\partial \rho_v}{\partial x}\right) + \dot{m}_{gs} + \dot{m}_{gl} = 0 \tag{6.8}$$

$$D_{eff} = \frac{\varepsilon_\gamma \cdot D_a}{\tau} \tag{6.9}$$

$$D_a = 2.23 \cdot 10^{-5} \left(\frac{T}{273.15}\right)^{1.75} \tag{6.10}$$

Assuming no advection and diffusion phenomena, the free liquid water and bounded water balances are stated as follows:

$$\rho_w \frac{\partial \varepsilon_l}{\partial t} = \dot{m}_{sl} + \dot{m}_{vl} \tag{6.11}$$

$$\rho_w \frac{\partial \varepsilon_{bw}}{\partial t} = \dot{m}_{gs} + \dot{m}_{ls} \tag{6.12}$$

$$\dot{m}_{gs} = \frac{8 D_f \rho_{ds}}{d_f^2} \left(Regain_{eq} - Regain_f\right) \tag{6.13}$$

$$\dot{m}_{gl} = \begin{cases} c \cdot \left(\rho_v - \rho_{v,sat}\right) & \rho_{v,sat} \geq \rho_v \\ h_m a_s \dfrac{\varepsilon_l}{\varepsilon_l^{cr}} \left(\rho_v - \rho_{v,sat}\right) & \rho_{v,sat} \leq \rho_v \end{cases} \tag{6.14}$$

$$a_s = \frac{4 \varepsilon_{ds}}{d_f} \tag{6.15}$$

$$\dot{m}_{ls} = h_m a_s \gamma_{ls} \left(\frac{Regain_{eq}}{Regain_f} - 1 \right) \tag{6.16}$$

$$Regain_f = \frac{\varepsilon_{bw} \rho_w}{\varepsilon_{ds} \rho_{ds}} \tag{6.17}$$

$$\begin{aligned} Regain_{eq} = & \frac{\varepsilon_{bw}|_{eq} \cdot \rho_w}{\varepsilon_{ds} \rho_{ds}} \\ & = 0.578 \cdot Regain_{f(\emptyset = 65\,\%)} \cdot \emptyset \\ & \cdot [(0.321 + \emptyset)^{-1} + (1.262 - \emptyset)^{-1}] \end{aligned} \tag{6.18}$$

$$\varepsilon_{ds} + \varepsilon_{bw} + \varepsilon_{PCM} + \varepsilon_{\gamma} + \varepsilon_l = 1 \tag{6.19}$$

Lastly, the volume fraction constraint now includes the PCM phase as well.

6.2.2.2 Skin model

The Pennes' bio-heat model was assumed to describe the heat exchanges in the firefighter's skin layers. The following equations describe heat transport in the epidermis, dermis and subcutaneous:

$$\rho_{ep} C_{ep} \frac{\partial T}{\partial t} = \frac{\partial}{\partial x} \left(k_{ep} \frac{\partial T}{\partial x} \right) \tag{6.20}$$

$$\rho_{derm} C_{derm} \frac{\partial T}{\partial t} = \frac{\partial}{\partial x} \left(k_{derm} \frac{\partial T}{\partial x} \right) - G \rho_b c_b (T - T_c) \tag{6.21}$$

$$\rho_{subcut} C_{subcut} \frac{\partial T}{\partial t} = \frac{\partial}{\partial x} \left(k_{subcut} \frac{\partial T}{\partial x} \right) - G \rho_b c_b (T - T_c) \tag{6.22}$$

where G, ρ_b, c_b and T_c represent the volumetric blood flow, blood density (kg/m^3), specific heat (J/(kg·K)) and core body temperature (K), respectively. The subscripts *ep*, *derm*, and *subcut* stand for epidermis, dermis and subcutaneous, respectively. The properties of the skin layers are in Table 6.4.

Like other studies in the field, Henriques' burn criterion was utilized to calculate second-degree burn time [43].

Table 6.4 - Properties of skin layers taken from [8].

Property	Epidermis	Dermis	Subcutaneous
Thermal conductivity (k) W/(m·K)	0.255	0.523	0.167
Specific heat (C_p) J/(kg K)	3600	3400	3060
Density (ρ) kg/m^3	1200	1200	1000
Thickness (w) mm	0.08	2	10
Blood perfusion rate (G) s^{-1}	1.25×10^{-3}	1.25×10^{-3}	1.25×10^{-3}

6.2.3 Boundary and initial conditions

Donnelly et al. [44] divided the firefighting scenario into four thermal classes that a firefighter can face. These classes are categorized based on the heat flux and air temperature. In this work, three heat exposure intensities were considered to simulate high- (84 kW/m^2), medium- (12 kW/m^2), and low-intensity (5 kW/m^2) heat exposure scenarios [17,20,45]. This incoming external heat flux (q_w) was imposed at boundary 1 (Figure 6.1) as a Newman condition (equation 6.23).

$$q_w = -k_{eff,outer} \left.\frac{\partial T}{\partial x}\right|_{x=0} \tag{6.23}$$

Also, at this boundary (1, Figure 6.1), water vapor is transferred from the garment to the ambient by convection (equation 6.24), assuming an ambient temperature of 34 °C with 65 % R.H.

$$k_c(\rho_v - \rho_{amb}) = -D_{eff,outer} \left.\frac{\partial \rho_v}{\partial x}\right|_{x=0} \tag{6.24}$$

At boundary 2* (Figure 6.1), continuity and symmetry boundary conditions were assumed for the energy and mass balances (equations 6.25 and 6.26, respectively).

$$-k_{epidermis}\frac{\partial T}{\partial x}\Big|_{x=L_{outer}+L_{moisture}+L_{inner}} = -k_{eff,inner}\frac{\partial T}{\partial x}\Big|_{x=L_{outer}+L_{moisture}+L_{inner}} \quad (6.25)$$

$$0 = -D_{eff,inner}\frac{\partial \rho_v}{\partial x}\Big|_{x=L_{outer}+L_{moisture}+L_{inner}} \quad (6.26)$$

where L_{outer}, $L_{moisture}$ and L_{inner} represent the outer shell, moisture barrier, and thermal inner widths, respectively.

A constant core body temperature of 37 °C (Dirichlet condition) was considered at boundary 2 (Figure 6.1). It was also assumed that the PCM FPC was initially at a constant temperature of 34 °C, and the skin temperature at a temperature which varied linearly between the epidermis and subcutaneous regions, i.e. between 34 °C and 37 °C [17,20]. An initial relative humidity of 65 % was assumed in the PCM FPC. All of the initial conditions assumed are shown in Table 6.5.

Table 6.5 - Initial conditions assumed for the firefighting protective clothing

Property	Outer shell	Moisture Barrier	Thermal Inner
$\varepsilon_{l,init}$	Distribution (0 to 0.27) (i.e. wetness level 0 to 1)	0	Distribution (0 to 0.25) (i.e. wetness level 0 to 1)
$\varepsilon_{b,init}$	0.025	0.007	0.008
T_{init}	34 °C	34 °C	34 °C
$Ø_{init}$	0.65	0.65	0.65

6.2.4 Grid independence tests

To ensure solution accuracy and promote computational efficiency, grid independence tests concerning time and space were performed. Figure 6.2a shows the difference in skin temperature histories obtained with the different indicated meshes in Table 6.6. As can be seen, spatial mesh independence is

obtained with mesh 2. A backward differentiation formula solver was used to choose the best time step, utilizing a relative tolerance as a criterion. The best relative tolerance obtained is 10^{-4} and a residual-based termination criterion was utilized (Figure 6.2a and b).

Table 6.6 – Meshes used to test for spatial mesh independence

Mesh no.	Elements in textile	Elements in skin
Mesh 1	50	5
Mesh 2	500	20
Mesh 3	1000	100

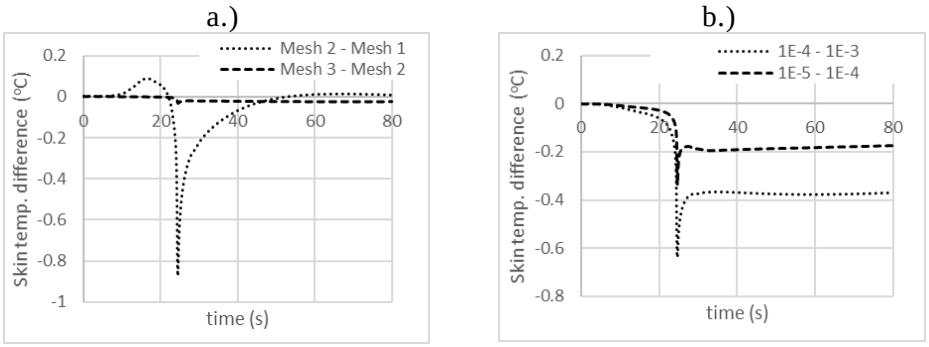

Figure 6.2 – a.) Differences in the skin temperature obtained for the different meshes b.) Differences in the skin temperature for the different relative tolerances.

6.2.5 Model validation

The textile model was validated with the experimental data outlined in [23]. Micro PCMs were incorporated in a polyester fabric and their thermoregulatory capabilities were tested by imposing step changes in the ambient temperature to promote their liquefaction/solidification. The PCM used was a paraffin. For such, two chambers were conditioned with different temperatures (i.e., 35 °C and 5 °C, corresponding to the hot and cold chamber, respectively) but with an equal relative humidity of 40 %. The polyester textile with PCM microcapsules was initially conditioned in the hot chamber. Thus, the PCM was initially in a liquid state. The garment was then moved into the cold chamber and remained there for 816 s. The temperature obtained at the center of the garment is shown

in Figure 6.3. The temperature decreased during this time and the PCM solidification released heat into its surroundings, delaying the temperature decrease at the center of the textile. The textile was then moved back into the hot chamber and remained there for another 600 s. During this period, the garment temperature increased and PCM melting occurred, which delayed the temperature increase in the textile.

Figure 6.3 shows the obtained experimental and numerical temperatures at the center of the textile. As can be seen, good agreement is obtained proving the adequacy of the model to simulate heat and mass transport in textiles incorporating micro encapsulated PCMs. The deviations which exist in the first part of the process (i.e., Figure 6.3, $t < 816$ s) are due to hysteresis phenomena regarding the phase change of the PCM, an effect neglected in the current model.

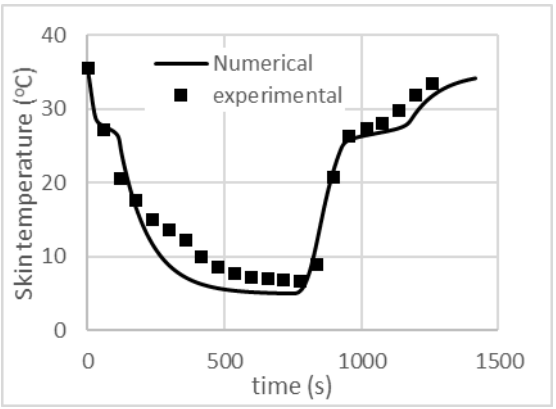

Figure 6.3 - Comparison between experimental [23] and numerical results for hot and cold chamber experiments to study the thermal properties of a polyester textile incorporated with micro PCMs.

6.2.6 PCM selection criteria

PCM selection criteria have been proposed in previous works to incorporate PCMs in dry FPCs [17]. There, it was determined that the significant variables to consider in PCM selection are its melting temperature, latent energy, and exposure scenario. A PCM with a substantially high melting temperature may only melt partially before the firefighter experiences a second-degree burnout,

thus the PCM not being efficient. Also, if the PCM disposes of insufficient latent energy, the increase in second-degree burnout time might not be significant. In this study, new PCM selection criteria for wet PCM FPCs will be established in function of the PCM melting temperature and latent energy for high- , medium- , and low-intensity exposures.

6.3 Results

When a PCM FPC suit is exposed to a heat source, the PCM will tend to melt, originating lower temperatures in the garment and thus at the firefighters skin [17,19–21,45]. This happens because part of the incoming dry heat accumulates as latent heat in the PCM [17]. When free water is present in a PCM FPC, the PCM's role on thermal performance changes as in some cases, the PCM might melt due to latent heat absorption from water condensation. Figure 6.4a shows the temperature profiles in a PCM FPC at 0, 5 and 10 s exposure to an 84 kW/m^2 heat flux when the outer shell is initially saturated with water. Two thermal inner layers with different PCM textile latent heats are considered in Figure 6.4. As can be seen, the incorporation of a garment with higher latent heat (e.g., greater amount of PCM incorporated in the textile fiber) originates lower temperature along the firefighting protective clothing (Figure 6.4a). This behavior was expected, as the presence of higher latent heat allows for heat storage at much lower temperature [17].

Figure 6.4c shows the relative humidity in the PCM FPC obtained for the PCM thermal inners at 0.5 and 10 s exposure time. At 10 s, for the PCM thermal inner with higher latent heat (black-line series in Figure 6.4c, 170 J/g), the relative humidity tends to be greater for positions further away from the skin (i.e., $0.0017 < x < 0.002$ m) while in the inner layer with the lowest latent heat, the skin is already saturated (black-dot series in Figure 6.4c, 40 J/g; $x = 0.003$ m). This occurs because the temperature in the PCM FPC is lower when the thermal inner has a higher latent heat (Figure 6.4a). Taking a closer look at the

tendency registered and considering the direction towards the skin (i.e., from 0 to 0.003 m), it is observed for the layer with higher latent heat (170 J/g; t = 10 s) that the relative humidity rises reaching a plateau (i.e., 0.0017 < x < 0.002 m), and then falls for positions closer to the skin (i.e., Figure 6.4c, x > 0.002 m). The reached plateau is where most of the water condensation happens and it is directly related to the PCM melting front (Figure 6.4b). As a significant amount of steam condenses in this position (Figure 6.4d), little is then left to diffuse towards the skin, explaining then the local lower relative humidity (i.e., Figure 6.4c, x > 0.002 m, t = 10 s, 170 J/g).

Figure 6.4b shows the PCM liquid fraction along the thermal inner. In this figure, the PCM melting front (i.e. at 0.0017 < x < 0.002 m, t = 10 s, 170 J/g) coincides directly with the relative humidity peak (Figure 6.4c, t = 10 s, 170 J/g). Thus, the PCM latent heat is used to lower the thermal inner temperature, promoting steam condensation. To show this more clearly, consider the condensation rate of water vapor in the thermal inner (i.e., $m_{gl,inner}$; Figure 6.4d). As is shown, there tends to be an increase in the condensation rate near the phase change front (i.e., Figure 6.4d and b; 0.0017 < x < 0.002 m). Notice that such behavior prevents the condensation from happening at the skin, as is the case when only a 40 J/g PCM thermal inner latent heat is considered. The PCM in such case has already fully melted at t = 10 s (Figure 6.4b). Thus, in the presence of wet protective clothing, the PCM reduces the garment temperature due to heat absorption from the flame and increases relative humidity as the lower temperature promotes steam condensation. Hence, the presence of free water in a PCM FPC suit will alter the thermal performance offered by the PCM as will be shown in the next sections. The first section explores in more detail the influence of the latent heat of the textile (with PCM) on the suit thermal performance. The second section deals with the implications in the PCM selection criteria when water is present in the outer shell or in the thermal inner. In the third section, similar analyses are done considering the presence of water in both layers simultaneously.

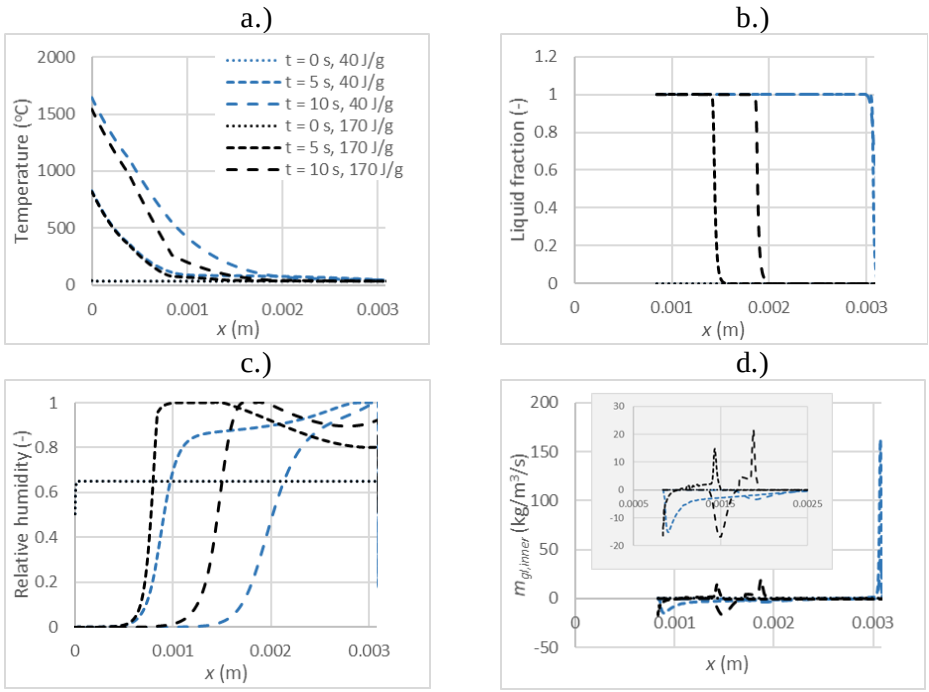

Figure 6.4- Calculated properties along the thickness of PCM FFPC suit considering the outer shell initially saturated and different amounts of PCM incorporated in the inner layer (represented by different latent heats), for an exposure of 84 kW/m^2, at the indicated times; a.) temperature profiles, b.) PCM liquid fraction, c.) relative humidity, and d.) rate of condensation of water vapor.

6.3.1 Influence of the latent heat of the textile with PCM

The incorporation of phase change materials may modify the textile fiber latent heat of the thermal inner. There are numerous techniques for incorporating PCMs in textile fibers. However, as it will be shown in this section, many of these methods fail to provide the PCM FPC with enough latent heat to cause a significant effect on thermal performance. A 40 J/g textile fiber latent heat is used as a reference to show how, for example, the recent microencapsulation incorporation techniques are not adequate to incorporate sufficient amounts of mass to a PCM FPC to provide adequate protection [27]. The effects of increasing textile latent heat on the thermal performance of a wet PCM FPC will also be shown for high- medium- and low-intensity exposures.

6.3.1.1 High-intensity heat exposures

As discussed in previous papers, increasing the PCM mass in a dry firefighting garment greatly increases its thermal performance [17]. However, when free water is present in the outer shell PCM FPC (i.e. assumed saturated in this case), a more complex behavior on the PCM thermal performance is registered when compared to the dry case [17].

Figure 6.5a shows the skin temperature histories obtained for an exposure intensity of 84 kW/m^2 for various textile latent heats. For exposure times less than 20 s, an increase in textile latent heat originates a decrease in the skin temperature. During this period, the incoming stream from the water vaporization in the outer shell is significant. This behavior explains, for example, the sudden temperature spike registered in the beginning (e.g., Figure 6.5a, t = 6.1 s, 40 J/g). For times greater than 20 s, the temperature differences between the various PCM textile latent heats tend to converge.

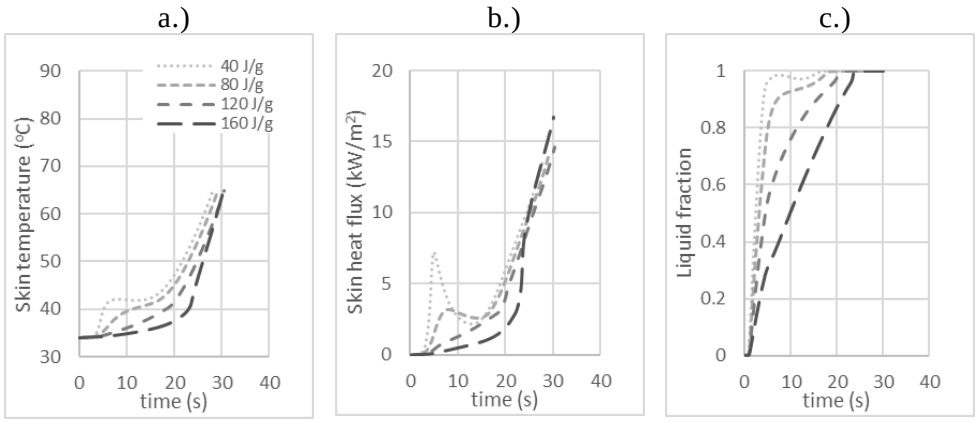

Figure 6.5 –a.) Skin temperature, b.) Skin heat fluxes, and c.) PCM liquid fraction histories for the indicated thermal inner textile latent heats; for a high-intensity heat exposure (84 kW/m^2).

Figure 6.5b shows the skin heat flux over time for the various textile latent heats considered. As can be seen, for low textile latent heats, an initial spike in the skin heat flux is registered (e.g., Figure 6.5b, t = 5 s, 40 J/g). This behavior is due to steam condensation near the skin, as evidenced by the skin temperature (Figure 6.5a). For higher textile latent heats and higher times of exposure (t > 25 s), the heat flux registered at the skin tends to surpass that of lower textile latent heats (i.e., Figure 6.5b). This behavior is in accordance with the skin temperature rates registered at such times.

The lower temperature and skin heat fluxes at the beginning obtained for higher textile latent heat are explained by the melting of the PCM in the textile. Figure 6.5c shows the PCM liquid fractions for the various textile latent heats. As shown, for all textile latent heats considered, the PCM in the textile melts before 25 s. However, unlike in dry case scenarios [17], the tendencies of the liquid fraction curves are not linear. For example, considering a textile latent heat of 40 J/g, the liquid fraction initially increases rapidly to about 0.95 but then decreases, followed by another increase up to 1. This variation happens due to evaporative cooling in the inner layer. During the exposure, when no more water is present in the outer shell, the incoming stream of water vapor towards the skin ceases. This gives rise to evaporative cooling phenomena in the thermal

inner, as the water which condensed now begins to evaporate. This allows for the PCM to re-solidify a bit. This effect ceases for higher textile latent heats and is substituted by another one with implications in the liquid fraction curve. For example, for a textile latent heat of 160 J/g, the liquid fraction initially increases abruptly up to 0.25 at t = 7 s; the PCM liquefaction is being utilized to condense the incoming steam from the water vaporization at the outer shell. Then, it increases less abruptly and linearly until 1; the PCM latent heat is mainly used to absorb the energy from the incoming heat flux from the exposure. When steam ceases to diffuse towards the inner layer, from the outer shell, there is still a significant amount of solid PCM (e.g., Figure 6.5c, t = 7 s, *liquid fraction* = 0.27, 160 J/g). Thus no evaporative cooling happens, as the temperature in the thermal inner is still low.

Therefore, when compared to the dry case, wet PCM FPCs exhibit a more complex thermal behavior for high heat exposures. This complex behavior naturally affects the second-degree burn time, as shown below.

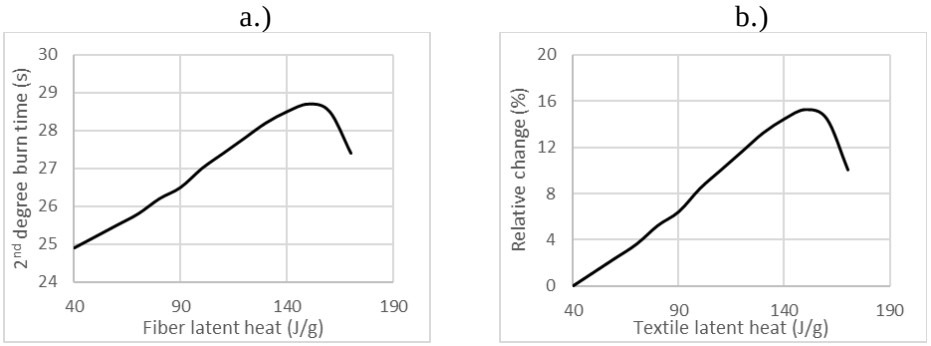

Figure 6.6 – a.) 2nd degree burn time variance with textile latent heat b.) Relative change in 2nd degree burn time with textile latent heat; for a high-intensity heat exposure (84 kW/m^2).

Figure 6.6a and b show the second-degree burn times and relative changes for the various textile latent heats considered, respectively. A positive almost linear trend is observed up to a textile latent heat of 150 J/g, followed by a decline in the thermal performance. This behavior is due to the thermal properties of the PCM FPC thermal inner where the bulkier thermal inner (i.e.,

with more PCM) has less pore space and hence its thermal diffusivity increases. Therefore, the incorporation of textiles with higher latent heats promotes thermal performance, even under wet conditions where steam condensation is present (Figure 6.4).

6.3.1.2 Medium intensity heat exposures

For medium intensity exposures, the phenomena observed are similar to those for flash fires but with a different intensity.

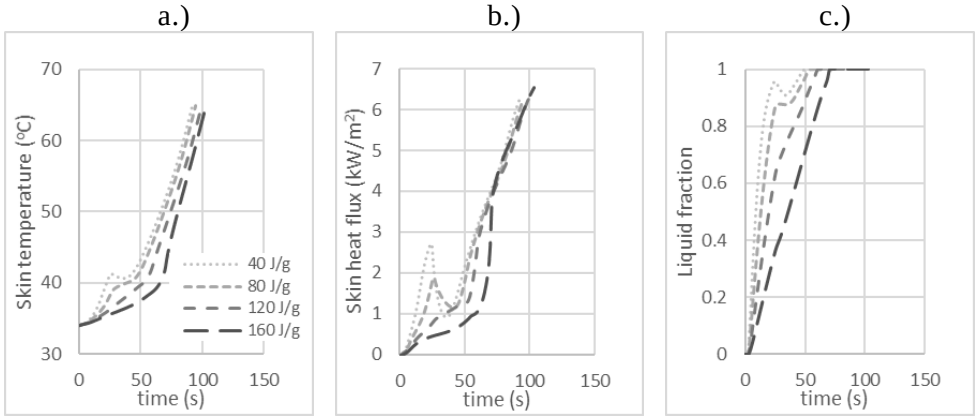

Figure 6.7 - a.) Skin temperature, b.) Skin heat fluxes, and c.) PCM liquid fraction histories obtained for the indicated thermal inner textile latent heats; for a medium – intensity heat exposure (12 kW/m^2).

Figure 6.7a shows the skin temperature for the various textile latent heats for a medium-intensity heat exposure of 12 kW/m^2. Compared to the high-intensity scenario (Section 6.3.1.1), the initial temperature rise is less intense since a lower heat flux causes less water vaporization in the outer shell, decreasing water vapor diffusion and, by consequence, the condensation of water at the skin. For example, for a 40 J/g textile, the initial temperature spike is reached at 40.6 °C at t = 25.3 s, whilst for a high heat exposure, it is 42.2 °C at t = 8.2 s (Figure 6.6a and Figure 6.7a). The different thermal diffusivities of the different latent heat textiles don't seem to influence skin temperature as significantly as in the flash fire case, despite there being an approximation of the curves and

parallel behavior of the lines for the various latent heat textiles (i.e., Figure 6.7a, $t > 70$ s). This parallel behavior in the skin temperature is more evident if the skin heat fluxes are considered (Figure 6.7b). As shown, for $t > 70$ s, the skin heat flux registered for the various latent heat textiles is approximately the same, explaining the parallel behavior in the skin temperature. The initial deviations in skin temperature and skin heat fluxes (i.e., Figure 6.7a and b, $t < 80$ s) are explained majorly by the deviation in the PCM liquid fraction curves (Figure 6.7c). Thus, as the water evaporation rate is less in medium-intensity heat exposures, the skin temperature, skin heat fluxes, and PCM liquid fraction are less affected.

Figure 6.7c shows the PCM liquid fraction for the various textile latent heats. As can be directly seen, steam condensation does not influence PCM liquid fractions tendency that much when compared to high-intensity exposures (Figure 6.5c). For example, considering a textile of 160 J/g, while for a high-intensity exposure, a clear change in PCM liquid fraction trend was observed when steam condensation was present in the inner layer (Figure 6.6c, $t = 5$ s), for a medium-intensity exposure, this is almost not visible (Figure 6.7c). However, during the evaporative cooling phase, the amount of PCM re-solidified in a medium-intensity exposure is greater than in a flash fire. For example for a 40 J/g textile latent heat, the amount of PCM re-solidified in a flash fire during evaporative cooling phase is about 2.2 % (Figure 6.6c, $7.6 < t < 13.1$ s) whilst for a medium-intensity exposure it is about 6.7 % (Figure 6.7c, $23.6 < t < 33.1$ s). In a medium-intensity exposure, temperature rise in the garment due to incoming heat from the flame takes longer, thus rendering more time for evaporative cooling to take place in the PCM thermal inner.

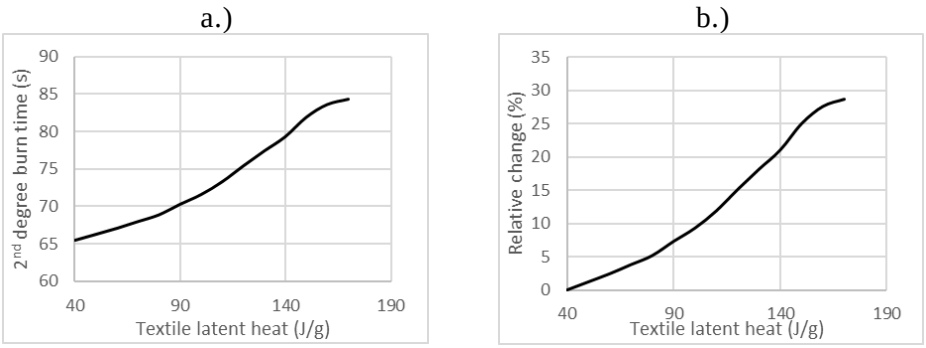

Figure 6.8- a.) 2nd degree burn time variance with textile latent heat b.) Relative change in 2nd degree burn time with textile latent heat; for a medium-intensity heat exposure (12 kW/m^2).

Figure 6.8 shows the second degree burn time and respective relative changes, for a medium – intensity exposure. A positive trend can be observed between the textile latent heat and second-degree burn time. A 30 % rise in time to second-degree burn is registered when the textile latent heat varies from 40 to 170 J/g. This is a significant improvement compared with the slight increase of 9 % for the high-intensity case (Figure 6.3b). The presence of free water augments the second-degree burn time almost in an equal fashion for all PCM thermal inners considered. Hence, the nearly linear tendencies registered, since the increase in latent heat is solely responsible for such.

6.3.1.3 Low-intensity heat exposures

When considering low-intensity heat exposures, condensation phenomena at the PCM thermal inner are even less pronounced.

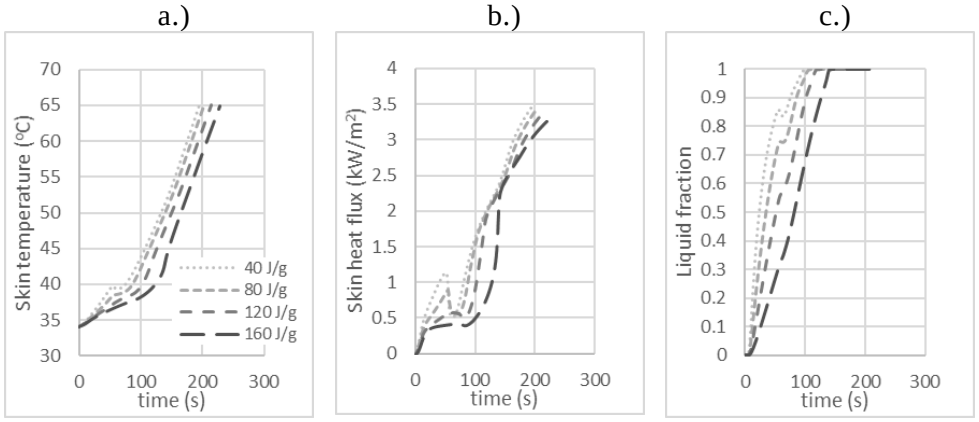

Figure 6.9 -a.) Skin temperature b.) Skin heat fluxes and c.) PCM liquid fraction histories for the indicated thermal inner textile latent heats; for a low-intensity heat exposure (5 kW/m^2).

Figure 6.9a shows the skin temperature obtained for the various textile latent heats. As shown, the initial temperature spike becomes very negligible when compared to the other two exposure scenarios (e.g., Figure 6.9a, 40 J/g, t = 50.3 s). For a 40 J/g textile latent heat, the maximum temperature at the spike is 39.3 ºC. Likewise, the corresponding spikes are also associated with lower registered skin heat fluxes (e.g., Figure 6.9b, 40 J/g, t = 50.3 s). For example, for a 40 J/g textile latent heat, a maximum skin heat flux of about 1 kW/m^2 is reached for low-intensity exposures, significantly smaller that in medium- and high-intensity heat exposure scenarios.

Figure 6.9c shows the PCM liquid fractions for the various textile latent heats. Evaporative cooling phenomena tend to happen when the PCM liquid fraction is lower when compared to the other two exposure scenarios. For example, considering a textile latent heat of 40 J/g, the evaporative cooling phenomenon begins when about 86 % of the PCM has fully melted. However, the PCM re-solidification is less when compared to a medium-intensity exposure. Only 4.5 % of the PCM re-solidifies before the temperature in the PCM FPC increases again due to the incoming external heat flux, and thus the PCM liquid fractions also rise. As less steam diffuses towards the inner layer due to a lower – heat flux, less also condenses, and thus the temperature in the thermal inner is lower when such ceases, giving rise to less evaporative cooling.

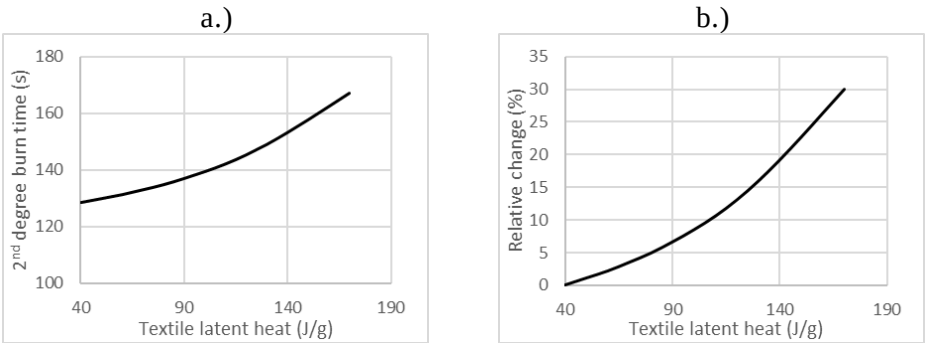

Figure 6.10 - a.) Second-degree burn time variance with textile latent heat b.) Relative change in second-degree burn time with the textile latent heat; for a low-intensity heat exposure (5 kW/m^2).

Figure 6.10 shows the second-degree burn times obtained for the indicated textile latent heats. A similar trend is obtained when compared to medium-intensity heat exposure. A slightly higher increase is obtained when the textile latent heat varies from 40 J/g to 170 J/g (Figure 6.10b).

Thus, for low-intensity heat exposures, textile latent heat influence on thermal performance tends to be marginally affected by the presence of moisture when such is solely present in the outer shell.

The presence of steam condensation alters the PCMs thermal behavior. PCMs liquefying behavior is altered also due to evaporative cooling phenomena which happen during the exposure phase.

6.3.2 Effect of water distribution on PCM selection

6.3.2.1 Water presence in the outer shell

Figure 6.11a shows the second-degree burn time for a high-intensity heat exposure scenario and different PCM melting temperatures, considering a dry or saturated outer shell and an inner layer with different latent heat. As shown, independently of the textile latent heat considered, differences in second-degree burn time exist whether the outer shell is dry or saturated. Higher second-degree burn times are obtained when the outer shell is saturated for all PCM melting temperatures considered. For example, consider a PCM FPC with a textile latent heat of 160 J/g incorporating a PCM with a melting temperature of 80 ºC. If its outer shell is initially dry, the second-degree burnout obtained when exposed to a high heat exposure is 24.5 s, but if it is initially wet and fully saturated, it increases up to 27.6 s (Figure 6.11a). Furthermore, if other PCM melting temperatures are considered, similar increases in second-degree burnout also occur. Such an increase in second-degree burn time is almost the same for all PCM melting temperatures considered.

Next, the liquid fractions obtained at second-degree burnout for the various PCM melting temperature do not vary significantly, whether the outer shell is considered saturated or dry (Figure 6.11d). For example, for a PCM with a melting temperature of 200 °C when the outer shell is saturated or dry, the PCM liquid fraction obtained at the second degree burn time is 0.54 and 0.57, respectively. Hence, it can be deduced that the presence of water in the outer shell does not affect PCM selection criterion for high-intensity exposures. The slight differences in the PCM liquid fractions at the second-degree burn time are due to steam condensation phenomena.

Figure 6.11b shows the second-degree burn times obtained for the various PCM melting temperatures when the outer shell is under dry or saturated conditions for the medium-intensity exposure. As is shown, similar trends are registered when compared to the high-intensity scenario. The second-degree

burn times are generally higher in magnitude due to the lower intensity of the heat flux. It can be observed that wetting the outer shell also causes a shift in the second-degree burn time but does not influence the quality of its tendency with PCM melting temperature. This is likewise for the low-intensity exposures (Figure 6.11c and f) but the magnitude of the second-degree burn times and PCM liquid fractions at second-degree burn time differ.

Also, independently of the heat exposure scenario considered, a protective garment with low PCM mass incorporation and thus low latent energy (i.e., with 40 J/g) does not provide a significant benefit in second-degree burn time (Figure 6.11a to c). However, this value corresponds to the maximum latent energy that was experimentally incorporated onto a textile [27], which means that, for firefighting applications, other methods of incorporation should be considered allowing greater PCM masses to be incorporated (e.g., macro encapsulation). Incorporation through microencapsulation methods still needs to have major technological breakthroughs either at the material level (e.g., PCMs with higher latent heats) or at the amount of mass that is actually incorporated onto the textile.

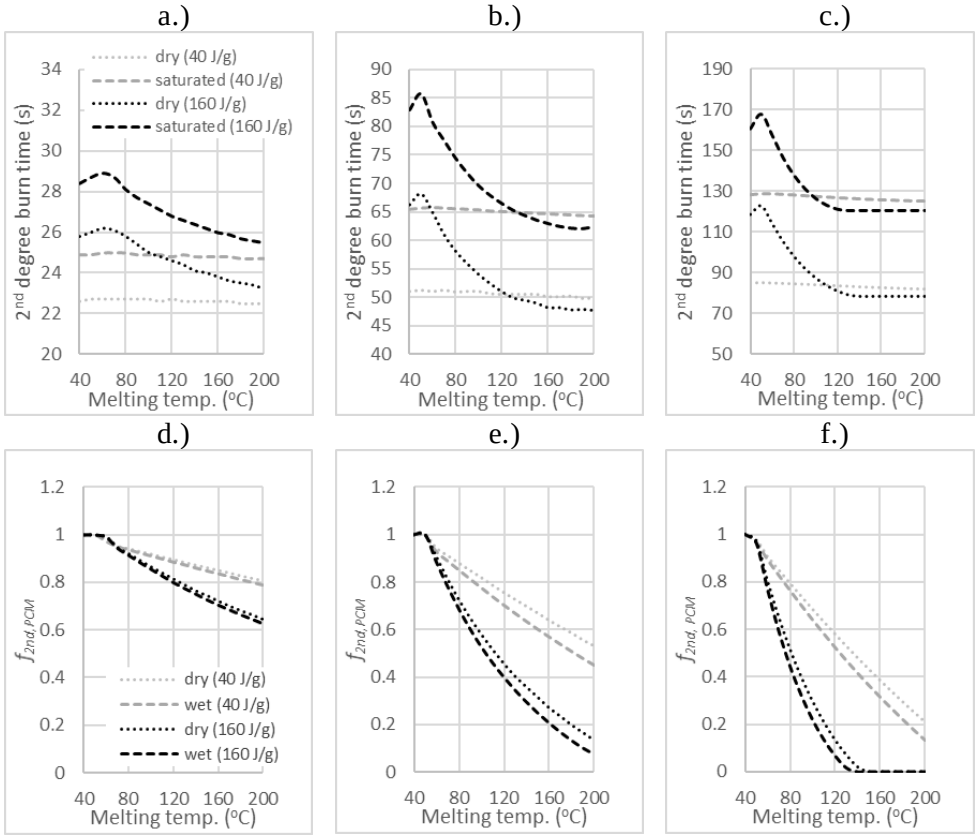

Figure 6.11 – Second-degree burn times for the indicated PCM melting temperature and textile latent heats for cases where the outer shell is dry or saturated for: a.) high, b.) medium, and c.) low–intensity exposures. PCM liquid fraction at second-degree burnout time ($f_{2nd,\ PCM}$) for the indicated PCM melting temperature and textile latent heats for cases where outer shell is dry or saturated for d.) high, e.) medium, and f.) low-intensity exposures

Thus, it can be concluded that the presence of water in the outer shell does not influence the PCM's impact on the PCM FPC thermal performance. The PCM choice will be dependent on other variables that have been explored in other studies in the literature where the PCM FPC suit was considered dry [17].

6.3.2.2 Water presence in the thermal inner

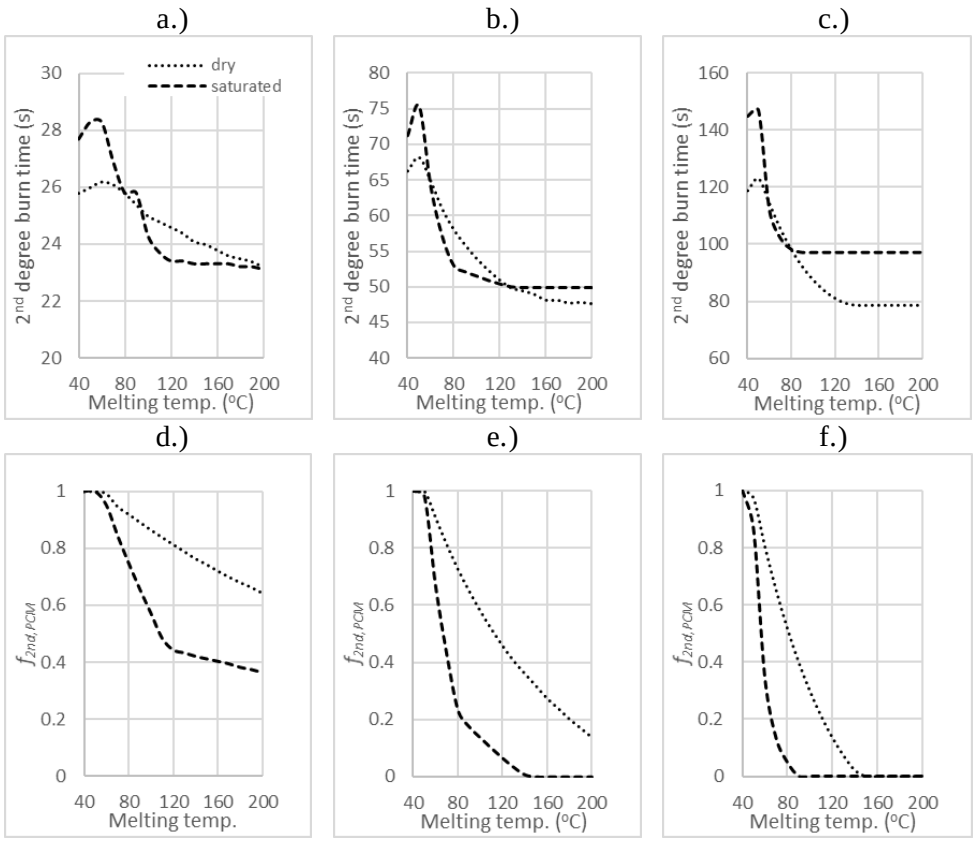

Figure 6.12 – Second-degree burn times for the indicated PCM melting temperature and a 160 J/g textile latent heat for cases where the thermal inner is dry or saturated for a.) high, b.) medium, and c.) low-intensity exposures. PCM liquid fraction at second-degree burnout time ($f_{2nd,\ PCM}$) for the indicated PCM melting temperature and a 160 J/g textile latent heat for cases where the thermal inner is dry or saturated for d.) high e.) medium and f.) low-intensity exposures

Figure 6.12 shows the times to second-degree burn and the liquid fractions at second-degree burnout for different PCM melting temperatures. The results were obtained for a PCM FPC with an inner layer with a fixed latent heat (160 J/g), dry or saturated, and exposed to high-, medium-, and low-intensity exposures. As can be seen, unlike in the case where the outer shell was considered saturated, the tendencies of the second-degree burn times differ whether the thermal inner is saturated or not. This behavior is valid for all heat

exposures (Figure 6.12a-c). For example, for medium-intensity heat exposure and very low PCM melting temperatures (i.e., 40 to 50 °C; Figure 6.12b), the time to second-degree burn slightly rises for both conditions (saturated and dry). For higher melting temperatures, however, with a saturated thermal inner, the second-degree burn time decreases abruptly until a PCM melting temperature of 80 °C, where another abrupt change in tendency happens. Between 80 and 150 °C, the second-degree burn time decreases slowly, while for a melting temperature greater than 150 °C, it does not vary. If a dry thermal inner is considered, such abrupt changes in the tendency do not appear (Figure 6.12b, *dry*). Such behaviors are also observed in the trends for other exposure scenarios when the thermal inner is saturated before the heat exposure. For example, in a high-intensity scenario, the former mentioned abrupt change happens at a melting temperature of 120 °C (Figure 6.12a). These sudden shifts in the tendencies of second-degree burn times with PCM melting temperature are directly related to the liquid fraction at second-degree burn time (Figure 6.12d - e). For example, for a high-intensity heat exposure scenario, the sudden shift in tendency in the second-degree burn, which happens at a melting temperature of 120 °C, is directly related to the sudden change in the trend of second-degree burn liquid fraction, which also happens at a melting temperature of 120 °C (Figure 6.12d).

These sudden shifts in the second-degree burn times and second-degree burnout liquid fractions are directly related to whether the PCM melting is used to absorb latent heat from water condensation or incoming heat directly from the flame. This phenomenon is shown more clearly in Figure 6.13.

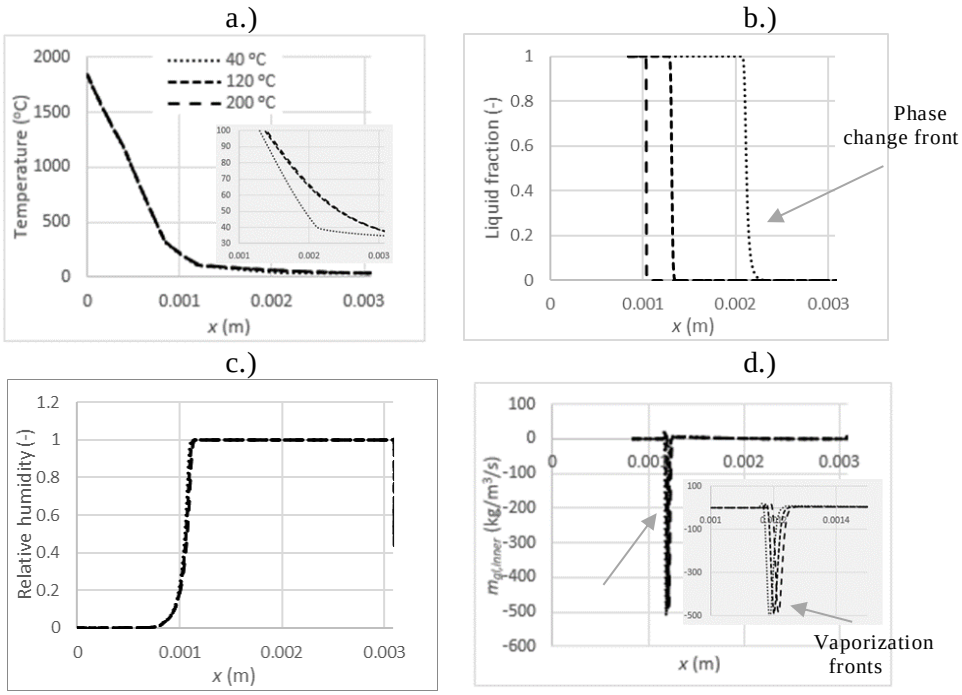

Figure 6.13- Calculated properties along with the thickness of PCM FFPC suit (i.e. *x*) considering the inner shell initially saturated and different PCM melting temperature, at t = 8 s for an exposure of 84 kW/m^2; a.) temperature profiles, b.) PCM liquid fraction, c.) relative humidity, and d.) rate of condensation of water vapor.

Figure 6.13a shows the temperature profiles obtained for the indicated PCM melting temperature after 10 s of exposure. As expected, an increase in the melting temperature of the PCM originates an increase in the temperature profiles. As the melting temperature of the PCM is higher, its liquefaction by the incoming heat flux happens later. Thus the phase change fronts associated with higher melting temperatures tend to lag behind. Figure 6.13b shows the phase change fronts for the respective PCM melting temperature. When the phase change front is compared to the vaporization front, it can be unraveled whether the PCM melting is used to absorb condensation heat or incoming heat from the flame (Figure 6.13d).

Figure 6.13d shows the rate of condensation of water vapor in the PCM thermal inner for the various PCM melting temperature considered. The dips in the rate indicate the vaporization fronts. When these fronts are compared to the phase change fronts (Figure 6.13b), it can be clearly seen that the phase change

front associated with the PCM melting temperature of 40 °C is ahead of the vaporization front. Hence, the PCM latent heat is mostly used for steam condensation. While if a PCM melting temperature of 200 °C is considered, the phase change front is behind the vaporization front, and thus the PCM latent heat will mostly be used to absorb the incoming dry heat from the flame as latent energy. When the PCM melting temperature is 120 °C, both fronts coincide with each other (Figure 6.13b and d). Under a high-intensity exposure, this is the melting temperature that marks the frontier. A PCM with a lower melting temperature will be used to absorb majorly heat of condensation, while a PCM with a higher melting temperature will be used to absorb majorly incoming dry heat from the heat exposure. This is reflected in the sudden change in the second-degree burn time with PCM melting temperature (Figure 6.12d, melting temperature = 120 °C).

Figure 6.13c shows the relative humidity obtained along the PCM thermal inner. As can be seen, the PCM thermal inner is virtually saturated, independently of the PCM melting temperature considered because liquid water is initially present in all of the PCM thermal inner. Thus, such a parameter is inadequate to observe the influence of PCM on thermal performance

In Figure 6.12, for low melting temperature and for all exposure scenarios, the sudden decrease in second degree burn time and PCM liquid fraction at second-degree burnout is explained by the fact that the melting of the PCM is majorly being used to condense the hot steam vapor and preventing it from reaching the skin. For greater melting temperature, the PCMs melting temperature is high enough to promote intense steam condensation no longer. Instead, it is used majorly to absorb the incoming heat flux directly from the flame. For high- and medium-intensity exposures, this shift happens at a PCM melting temperature of 120 °C, 80 °C. However, for low-intensity heat exposure, such a shift is not visible, thus the melting of the PCM occurring only due to steam condensation (Figure 6.12).

Thus, the PCMs efficiency is highly prejudiced by the presence of water in the thermal inner. In some cases, second-degree burnouts tend to happen earlier due to the diffusion of steam towards the skin, thus not leaving enough time for

the PCM to melt before a second-degree burnout happens. Comparisons of the PCM liquid fractions at second-degree burn time between the dry and saturated cases clearly show this (Figure 6.12d - f).

6.3.2.3 Water presence in the outer shell and thermal inner

During firefighting, the presence of moisture simultaneously in the outer shell and thermal inner is likely due to external (e.g., hose spraying) and internal (e.g., perspiration) moisture sources. When water is present in both layers, PCM selection criterion is determined mainly by water in the thermal inner (similar tendencies between Figure 6.12 and Figure 6.14).

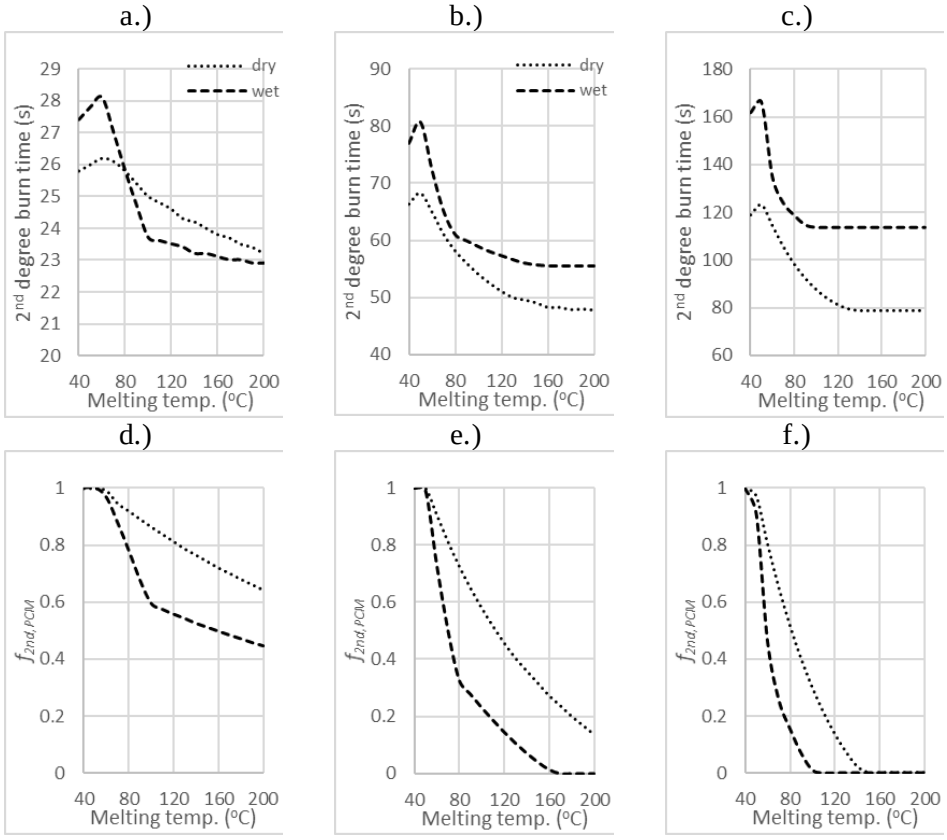

Figure 6.14 – Second-degree burn times for the indicated PCM melting temperature and a 170 J/g textile latent heat for cases where thermal inner and outer shell are at a 50 % saturation wetness level for a.) high, b.) medium, and c.) low-intensity exposures. PCM liquid fraction at second degree burnout time ($f_{2nd,PCM}$) for the

indicated PCM melting temperature and a 160 J/g textile latent heat for cases where thermal inner and outer shell are at a 50 % saturation wetness level for d.) high, e.) medium, and f.) low-intensity exposures

Figure 6.14 shows the second-degree burn time and PCM liquid fraction at burnout variance with melting temperature, wetness level (0 or 50 %) for high, medium, and low-intensity exposures. In this case, both the outer and inner layers have a 50 % saturation wetness level. However, the tendencies of second-degree burn time and PCM liquid fraction (Figure 6.14) are comparable with the results obtained when only the inner layer is saturated, with a wetness level of 100 % (Figure 6.9). However, the melting temperatures at which they happen decrease. For example, whilst for a fully saturated thermal inner and dry outer shell, the shift in tendencies happened at a melting temperature of 120 °C (Figure 6.13a), while for a 50 % saturated thermal inner and outer shell, it happens at 100 °C (Figure 6.14a). This discrepancy is related to the lower quantity of water present in the thermal inner rather than the water presence in the outer shell.

The presence of water in the thermal inner is the major factor in altering the PCM selection criterion whether there is water in the outer shell or not before a heat exposure.

6.4 Conclusions

In this study, the effect of the presence of free water in a PCM FPC was analyzed. At first, the effect of incorporating the thermal inner with different PCM masses was studied for high- (84 kW/m^2), medium- (12 kW/m^2) and low-intensity (5 kW/m^2) heat exposure scenarios. Such was done assuming an initially saturated outer layer. Then, the influence of PCM melting temperature on thermal performance was studied considering a wet outer shell and/or thermal inner. The following major conclusions were obtained:

- Independently of the heat exposure scenario considered, incorporating PCMs through micro or nanoencapsulation configures the textile with insufficient PCM mass to benefit second-degree burn time significantly.
- When there is water in the outer shell is present, part of the steam that diffuses in the direction of the skin is condensed due to the presence of the PCM. Hence, the PCMs latent heat is used to absorb the heat of condensation.
- Also, when water is exclusively present in the outer shell, its impact on the extra time to second-degree burn that the PCM provides is negligible. The implications are that whether free water is present in the outer shell or not, a PCM may be selected independently of such an issue.
- Such is not the case when free water is present in the thermal inner as such is closer to the skin resulting in higher mass fluxes towards the skin. In such a case, the PCMs will demonstrate significant partial melting phenomena for all exposure scenarios. If the role of the PCM is to protect the firefighter from dry incoming heat flux, then the presence of steam dramatically decreases the efficiency of the PCMs. In order to eliminate the partial melting phenomena, water vapor management solutions need to be included in the PCM FPC.

- When free water is present in the outer shell and thermal inner, the water in the thermal inner tends to determine the efficacy of the PCM in increasing second degree burn time, because such is determined to know how well the PCM is able to promote the condensation of the water vapor instead of letting it diffuse and condense at the skin.

This study intends to shine a light on how the presence of free water in the PCM FPC may impact the PCMs thermal performance. It will help in the adequate choice of a PCM and guide PCM FPC design when the presence of free water is verified. Such is very important because, as seen above, its presence may take away the benefit of adding a PCM into a FPC.

Acknowledgments

National funds supported the present study through F.C.T. –Fundação para a Ciência e a Tecnologia, I.P., within the scope of the project UIDB/00532/2020 as well as by PCIF/SSO/0106/2018 - Project for "Development of an innovative firefighter's jacket", funded by national funds through FCT/MCTES (PIDDAC). Malaquias acknowledges the financial support provided by F.C.T. through the PhD Grant PD/BD/ 135097/2017.

References

[1] R.L. Barker, C. Guerth-Schacher, R. V. Grimes, H. Hamouda, Effects of Moisture on the Thermal Protective Performance of Firefighter Protective Clothing in Low-level Radiant Heat Exposures, Text. Res. J. 76 (2006) 27–31. https://doi.org/10.1177/0040517506053947.

[2] Y. Su, J. Li, G. Song, The effect of moisture content within multilayer protective clothing on protection from radiation and steam, Int. J. Occup. Saf. Ergon. 24 (2018) 190–199. https://doi.org/10.1080/10803548.2017.1321890.

[3] C. Keiser, C. Becker, R.M. Rossi, Moisture Transport and Absorption in Multilayer Protective Clothing Fabrics, Text. Res. J. 78 (2008) 604–613. https://doi.org/10.1177/0040517507081309.

[4] M. Guan, S. Annaheim, M. Camenzind, J. Li, S. Mandal, A. Psikuta, R.M. Rossi, Moisture transfer of the clothing–human body system during continuous sweating under radiant heat, Text. Res. J. 89 (2019) 4537–4553. https://doi.org/10.1177/0040517519835767.

[5] C. Keiser, R.M. Rossi, Temperature Analysis for the Prediction of Steam Formation and Transfer in Multilayer Thermal Protective Clothing at Low Level Thermal Radiation, Text. Res. J. 78 (2008) 1025–1035. https://doi.org/10.1177/0040517508090484.

[6] C. Keiser, P. Wyss, R.M. Rossi, Analysis of steam formation and migration in firefighters' protective clothing using x-ray radiography, Int. J. Occup. Saf. Ergon. 16 (2010) 217–229. https://doi.org/10.1080/10803548.2010.11076839.

[7] S. Mandal, G. Song, F. Gholamreza, A novel protocol to characterize the thermal protective performance of fabrics in hot-water exposure, J. Ind. Text. 46 (2016) 279–291. https://doi.org/10.1177/1528083715580522.

[8] P. Chitrphiromsri, Modeling of Thermal Performance of Firefighter Protective Clothing during the Intense Heat Exposure, NCSW, 2004.

[9] P.W. Gibson, Multiphase heat and mass transfer through hygroscopic porous media with applications to clothing materials, 1996. https://www.researchgate.net/publication/216777883_Multiphase_Heat_and_Mass_Transfer_Through_Hygroscopic_Porous_Media_with_Applications_to_Clothing_MaterialsFinal_Report_Jan_1994-_Mar_1996.

[10] D. Huang, S. He, Influence of Initial Moisture Content on Heat and Moisture Transfer in Firefighters' Protective Clothing, Sci. World J. 2017 (2017). https://doi.org/10.1155/2017/9365814.

[11] Y. Su, R. Li, G. Song, J. Li, C. Xiang, Modeling steam heat transfer in thermal protective clothing under hot steam exposure, Int. J. Heat Mass Transf. 120 (2018) 818–829. https://doi.org/10.1016/j.ijheatmasstransfer.2017.12.074.

[12] Y. Su, J. Li, X. Zhang, A Coupled Model for Heat and Moisture Transport Simulation in Porous Materials Exposed to Thermal Radiation, Transp.

Porous Media. (2019). https://doi.org/10.1007/s11242-019-01347-2.
[13] H. Zhang, G. Song, H. Su, H. Ren, J. Cao, An exploration of enhancing thermal protective clothing performance by incorporating aerogel and phase change materials, Fire Mater. 41 (2017) 953–963. https://doi.org/10.1002/fam.2435.
[14] L. Wang, Y. Lu, J. He, On the Effectiveness of Temperature-Responsive Protective Fabric Incorporated With Shape Memory Alloy (SMA) Under Radiant Heat Exposure, Cloth. Text. Res. J. 38 (2020) 212–224. https://doi.org/10.1177/0887302X19892095.
[15] A. Šalej Lah, P. Fajfar, G. Kugler, T. Rijavec, A NiTi alloy weft knitted fabric for smart firefighting clothing, Smart Mater. Struct. 28 (2019). https://doi.org/10.1088/1361-665X/ab18b9.
[16] A. Dąbrowska, G. Bartkowiak, R. Kotas, Evaluation of functionality of warning system in smart protective clothing for firefighters, Sensors. 21 (2021) 1–14. https://doi.org/10.3390/s21051767.
[17] A. Fonseca, T.S. Mayor, J.B.L.M. Campos, Guidelines for the specification of a PCM layer in firefighting protective clothing ensembles, Appl. Therm. Eng. 133 (2018) 81–96. https://doi.org/10.1016/j.applthermaleng.2018.01.028.
[18] F.L. Zhu, Q.Q. Feng, R.T. Liu, B.G. Yu, Y. Zhou, Enhancing the Thermal Protective Performance of Firefighters' Protective Fabrics by Incorporating Phase Change Materials, Fibres Text. East. Eur. 23 (2015) 68–73.
[19] Y. Su, W. Zhu, M. Tian, Y. Wang, X. Zhang, J. Li, Intelligent bidirectional thermal regulation of phase change material incorporated in thermal protective clothing, Appl. Therm. Eng. 174 (2020) 115340. https://doi.org/10.1016/j.applthermaleng.2020.115340.
[20] H. Phelps, H. Sidhu, A mathematical model for heat transfer in fire fighting suits containing phase change materials, Fire Saf. J. 74 (2015) 43–47. https://doi.org/10.1016/j.firesaf.2015.04.007.
[21] Y. Hu, D. Huang, Z. Qi, S. He, H. Yang, H. Zhang, Modeling thermal insulation of firefighting protective clothing embedded with phase change material, Heat Mass Transf. 49 (2012) 567–573. https://doi.org/10.1007/s00231-012-1103-x.
[22] A. Fonseca, S.F. Neves, J.B.L.M. Campos, Thermal performance of a PCM firefighting suit considering transient periods of fire exposure, post – fire exposure and resting phases, Appl. Therm. Eng. 182 (2020) 115769. https://doi.org/10.1016/j.applthermaleng.2020.115769.
[23] F. Li, L. Yi, A computational analysis for effects of fibre hygroscopicity on heat and moisture transfer in textiles with PCM microcapsules, Model. Simul. Mater. Sci. Eng. 15 (2007) 223–235. https://doi.org/10.1088/0965-0393/15/3/003.
[24] M. Itani, N. Ghaddar, K. Ghali, Innovative PCM-desiccant packet to provide dry microclimate and improve performance of cooling vest in hot environment, Energy Convers. Manag. 140 (2017) 218–227. https://doi.org/10.1016/j.enconman.2017.03.011.

[25] X. Wan, F. Wang, Udayraj, Numerical analysis of cooling effect of hybrid cooling clothing incorporated with phase change material (PCM) packs and air ventilation fans, Int. J. Heat Mass Transf. 126 (2018) 636–648. https://doi.org/10.1016/j.ijheatmasstransfer.2018.05.155.

[26] M. Zhao, C. Gao, F. Wang, K. Kuklane, I. Holmér, J. li, The torso cooling of vests incorporated with phase change materials: A sweat evaporation perspective, Text. Res. J. 83 (2013) 418–425. https://doi.org/10.1177/0040517512460294.

[27] K. Iqbal, A. Khan, D. Sun, M. Ashraf, A. Rehman, F. Safdar, A. Basit, H.S. Maqsood, Phase change materials, their synthesis and application in textiles—a review, J. Text. Inst. 110 (2019) 625–638. https://doi.org/10.1080/00405000.2018.1548088.

[28] a. Izzo Renzi, C. Carfagna, P. Persico, Thermoregulated natural leather using phase change materials: An example of bioinspiration, Appl. Therm. Eng. 30 (2010) 1369–1376. https://doi.org/10.1016/j.applthermaleng.2010.02.026.

[29] Bendkowska, Experimental Study of the Thermoregulating Properties of Nonwovens Treated with Microencapsulated PCM, Fibres Text. East. Eur. 17 (2009) 87–91. http://www.fibtex.lodz.pl/issue76.html.

[30] H. Yoo, J. Lim, E. Kim, Effects of the number and position of phase-change material-treated fabrics on the thermo-regulating properties of phase-change material garments, Text. Res. J. 83 (2012) 671–682. https://doi.org/10.1177/0040517512461700.

[31] R. Rossi, W. Bolli, Phase change materials for improvement of heat protection, Adv. Eng. Mater. 7 (2005) 368–373. https://doi.org/10.1002/adem.200500064.

[32] H. Zhang, G. Song, H. Ren, J. Cao, The effects of moisture on the thermal protective performance of firefighter protective clothing under medium intensity radiant exposure, Text. Res. J. 88 (2018) 847–862. https://doi.org/10.1177/0040517517690620.

[33] J.W.S. Hearle, M.W. E, Physical Properties of Textile Fibres, 4th ed., Woodhead Publishing Limited, 2008.

[34] DuPont, Technical Guide for NOMEX Brand Fiber, 2001.

[35] S.F. Neves, J.B.L.M. Campos, T.S. Mayor, On the determination of parameters required for numerical studies of heat and mass transfer through textiles - Methodologies and experimental procedures, Int. J. Heat Mass Transf. 81 (2015) 272–282. https://doi.org/10.1016/j.ijheatmasstransfer.2014.09.038.

[36] E. Onofrei, T.C. Codau, S. Petrusic, G. Bedek, D. Dupont, D. Soulat, Analysis of moisture evaporation from underwear designed for fire-fighters, Autex Res. J. 15 (2015) 35–47. https://doi.org/10.2478/aut-2014-0015.

[37] H. Zhang, G. Song, H. Ren, J. Cao, The effects of moisture on the thermal protective performance of firefighter protective clothing under medium intensity radiant exposure, Text. Res. J. 88 (2018) 847–862.

https://doi.org/10.1177/0040517517690620.
[38] D.A. Torvi, Heat transfer in thin fibrous materials under high heat flux conditions, 1997.
[39] Y. Su, J. Li, X. Zhang, A Coupled Model for Heat and Moisture Transport Simulation in Porous Materials Exposed to Thermal Radiation, Transp. Porous Media. 131 (2020) 381–397. https://doi.org/10.1007/s11242-019-01347-2.
[40] H. Zhang, X. Liu, G. Song, H. Yang, Effects of microencapsulated phase change materials on the thermal behavior of multilayer thermal protective clothing, J. Text. Inst. 0 (2020) 1–10. https://doi.org/10.1080/00405000.2020.1832363.
[41] Rubitherm PCMs, (n.d.). http://www.rubitherm.de/english/pages/02a_latent_heat_pcms.htm.
[42] A. Fonseca Malaquias, S.F. Neves, J.B.L.M. Campos, The impact of water on firefighter protective clothing thermal performance and steam burn occurrence in firefighters, Fire Saf. J. 127 (2022). https://doi.org/10.1016/j.firesaf.2021.103506.
[43] F.C. Henriques, Studies of thermal injury V. The predictability and the significance of thermally induced rate processes leading to irreversible epidermal injury, Arch. Pathol. 43 (1947) 489–502.
[44] M.K. Donnelly, W.D. Davis, J. Lawson, M. Selepak, Thermal Environment for Electronic Equipment Used by First Responders, Natl. Inst. Stand. Technol. Spec. Publ. 1474. (2006) 41.
[45] G.N. Mercer, H.S. Sidhu, A Theoretical Investigation into Phase Change Clothing Benefits for Firefighters under Extreme Conditions, Chem. Prod. Process Model. 4 (2009). https://doi.org/10.2202/1934-2659.1349.
[46] H. D., H. S., Influence of Initial Moisture Content on Heat and Moisture Transfer in Firefighters' Protective Clothing, Sci. World J. 2017 (2017). https://doi.org/10.1155/2017/9365814.

7

Chapter 7

Conclusions and future work

7

Conclusions and future work

7.1 Thesis conclusions

In an effort to understand the benefits that the application of PCMs could have in the thermoregulation of the human body under extreme heat stressful conditions, in this thesis the incorporation of PCMs into a typical fire protective clothing (FPC) garment assembly is numerically analyzed. This is done to see if it could increase the thermal protection offered by the textile, and also quantify it in terms of the various parameters associated to the heat stress environment, the PCM, and the clothing itself.

In a first phase of the study, the increase in thermal performance by the PCM incorporation in an FPC is studied considering constant heat exposure scenarios for specific times. Namely a high – (84 kW/m^2 for 8 s), medium – (12 kW/m^2 for 300 s) and low- (5 kW/m^2 for 300 s) heat exposure scenarios. Parameters associated to the PCM (i.e. latent heat, mass, melting temperature, position) are subject to independent parametric studies and correlations are established. Hence, a PCM selection criteria, under the tested conditions is proposed. It is shown that, by selecting PCM properties which promote PCM melting during the fire exposure, great gains in second – degree burn time are obtained, contrary to the case where the PCM does not melt due to inadequate PCM property choice (e.g. too high a melting temperature).

In a second phase, using the correlations generated in the first phase, potential PCM candidates are chosen and numerically incorporated into a FPC assembly to study how such assemblies would behave in the post – fire and resting phases which also occur in typical firefighting scenarios. Third – degree burn time is found to depend on the environmental conditions that

the firefighter faces after the extreme heat exposure as well as on the PCM properties, and also its mass. If the PCM FPC is not doffed after a fire exposure, the accumulated heat in the PCM liberates towards the skin eventually causing a burnout in the most unexpected times to the firefighter, way after quitting the fire scenario. This information must thus also be considered in the PCM choice.

It has been known that presence of water in fire protective clothing can alter its thermal performance. As such is common, it is also of interest to numerically study the influence of the presence of water in a PCM FPC. However, before such could be done, the influence of water presence on the thermal performance of a FPC has to be studied in detail in function of the environmental conditions as well as initial water content and location in the FPC. Such is done for a wide range of heat exposures and initial water contents, essentially establishing maps, which demonstrate how the presence of water altered second-degree burn times. Steam burns tend to be common when presence of water is verified in the thermal inner and/or in the outer shell of the textile.

Hence in a fourth phase, the incorporation of PCMs into a FPC is studied considering different levels of water presence in the textile. It is shown that, when steam is present in the FPC, part of the PCMs latent energy is utilized to condense steam which would otherwise condense at the skin. Such happens if the PCMs melting temperature is low enough. Correlations are then established for high – medium- and low – intensity heat exposures scenarios regarding PCM choice for wet FPCs.

The work outlined in this thesis allows for understanding of the basic heat and mass transport mechanisms that occur in a PCM textile under extreme temperatures as well as the providence of correlations, which can be utilized as first estimates to aid in the design of such apparel.

7.2 Future work

The work developed in this thesis contains a significant amount of numerical data. Experimental validation of such is suggested as future work. The practical design of a PCM FPC prototype would provide valuable information as not only to the validity of the information generated in this thesis, but also shine light as to what aspects still need to be considered in order to have a functionable PCM FPC.

Extreme environments are not only present in firefighting duties, but also in other activities in which humans tend to engage in. Hence, the numerical analysis of textile application of PCMs in other high temperature environments such as in certain industries is proposed as these are also areas where the potential application of PCMs could be of great benefit.

From a modeling point of view, improvements to the model can be made so as to consider the heterogeneous arrangement of the PCM in the textile which can only be considered utilizing a three dimensional domain. Encapsulation method influence on PCMs melting behavior can also be more thoroughly investigated with such a model as there could be certain textile applications where geometrical features are responsible for the lack of PCM melting. Such would also allow to better evaluate the position and severity of the burns obtained. Also, dripping and wicking mechanisms in the FPC were neglected, but can be important factors which influence heat and mass transport in the FPC under certain conditions. Hence, these two factors should be further experimentally investigated so that an improved model considering such can be formulated.